An investigation into the relationship between cellular metabolism and small extracellular vesicle release in metastatic breast cancer

Michail D. Gounis

M.Sc.

Submitted in fulfilment of the requirements for the Degree of

Doctor of Philosophy

School of Cancer Sciences

College of Medical, Veterinary and Life Sciences

University of Glasgow

September 2022

Abstract

Altered cellular metabolism and release of small extracellular vesicles (sEVs) contribute to acquisition of invasive phenotypes that drive tumour dissemination and metastasis, the main cause of cancer-related death. Both these processes depend on membrane trafficking events that allow communication of cancer cells with different microenvironments on the path to metastasis, and thus shape their ability to colonise and outgrow in distant organs. To investigate these processes, we have combined the MMTV-PyMT mouse model of mammary carcinoma with a syngeneic transplantation and primary tumour resection approach to generate isogenic cells from primary tumours and their corresponding lung micrometastases. Phenotypic characterisation of these cell lines showed that, despite similar growth rates, lung micrometastatic cells exhibited more mesenchymal characteristics than primary tumour-derived cells. In particular, gene set enrichment analysis (GSEA) of differentially expressed genes identified an epithelial-to-mesenchymal transition (EMT) signature in micrometastatic cells, despite the retention of some epithelial characteristics, such as E-cadherin expression. Furthermore, when plated in 3D microenvironment, cells lines from lung metastases were more invasive than those from primary tumours.

Liquid chromatography-mass spectrometry (LC-MS) analysis indicated that there were significant differences between the steady-state metabolome of primary tumour and micrometastatic cells – notably that glutathione levels were decreased in micrometastatic cells and that they synthesised and secreted more proline than their primary tumour counterparts. We also used LC-MS to compare the lipidome of PyMT-derived cell lines and found that micrometastatic cells differed in lipid composition. Notably, micrometastatic cells were enriched in certain sphingolipid species, in particular (C16-, C18-) ceramide, which is known to influence sEV biogenesis.

Using differential centrifugation in combination with nanoparticle tracking and Western blotting, we found that cells from lung micrometastases secreted more sEVs than their primary tumour counterparts, and these vesicles are highly enriched in the sEV markers, CD63, CD81, and TSG101. We then explored the role of ceramide in sEV release by generating neutral sphingomyelinase (nSMase) CRISPR-knockout isogenic cell lines, and demonstrated that increased sEV release

from micrometastatic cells, but not from their matched primary tumour cells, was opposed following deletion of nSMase2. However, no significant differences were found in the size or number of sEVs released from nSMase1-knockout PyMT-derived cells. Furthermore, pharmacological depletion of glutathione led to upregulation of CD63 positive sEVs released from primary tumour cells in a nSMase2-dependent manner. Deletion of nSMase2 did not affect the invasive migration of PyMT-derived micrometastatic cells on fibroblast-derived ECM, but abrogated their ability to invade into a collagen-rich organotypic environment. Collectively, these data indicate that increased sEV release by micrometastatic cells contributes to the generation of microenvironment that supports invasiveness.

Taken together, these data provide evidence that metabolic rewiring, and in particular glutathione and ceramide levels, influence production of sEVs in cells from mammary carcinoma-derived lung micrometastases in a way that supports a more invasive microenvironment.

Table of Contents

List of Tables

List of Figures

Acknowledgements

I would like to thank Jim Norman for giving me the unique opportunity to join the lab, and for his thorough guidance, teaching and supervision throughout my PhD. I am equally grateful to Cassie Clarke for her co-supervision and invaluable input, and for keeping me sane over the last 4 years. I would also like to express my gratitude to both Jim and Cassie for critical review of this thesis and helpful suggestions throughout the writing process. My special thanks to Louise Mitchell for her unconditional support and advice in the course of my PhD, and to David Novo for his constant encouragement and insightful feedback on this project. I would also like to thank them for being such great friends. I am especially thankful to all R20 lab members (past and present) for their endless support, fruitful discussions and for having so much fun over these years. I would like to gratefully acknowledge Cancer Research UK for generously funding the research work during my PhD.

None of the progress I have made throughout my time at the Beatson would have been possible without the contribution of collaborators and services to this work. A massive thank you to David Sumpton and Engy Shokry for their metabolomics expertise, Karen Blyth for her *in vivo* advice, Saverio Tardito for his metabolic insights, Billy Clark, Andy Keith and Jillian Murray for their molecular services, Ann Hedley and Ryan Kwan for their bioinformatics input, David Strachan, Peter Thomason, Nikki Paul, and Lynn McGarry for their help with microscopy, Colin Nixon, Gemma Thomson and rest of the team for their histology services, and the BSU/BRU staff for their practical support with the *in vivo* models.

I am eternally grateful to my family, especially my dad (Dimitris), my sister (Katerina) and her partner (Nikos), for all of their unconditional love, support, and understanding throughout my studies. I would also like to thank my friends (Iliana, Maria, Mara, Sofia, Chrysa, and Giorgos) who always believed in me and can't express how grateful I feel for having them in my life. Finally, I would like to dedicate this thesis to the memory of my Mum, Vassiliki; I miss you very much and your love and guidance continue to inspire me every day to pursue my dreams.

Author's Declaration

I declare that, except where explicit reference is made to the contribution of others, this thesis is the result of my own work and has not been submitted for any other degree at the University of Glasgow or any other institution.

Michalis Gounis

Abbreviations

4EBP1,2	4E-binding proteins 1 and 2
α-KG	α-ketoglutarate
ACC1	acetyl-CoA carboxylase 1
ACSL3	Acyl-CoA synthetase long-chain family member 3
AMPK	Adenosine monophosphate (AMP) activated protein kinase
ANGPTL4	Angiopoietin Like 4
Arp2/3	Actin-related protein 2/3
Asns	Asparagine synthetase
ATP	Adenosine triphosphate
BMDCs	Bone marrow derived cells
BMP	Bone morphogenetic protein
BSO	Buthionine sulfoximine
CAV1	Caveolin-1
CCL2	C-C Motif Chemokine Ligand 2
CDM	Cell-derived matrix
Cer	Ceramide
CerK	Ceramide kinase
CerP	Ceramide phosphate
Cldn1	Claudin 1
CLIC3	Chloride intracellular channel 3
CM	Conditioned media
CRISPR	Clustered regularly interspaced short palindromic repeats
CTCs	Circulating tumour cells
DAG	Diacylglycerol
Ddr2	Discoidin domain receptor tyrosine kinase 2
DGKα	Diacylglycerol kinase α
Dkk1	Dickkopf-related protein 1
DTCs	Disseminated tumour cells
ECM	Extracellular matrix
ECs	Endothelial cells
EEs	Early endosomes
EGFR	Epidermal growth factor receptor
EMT	Epithelial-to-mesenchymal transition
ER	Oestrogen receptor
ESCRT	Endosomal sorting complex required for transport
FASN	Fatty acid synthase
FHOD3	Formin homology-2 domain containing 3
FRAP	Fluorescence recovery after photobleaching
GCL	Glutamate-cysteine ligase
GEMM	Genetically engineered mouse model
Glipr1	GLI pathogenesis related 1
GLUT1	Glucose transporter type 1
Gpx	Glutathione peroxidase

Gr	Glutathione reductase
GRM3	Glutamate metabotropic receptor 3
GSEA	Gene set enrichment analysis
GSH	Reduced glutathione
GSS	Glutathione synthetase
GSSG	Oxidised glutathione
HCC	Hepatocellular Carcinoma
HER2	Human epidermal growth factor receptor 2 (ERBB2/NEU)
HexCer	Hexosylceramide
HSC	Hepatic stellate cell
IDH1	Isocitrate dehydrogenase 1
IL-1β	Interleukin-1β
ILVs	Intraluminal vesicles
ISH	In-situ hybridisation
Itga5	Integrin subunit alpha 5
LC-MS	Liquid chromatography-mass spectrometry
LEs	Late endosomes
lEVs	Large extracellular vesicles
LOH	Loss of heterozygosity
LOX	Lysyl oxidase
MAMs	Metastasis associated macrophages
MCT1	Monocarboxylate transporter 1
MET	Mesenchymal-to-epithelial transition
MHC	Major Histocompatibility Complex
MIF	Migration inhibitory factor
miRNA	MicroRNA
mLST8	Mammalian lethal with SEC13 protein 8
MMTV	Murine mammary tumour virus promoter/enhancer
MRD	Minimal residual disease
MT1-MMP	Membrane type I matrix metalloproteinase
mtDNA	Mitochondrial DNA
mTOR	Mechanistic target of rapamycin
Mutp53	Mutant p53
MVEs	Multivesicular endosomes
NAC	N-acetylcysteine
NADPH	Reduced nicotinamide adenine dinucleotide phosphate
NEM	N-ethylmaleimide
NETs	Neutrophil extracellular traps
NK	Natural killer cells
NMuMG	Normal murine mammary gland
Nrf2	Nuclear factor erythroid 2–related factor 2
nSMase	Neutral sphingomyelinase
NTA	Nanoparticle tracking analysis
NTC	Non-targeting control
OXPHOS	Oxidative phosphorylation

P4HA	Prolyl-4-hydroxylase
P5C	Pyrroline-5-carboxylic acid
PA	Phosphatidic acid
PC	Pyruvate carboxylase
PC	Phosphatidylcholine
PDX	Patient derived xenograft
PE	Phosphatidylethanolamine
PHGDH	Phosphoglycerate dehydrogenase
PI	Phosphatidylinositol
PI3K	Phosphatidylinositol-3-kinase
PKB	Protein kinase B/Akt
PKC	Protein kinase C
PKD1	Protein kinase D1
PKM2	Pyruvate kinase type M2
PLCγ-1	Phospholipase Cγ-1
PMN	Pre-metastatic niche
PNRC	Perinuclear recycling compartments
PPP	Pentose phosphate pathway
PR	Progesterone receptor
Prodh	Proline dehydrogenase
PS	Phosphatidylserine
PSAT1	Phosphoserine aminotransferase 1
PSPH	Phosphoserine phosphatase
PTM	Post-translational modification
Ptprf	Protein tyrosine phosphatase receptor type F
PUFA	Polyunsaturated fatty acid
Pycr1	Pyrroline-5-carboxylate reductase 1
PyMT	Polyoma virus middle T antigen
RAPTOR	Regulatory-associated protein of mTOR
RCP	Rab-coupling protein
Rhpn2	Rhophilin Rho GTPase binding protein 2
RNA-Seq	RNA-Sequencing
ROS	Reactive oxygen species
RT	Room temperature
RTKs	Receptor tyrosine kinases
RT-qPCR	Reverse transcription quantitative real-time PCR reaction
S1P	Sphingosine 1-phosphate
S6K1	S6 kinase 1
SASP	Senescence-associated secretory phenotype
sEVs	Small extracellular vesicles
sgRNA	Single guide RNA
ShcA	Src homology domain–containing protein (also known as Shc1)
SHMT2	Serine hydroxymethyltransferase 2
SM	Sphingomyelin
Smpd	Sphingomyelin phosphodiesterase

TAMs	Tumour associated macrophages
TC	Tissue culture
TCA	Tricarboxylic acid
TEM	Transendothelial migration
TFEB	Transcription factor EB
TfnR	Transferrin receptor, also known as TRFC
TGF-ß	Transforming growth factor ß
TGN	Trans-Golgi network
TIFs	Telomerase-immortalised fibroblasts
TMEM	Tumour Microenvironment of Metastasis
UGDH	UDP-glucose 6-dehydrogenase
ULK1	Unc-51-like kinase 1
V-ATPase	Vacuolar H^+-ATPase
VCAM-1	Vascular cell adhesion molecule 1
VEGF	Vascular endothelial growth factor
WASH	WASP and SCAR homologue complex
xCT	xC- cystine/glutamate antiporter system

Chapter 1 Introduction

1.1 Metastasis as a systemic disease

Despite considerable progress in early detection and development of systemic therapies for different types of cancer, metastatic disease accounts for the majority of cancer-related deaths. This might seem paradoxical considering that colonisation of distant organs by disseminated cancer cells is a highly inefficient process, with clinical manifestation of overt metastases often occurring after years of undetectable disease following surgery and/or therapy (Lambert et al., 2017; Pollard, 2016). Advances in our understanding of disease progression have partially resolved this paradox by establishing that systemic spread of cancer occurs very early, challenging the traditionally held view of metastatic dissemination being a late event in tumour progression (Hosseini et al., 2016; Hüsemann et al., 2008; Rhim et al., 2012; Podsypanina et al., 2008). Furthermore, it involves a complex interplay between disseminated tumour cells (DTCs), immune and stromal cells. It is now clear that the presence of a primary tumour leads to systemic changes that may elicit spatiotemporal responses, which regulate tissue-specific processes (inflammation, angiogenesis, immunosuppression, stromal and metabolic reprogramming) in distant tissues, to promote the formation of pre-metastatic niches, colonisation, and eventual outgrowth of previously latent metastatic cells (McAllister & Weinberg, 2014). However, current therapies directed at minimal residual disease, which originates from survival of local and/or disseminated cancer cells following treatment, are mostly empirical, and target rapidly proliferating cells with little or no consideration of the molecular characteristics of dormant cells and/or the niche in which they reside (Ghajar, 2015). Thus, a deeper understanding of the cellular and molecular events that discern primary tumours from their metastatic descendants could be key to the development of future therapies targeting elimination or prevention of systemic cancer spread (Klein, 2020; Lambert et al., 2017).

1.2 Steps of the metastatic cascade

During the course of disease progression, a few clones of cells within the primary tumour may display enhanced potential for seeding metastatic colonies in distant

organs, but these founder cells first need to traverse different microenvironments through a multi-step process, known as the invasion-metastasis cascade (Joyce & Pollard, 2009; Lambert et al., 2017). For carcinoma cells to metastasise, the first step in the cascade (Figure 1-1) involves breaching the basement membrane and locally invading the surrounding stroma, followed by entrance into the circulatory and/or lymphatic system, survival of tumour cells in the circulation and endurance of shear stress in the vasculature. Subsequently, these circulating cells can extravasate into the parenchyma of distant organs, adapt to new microenvironments and seed small colonies (micrometastases) that will eventually give rise to clinically detectable metastases (macrometastases) (Lambert et al., 2017). These processes require cancer cells to acquire properties that foster migratory and invasive phenotypes, and interact with non-tumour cell types that help them survive this intricate journey, as briefly described below in the context of carcinomas (with a particular focus on breast cancer studies).

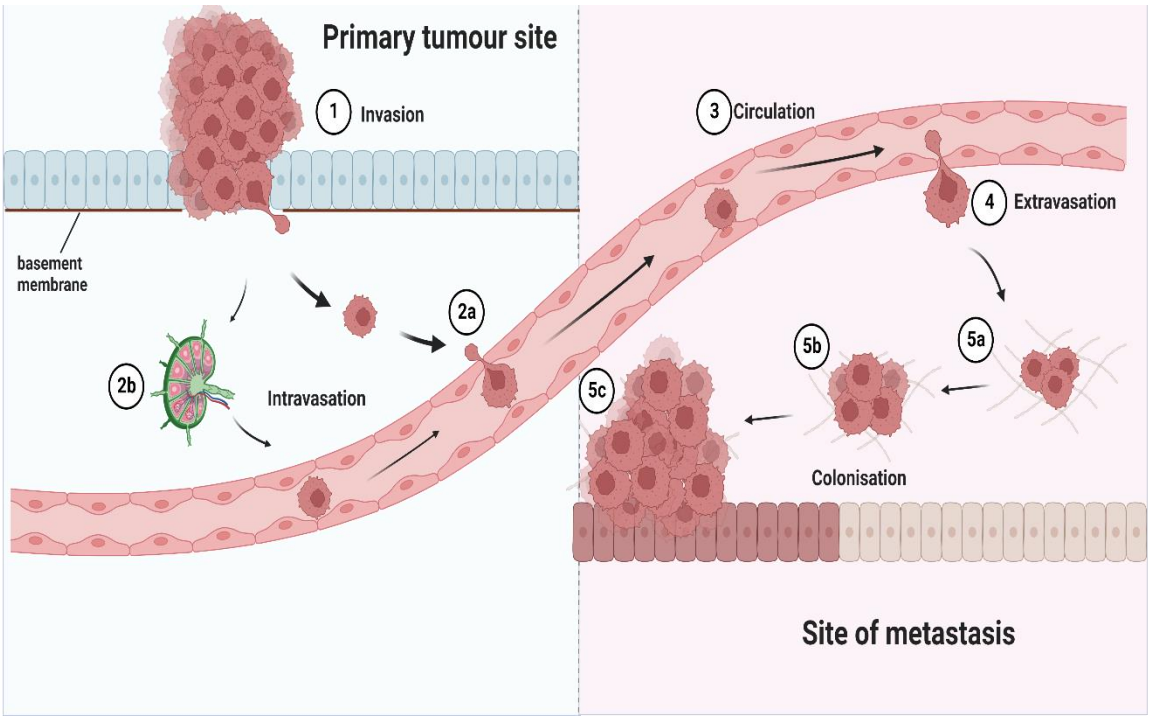

Figure 1-1 Overview of the metastatic cascade.
Cancer cell clones within the primary tumour need to complete several steps in order to metastasise to distant sites through a process known as the 'metastatic cascade'. Firstly, they need to breach the basement membrane and locally invade into the surrounding stroma (1). Cancer cells mainly enter the circulation via the capillary bed (2a) or the lymphatic system (2b), where adaptation strategies are critical for cancer cells to survive in a highly inhospitable environment. Having successfully escaped cell death signals, tumour cells reach the capillaries of distant organs via the circulation (3) where their ability to extravasate into the parenchyma of metastatic target organs (4) depends on interactions with other cell types in the circulation, as well as systemic changes (termed 'metastatic niche priming') that had previously been induced in these organs by factors emanating from the primary tumour. Metastatic colonisation (5) is the last step in the cascade, but the journey is not complete until cancer cells adapt to the new microenvironment, escape immune surveillance and settle in a favourable niche that supports their survival and maintains their tumour initiating capacity

(5a). Even then, disseminated cancer cells may enter a state of quiescence (5b), which can last for years before the appearance of frank metastasis (5c) in the target organ.

1.2.1 Invasion into surrounding stroma

Cell motility and invasion are crucial processes for metastatic dissemination as they enable cancer cells to move into the surrounding tumour stroma, and are highly orchestrated by responses to both cell-intrinsic and extrinsic cues present in the microenvironment (Sahai, 2005). In particular, acquisition of mesenchymal-like traits associated with elongated cell morphology, integrin-mediated cell adhesion and proteolytic degradation of extracellular matrix (ECM) components are key to cancer cell invasiveness, with the latter phenotype frequently displayed by cancer cells invading alone (Giampieri et al., 2009), collectively (Haeger et al., 2014) or in multicellular streams (Roussos et al., 2011). A well-studied biological program that drives the acquisition of such characteristics is the epithelial-to-mesenchymal transition (EMT) (Lambert et al., 2017), described in more detail in 1.4, with this term often being used synonymously with phenotypic plasticity (Jehanno et al., 2022). Activation of programs regulating cell motility is not only restricted to successful invasion of cancer cells into stroma, but can also shape paracrine signalling interactions between macrophages and tumour cells influencing the next step of the cascade, intravasation (Roussos et al., 2011).

1.2.2 Entry into circulation in clusters or single cells

At the primary site, tumour cells that have locally invaded the surrounding stroma can enter into blood or lymphatic vasculature either in neighbouring tissues or newly formed vessels within the tumour. Although haematogenous dissemination of cancer is considered the main route towards metastatic seeding (Lambert et al., 2017), the presence of cancer cells in the draining lymph nodes close to the primary tumour has prognostic value since it is associated with poor disease-free and overall survival (De Boer et al., 2010). Both cell clusters and single cancer cells (Figure 1-2), escorted by immune cells, can be found in the bloodstream, with the former being associated with a more aggressive disease progression (Aceto et al., 2014; Szczerba et al., 2019). Intravital imaging studies have shown that physical contacts between macrophages and tumour cells trigger invadopodia formation in the latter promoting transendothelial migration, and thus enhancing intravasation (Wyckoff et al., 2000; Roh-Johnson et al., 2014). Indeed, the initial

pioneering work into the role of macrophages in intravasation (by Jeff Pollard's and John Condeelis's groups) (Wyckoff et al., 2007) led to the discovery of micro-doorways on endothelial cells, called Tumour Micro Environment of Metastasis (TMEM) (Figure 1-2), through which breast cancer cells enter the circulation (Harney et al., 2015; Ginter et al., 2019). Each functional doorway consists of three different cell types in direct physical contact, a perivascular macrophage (Tie2-high VEGFA-high causing transient vascular permeability), a tumour cell (highly expressing Mena, which regulates actin polymerisation and cell migration) and an endothelial cell (ANG2) acting as a doorway for haematogenous spread (Harney et al., 2015; Ginter et al., 2019). Importantly, these micro-anatomical structures have been identified both in mice and human mammary carcinomas, and increased TMEM density positively correlates with development of systemic metastases in breast cancer patients (Robinson et al., 2009; Rohan et al., 2014). It is, therefore, conceivable that understanding the mechanisms involved in intravasation of cancer cells into the circulation may uncover novel targets to prevent systemic spread at the start of the metastatic cascade (Sznurkowska & Aceto, 2021).

1.2.3 Survival of cells while in transit

Once in the bloodstream, circulating cancer cells must overcome major survival bottlenecks on their way to seed the parenchyma of distant organs (Figure 1-2), notably due to loss of integrin-dependent adhesion to ECM, shear stress in the vasculature and/or immune attack, especially by natural killer (NK) cells (Labelle & Hynes, 2012). To overcome these challenges, circulating tumour cells (CTCs) interact with other cell types, namely neutrophils and platelets, which can facilitate their journey to distant sites. For example, neutrophil extracellular traps (NETs), which are web-like chromatin structures that combat pathogens upon infection, can entrap circulating carcinoma cells via ß1-integrin mediated interactions (Najmeh et al., 2017), and NET formation has been associated with the appearance of lung venous thrombosis in a mammary carcinoma model (Demers et al., 2012). In addition, formation of clusters between CTCs and neutrophils has been reported to support cell cycle progression in the former leading to enhanced metastatic seeding in mouse and human mammary carcinoma (Szczerba et al., 2019). Consistent with exerting a protective role against shear forces and NK cell-mediated attack (Palumbo et al., 2005), platelets associate

with CTCs and form aggregates which have been known to support metastatic progression (Gasic et al., 1968; Gay & Felding-Habermann, 2011). Platelet-rich thrombi around tumour cells are formed upon activation of platelets either by direct contact with cancer cells (expressing tissue factor on their cell surface) or via release of tumour-derived soluble factors (e.g. ADP, TXA2, thrombin) (Schlesinger, 2018). Platelet coating can physically protect CTCs from recognition and lysis by NK cells (Palumbo et al., 2005) or even grant them a pseudo-normal phenotype (MHC I transfer onto cancer cells) (Placke et al., 2012), while platelet-derived transforming growth factor ß (TGF-ß) activates TGF-ß/Smad and NF-κB signalling in tumour cells to sustain invasive mesenchymal-like traits (Labelle et al., 2011), potentially substituting for the absence of stromal interactions previously found in the context of primary tumour (Lambert et al., 2017). Interestingly, it has been reported that carcinoma cell-derived mucins bind to selectins on neutrophils and platelets promoting their physical interaction and leading to release of cathepsin G from neutrophils that stimulates platelet aggregation (Shao et al., 2011). Thus, neutrophils and platelets may display synergistic action on supporting survival, or avoiding cell killing, of tumour cells in the circulation.

1.2.4 Arrest and extravasation at distant sites

Following survival in the circulation, and prior to entry into the parenchyma of distant organs, cancer cells can arrest in capillaries due to physical restrictions and/or adherence to vessel walls. Transient entrapment of cancer cells into capillary beds shortly after intravasation is mostly dictated by circulation patterns, while sustained adhesion to the endothelium probably requires specific adhesion molecules and the involvement of other cell types (Labelle & Hynes, 2012). For example, after intravasation, breast and colon cancer cells travel first to the capillaries of the lungs and liver (sinusoids) respectively, where tumour-host cell clusters (as described in 1.2.3) may initially arrest due to the small diameter of the capillaries (Chambers et al., 2002). However, cancer cells can also arrest in blood vessels of larger diameter (Al-Mehdi et al., 2000), suggesting that adhesion to the endothelium is not merely a passive mechanical process, and involves complex interactions with non-tumour cells, particularly platelets and components of the innate immune system (immature myeloid cells, neutrophils, monocytes) (Labelle & Hynes, 2012). These interaction networks influence the

ability of tumour cells to pass through the endothelial walls via a process known as transendothelial migration (TEM) (Figure 1-2). Mechanistically, tumour cell-activated platelets enhance TEM by releasing several growth factors and cytokines, which can promote invasive mesenchymal characteristics in cancer cells (TGF-mediated signalling) (Labelle et al., 2011), increase vascular permeability (endothelial P2Y2 receptor activation) (Schumacher et al., 2013) or directly lead to the recruitment of bone marrow derived cells (BMDCs) (Massberg et al., 2006). Likewise, neutrophils have been shown to facilitate TEM of tumour cells through the secretion of IL-1β and matrix metalloproteinases (MMP9), which activate endothelial cells and degrade the perivascular ECM respectively (Spiegel et al., 2016). Furthermore, recruitment of classical (inflammatory) monocytes (which may differentiate into metastasis-associated macrophages) to metastatic sites depends on tumour- and stroma-derived CCL2, which is upregulated following activation of NF-κB signalling pathway in cancer cells interacting with platelets (Labelle et al., 2011), and promotes vascular permeability and extravasation of cancer cells into the distant tissue parenchyma (Qian et al., 2011). Lastly, extravasation efficiency depends on tumour cells' intrinsic ability to express factors involved in vascular and ECM remodelling, including epidermal growth factor receptor ligand epiregulin, cyclooxygenase COX2, matrix metalloproteinases, VEGF, and ANGPTL4 (Gupta et al., 2007; Padua et al., 2008; Weis et al., 2004). Indeed, cancer cells expressing high levels of VEGF or Angptl4 are very efficient in metastasising to the lungs, since these factors disrupt endothelial cell-cell junctions and enhance permeability of lung capillaries facilitating extravasation (Padua et al., 2008; Weis et al., 2004). Overall, the formation of cooperative interactions between cancer cells and different types of host cells during metastasis shape the potential of CTCs to adhere and transmigrate into the metastatic sites.

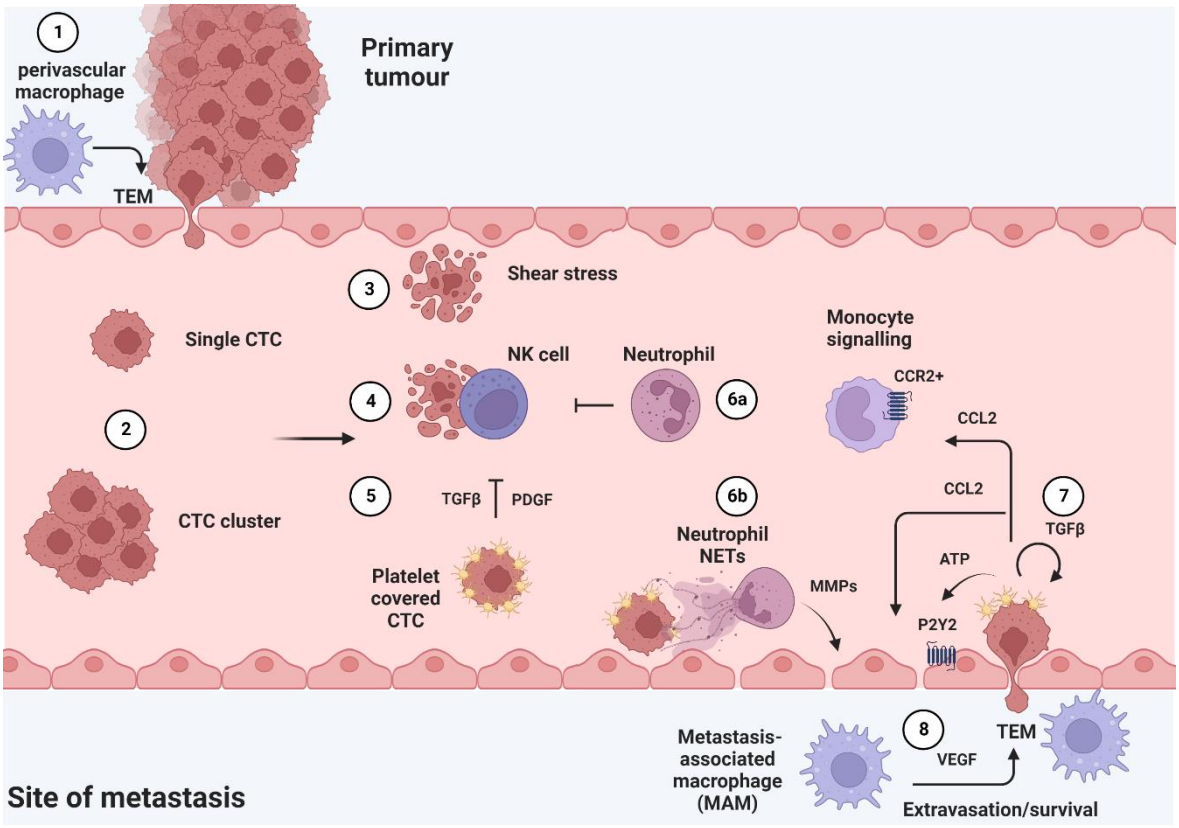

Figure 1-2 Interplay between tumour, immune and stromal cells during intravasation, survival in circulation and extravasation.
Intravasation involves physical contacts between perivascular macrophages and tumour cells (1) that promote disruption of endothelial cell-cell junctions enabling transendothelial migration (TEM). Cancer cells enter the bloodstream either as single circulating tumour cells (CTCs) or multicellular clusters (2), which can be fragmented due to mechanical (shear) stress encountered in their journey through the vasculature (3) or can be rapidly eliminated by natural killer (NK) cells (4). Following intravasation, some cancer cells can survive by associating with platelets, which confer both physical and immune protection (5), and/or neutrophils that either inhibit NK cell function (6a) or entrap cancer cells following formation of neutrophil extracellular traps (NETs). Neutrophil-mediated physical entrapment of cancer cells and release of matrix metalloproteinases (MMPs) also contribute to extravasation (6b), which is further enhanced by the coordinated action of activated platelets and tumour cells once arrested in the capillaries. In particular, tumour-associated platelets activate endothelial P2Y2 receptor to induce vascular permeability, and release various growth factors (e.g. TGFβ) and cytokines (e.g. CCL2) to promote invasive mesenchymal traits in cancer cells, and activate monocyte signalling respectively (7), leading to their recruitment to the metastatic site. These effects promote TEM of cancer cells into metastatic target organs, which is further supported by differentiation of the recruited inflammatory monocytes into metastasis-associated macrophages (MAM) through growth factor secretion (8) in the target organ parenchyma. Adapted from (Lambert et al., 2017).

1.2.5 Metastatic colonisation

A major rate-liming step for development of clinically detectable metastases is the last stage of the metastatic cascade, which includes the foundation of micrometastatic colonies and their outgrowth into overt tumours. Following extravasation, the vast majority of disseminated cancer cells are not able to grow in distant organ environments, with only 0.02% forming macroscopic tumours in a metastatic melanoma model (Luzzi et al., 1998). Metastatic colonisation is highly inefficient most probably due to elimination of DTCs by immune cells or entry of

cancer cells into a quiescent state triggered by the absence of microenvironmental signals that previously sustained their growth in the primary site (Aguirre-Ghiso, 2007). In fact, these dormant disseminated cancer cells can be present for years or even decades before they form overt metastases ('awakening'), which is supported by clinical observations of patients (20-45%) with breast or prostate cancer that will relapse with metastatic disease after long periods of remission following primary tumour removal (Aguirre-Ghiso, 2007). Consistent with this, the presence of DTCs in the bone marrow at the time of diagnosis of breast cancer is associated with an increased risk of recurrence and poor disease-free survival in a 10-year follow-up study (Braun et al., 2005). Despite their clinical relevance, little is known about the nature of dormant disseminated cells and the mechanisms (further described in 1.3) that enable them to sustain quiescence, and evade immune surveillance, while retaining tumour initiating capacity and eventually form macroscopic lesions (Massagué & Obenauf, 2016). It has been demonstrated that, in the lung, stromal expression of bone morphogenetic protein (BMP) or DKK1-mediated inhibition of WNT signalling (Figure 1-3) promotes dormancy of disseminated breast cancer cells by inhibiting cancer stem cells traits (self-renewal) or by downregulating ligands for NK cell activation respectively (Malladi et al., 2016; Gao et al., 2012). Interestingly, another study has also shown that DKK1 differentially regulates the metastatic tropism of breast cancer cells to the lung and bone by inhibiting non-canonical and canonical WNT signalling pathways respectively (Zhuang et al., 2017), but the exact relationship between organ tropism and 'awakening' in proliferating metastatic lesions remains to be determined (Zheng & Pollard, 2017). Understanding, therefore, the molecular mechanisms that shape metastatic latency within different organ microenvironments could be key to target the dormant niche that contributes to disease recurrence.

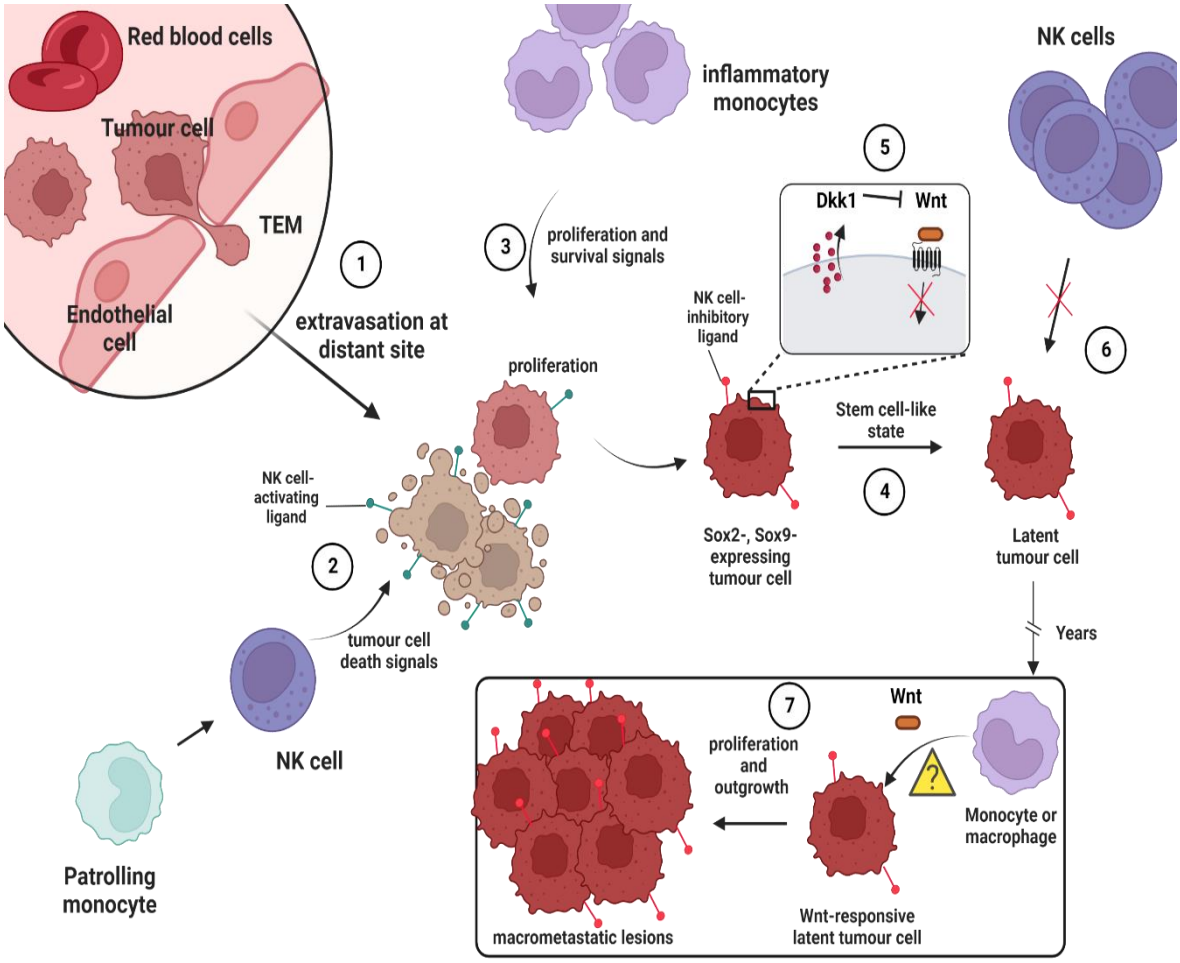

Figure 1-3 Mechanisms of metastatic cell latency.
Following extravasation at metastatic target organs (1), the majority of disseminated cancer cells undergo apoptosis. This is triggered by NK cells, which are recruited to the target organ parenchyma by patrolling monocytes, which recognise cancer cells and mediate their killing through ligand stimulation of NK cell receptors (2). Recruitment of inflammatory monocytes, on the other hand, can promote survival and proliferation of cancer cells by counteracting NK cell-induced cytotoxicity (3). Infiltrating cancer cells can adopt stem cell-like programs (characterised by high expression of Sox2 and Sox9) and are able to enter a quiescence state (4) in a stochastic manner by upregulating dickkopf-related protein 1 (Dkk1), a Wnt inhibitor (Sox2-mediated transcription), and thus preventing β-catenin driven proliferation in the presence of Wnt signals (5). This autocrine signalling leads to downregulation of NK-cell activating ligands and allows latent cancer cells to evade NK cell-mediated clearance and efficiently seed target organs (6). However, additional traits that latent cancer cells acquire to break these stochastic cycles of proliferation-death, respond to Wnt signalling and promote metastatic outgrowth (7). Adapted from (Malladi et al., 2016; Pollard, 2016).

1.3 Dormancy of disseminated tumour cells

It is now clear that disseminated cancer cells that persist as minimal residual disease (MRD) following primary tumour removal and/or systemic treatment serve as a substrate for tumour recurrence and manifestation of metastatic lesions, which can become clinically evident years or decades after successful therapy (Aguirre-Ghiso, 2007; Sosa et al., 2014). The notion of metastatic latency (Figure 1-3) and MRD is further supported by the persistence of DTCs, which are associated with increased risk for disease relapse in breast cancer patients following

neoadjuvant therapies, suggesting that DTCs are not immediately capable of initiating growth in distant sites (Hartkopf et al., 2013). Despite the presence of cancer-driver mutations, the inability of these cancer cells to reinitiate growth can be controlled by microenvironmental and epigenetic mechanisms (Sosa et al., 2014), similar to the concept previously introduced (Bissell et al., 1982; Parry et al., 1980), in which host-derived microenvironmental cues regulating tissue homeostasis might have a suppressive role in cell growth over cancer genetics. Cancer dormancy refers to the paused growth of DTCs in distant tissues before the outgrowth of overt metastases (Sosa et al., 2014; Risson et al., 2020), with two forms being observed: tumour mass dormancy, where a balance between cancer cell proliferation and death due to immune surveillance and/or impaired angiogenic response maintains tumour mass constant with no significant change in cell number, and cellular dormancy, in which DTCs or small cell clusters enter a reversible mitotic arrest (G0 phase) and are resistant to host defences and therapy (Aguirre-Ghiso, 2007; Ghajar, 2015). The switch of DTCs from a dormant to a proliferative state ('awakening'), and vice versa, is under constant dynamic control and can be mediated via cancer cell-intrinsic or extrinsic mechanisms in response to changes in the surrounding microenvironment (Risson et al., 2020). For example, recent work has shown that sustained inflammation results in awakening of DTCs through ECM remodelling in mouse models of breast and prostate cancer (Albrengues et al., 2018). In particular, inflammation-activated neutrophils form NETs and release the proteolytic enzymes elastase (NE) and MMP9, leading to remodelling of laminin, the cleavage of which triggers proliferation of dormant cancer cells via activation of $\alpha_3\beta_1$ integrin and downstream signalling (Albrengues et al., 2018). Conversely, DTCs may reside in niches that support their survival and induce dormancy programs, such as the bone marrow microenvironment or the perivascular niche of different metastatic sites (Ghajar, 2015). Indeed, it has been reported that $NG2^+$/$Nestin^+$ mesenchymal stem cells (MSCs) present in the bone marrow perivascular niche secrete TGF-ß2 and BMP7 to signal through TGFBRIII and BMPRII on breast DTCs resulting in activation of the SMAD, p38 and p27 pathways and subsequent dormancy (Nobre et al., 2021). Similarly, another study demonstrated that dormant breast DTCs reside on the microvascular endothelium of lung, bone marrow and brain, and endothelial-deposited thrombospondin-1 is able to sustain quiescence of these cancer cells by acting as an angiocrine tumour suppressor (Ghajar et al., 2013). Taken together,

these studies reflect the ability of DTCs to enter or exit cellular dormancy depending on the microenvironmental signals, thus highlighting their phenotypic plasticity.

1.4 Phenotypic plasticity of metastasising cancer cells

As mentioned above (in 1.2.1), acquisition of highly motile phenotypes and invasive characteristics is critical for carcinoma cells to leave the primary site and disseminate to distant tissues. One centrally important concept encompassing these steps is the phenotypic plasticity of cancer cells - which refers to the reversible transition between cellular states over disease progression and is shaped by the integration of both intrinsic factors (genetic, epigenetic changes) and external stimuli (tumour microenvironment) (Jehanno et al., 2022). One of the best studied examples of plasticity is the activation of EMT-like programmes in carcinoma cells leading to transient and reversible acquisition of certain mesenchymal traits, while resulting in loss of some epithelial features (Lambert & Weinberg, 2021). During cancer progression, the tumour-associated stroma (consisting of fibroblasts, myofibroblasts, endothelial and immune cells recruited from host tissues) becomes 'reactive' resembling the type of stroma typically observed during tissue-healing responses and is coupled with the release of various paracrine signals (LeBleu & Kalluri, 2018). These secreted molecules, including TGF-ßs and certain interleukins, activate multiple signalling pathways (Wnt/ß-catenin, Notch) and master transcription factors (Snail, Slug, Twist, Zeb1) resulting in induction of EMT, which confers cancer cells tumour initiating capacity and therapeutic resistance (Lambert et al., 2017; Lambert & Weinberg, 2021). Although EMT-like processes might have occasionally been described to act as a binary switch, with cancer cells residing in either an epithelial or mesenchymal state, a recent study revealed distinct hybrid EMT states in skin and mammary primary tumours (Figure 1-4A, B), with cancer cells in the hybrid state displaying higher plasticity and metastatic potential compared with solely epithelial or mesenchymal cells (Pastushenko et al., 2018). Interestingly, subpopulations of cancer cells with various EMT transition states were detected in spatially distinct areas within the tumour microenvironment, where macrophage infiltration was associated with progression towards the mesenchymal phenotype (Pastushenko et al., 2018). The requirement of hybrid EMT cell states, or partial EMT, for metastasis formation is further supported by an independent study using lineage

tracing in a model of metastatic breast cancer (Lüönd et al., 2021). In contrast, induction of a fully mesenchymal phenotype (full EMT), which can be achieved experimentally through upregulation of EMT transcription factors or complete loss of epithelial features, results in cancer cells that have reduced both their tumour initiating capacity and ability to form metastases (Ocaña et al., 2012; Padmanaban et al., 2019). Mechanistically, while loss of E-cadherin was shown to increase invasion, it was able to trigger apoptosis in breast DTCs by influencing TGF-ß signalling and ROS accumulation, which ultimately led to decreased metastasis (Padmanaban et al., 2019) (Figure 1-4C). Phenotypic plasticity can be extended to other processes in addition to EMT-like transitions critical to metastatic colonisation, where DTCs may acquire stem-like features, display altered metabolism, mimic characteristics of the host organ or reside in dormant niches to be reawakened later (Jehanno et al., 2022). This notion might not come as a surprise considering evidence that supports a hierarchical model for metastasis (Malanchi et al., 2012; Lawson et al., 2015). Indeed, it has been shown that a small population of cancer stem cells is responsible for lung colonisation in a model of metastatic breast cancer, and cross-talk with the stromal niche of the target organ is required to allow cancer stem cell maintenance through enhanced Wnt signalling (Malanchi et al., 2012). Consistent with this, single-cell expression analyses have demonstrated that DTCs from low-burden metastatic tissues of patient-derived xenograft (PDX) models of breast cancer display a distinctive expression profile, relative to cancer cells from advanced metastatic lesions, that was characterised by expression of stem cell, EMT and survival/dormancy-associated genes (Lawson et al., 2015). Taken together, these studies implicate EMT-like, stem cell and dormancy programs in metastatic dissemination, and cellular state switches in these processes appear to be crucial for the establishment and eventual outgrowth of metastases in distant organs.

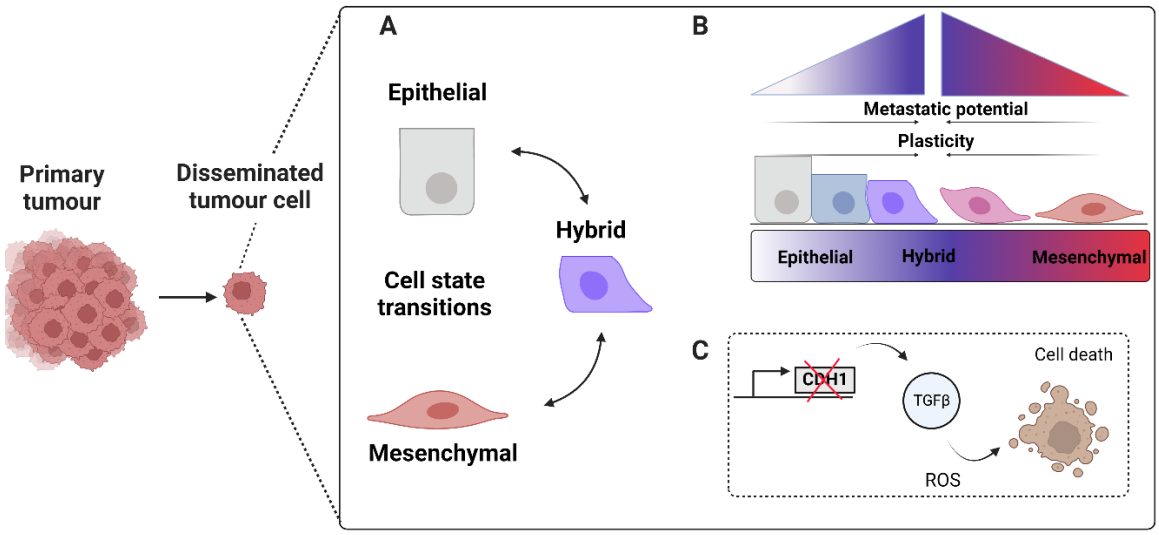

Figure 1-4 Disseminated tumour cells exhibit phenotypic plasticity in EMT programs. (A) During disease progression, cancer cells undergo reversible transitions between cellular states associated with EMT programs. Rather than residing in one state (epithelial or mesenchymal), carcinoma cells can acquire mesenchymal traits in a dynamic and transient manner, while retaining epithelial features, thus exhibiting hybrid phenotypes. (B) Tumour cells which display plasticity in switching between EMT states have increased metastatic potential than cells found only in epithelial or mesenchymal states, and this plasticity has been associated with immune infiltration in subpopulations of cancer cells within the tumour microenvironment. (C) Genetic depletion of E-cadherin (CDH1) in breast disseminated tumour cells results in TGFβ-induced accumulation of ROS and nuclear enrichment of SMAD2/3, leading to oxidative stress and increased apoptosis with concomitant loss of tumour initiating and metastatic capacity. Adapted from (Jehanno et al., 2022).

1.5 Lung as a metastasis-permissive microenvironment

1.5.1 Formation of the pre-metastatic niche

Seminal observations by Stephen Paget in 1889 which reported preferential patterns of metastatic colonisation in autopsies from breast cancer patients, led him to postulate that metastasis is not a random process, but rather depends on the interactions between disseminated tumour cells ('seeds') and the host microenvironment ('soil') (Paget, 1889). Increasing evidence over the last two decades suggests that, during disease progression, primary tumours release factors, which condition distant organs before the arrival of tumour cells, thus generating microenvironments permissive to cancer cell seeding and survival, which are termed 'pre-metastatic niches' (PMNs) (McAllister & Weinberg, 2014; Psaila & Lyden, 2009). Indeed, these factors can promote vascular leakiness, which is followed by changes in resident stromal cells and the recruitment of non-resident BMDCs helping to create a microenvironment receptive to colonisation by circulating tumour cells (Peinado et al., 2017). During PMN formation, ECM deposition and remodelling, with accumulation of fibronectin and collagen crosslinking (via lysyl oxidase or LOX), is critical for the adhesion of BMDCs (Erler

et al., 2009), likely providing a platform for sites of immune deregulation, due to the presence of a tumour-derived inflammatory landscape in distant organs where malignant cells are able to survive and proliferate escaping immune cell clearance (McAllister & Weinberg, 2014; Peinado et al., 2017).

1.5.2 Neutrophils and macrophages can engender metastasis-permissive niches

Myeloid-derived cells, recruited to distant sites through systemic signalling by primary tumours, are crucial components of the PMN environment. During early steps of the metastatic cascade, primary mammary tumours have been shown to secrete inflammatory factors leading to the recruitment of neutrophils to the lung PMN (Coffelt et al., 2015; Wculek & Malanchi, 2015). For example, a study in a mouse model of spontaneous breast cancer metastasis showed that tumour-induced expansion and polarisation of neutrophils, mediated by IL-17-producing γδ T cells, promoted lung metastasis (Coffelt et al., 2015). The authors further demonstrated that tumour-associated macrophages (TAMs) orchestrate recruitment of neutrophils to the metastatic site by secreting systemic factors. Specifically, mammary tumour-bearing mice showed elevated intratumoural and serum levels of CCL2, which induced the expression of IL-1β by TAMs ultimately leading to systemic production of γδ T-derived IL-17, IL-12 and G-CSF mediated expansion of neutrophils, to create an immunosuppressive environment in the lung by suppressing proliferation of cytotoxic $CD8^+$ T cells (Kersten et al., 2017; Coffelt et al., 2015). Consistent with this, neutrophils were found to accumulate in the pre-metastatic lungs of mammary tumour-bearing mice (PyMT genetically engineered mouse model), and promoted metastatic colonisation by supporting the tumour initiating capacity of cancer cells via leukotriene signalling (Wculek & Malanchi, 2015).

While patrolling monocytes prevent the seeding of cancer cells that arrive in the PMN (Hanna et al., 2015), macrophages, inflammatory monocytes (classical) and bone-marrow derived cells are recruited to pre-metastatic sites favouring metastasis. Indeed, an increase in $Ly6C^+$ monocytes has been observed in the pre-metastatic lungs in a melanoma model (van Deventer et al., 2013), and the recruitment of monocytes/macrophages to this site was required for homing and survival of melanoma cells in a process involving clot formation (induced by

tumour-expressing TF) (Gil-Bernabé et al., 2012). Similarly, it has been reported that pre-metastatic clusters of bone marrow-derived cells (VEGFR1$^+$ hematopoietic progenitors) are recruited to the lungs promoting adherence and growth of cancer cells, which can display different metastatic tropism upon conditioning with humoral factors secreted from different tumour types (Kaplan et al., 2005). In addition, a unique population of macrophages (metastasis-associated macrophages (MAMs)) derived from circulating Ly6C$^+$ monocytes has been found in metastatic lungs, and is distinct from resident lung macrophages (Qian et al., 2009). Interestingly, MAMs were reported to interact with CTCs at the site of the vessel during extravasation, and depletion of MAMs significantly reduced metastatic burden (Qian et al., 2009). Mechanistically, vascular cell adhesion molecule 1 (VCAM-1)-expressing breast cancer cells can be tethered to MAMs via α_4 integrins, and clustering of VCAM-1 induces Akt activation protecting cancer cells from proapoptotic cytokines (Chen et al., 2011). These heterotypic interactions can be enhanced by a CCL2-triggered chemokine cascade in MAMs further promoting metastatic seeding (Kitamura et al., 2015). Following metastatic seeding, VEGFR1 signalling in MAMs has also been suggested to promote survival of metastatic cells through the induction of CSF1 (Qian et al., 2015). Lastly, an increase of inflammatory monocytes in the lungs of mammary-tumour bearing mice has been associated with an increase of CD25$^+$FoxP3$^+$ Tregs and a decrease in NK cell numbers and activity (Eisenblaetter et al., 2017). Taken together, neutrophils and macrophages can act through different mechanisms towards the establishment of a supportive and immunosuppressive microenvironment in the lungs favouring metastatic formation.

1.5.3 Lungs, a common site of metastatic spread

Lungs are among the most common sites of metastasis in a range of solid carcinomas, with about 21% to 26% of malignant tumours successfully colonising the lungs and forming clinically-detectable metastases (Riihimäki et al., 2018).The high propensity of cancer cells to metastasise to the lungs has been attributed to anatomical features of the organ, as well as cellular and molecular components shaping the lung PMN microenvironment (Ewing, 1928; Paget, 1889; Psaila & Lyden, 2009). Indeed, lungs possess unique characteristics, such as the densest capillary beds in the body receiving the entire cardiac output every minute, and are one of the first tissues encountered after lymphatic drainage into

the venous system, thus providing favourable conditions that could, to some extent, result in non-specific dissemination of cancer cells to this organ (Schueller & Herold, 2003; Gerull et al., 2021). Recently, in an attempt to address this, a study simulated cancer cell trajectories in a high-resolution humanoid model of global blood circulation. Comparison of stochastic adhesion events with metastatic patterns in human autopsies from different cancer types revealed that blood circulation can account for approximately 40% of the variation in metastatic distribution (Font-Clos et al., 2020). Interestingly, geometric and haemodynamic factors were shown to be particularly relevant in the metastatic spread of lung primary cancer cells, whereas variations in metastasis to the lung could be mostly attributed to the seed-and-soil hypothesis (Font-Clos et al., 2020), pointing towards the contribution of primary tumour-induced systemic changes in metastatic tropism. Once disseminated, breast carcinoma cells can metastasise to various organs, with lungs being one of the most common sites (Weigelt et al., 2005; Kennecke et al., 2010). Notably, breast cancer patients with metastatic disease exhibit reduced 5-year survival rate (18-36%) compared to non-metastatic patients (>90%) (Jamil & Kasi, 2022; Hayman et al., 2020). Although mortality from early breast cancer has declined substantially, due to advances in adjuvant systemic therapies, metastatic breast cancer remains incurable with lung metastases representing a significant burden and leading cause of cancer-related complications (Hayman et al., 2020).

1.6 Metabolic reprogramming during metastasis

As our understanding of the complex processes involved in tumour progression increases, so does our appreciation of the metabolic adaptations that allow cancer cells to overcome fitness constraints on the path to metastasis. Progression from locally aggressive solid tumours to metastatic lesions entails clonal expansion of cancer cells with acquisition of additional mutations, and implementation of migratory/invasive phenotypes as cancer cells navigate the changing microenvironments of the metastatic cascade (previously described in 1.2). Accumulating evidence supports that successful transition through the steps of this cascade requires cancer cells to dynamically rewire their metabolism (Figure 1-5) maintaining cellular homeostasis in response to challenges imposed by the (epi)genomic landscape and tissue-specific microenvironments (Faubert et al., 2020). Although different metabolic pathways have been described to be

important for metastatic colonisation (depending on the target organ), they all converge to fuel energy production (Elia et al., 2018; Bergers & Fendt, 2021). However, the reasons for these high energetic requirements of colonising metastatic cells, which are distinct from those that support hyperplastic growth and anabolism in the context of the primary tumour (Faubert et al., 2020), remain unclear and recent studies point towards energy-consuming processes that involve cytoskeletal reorganisation promoting cancer cell migration (Zanotelli et al., 2018; Wu et al., 2021). It is, therefore, conceivable that metabolic plasticity is intricately linked to invasive phenotypes exhibited by disseminating cancer cells, and understanding the functional contribution of such metabolic pathways to cancer progression is crucial for the identification of reprogrammed activities that are most relevant to therapeutic vulnerabilities.

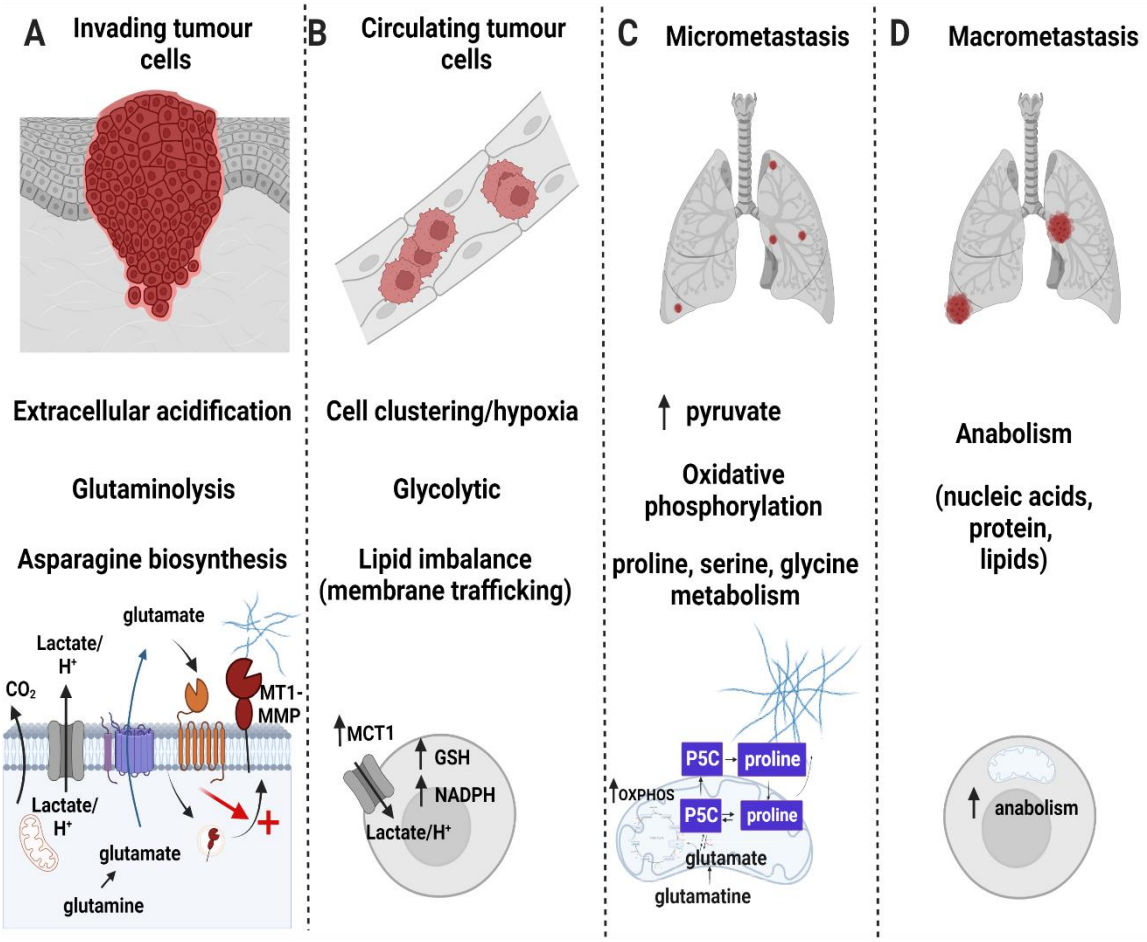

Figure 1-5 Metabolic reprogramming of cancer cells during the metastatic cascade.
(A) The first step in the metastatic cascade requires breaching of the basement membrane and invasion of cancer cells into the surrounding stroma. Extracellular acidification enables metabolically active cancer cells to overcome such physical barriers though release of lactate, CO_2 and other organic acids leading to disruption of adherens junctions in the basement membrane and release of proteolytic enzymes to degrade the ECM. In addition, cancer cells secrete glutamine-derived glutamate that supports invasive behaviour by increasing recycling of a matrix metalloprotease, MT1-MMP, to the cell surface and further promoting ECM degradation. Acquisition of a more mesenchymal phenotype in epithelial cancer cells can be supported by incorporation of aspartate-

derived asparagine into EMT-associated proteins to drive invasiveness. (B) Loss of ECM attachment leads to cell death (anoikis) due to oxidative insults unless counteracted by NADPH production via the pentose phosphate pathway (PPP) to provide reducing equivalents for glutathione synthesis and detoxification. (C) Increased pyruvate levels in the lung microenvironment promote metastatic colonisation through different mechanisms; (i) metastatic cells depend on pyruvate-carboxylase anaplerosis to fulfil biosynthetic needs and support growth, (ii) pyruvate levels influence the enzymatic activity of prolyl-4-hydroxylase to create a collagen-rich ECM permissive to metastatic seeding, (iii) Mct2-dependent pyruvate uptake boosts mTORC1 signalling in breast cancer lung metastases. Micrometastatic cells can also upregulate mitochondrial OXPHOS and oligomycin treatment reduces metastatic seeding in the lungs. (D) During metastatic outgrowth, anabolic processes are reactivated, to support proliferation. Adapted from (Faubert et al., 2020; Dornier et al., 2017).

1.6.1 Invading cells at the primary site

The metastatic cascade starts with dissemination of tumour cells from the primary site, which can be achieved by first overcoming physical barriers posed by the ECM, such as the basement membrane underlying the epithelium and endothelium, and the desmoplastic stroma that separates them. When metabolically-active cancer cells invade into the stroma they can release CO_2, lactate and other organic acids (Figure 1-5A), thus increasing extracellular acidification, which in turn allows cancer cells to detach from adjacent cells (decrease in abundance of adherens junctions) and promotes ECM degradation through stimulation of proteolytic enzymes (Helmlinger et al., 2002). Of note, glutamine-derived glutamate released by cancer cells in the extracellular milieu (via Xc- antiporter system or xCT) can also drive disruption of the basement membrane and promote invasive phenotypes by upregulating Rab27-dependent recycling of the transmembrane matrix metalloprotease, MT1-MMP (Dornier et al., 2017)(Figure 1-5A). Another example of metabolic reprogramming in cancer cells is the oncogene (HER2, SRC)-induced activation of lactate dehydrogenase A (LDHA), an enzyme catalysing the interconversion of pyruvate and lactate, through phosphorylation, where inhibition of this modification results in anoikis-induction, decreased invasiveness and low metastatic potential in breast cancer xenograft mouse models (Jin et al., 2017). Interestingly, supplementation of lactate and the antioxidant N-acetylcysteine (NAC) rescues this phenotype in vitro, suggesting a redox homeostasis-related mechanism (Jin et al., 2017).

Other metabolic adaptations promote EMT and acquisition of mesenchymal-like phenotypes to facilitate cancer cell invasion into the surrounding stroma. Indeed, EGFR-induced activation of UDP-glucose 6-dehydrogenase (UGDH) depletes UDP-glucose and increases production of *SNAI1* (via enhanced mRNA stability), an EMT-

TF, which promotes mesenchymal characteristics leading to increased cancer cell migration and lung metastasis (Wang et al., 2019). In addition, the ability of cancer cells to synthesise the nonessential amino acid asparagine from aspartate (via expression of asparagine synthetase (*Asns)*) supports EMT due to the disproportionately high asparagine content of EMT-associated proteins (Figure 1-5A). In this model of breast cancer, high asparagine levels promote cancer cell invasiveness and lung metastasis, while its systemic depletion or Asns silencing reduces metastasis by decreasing the ratio of epithelial-to mesenchymal-like tumour cells both in primary and metastatic lesions (Knott et al., 2018). EMT programs can also be induced by elevated intracellular levels of acetyl-CoA, which is produced following pyruvate oxidation (via PDH) and further accumulated through phosphorylation-induced inhibition (leptin, TGF-β/TAK1/AMPK signalling axis) of its consuming enzyme acetyl-CoA carboxylase 1 (ACC1), resulting in the acetylation and activation of the transcription factor Smad2, the nuclear translocation of which is known to promote EMT expression patterns (Rios Garcia et al., 2017).

Hypoxic regions within the primary tumour influence intrinsic characteristics of cancer cells and vascular permeability increasing the risk of metastasis. Specifically, transcriptional programs downstream of HIF-1 and HIF-2 enable hypoxic breast cancer cells to intravasate and extravasate by disrupting endothelial cell (EC)-cell interactions (via secretion of ANGPTL4) and promoting adherence of cancer cells (expressing L1CAM) to ECs respectively (Zhang et al., 2012). To enhance the entry into the vasculature, both perivascular stromal and cancer cells can release permeability factors, such as VEGF and angiopoietin, thus creating leaky and disorganised vessels, which are lined by hypermotile ECs with excessive filopodia and deregulated EC rearrangements (Carmeliet & Jain, 2011). Interestingly, glycolytic (PFKFB3-driven) production of ATP in ECs drives EC rearrangements by promoting filopodia formation and intercellular adhesion, while blocking glycolysis during vessel sprouting is sufficient to normalise EC dynamics exhibiting an anti-angiogenic effect in vivo (Cruys et al., 2016).

Migratory and invasive traits of cancer cells can be further supported by enhanced uptake of fatty acids, accumulation of lipids and upregulation of genes associated with fatty acid transport and metabolism. For example, a subpopulation of cells

in human oral carcinomas express high levels of the lipid transporter CD36 that imports fatty acids for oxidation and confers a metastasis-initiating ability to these cells (Pascual et al., 2017). Consistent with this, CD36 expression is induced in breast cancer cells to facilitate fatty acid uptake in the presence of breast-associated adipocyte secretome, which promotes cancer cell migration and invasion in vitro (Zaoui et al., 2019), though the underlying mechanisms are not clear or have been associated with EMT phenotypes in different cancer types (hepatocellular, cervical) (Nath et al., 2015; Deng et al., 2019). Cancer cells are also able to synthesise fatty acids *de novo* (via fatty acid synthase or FASN), with recent evidence supporting that colorectal cancer cells upregulate FASN-mediated sphingolipid metabolism (FASN/SPHK/S1P axis), which promotes the proliferation, adhesion and migration of these cells by modulating focal adhesion signalling (Jafari et al., 2019).

1.6.2 Circulating tumour cells

Circulating cancer cells can employ antioxidant defence strategies to avoid cell death following detachment from the extracellular matrix (anoikis) (Figure 1-5B). Mammary epithelial cells display altered glucose metabolism (reduction of glucose uptake and concomitant ATP deficiency) upon loss of ECM-induced signals leading to accumulation of reactive oxygen species (ROS), which results in cell death unless counteracted via oncogene-induced (Erbb2 or Her2) production of reduced nicotinamide adenine dinucleotide phosphate (NADPH) through the pentose phosphate pathway (PPP) (Schafer et al., 2009). This pathway contributes to detoxification of oxidative insults by providing reducing equivalents to regenerate reduced glutathione (Figure 1-5B), the most abundant antioxidant in the cytosol. Indeed, it is because of its role in regenerating reduced glutathione that NADPH shuttling from the cytosol into the mitochondria is required for efficient cancer cell growth after loss of ECM attachment (Jiang et al., 2016). Moreover, this survival mechanism is supported by an unconventional pathway of redox regulation during anchorage-independent growth, in which cancer cells limit mitochondrial ROS by promoting isocitrate dehydrogenase 1 (IDH1)-dependent reductive carboxylation of glutamine into citrate (Jiang et al., 2016). Loss of matrix attachment has been shown to influence mitochondrial morphology and function in cancer cells, leading to increased production of mitochondrial ROS levels. In this case, formation of cell clusters upon ECM detachment promotes

survival by protecting from ROS-induced death via hypoxia-mediated mitophagic clearance of damaged mitochondria. However, this adaptation renders cancer cells metabolically inflexible due to their dependence on glycolysis for ATP production and inability to utilise alternative nutrient sources that require oxidative phosphorylation (OXPHOS) for energy production (Labuschagne et al., 2019). Consistent with this, dynamic labelling of cancer cells during mammary carcinoma progression reveals that the majority of CTC clusters escaping from the primary site undergo hypoxia, whereas single CTCs are highly normoxic (Donato et al., 2020). Specifically, hypoxic regions within the primary tumour retain functional blood vessels and upregulate cell-cell adhesion proteins, leading to the formation of CTC clusters with high metastatic potential, which can be targeted using a pro-angiogenic therapy that reduces hypoxia and prevents CTC cluster generation (Donato et al., 2020).

Antioxidant defence mechanisms that protect circulating tumour cells against the oxidising environment of the bloodstream has been shown to influence their metastatic efficiency (Piskounova et al., 2015; Gal et al., 2015; Ubellacker et al., 2020). For example, in PDX and syngeneic models of melanoma, high expression of monocarboxylate transporter 1 (MCT1) confers a subpopulation of circulating tumour cells with enhanced metastatic efficiency (Figure 1-5B). Indeed, MCT1-dependent lactate(/proton) transport influences intracellular pH and NAD+/NADH ratio to support the pentose phosphate pathway and help metastasising cells cope with oxidative stress (Tasdogan et al., 2020). In these melanoma models, an independent study also demonstrated that cancer cells in transit through the lymphatics are more likely to form distant metastases since they display reduced levels of ROS-mediated ferroptosis compared with cells attempting to metastasise through the circulation (Ubellacker et al., 2020). Reduced sensitivity of lymph-circulating melanoma cells to lipid peroxidation (and the ferroptosis that results from this) is due to acyl-CoA synthetase long-chain family member 3 (ACSL3)-mediated membrane incorporation of oleic acid, which is enriched within ApoB+ vesicles in the lymph (by comparison with plasma), resulting in fewer peroxidation-sensitive double bonds in membrane lipids (Ubellacker et al., 2020). Similarly, another study has reported a link between imbalance in monounsaturated to saturated fatty acids and reduced capacity of cancer cells to metastasise to lymph nodes and lungs (Blomme et al., 2017). Mechanistically, this

imbalance is caused by impairment of vesicular trafficking between the plasma membrane and an endosomal compartment in cancer cells following depletion of myoferlin (Blomme et al., 2017; Gupta et al., 2021). Intriguingly, the improper function of the endosomal system (accumulation of vesicles near the plasma membrane, reduction in frequency and size of late endosomes/lysosomes and decrease in microvilli number) induces metabolic stress, characterised by mitochondrial dysfunction, AMP activated protein kinase (AMPK) activation and HIF1α stabilisation under normoxic conditions, leading to metabolic rewiring of breast cancer cells towards glycolysis (Blomme et al., 2017), a phenotype similar to the one observed after ECM detachment (as previously described) (Labuschagne et al., 2019). These observations highlight a critical role for the endosomal system in regulating cellular metabolism associated with invasive phenotypes, suggesting that crosstalk between these processes can shape the metastatic efficiency of cancer cells depending on the cancer type and metastatic route.

Over the last decade, it has become clear that alterations in the redox homeostatic mechanisms of transformed cells, particularly those controlling oxidative stress and ROS production, have a dual role in cancer progression (Reczek & Chandel, 2017). ROS accumulation drives pro-tumourigenic signalling pathways via genomic instability, cellular transformation, proliferation, and adaptation to hypoxia, while it leads to oxidative stress-induced death unless the stress can be mitigated by an increase in the antioxidant capacity of cancer cells (Reczek & Chandel, 2017). In fact, administration of systemic antioxidants (e.g. NAC, and Trolox (a vitamin E analogue)) to suppress oxidative stress or to activate endogenous antioxidant pathways (e.g. NADPH generation, de novo glutathione synthesis, mutations in Keap1 or Nfe2l2, the master transcriptional regulator of antioxidant response) supports distant metastasis in PDX models of melanoma (Piskounova et al., 2015), and in autochthonous mouse models of melanoma (Gal et al., 2015) and lung cancer (Wiel et al., 2019; Lignitto et al., 2019). For example, two independent studies provide complementary evidence supporting that constitutive activation of endogenous antioxidant responses (loss of Keap1, Nrf2 accumulation) or chronic supplementation with pharmacological/dietary antioxidants (NAC, vitamin E) promotes distant metastasis in mouse models of KRAS-driven lung cancer by inhibiting the Ho1 (haem catabolising enzyme)-induced degradation of the transcription factor Bach1, which stimulates

glycolysis-dependent metastasis of mouse and human lung cancer cells (Wiel et al., 2019; Lignitto et al., 2019). However, oxidative stress has been also shown to promote metastasis in some models (Porporato et al., 2014; Ishikawa et al., 2008), suggesting that the exact role of ROS in disease progression may depend on the type and stage of cancer (Reczek & Chandel, 2017).

1.6.3 Metabolic rewiring during metastatic colonisation

Following extravasation into the parenchyma of distant organs, disseminated cancer cells need to adapt to a microenvironment, which may differ in nutrient and oxygen availability compared to the primary site, and create a permissive niche that eventually allows reactivation of growth, leading to clinically detectable macrometastases. For example, it has been shown that pyruvate (Figure 1-5C), which is present at higher concentrations in lung interstitial fluid than in plasma, results in increased intracellular levels of pyruvate in lung metastases and this contributes to pyruvate carboxylase (PC)-dependent anaplerosis (conversion of pyruvate to oxaloacetate to replenish TCA cycle intermediates) (Christen et al., 2016). This mode of anaplerosis (as opposed to glutaminolysis-mediated anaplerosis) is critical for cancer cell proliferation in patients with early-stage non-small cell lung cancer and in a mouse xenograft model (Sellers et al., 2015), suggesting that breast cancer cells undergoing metastatic colonisation in the lung microenvironment utilise pyruvate to replenish precursor intermediates required for anabolic biosynthesis (Christen et al., 2016). Another study has confirmed that PC expression is required for growth of breast cancer cells in the lung, while it is dispensable for growth of extrapulmonary metastases (beyond the lung), further reinforcing the tissue-specific requirement for PC activity (Shinde et al., 2018). In addition, extracellular pyruvate promotes generation of α-ketoglutarate (α-KG) through alanine aminotransferase (ALT2) conversion, and boosts the enzymatic activity of prolyl-4-hydroxylase (P4HA), which is involved in collagen deposition (Gilkes et al., 2013), leading to the generation of a supportive metastatic niche through ECM remodelling (Elia et al., 2019). Indeed, inhibition of pyruvate metabolism impairs collagen hydroxylation and subsequent growth of breast-cancer-derived lung metastases (Elia et al., 2019). In these mammary cancer models it is thought that, pyruvate availability in the mouse lung reflects that of the human lung, and this has been also shown to support mTORC1 mediated growth signalling in breast-cancer derived lung

metastases by increasing the activity of the serine biosynthesis pathway in the former (Rinaldi et al., 2021). Mechanistically, Mct2-mediated pyruvate uptake stimulates serine biosynthesis, which potentiates mTORC1 signalling through the equimolar production of α-KG (via the phosphoserine aminotransferase 1 or PSAT-1-mediated conversion of 3-phosphohydroxypyruvate and glutamate to 3-phospho-serine and α-KG), and defines (through phosphoglycerate dehydrogenase or Phgdh expression) the sensitivity of breast-cancer derived lung metastases, and not primary breast tumours, to mTORC1 inhibition (through use of rapamycin) (Rinaldi et al., 2021).

Metabolic adaptations associated with the biosynthesis and/or catabolism of non-essential amino acids, such as serine, glycine and proline (Figure 1-5C), have been reported to influence the metastatic propensity of mammary cancer cells depending on the target organ. In particular, a breast cancer cell line variant with enhanced bone metastatic efficiency has been reported to show increased levels of all the enzymes involved in the serine biosynthesis pathway, namely phosphoglycerate dehydrogenase (PHGDH), phosphoserine aminotransferase 1 (PSAT1), and phosphoserine phosphatase (PSPH), with high expression of PHGDH and PSAT1 in primary breast cancer being significantly linked to poor relapse-free and overall survival of patients (Pollari et al., 2011). Similarly, positivity of PHGDH and PSPH have been associated with reduced overall survival of patients with breast cancer-derived liver and bone metastases respectively (Kim et al., 2014), while high expression levels of serine hydroxymethyltransferase 2 (SHMT2), which converts serine to glycine, are detected in lymph node metastases and correlate with poor survival in breast cancer patients with metastatic recurrence (Li et al., 2020). Conversely, the scarcity of serine and glycine in the brain microenvironment has been shown to create metabolic inflexibility depending on serine biosynthesis, and thus pharmacological or genetic inhibition of PHGDH impairs their growth (Ngo et al., 2020). Another metabolic liability can be found in the lung microenvironment, where formation of breast cancer-derived metastases depends on proline catabolism via proline dehydrogenase (Prodh) which supports their growth and ATP production, while recycling of pyrroline-5-carboxylic acid (P5C) back to proline via P5C reductase 1 (Pycr1) sustains Prodh activity (Elia et al., 2017) (Figure 1-5C). Accordingly, PRODH is more highly expressed in metastases than primary tumours in breast cancer patients (Elia et

al., 2017). Furthermore, high PYCR1 is frequently observed in invasive ductal breast carcinoma (Loayza-Puch et al., 2016), and pharmacological inhibition of Prodh impairs lung metastases formation in an orthotopic breast cancer mouse model (Elia et al., 2017).

As previously described (in 1.3), disseminated tumour cells enter a dormant state, which is influenced by the microenvironment of the target organ, and may endure for years after the initial diagnosis before triggering metastatic relapse. The mechanisms these cancer cells employ in order to survive, along with the metabolic adaptations acquired during prolonged dormancy are not completely known (Pollard, 2016). In a recent study, isolation and characterisation of latency-competent cancer cells from early stage human lung and breast carcinoma lines through *in vivo* selection have revealed that these cells display quiescent-like traits, reminiscent of stem and progenitor cells (Malladi et al., 2016). In a similar vein, an independent study has reported that minimal residual cancer cells derived from conditional mouse models of recurrent mammary carcinogenesis, exhibit a dormancy signature along with upregulation of OXPHOS, PPP, and altered lipid metabolism (elevated fatty acid synthesis) leading to oxidative DNA damage. These are features which have also been observed in tissues obtained from breast cancer patients following successful neoadjuvant therapy (Havas et al., 2017). Indeed, inhibition of oxidative stress by scavenging ROS or abrogation of hormone-driven proliferation of mammary cells attenuated tumour recurrence *in vivo* (Havas et al., 2017). Consistent with this, it has been recently reported that, in human breast cancer PDX models, both primary tumours and micrometastases display transcriptional diversity. However, only micrometastatic cells seem to commonly upregulate mitochondrial OXPHOS (Figure 1-5C), and its pharmacological inhibition (by oligomycin) is sufficient to attenuate metastatic seeding in the lungs (Davis et al., 2020). It is, therefore, conceivable that once dormant cancer cells begin to proliferate in the distant organ, anabolic processes supporting macromolecule biosynthesis (Figure 1-5D) are presumably required for metastatic outgrowth, and it will be interesting to determine whether these processes differ from the ones observed in the context of primary tumour growth. So far, at the single cell transcriptomic level, it has been demonstrated in PDX models of metastatic breast cancer that micrometastatic lesions are more enriched in stem-like traits than macrometastases; the latter displaying a more

luminal differentiation state, akin to the primary tumour identity (Lawson et al., 2015). All these observations depict specific metabolic adaptations in cancer cells during their metastatic journey, with a paradigm emerging in which cancer cells need to retain a degree of metabolic plasticity in order to switch between different cellular states (e.g. dormant-proliferating, stem-like-differentiated, epithelial-mesenchymal-like, migrating- proliferating) (Jehanno et al., 2022).

1.7 Crosstalk between cellular metabolism and endosomal trafficking

1.7.1 An evolutionarily conserved relationship

From invertebrates to humans, the maintenance of metabolic homeostasis requires proper sensing of nutrient availability and fine-tuning of distinct integrated responses to such signals across different tissues. On a cellular level, this implies a requirement for expression of plasma membrane nutrient sensors and transporters whose surface expression may be dynamically controlled by components of the endosomal system through vesicular trafficking between intracellular compartments responsible either for its degradation (lysosomes) or recycling back to the plasma membrane. Strikingly, genome-wide screens performed in invertebrate model organisms (*C. elegans*, *D. melanogaster* or *D. rerio*) to identify genes implicated in glucose or lipid metabolism have revealed significant associations with more than thirty endocytic components belonging to different endocytic pathways (as reviewed in (Gilleron et al., 2019)), though the metabolic functions of these genes remain uncharacterised. In addition, changes in the internalisation and/or recycling rates of several nutrient transporters, namely transferrin receptor 1 (decreased TfR1 internalisation limits iron uptake), GLUT family of transporters (endocytosis of GLUT limits the rates of cellular glucose uptake), CTR1 (endocytosis and/or degradation of CTR1 stimulated by increased copper levels to prevent excessive accumulation), have been reported to influence cellular metabolism by determining the levels of these transporters at the cell surface (Wang et al., 2011; Antonescu et al., 2014). One of the best examples that demonstrate the critical contribution of endosomal transport to metabolic homeostasis is membrane trafficking of GLUT4. In particular, insulin (during the postprandial period) triggers redistribution of GLUT4, whose expression is limited to insulin-responsive cells such as muscle and fat cells, from

specialised intracellular compartments to the plasma membrane leading to increased glucose uptake in these tissues (Foley et al., 2011; Rowland et al., 2011). In contrast to insulin stimulation, metabolic stress in cardiomyocytes treated with oligomycin (and thus shifting towards glycolysis) has been reported to reduce the rate of GLUT4 endocytosis increasing the glucose influx (Yang & Holman, 2005), a phenotype similar to the one observed in physiological conditions, where muscle contraction increases surface GLUT4 levels through AMPK- and Ca^{2+}- dependent signals in order to support energetic demands (Douen et al., 1990; Goodyear et al., 1991). Consistent with these data, defective translocation of GLUT4 in response to insulin is an early step in the development of insulin resistance and type 2 diabetes mellitus in humans (Lizunov et al., 2013; Maianu et al., 2001). Altogether, these studies support an essential function of the endosomal system in influencing metabolic responses depending on external cues and different microenvironments, pointing to a reciprocal regulatory relationship of endocytosis and metabolism.

1.7.2 Membrane trafficking and cell migration

Cell migration is essential to several physiological processes including tissue homeostasis, wound healing, angiogenesis and morphogenetic movements during embryonic development. As previously mentioned (in 1.2.1), acquisition of highly migratory phenotypes is the first crucial step in metastatic dissemination (Sahai, 2005), with extensive evidence indicating an important regulatory role of membrane trafficking in cell migration. In cancer cells, internalisation and recycling of integrins (Figure 1-6A), which mediate interaction of cells with the ECM, can influence cell migratory functions by controlling cell-ECM adhesion dynamics at the cell front and rear, while cross-talk with other receptor classes, for example co-trafficking of receptor tyrosine kinases (RTKs) with these adhesion receptors, has also been reported to promote cell migration through spatiotemporal regulation of growth factor signalling (Jacquemet, Humphries, et al., 2013), as described below.

1.7.2.1 Integrin trafficking and invasive cell migration

Integrins are the major transmembrane receptors that cells use to bind and respond to components of the surrounding ECM, and represent a diverse family of

24 heterodimeric receptors that are composed of a non-covalently linked α and ß subunit, with each subunit possessing a large extracellular domain (ECM binding), a single-spanning transmembrane domain, and a short cytoplasmic tail (interacting with several cytoplasmic partners to link to the cytoskeleton or membrane trafficking machinery) (Hynes, 2002). Integrins can be internalized from the cell surface via clathrin-dependent or independent endocytosis, caveolin-mediated or macropinocytosis (Gu et al., 2011; de Franceschi et al., 2015). After internalisation, integrins are delivered to early endosomes for recycling back to the cell surface or targeting for degradation, processes that are regulated by small GTPases including members of the Ras superfamily, namely those of the Rho, Rab (Figure 1-6A) and Arf groups, and can influence cell migration. For example, members of the Rho family, Rho, Rac and Cdc42, affect integrin trafficking and cell migration through regulation of actin polymerisation dynamics (Ridley, 2006). By contrast, the Rab and Arf GTPases play a more direct role in integrin trafficking by regulating the recycling and trafficking of internalised receptors to the cell surface. Indeed, Rab-4 dependent pathway can regulate rapid or short-loop recycling of integrins from early endosomes, while integrins recycled through the slow or long-loop pathway are trafficked to perinuclear recycling compartments (PNRC) in a Rab11- and Arf6-dependent way (Caswell & Norman, 2006; Paul, Jacquemet, et al., 2015; de Franceschi et al., 2015) (Figure 1-6A). For example, growth factor-induced autophosphorylation of protein kinase D1 (PKD1) and its direct interaction with the cytoplasmic tail of $ß_3$, as well as PKD1-dependent phosphorylation of Rabaptin-5 (Rab5 effector), are required for the rapid recycling of integrin $α_vß_3$ from early endosomes to the plasma membrane via the Rab-4 dependent pathway (Roberts et al., 2001; Woods et al., 2004; White et al., 2007; Christoforides et al., 2012). Integrin $α_5ß_1$, instead, can be trafficked via the long-loop pathway from early endosomes to the Rab11 positive PNRC prior to recycling to the cell surface, and this trafficking pathway can be regulated by several different kinases, including PKB/Akt (Roberts et al., 2004) and PKCε (Ivaska et al., 2005), as well as actin related proteins like Arp2/3(Actin related protein 2/3) and WASH (WASP and SCAR homologue) (Duleh & Welch, 2012; Zech et al., 2011).

Interestingly, an antagonistic relationship between $α_vß_3$ and $α_5ß_1$ has been reported, and disruption of the rapid Rab4-dependent pathway (by inhibiting $α_vß_3$

integrin or through PKD1/Rabaptin-5 mutation) promotes increased recycling of $\alpha_5\beta_1$ integrin to the plasma membrane via Rab-coupling protein (RCP; Rab11-FIP1) (Figure 1-6B), and its mobilisation to dynamic ruffling protrusions at the cell front (Caswell et al., 2008; Christoforides et al., 2012; Woods et al., 2004; White et al., 2007). RCP promotes the fibronectin-dependent migration of cancer cells by controlling the endosomal trafficking of $\alpha_5\beta_1$ and RTKs. This RCP-driven increase in cell invasion is not due to changes in adhesive function, but rather coordinated recycling of $\alpha_5\beta_1$ and EGFR1, which promote downstream RTK signalling and activation of the pro-invasive kinase AKT and a RhoA-FHOD3 (Formin homology-2 domain containing 3) pathway leading to the formation of filopodia at the cell front (Caswell et al., 2008; Paul, Allen, et al., 2015), with the latter pathway driving actin spike formation and invasion both in vivo and in cell-derived 3D matrices (Paul, Allen, et al., 2015) (Figure 1-6B). Notably, $\alpha_v\beta_3$ recycling is associated with slow and persistent migration through Rac activation and promotes invasion into ECM containing low fibronectin concentrations, whereas $\alpha_5\beta_1$ recycling can induce rapid and random migration through the Rho-ROCK-Cofilin pathway and its compensatory increase following inhibition of $\alpha_v\beta_3$ in matrices with high fibronectin abundance drives increased migration (Danen et al., 2005; Caswell et al., 2008; Christoforides et al., 2012). Integrin recycling, therefore, influences invasive migration in 3D matrices depending on the availability of ECM ligands (or matrix composition) for those integrins.

Gain-of function mutant p53 (mutp53) expression can also activate RCP-dependent recycling of integrins and RTKs to promote migratory and invasive phenotypes. In particular, mutp53-mediated inhibition of p63 function leads to suppression of endoribonuclease Dicer and impairment of miRNA processing, which in turn attenuates an inhibition of RCP-$\alpha_5\beta_1$ association and stimulates $\alpha_5\beta_1$ trafficking from recycling endosomes to the plasma membrane (Muller et al., 2009, 2014) (Figure 1-6B). RCP can also associate, through its N-terminus, with a number of RTKs, including EGFR and cMET (Caswell et al., 2008; Muller et al., 2009, 2014), and mutp53 can stimulate RCP-dependent co-recycling of adhesion and growth factor receptors to the plasma membrane, which requires DGKα (diacylglycerol kinase α)-mediated production of phosphatidic acid at the tips of invasive protrusions (Rainero et al., 2012). Consistent with RTK trafficking influencing their signalling, mutp53-driven increased recycling of EGFR and c-MET

have been shown to activate the Akt and MAP kinase (MAPK) pathways respectively (Muller et al., 2009, 2014). Indeed, RCP/DGKα-dependent recycling of $\alpha_5\beta_1$ and RTKs leads to localised RTK signalling with activation of Akt, subsequent recruitment of the RacGAP1/IQGAP1 complex that inhibits Rac1, and in turn increases RhoA activity at the cell front (Jacquemet, Green, et al., 2013). RhoA activates the formin FHOD3, which promotes nucleation of actin filaments to drive the formation of filopodial spike-based protrusions and invasive migration into fibronectin-rich ECM (Jacquemet, Green, et al., 2013; Paul, Allen, et al., 2015) (Figure 1-6B). Further interrogation of this signalling network by computational modelling reveals the presence of a MAPK (Raf/MEK/ERK signalling)-driven feedback loop to maintain RhoA activity in the invasive protrusions by suppressing Rac1 via inhibition of the Rac-activating Sos1-Eps8-Abi1 complex, which can be rescued through MEK inhibition abrogating RCP-driven cancer cell invasion (Hetmanski et al., 2016).

Rab25, a member of the Rab11 subfamily, displays a restricted expression profile (epithelial tissues) (Goldenring et al., 1993), has been linked to tumour aggressiveness and metastasis (Cheng et al., 2004), and can modulate $\alpha_5\beta_1$ integrin recycling to promote invasiveness of cancer cells. In particular, Rab25 has been shown to directly interact with the cytoplasmic tail of β_1 integrin, which drives recycling of $\alpha_5\beta_1$ to the plasma membrane at the tips of cancer cells, as well as retention of an actively cycling $\alpha_5\beta_1$ at the cell front, during migration on a fibronectin-rich 3D matrix to support pseudopod-driven migration (Caswell et al., 2007). Interestingly, Rab25 expression does not affect 2D migration, suggesting that this GTPase is not involved in processes like actin polymerisation or recruitment of integrins to focal adhesions (Caswell et al., 2007). In Rab25-expessing cancer cells, chloride intracellular channel 3 (CLIC3) (Figure 1-6A) is upregulated and colocalises with $\alpha_5\beta_1$ in late endosomes/lysosomes, where the active conformation of this integrin (ligand-occupied) is trafficked in a Rab25-dependent way, but is not degraded. Instead, CLIC3 mediates retrograde transport and recycling of lysosomally-targeted $\alpha_5\beta_1$ to the plasma membrane at the cell rear, where subsequently localised Src activity promotes invasion by enabling release of the cell rear during migration on 3D matrices (Dozynkiewicz et al., 2012). In addition, CLIC3 has been reported to promote invasiveness in breast cancer cells (lacking Rab25 expression), with little influence on integrin recycling,

by controlling the recycling of the pro-invasive matrix metalloproteinase MT1-MMP from late endosomes/lysosomes to sites of cell-ECM adhesion, and thus supporting disruption of basement membrane (Macpherson et al., 2014). Membrane trafficking control is therefore integral to cell migration and invasion, while the nature of pro-invasive cargo (integrins, metalloproteinases) and the site to which is trafficked within different subcellular compartments (from late endosomes to plasma membrane of invadopodia or cell rear) can depend on the cellular machinery involved in these processes and expression of membrane trafficking regulators (e.g. expression of particular GTPases).

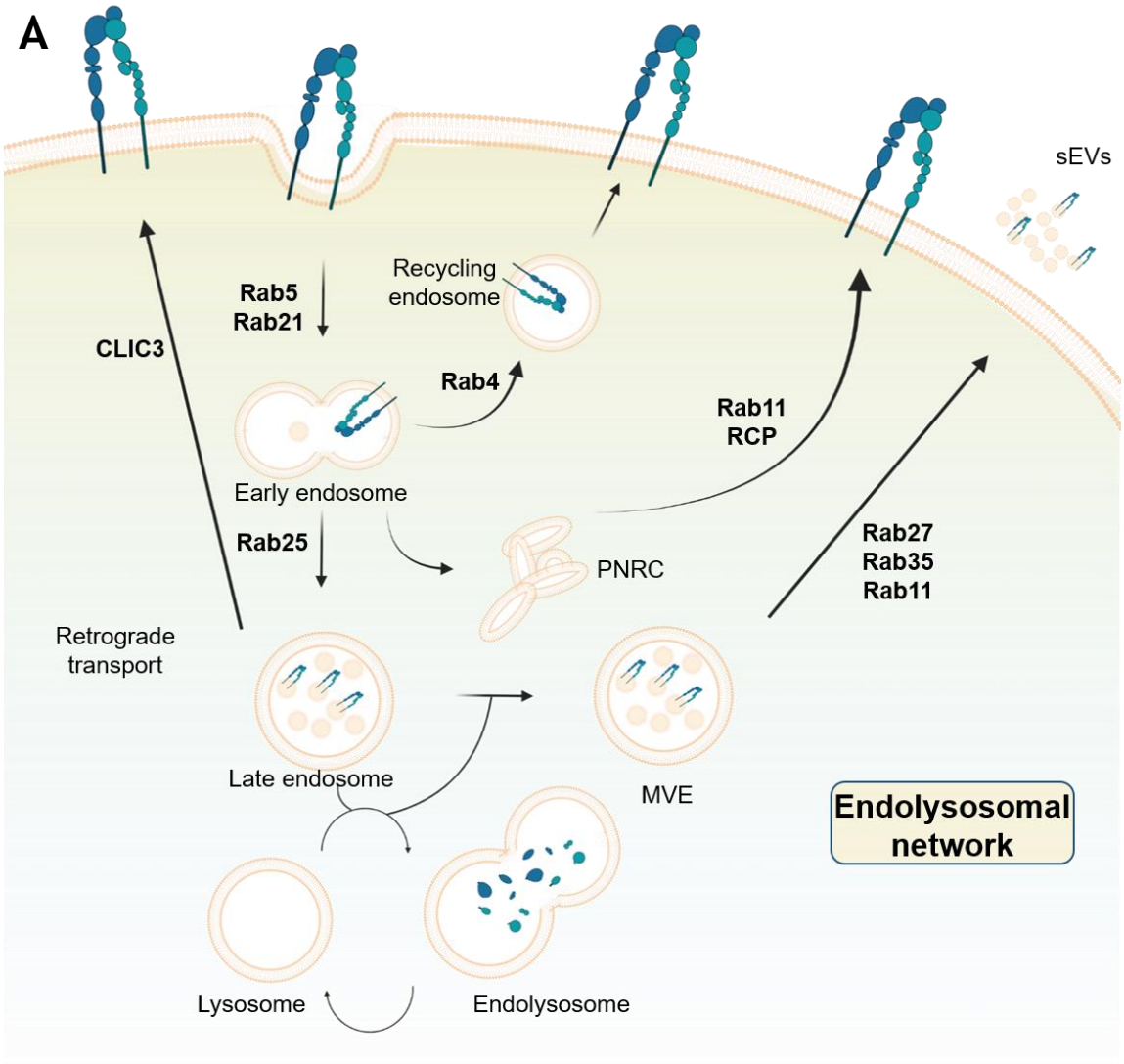

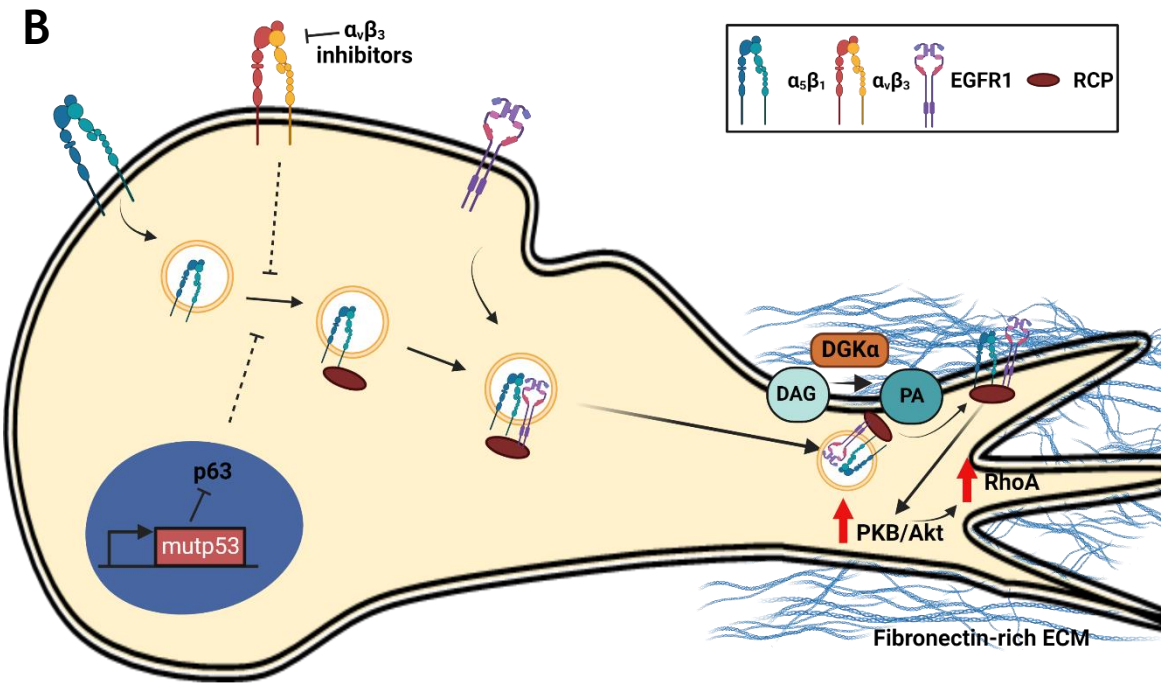

Figure 1-6 Integrin trafficking control and invasive cell migration.
(A) Integrins can be internalised into Rab5-positive early endosomes (EEs) under control of Rab21. Integrin trafficking from EEs to late endosomes (LEs) can be controlled by Rab25, and integrin-containing LEs can fuse with lysosomes for degradation. Integrins can be recycled back to the plasma membrane from many endosomal compartments. $\alpha_5\beta_1$ integrin can recycle from LEs in Rab25-expressing cells under control of Chloride Intracellular Channel Protein 3 (CLIC3). Integrin recycling back to the cell surface can be also mediated by the Rab-4 dependent short-loop pathway or the long-loop pathway in which integrins are trafficked to and recycled from perinuclear recycling compartments (PNRC) via Rab11-, RCP-mediated processes. Trafficking to multivesicular endosomes (or bodies) (MVEs) can further lead to their sorting into intraluminal vesicles (ILVs) and secretion in small extracellular vesicles following MVE transport, docking and fusion with the plasma membrane (Rab27-, Rab11-, Rab35- dependent). Adapted from (Caswell & Norman, 2006; Bridgewater et al., 2012). **(B)** In fibronectin-rich ECM, inhibition of $\alpha_v\beta_3$ integrin or gain-of-function mutant p53 (via inhibition of p63) expression leads to association of $\alpha_5\beta_1$ integrin with Rab-coupling protein (RCP) and its recycling to the cell surface. Receptor tyrosine kinases (RTKs), such as EGFR1, are also recruited to RCP-positive vesicles which can be tethered to the front of migrating cells (pseudopod tips) via RCP, which requires the production of phosphatidic acid (PA) from diacyglycerol (DAG) catalysed by diacylglycerol kinase α (DGKα). This results in spatially restricted EGFR signalling which locally activates PKB/Akt which in turn, suppresses Rac through recruitment of phosphorylated RacGAP1 to IQGAP1 (not shown). The inhibition of Rac allows increased RhoA activity and activation of the formin, FHOD3 that mediates actin filament nucleation to drive formation of invasive protrusions. Adapted from (Rainero et al., 2012; Jacquemet, Green, et al., 2013; Paul, Jacquemet, et al., 2015).

1.7.3 Extracellular vesicles

Although initially described as a way to export excess membrane during reticulocyte maturation (Johnstone et al., 1987), extracellular vesicles (EVs) have now been recognised as important mediators of intercellular communication. Release of these membrane-bound vesicles into the extracellular space is an evolutionarily conserved process from bacteria to humans (Deatheragea & Cooksona, 2012), and their ability to transfer a variety of cargoes (nucleic acids, proteins, lipids) from donor to recipient cells that may trigger phenotypic changes

in the latter has placed EVs as part of the intercellular signalling network in multicellular organisms. The compositional repertoire of EVs can, therefore, reflect the physiological state of the cells contributing to the extracellular milieu (Yáñez-Mó et al., 2015), or in the case of pathological conditions, such as cancer, the content of tumour-derived EVs can be used as biomarkers and may further contribute to disease progression. Indeed, EVs are among the factors (described in 1.5.1) that primary tumours release towards the generation of microenvironments that either support local growth and survival (Li & Nabet, 2019) or favour metastatic dissemination and seeding though the formation of PMNs (Peinado et al., 2012; Costa-Silva et al., 2015; Novo et al., 2018), as discussed below.

1.7.3.1 EV classes

Despite controversy surrounding the nomenclature of EVs due to the presence of heterogeneous populations of membrane vesicles and limitations in isolation techniques (Théry et al., 2018), EVs can be broadly divided into two main categories according to their biogenesis: microvesicles (or large EVs; lEVs, (here, oncosomes refer to tumour-derived lEVs)) and exosomes (or small EVs; sEVs) (van Niel et al., 2022) (Figure 1-7). The former comprises types of EVs that are generated at the plasma membrane from its outward budding and fission, while exosomes originate from intraluminal vesicles (ILVs) formed by inward budding of maturating multivesicular endosomes (MVEs), followed by fusion of these with the plasma membrane. Notably, exosomes are small having the same size as ILVs (<200nm in diameter), whereas microvesicles range in size (50nm to 1,000nm in diameter), and can be even larger in the case of oncosomes (up to 10μm) (Mathieu et al., 2019; Van Niel et al., 2018).

1.7.3.2 EV biogenesis

EV biogenesis begins with the formation of microdomains, where membrane-associated proteins and lipids form clusters through the action of several sorting machineries, in discrete sites of the plasma membrane for microvesicles, and of the MVE limiting membrane for exosomes (Figure 1-7). These microdomains, together with additional machineries, participate both in the sequestration of soluble components, such as nucleic acids and cytosolic proteins, and the

promotion of membrane budding and fission processes at the plasma membrane for microvesicle release or at the limiting membrane of MVE for ILV formation. Of note, a common characteristic of plasma membrane-derived EVs and endosomal ILVs (future exosomes) is that they bud away from the cytosol, and thus, the orientation of transmembrane proteins sorted on these EVs is identical to that of the plasma membrane (Van Niel et al., 2018). Despite the fact that biogenesis of microvesicles and exosomes occurs at distinct sites in the cell, some of the sorting machineries and mechanisms involved in the biogenesis of both EV classes are common, as described in the following sections, and this makes it particularly challenging to distinguish between different EV subpopulations (van Niel et al., 2022).

1.7.3.3 Endosomal sorting complex required for transport (ESCRT)

The endosomal sorting complex required for transport (ESCRT) machinery consists of cytosolic protein complexes (ESCRT-0, -I, -II and –III) acting sequentially at the limiting membrane of MVEs to modulate cargo sequestration leading to ILV formation (Colombo et al., 2013) (Figure 1-7). The ESCRT-0 complex recognises and sequesters ubiquitinated proteins on microdomains of the limiting MVE membrane, followed by recruitment of ESCRT-I, which interacts with ESCRT-II leading to membrane deformation into buds, and subsequent recruitment of ESCRT-III which drives vesicle scission and ILV formation (Colombo et al., 2013; Hurley & Hanson, 2010). Alternatively, syntenin, which binds to the cytosolic domain of syndecan-1, can recruit the ESCRT-accessory protein Alix, which together with an ESCRT-III member (VPS32; also known as CHMP4), allows intraluminal budding of endosomal membranes (Baietti et al., 2012). However, these pathways may not be specific for MVE-derived exosomes in all types of cells, as syntenin is also detected in larger EVs (Durcin et al., 2017), and ESCRT factors are involved in membrane budding and scission events at the plasma membrane (Nabhan et al., 2012).

1.7.3.4 Cellular machineries other than ESCRT

In addition to the ESCRT machinery, cone-shaped lipids and proteins of the tetraspanin family have been reported to influence ILV formation, and exosome biogenesis. Specifically, ceramide, the catabolic product of sphingomyelin

following hydrolytic removal of phosphocholine moiety by neutral sphingomyelinases, promotes inward budding into the endosomal lumen (MVEs) leading to increased ILV generation (Trajkovic et al., 2008) (Figure 1-7). Ceramide can also be converted to sphingosine 1-phosphate (S1P), which has been shown to influence cargo sorting into ILVs through activation of inhibitory G protein (Gi)-coupled S1P receptors (Kajimoto et al., 2013). At the plasma membrane, Ca^{2+}-dependent enzymatic machineries, including aminophospholipid translocases (flippases and floppases), can drive phospholipid translocation from the inner to the outer leaflet leading to physical bending of the membrane, and subsequent restructuring of the underlying actomyosin cytoskeleton which promotes plasma membrane-derived vesicle budding and microvesicle biogenesis (Hugel et al., 2005; Minciacchi et al., 2015). However, the effects of these mechanisms on exosome secretion are yet to be defined. Furthermore, proteins of the tetraspanin family, like CD63, CD81 and CD9 can influence either cargo sorting into exosomes or ILV biogenesis (Van Niel et al., 2018), probably via clustering with other proteins (tetraspanin members or different transmembrane and cytosolic proteins) leading to the formation of microdomains that promote inward budding (Charrin et al., 2014). Indeed, inward budding can be supported by a cone-like structure present in some tetraspanin members. For instance, CD81 possesses a cone-like structure with an intramembrane cavity for cholesterol binding which can influence its trafficking within the cell (Zimmerman et al., 2016). Taken together, EV biogenesis can be dictated by both ESCRT-dependent and alternative mechanisms, while the relative contribution of these cellular machineries may vary depending on the cell type and nature of the sequestered cargo.

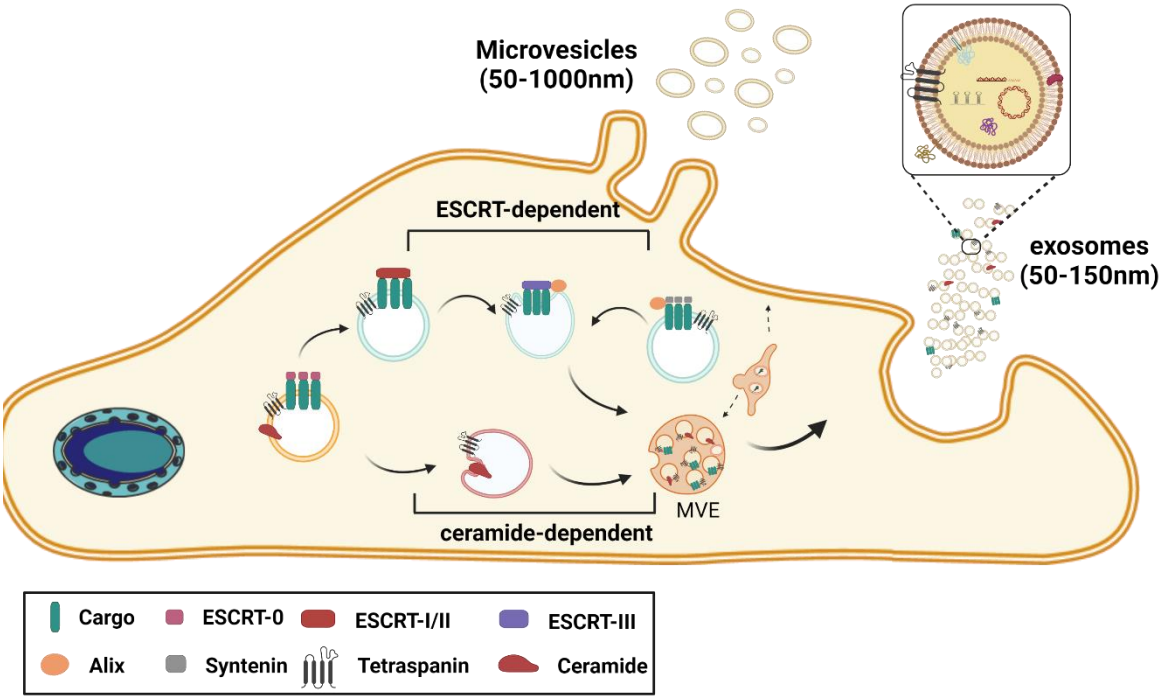

Figure 1-7 EV classes and exosome biogenesis.
Extracellular vesicles (EVs) are membrane-bound structures released by cells, and can be broadly classified in two categories based on their site of biogenesis. Microvesicle biogenesis starts with microdomain formation at the plasma membrane, whereas exosome formation is initiated upon intraluminal budding of the limiting membranes of multivesicular endosomes (MVEs). The biogenesis mechanisms for these two EV classes involve coordinated action of several sorting machineries consisting of membrane-associated proteins and lipids to control membrane budding and fission processes. Exosome biogenesis may occur through the action of the endosomal sorting complex required for transport (ESCRT) machinery (top pathway) or generation of ceramide (bottom pathway) in the limiting membrane of MVEs. In the ESCRT-dependent pathway, ubiquitinated cargoes are recognised and sequestered to the limiting MVE membrane by ESCRT-0 complex, which further recruits ESCRT-I that interacts with ESCRT-II leading to membrane deformation into buds, and further sequestration of ESCRT-III to promote vesicle scission and ILV formation. Intraluminal budding of endosomal membranes can be, alternatively, achieved through the recruitment of an ESCRT-accessory protein, Alix, which is recruited by syntenin. In the ceramide-dependent pathway, ceramide induces budding of endosomal membranes towards the lumen of MVEs, thus increasing ILV formation. In addition to ILV biogenesis, these pathways contribute to the sorting of different cargoes into ILVs, and therefore shape the compositional repertoire (shown on the top right) of exosome cargoes, which can vary from nucleic acids to proteins and lipids. Adapted from (Van Niel et al., 2018).

1.7.3.5 Tumour-derived EVs participate in formation of pre-metastatic niches

As previously described in 1.5.1, primary tumours can release factors to support the formation of PMNs, that is, microenvironments in distant organs that are highly permissive to metastatic colonisation and outgrowth. EVs are amongst the factors released by tumours which can contribute to establishment of PMNs. Indeed, tumour cells release EVs which contribute to disruption of endothelial integrity of the blood and lymphatic system, an important barrier to extravasation of cancer and immune cells at distant sites. For example, metastatic melanoma-derived EVs, but not EVs from non-metastatic cells, increase lung vascular permeability to promote spontaneous lung metastasis, with minimal effects on primary tumour

growth (Peinado et al., 2012). Similarly, increased permeability of the blood-brain barrier resulting from highly invasive breast cancer-derived EVs leads to enhanced brain metastasis of less invasive cells (Tominaga et al., 2015), with these EVs being taken up by brain endothelial cells inducing endothelial cell branching and inflammation in the perivascular niche (Rodrigues et al., 2019). Several studies have reported that tumour-derived EVs mediate disruption of endothelial cell junctions by transferring certain cargoes, and these often include microRNAs that target factors controlling vascular integrity (Tominaga et al., 2015; Lucotti et al., 2022).

Since tissue-resident immunity is typically inhibitory to metastatic colonisation, generation of an immune permissive environment though recruitment of BMDCs or activation of resident immune cells at distant pre-metastatic organs is considered crucial for successful metastatic seeding and outgrowth (Kaplan et al., 2005; Kaczanowska et al., 2021). When systemically introduced into mice, EVs from highly metastatic tumour cells have been reported to modulate these processes towards the formation of immune-suppressive environments in different PMNs (Costa-Silva et al., 2015; Peinado et al., 2012; Hoshino et al., 2015). Indeed, Rab27a-dependent EV secretion from invasive murine breast cancer cells, together with release of cytokines and/or metalloproteinases, have been shown to induce systemic mobilisation of neutrophils promoting metastatic dissemination, with barely any effect on non-metastatic carcinoma (Bobrie et al., 2012). Similarly, murine mammary carcinoma-derived EVs can induce an immunosuppressive microenvironment supporting the formation of lung and liver PMNs in naïve mice. These PMNs are characterised by accumulation of granulocytic myeloid-derived suppressor cells and reduced infiltration of CD8+ T cells, while the mammary carcinoma-derived EVs can directly suppress CD4+/CD8+ T cell proliferation and reduce the tumour-suppressive activity of NK cells (Wen et al., 2016). Tumour-derived EVs can, therefore, modulate immunologic responses in distant organs, while their ability to promote immune suppressive phenotypes depends on the metastatic capacity of EV-releasing cells (Bobrie et al., 2012).

In addition to promoting mobilisation of BMDCs, release of systemic factors from the primary tumour, and these include tumour-derived EVs, can promote activation of stromal resident cells in pre-metastatic organ sites. ECM deposition

and remodelling by such 'educated' fibroblasts contribute to the establishment of PMNs and can determine the metastatic potential of a tumour (Peinado et al., 2017). In the liver niche, for example, pancreatic cancer-derived EVs expressing migration inhibitory factor (MIF) have been shown to educate Kupffer cells to release TGFß which, in turn, induces hepatic stellate cell (HSC) activation and fibronectin deposition (Costa-Silva et al., 2015). In the lung niche, breast cancer–derived EVs promote upregulation of pro-inflammatory S100 proteins that activate resident fibroblasts, and these authors suggested that it was the presence of the laminin binding integrin, $\alpha_6\beta_4$ on the surface of these EVs that guided them to the laminin-rich lung microenvironment (Hoshino et al., 2015). Moreover, the ECM-rich microenvironments in both the liver and lung niches can enhance the recruitment of immune-suppressive BMDCs, suggesting that changes in ECM deposition and/or structure contribute to PMN formation and metastasis (Hoshino et al., 2015; Costa-Silva et al., 2015; Kaplan et al., 2005). Consistent with this, expression of mutp53 by pancreatic tumours alters the quantity of podocalyxin present on EVs released by the cancer cell. This, in turn, influences RCP-dependent trafficking of $\alpha_5\beta_1$ integrin in normal fibroblasts to promote deposition of a highly pro-invasive ECM in the lung (Novo et al., 2018) and liver (D. Novo, personal communication) microenvironments.

Given their ability to dispatch cargoes over long distances, it is not surprising that tumour-derived EVs have emerged as messengers creating a favourable 'soil' for the 'seed', but it is remarkable that they can accomplish this in an organ-specific manner (organotropic metastasis) (Hoshino et al., 2015). Indeed, the protein cargo of tumour-derived EVs has been reported to correlate with their metastatic potential (Peinado et al., 2012; Costa-Silva et al., 2015; Novo et al., 2018), while expression of different integrin heterodimers at the surface of EVs has been shown to dictate the organs to which are targeted for the formation of PMNs (Hoshino et al., 2015). For example, $\alpha_6\beta_4$ and $\alpha_6\beta_1$ integrins are upregulated in EVs which end-up in the lungs, while $\alpha_v\beta_5$ is enriched in EVs accumulating in the liver. In this case, the pattern of EV uptake by the different tissue microenvironments reflects the organotropism of donor cells, suggesting that EV-associated integrins can mediate organotropic metastasis (Hoshino et al., 2015).

1.7.4 Endo-lysosomal system as a metabolic regulator

Metabolic reprogramming of cancer cells is tightly linked to their enhanced ability to take-up and utilise nutrients required for survival and increased biosynthetic demands in adverse environments (Pavlova & Thompson, 2016). In particular, glucose uptake is often dysregulated in cancer cells though altered expression and trafficking of membrane transporters, mostly due to aberrant growth factor signalling cues. For example, activation of PI3K/Akt signalling promotes upregulation of GLUT1 mRNA levels and Rab11a-dependent recycling of GLUT1 to the cell surface supporting glucose uptake (Barthel et al., 1999; Wieman et al., 2007), indicating that proper function of the GLUT1 transporter depends on its translocation to the plasma membrane. Indeed, the spatial organisation and abundance of cellular cargoes, including nutrient transporters, signalling and adhesion receptors, on the cell surface are determined by membrane trafficking events within the endo-lysosomal network, which directs cargoes either for degradation (within the lysosome) or cargo retrieval and recycling back to the plasma membrane or the trans-Golgi network (TGN) (Cullen & Steinberg, 2018). Similarly, during endosomal maturation, MVEs can be sorted for lysosomal degradation or can be transported towards the periphery and fuse with the plasma membrane to release exosomes (Van Niel et al., 2018), although the molecular events that drive the degradative versus the secretory capacity of MVEs remain largely unexplored.

1.7.4.1 Balancing lysosomal degradation and endocytic recycling towards exosome secretion

The fine tuning of several intracellular trafficking events, together with cytoskeletal rearrangements, within the endolysosomal system are required for cargo sorting to the site of ILV biogenesis, and determining the subsequent fate of MVEs (to lysosome or plasma membrane) from which these vesicles stem (Van Niel et al., 2018). Mechanisms that promote or prevent degradation of MVEs in lysosomes, the compartment to which they are primarily targeted, can lead to downregulation or upregulation of exosome release respectively. For example, it has been shown that a post-translational modification (PTM; ubiquitin-like) of an ESCRT (-I) machinery component (TSG101) promotes its aggregation leading to lysosomal degradation, decreased MVEs and inhibition of exosome release

(Villarroya-Beltri et al., 2016). Conversely, impairment of lysosomal function or endosome-lysosome fusion (via expression of a Rab7 dominant-negative mutant, Rab7T22N) can rescue exosome secretion even in the presence of this PTM, supporting its effect is mediated through lysosomal degradation (Villarroya-Beltri et al., 2016). Similarly, cargo ubiquitination (probably recognised by ESCRT-dependent machinery) of Major Histocompatibility Complex (MHC) class II drives its recruitment to MVEs destined for degradation, while non-ubiquitinated MHC-II is targeted to the luminal vesicles in MVEs that are then secreted as exosomes (Buschow et al., 2009). Consistent with the observation that syntenin function may be restricted to exosome secretion, overexpression of tetraspanin-6 causes impaired lysosomal degradation and upregulation of exosome release by recruiting syntenin (Guix et al., 2017).

Autophagy is another degradative process that can affect exosome release. Indeed, increased autophagic flux prevents exosome secretion due to the fusion of MVEs with the autophagosome, and their subsequent degradation in the autolysosome. Indeed, pharmacological or genetic inhibition of PIKfyve (kinase generating PI(3,5)P2, which is localised to MVEs/late endosomes and lysosomes) reduces autophagic flux and increases exosome generation, with a prominent recovery of autophagic markers (NBR1,p62, LC3-II) (but not exosome-related proteins) in the exosomal pellet, indicating that ILVs are secreted via a pathway distinct from that responsible for releasing MVE-autophagosome-derived vesicles (Hessvik et al., 2016). Another study has demonstrated that expression of prion protein (PRNP) promotes internalisation of caveolin-1 (CAV1) and subsequent cytoplasmic inhibition of ATG12-ATG5 complex, leading to autophagic impairment. This autophagic impairment is paralleled by increased exosome release, further supporting a reciprocal relationship between exosome production and autophagy (Dias et al., 2016).

During endosomal maturation, transport of MVEs to the lysosome for degradation, or to the plasma membrane for release of ILVs as exosomes, entails the association of these organelles with cytoskeletal elements (microtubules and actin) and motor proteins (dynein, kinesin and myosin). These cytoskeletal-vesicle interactions and the function of the motors and adaptors that mediate these are regulated by small GTPases. Lysosomal targeting involves transport of MVEs towards the minus end

of microtubules (retrograde) and this is mediated by recruitment of a dynein motor via Rab7 and its effectors (Vanlandingham & Ceresa, 2009; Rocha et al., 2009). Trafficking of MVEs to the plasma membrane, on the other hand, occurs by kinesin-mediated transport towards the plus end of microtubules (anterograde). Upon reaching the sub-plasmalemmal region, MVEs must detach from microtubules and associate with the actin cytoskeleton so that they can dock and fuse with the plasma membrane. This switch of allegiance from the microtubular to the actin cytoskeleton requires the action of Rab27s (Rab27a and Rab27b), and their effectors synaptotagmin-like protein 4, exophilin 5 and myosin Vb (Sinha et al., 2016; Ostrowski et al., 2010). Notably, Rab27s are not expressed in all types of cells, and the involvement of additional Rab members and their effectors, such as Rab11 and Rab35, has been proposed to contribute to MVE transport towards the plasma membrane and exosome secretion (Savina et al., 2003; Hsu et al., 2010).

All the processes described so far underline crosstalk between the endosomal and lysosomal or autophagic system, indicating a dynamic balance between degradative and secretory functions, and the last step towards exosome secretion could not be a better example to reflect this. The fusion of MVEs with the plasma membrane, and subsequent release of ILVs into the extracellular milieu as exosomes, can be achieved through the action of SNARE and synaptotagmin family members. Indeed, some cells employ the SNARE complex consisting of VAMP7, plasma membrane syntaxin 7, and the lysosomal synaptotagmin 7, to promote exosome secretion, while this complex is also known to be involved in lysosomal exocytosis (Fader et al., 2009). Similarly, regulation of exosome secretion can be mediated by Ca^{2+} through activation of SNARE complexes (Savina et al., 2005) or even by pyruvate kinase type M2 (PKM2) through phosphorylation and activation of SNAP23 (Wei et al., 2017). Despite the diversity of SNARE proteins controlling exosome release across different cell types, the similarities between MVE fusion events and lysosomal exocytosis, which is under the transcriptional control of TFEB (Medina et al., 2011), point towards the exciting possibility that exosome release may represent an important node between catabolic and secretory processes whose activity reflects responses to cellular metabolic needs.

1.7.4.2 Nutrient sensing

In addition to its role in catabolic processes, the lysosome acts as a central hub for metabolic signalling and nutrient sensing, and as such, performs critical functions related to macromolecular recycling, vesicular trafficking, metabolic rewiring and growth signal transduction. This requires dynamic recruitment and activation of mTORC1 to the lysosomes in response to the presence of growth factors and nutrients (Ballabio & Bonifacino, 2020; Lawrence & Zoncu, 2019). mTORC1 is a protein complex consisting of mTOR (mammalian target of rapamycin, a serine/threonine kinase, also part of the independent mTORC2 complex), RAPTOR (regulatory-associated protein of mTOR), and mLST8 (mammalian lethal with SEC13 protein 8) (Hara et al., 2002; Kim et al., 2002), and its activation status depends on nutrient (especially amino acid) sensing and growth factor abundance. In particular, a complex machinery, which is composed of amino acid channels, the proton pump v-ATPase, and the Ragulator complex (Lawrence & Zoncu, 2019; Ballabio & Bonifacino, 2020), is located on the cytosolic leaflet of the late endosomal/lysosomal membrane. This allows sensing of amino acids, and promotes activation of heterodimeric Rag GTPases that directly bind to RAPTOR (Sancak et al., 2008) leading to lysosomal recruitment of mTORC1 and allosteric activation by RHEB (another lysosome-bound small GTPase activated by growth factors) (Menon et al., 2014). The nucleotide state of Rag GTPases in these heterodimers (RagA/B bound to GTP, RagC/D bound to GDP) is crucial for mTORC1 recruitment to the lysosome (Sancak et al., 2008; Kim et al., 2008), and nutrient depletion suppresses mTORC1, which remains inactive in the cytoplasm, by promoting GTP hydrolysis on RagA by the GATOR1 complex (Bar-Peled et al., 2013; Panchaud et al., 2013). When nutrients and growth factors are abundant, mTORC1 activation induces phosphorylation of substrates such as S6 kinase 1 (S6K1) and 4E-binding proteins 1 and 2 (4EBP1,2) leading to phosphorylation of downstream targets that regulate biosynthetic pathways (nucleotides, lipids, ribosomes), translation and cellular growth, whereas these processes are inhibited upon nutrient depletion due to inactivation of mTORC1 (Lawrence & Zoncu, 2019). mTORC1 inactivation also leads to activation of catabolic pathways, such as autophagy (through lack of phosphorylation of Unc-51-like kinase 1 (ULK1)) (Hosokawa et al., 2009)), and interestingly, during prolonged starvation mTORC1 signalling can be reactivated in an autophagy-dependent manner to maintain lysosome (reformation) homeostasis (Yu et al., 2010). Since lysosome-mediated

signalling pathways can sense cellular metabolism and are critical nodes for switching between catabolic and anabolic processes, it is not surprising that mTORC1 signalling is implicated in cancer, while its significance for amino acid homeostasis extends to primordial functions of nutrient sensing to maintain cell viability across different organisms (Lawrence & Zoncu, 2019; Li & Kane, 2009).

1.7.4.3 ECM, membrane trafficking and metabolism

Although integrin trafficking can partially mediate disassembly and reassembly of focal adhesions that support migration, it is becoming increasing clear that it can also influence intracellular signalling either directly or by co-trafficking of other membrane receptors (Bridgewater et al., 2012; Paul, Jacquemet, et al., 2015; Wilson et al., 2018)). Indeed, it has been recently shown that trafficking of ECM ligand-bound integrins to late endosomes/lysosomes can support mTOR signalling upon glucose starvation (Rainero et al., 2015). Specifically, glucose deprivation promotes tensin-dependent centripetal movement of $\alpha_5\beta_1$ integrins from focal adhesions in the cell periphery towards fibrillar adhesions in the subnuclear zone and subsequent endocytosis of fibronectin-bound $\alpha_5\beta_1$. This Arf4-dependent internalisation pathway leads to mTORC1 activation by controlling its recruitment to late endosomes/lysosomes. Conversely, mTORC1 inhibition promotes internalisation of active $\alpha_5\beta_1$, indicating that nutrient availability modulates ligand-engaged integrins (Rainero et al., 2015). Consistent with this, after dietary restriction or growth factor starvation, mammary epithelial cells internalise laminin-bound integrin β_4, leading to mTORC1 activation which prevents starvation-induced death (Muranen et al., 2017). Another study has demonstrated that the major energy sensor AMPK, which is known to inhibit mTORC1 by phosphorylating one of its components (Raptor) (Gwinn et al., 2008), inhibits $\alpha_5\beta_1$-integrin activity preventing its centripetal translocation to fibrillary adhesions and fibronectin remodelling by downregulating gene expression of the integrin-binding protein, tensin (Georgiadou et al., 2017). In addition, there have been several studies reporting (Steinberg et al., 2013; Kvainickas et al., 2017; Shinde & Maddika, 2017) the involvement of retrieval machineries, especially the retromer complex, in translocation of nutrient transporters from secretory vesicles or recycling endosomes to the plasma membrane, thus maintaining their surface levels and supporting nutrient demands. Taken together, these studies indicate the presence of mechanistic links between trafficking of membrane receptors,

nutrient sensing and the cell migration machinery. The likelihood that these links may be important to the acquisition of invasive and metastatic behaviour in cancer is now beginning to attract interest. Indeed, understanding the mechanistic relationships between membrane trafficking, metabolism and cell adhesion/migration will be critical to determining how cancer cells survive as they move through the widely differing microenvironments that exist en route to metastatic seeding and awakening of dormancy. We anticipate that a full understanding of these mechanisms will expose the key vulnerabilities of metastasising cells and reveal opportunities for targeting these therapeutically.

Using a murine model of metastatic mammary cancer, we have generated isogenic cell lines from primary mammary tumours and their corresponding metastases in the lung, and hypothesised that these isogenic pairs of cells differ in features that contribute to the acquisition of invasive behaviour.

1.8 PhD Objectives

Metastatic recurrence remains the main cause of cancer-related death, and further understanding of the mechanisms that drive metastasis are crucial to improve patient survival. Despite advances in systemic adjuvant therapies, targeting the occult nature of disseminated cancer cells (that are the origin of incurable metastatic disease) has proven challenging for two reasons. First, cancer cells leave the primary site very early in the malignant progression of cancer, and can enter a state of cellular dormancy that allows them to survive in distant sites, sometimes for years before manifesting as clinically-detectable metastases. Second, cancer cells navigate through different microenvironments on their metastatic journey, and on the way must evolve strategies that promote cellular fitness and characteristics that ultimately render them resistant to host defences and therapy. Among these strategies, altered metabolism is a key characteristic of cancer cells from early stages of tumour growth; with energy production, biosynthesis of macromolecules and redox homeostasis being critical for exponential growth and proliferation, while additional metabolic requirements emerge as disease progresses. In addition, cancer cells release EVs, membrane bound vesicles, through which they are able to communicate with other cell types within the tumour microenvironment, and can support the formation of favourable conditions in distant organs for future metastatic colonisation and outgrowth. EV cargo composition usually mediates these functions and differs between biogenesis pathways, which depend on membrane trafficking processes. A relationship between membrane trafficking and cellular metabolism has recently emerged, however it is currently unknown whether this also applies to EV biogenesis programs, or if it plays any role in invasive behaviour of cancer cells. The objective of this work is therefore to establish and phenotypically characterise cancer cell lines derived from primary mammary tumours and matched metastases in the lung, a common site of metastasis across a variety of carcinomas, with a particular interest in understanding whether breast cancer-derived lung metastatic cells rewire their metabolism in a way that could influence the cellular machinery controlling EV production and invasive behaviour.

Chapter 2 Materials and methods

2.1 Materials

2.1.1 Reagents

Reagent	Supplier
0.02µM Whatman Anotop filter	Merck
0.2um PES Filter unit (Nalgene)	ThermoFisher Scientific
0.45µm PTFE filter	Gilson
70µm cell strainer	Corning
1.5mL microcentrifuge tubes	Eppendorf
27G needle	Becton Dickinson
gelatin	Sigma
96 well PCR plate	Bio-Rad
Acetonitrile (HPLC grade)	ThermoFisher Scientific
Agarose	Sigma
All blue protein standard	Bio-Rad
Ampicillin	Sigma
BSA	First Link
BsmBI enzyme	New England Biolabs
Buthionine sulfoximine	Sigma
$CaCl_2$	Sigma
Casyton	Roche
Cell lifter	Corning
Chloroform	Sigma
Citric acid	Sigma
DMSO	Fisher Scientific
DNaseI	Roche
DTT	Melford Laboratories
Dulbecco's Modified Eagle Medium(DMEM)	Life Technologies
ECL Western blotting substrate	Pierce
EGF	Life Technologies
Ethanol	VWR
Foetal Calf Serum	PAA
Fungizone	Life Technologies
Glass bottom 35mm dish	MatTek
Glass bottom 6 well plate	MatTek
Glucose	Sigma
Glutaraldehyde	Sigma
Glycerol	Fisher Scientific
Halt Protease Inhibitor Cocktail, EDTA-free	Fisher Scientific

Human epidermal growth factor	Invitrogen
Hybond-P PVDF membrane	GE Healthcare
Hydrogen peroxide	Sigma
Insulin	Sigma
L-Glutamine	Sigma
Matrigel	BD Biosciences
MesNa	Fluka
Methanol (HPLC grade)	ThermoFisher Scientific
Milk powder	Marvel
Na_2CO_3	Fisher Scientific
Na_2HPO_4	Fisher Scientific
Na_3V0_4	Fisher Scientific
NaCl	Fisher Scientific
NaF	Sigma
NEBuffer 3.1	New England Biolabs
Nunc MaxiSorp plates	ThermoFisher
NuPage MOPS running buffer	Life Technologies
NuPAGE pre-cast gel (4-12 % & 10%)	Life Technologies
NuPage sample buffer	Life Technologies
NuPAGE transfer buffer	Life Technologies
Ortho-phenylenediamine	Sigma
Paraformaldehyde (PFA)	Fisher Scientific
PBS containing calcium and magnesium	Sigma
Penicillin/Streptomycin	Life Technologies
PerfeCTa SYBR Green Fast Mix	Quantabio
Polybrene	Sigma
Propan-2-ol	Fisher Scientific
RNase free water	Sigma
Puromycin	Sigma
SDS	Fisher Scientific
Slc7a11 ISH probe (422518)	Bio-Techne
S.O.C medium	ThermoFisher
Splash II lipidomix Mass Spec standard	Avanti
Stbl3 competent cells	ThermoFisher
Streptavadin-conjugated HRP	GE Healthcare
Sulfo-NHS-SS-Biotin	Pierce
Surgical scalpel blade (No.23)	Swann-Morton Ltd
T4 DNA ligase	New England Biolabs
T4 DNA ligation buffer	New England Biolabs
T4 polynucleotide kinase	New England Biolabs
T4 polynucleotide kinase reaction buffer	New England Biolabs
Thinwall Polypropylene Tube (38.5 mL)	Beckman
Tissue culture dishes (10 and 15 cm)	Corning

Tissue culture plate (6 well)	Corning
Tris HCl Melford Laboratories	Melford Laboratories
Triton-X100	Sigma
Trizol	Life Technologies
Trypsin	Life Technologies
Tween-20	Sigma
Vectashield mounting media + DAPI	Vector laboratories
Water (HPLC grade)	ThermoFisher Scientific

Table 2-1 Reagents and suppliers.

2.1.2 Solutions

Solution	Components
2x HBS	274mM NaCl, 10mM KCl, 1.4mM Na_2HPO_4, 15mM glucose, 42mM HEPES, pH 6.8
Biotin reduction buffer buffer	50mM Tris-HCl pH7.4, 10mM NaCl, pH 8.6 at 4˚C
ELISA coating buffer	0.05M Na_2CO_3, pH 9.6 at 4˚C
ELISA development reagent	0.56 mg/mL ortho-phenylenediamine, 25.4mM Na_2HPO_4, 12.3mM citric acid, pH 5.4 with 0.003% H_2O_2
LB Broth	85mM NaCl, 1% bacto-trypton (w/v), 0.5% yeast extract (w/v)
Non-denaturing lysis buffer	50mM Tris-HCl pH 7.0, 150mM NaCl, 10mM NaF, 1mM Na_3V0_4, 5mM EDTA, 5mM EGTA, 1.5% Triton-X100 (v/v), 0.75% Igepal CA-630 (v/v)
PBS-T	PBS, 0.1% Tween-20 (v/v)
RIPA buffer	10mM Tris-HCl pH 8.0, 1mM EDTA, 1% Triton X-100 (v/v), 0.1 % sodium deoxycholate (v/v), 0.1% SDS (v/v), 140mM NaCl, 1mM PMSF
TBS	10mM Tris-HCl pH 7.4, 150mM NaCl
TBS-T	TBS, 0.1% Tween-20 (v/v)

Table 2-2 Solutions and their components.

2.1.3 Kits

Kit	Supplier
Calcium phosphate kit	Thermo Fisher
Pierce BCA Protein Assay Kit	Thermo Fisher
QIAquick Gel Extraction Kit	Qiagen
Quantitech Reverse Transcription Kit Qiagen	Qiagen
Quick ligation kit	New England Biolabs

Table 2-3 Kits and suppliers.

2.1.4 Primer pairs

Primer	Sequence
ARPP P0 Forward	GCACTGGAAGTCCAACTACTTC
ARPP P0 Reverse	TGAGGTCCTCCTTGGTGAACAC
Gclc Forward	CCACAAGAGCTCATCCTCCCT
Gclc Reverse	GGGTCGGATGGTTGGGGTT
LKO.1 forward	GACTATCATATGCTTACCGT
PyMT Forward	CTGCTACTGCACCCAGACAA
PyMT Reverse	GCAGGTAAGAGGCATTCTGC
SLC7A11 (xCT) Forward	CTTTGTTGCCCTCTCCTGCTTC
SLC7A11 (xCT) Reverse	CAGAGGAGTGTGCTTGTGGACA
Smpd2 (nSMase1) Forward	CATCCCCTACCTGAGCAAAC
Smpd2 (nSMase1) Reverse	CCAGGAGAGCCAGATCAAAGTT
Smpd3 (nSMase2) Forward	TGGTGGTGTTTGACGTCATCT
Smpd3 (nSMase2) Reverse	GCGAGTAAAGAGCGAGTGCT

Table 2-4 RT-qPCR primer sequences.

2.1.5 Single guide RNA (sgRNA) oligos

Primer	Sequence
Smpd2 CRISPR Guide RNA F1	CACCGGCGGACCGCATGAAGCGCTT
Smpd2 CRISPR Guide RNA R1	AAACAAGCGCTTCATGCGGTCCGCC
Smpd2 CRISPR Guide RNA F2	CACCGCGCCCTATGTTTGCTCAGGT
Smpd2 CRISPR Guide RNA R2	AAACACCTGAGCAAACATAGGGCGC
Smpd2 CRISPR Guide RNA F3	CACCGCTTCTGAAGTAGTGTGCATC
Smpd2 CRISPR Guide RNA R3	AAACGATGCACACTACTTCAGAAGC
Smpd2 CRISPR Guide RNA F1	CACCGCACAAACGGTCTCTCTATGATG
Smpd2 CRISPR Guide RNA R1	AAACCATCATAGAGACCGTTTGTGC
Smpd2 CRISPR Guide RNA F3	CACCGCGATGTACCCAACAATT
Smpd2 CRISPR Guide RNA R3	AAACAAGAATTGTTGGGTACATCGC
Smpd2 CRISPR Guide RNA F5	CACCGGTGGTGTTTGACGTCATCTG
Smpd2 CRISPR Guide RNA R5	AAACCAGATGACGTCAAACACCACC

Table 2-5 Single guide RNA sequences.

2.1.6 Plasmids

Plasmid	Supplier (catalogue number)
lentiCRISPR vector	Addgene (#52961)
pSPAX2	Addgene (#12260)
pVSVG	Addgene (#12259)

Table 2-6 Plasmids and suppliers.

2.1.7 Primary antibodies

Antibody	Host species	Application (dilution)	Supplier (cat. Number)
CD63	rabbit	WB (1/1000)	Abcam (ab217345)
CD81	mouse	WB (1/1000)	Santa Cruz (sc-166029)
Ceramide	mouse	IF (1/100)	Enzo(ALX-804-196)
E-cadherin	mouse	IF (1/300)	BD Pharmingen (610181)
Integrin α_5	Rat	ELISA (1/100)	BD Pharmingen (553319)
Integrin α_5	rabbit	WB (1/1000)	Chemicon (AB1928)
Integrin β_1 (9EG7)	rat	ELISA (1/100)	BD Pharmingen (550531)
Integrin β_1 (9EG7)	rat	WB (1/500)	BD Pharmingen(553715)
Transferrin receptor	rat	ELISA (1/100)	BD Pharmingen (553264)
TSG101	mouse	WB (1/1000)	GeneTex (GTX70255)
Vinculin	mouse	WB (1/5000)	Sigma (MAB3574-C)

Table 2-7 Primary antibodies.

2.1.8 Secondary antibodies

Antibody	Host species	Application (dilution)	Supplier (cat. Number)
Alexa Fluor 488 anti-Mouse IgG	donkey	IF (1/500)	ThermoFisher (A-21202)
Alexa Fluor 488 anti-Mouse IgM	goat	IF (1/500)	ThermoFisher (A-21042)
HRP-linked anti-Mouse IgG	horse	WB (1/5000)	Cell Signalling (#7076)
HRP-linked anti-Rabbit IgG	goat	WB (1/5,000)	Cell Signalling (#7074)
IRDye 680RD anti-rabbit IgG	goat	WB (1/10,000)	LI-COR
IRDye 680RD anti-rat IgG	goat	WB (1/10,000)	LI-COR
IRDye 800CW anti-mouse IgG	goat	WB (1/10,000)	LI-COR

Table 2-8 Secondary antibodies.

2.2 Methods

2.2.1 Mouse models of metastatic breast cancer

2.2.1.1 Autochthonous model of mammary carcinoma

All mice carrying a mouse mammary tumour virus (MMTV) promoter-driven polyoma middle T (PyMT) transgene had been backcrossed >20 generations in FVB/N background. The MMTV-PyMT mice have been described previously(Guy et al., 1992). MMTV-PyMT mice (The Jackson Laboratory, ME, USA) were housed in

individual cages with environmental proactive enrichment, ventilated in a barrier facility (12-hour light/dark cycle). Monitoring of mice for tumour development was performed two to three times per week. Tumour growth was monitored by calliper measurement three times per week. The clinical endpoint was 15 mm diameter, and once this was reached, mice were euthanised with rising concentrations of CO_2. Metastatic burden (number of metastases, metastatic index) in the lungs was confirmed and further assessed by H&E staining (in collaboration with Karen Blyth's lab, CRUK Beatson Institute, Glasgow). All work was carried out with ethical approval from CRUK Beatson Institute and University of Glasgow under the revised Animal (Scientific Procedures) Act 1986 and the EU Directive 2010/63/EU (PP6345023). All animal experiments were performed in accordance with relevant guidelines and regulations (3Rs).

2.2.1.2 Syngeneic transplantation and resection model

For orthotopic transplantation experiments, 8-to-10-week-old female FVB/N mice were obtained from Charles River (UK). 0.5 $x10^6$ cells (either from PyMT#1 or PyMT#2 series) in 50µl PBS/matrigel were transplanted into the fourth mammary fat pad of FVB mice. Following recovery from surgery, mice were housed in individual cages and monitored for tumour development three times per week. Once tumour was palpable, growth was assessed by calliper measurement three times per week, and tumour was surgically removed when the diameter reached ~8-9mm. The tumour was kept in ice-cold PBS prior to downstream processing for cell line generation (as described in 2.2.2.1). After surgical resection, mice were closely monitored (three or more times per week) for clinical signs of metastasis, which included weight loss, altered respiration or abdominal distension. All the animals were scored based on these signs (mild, moderate, advanced) and were euthanised in rising concentrations of CO_2, if they displayed two or more moderate signs (e.g. weight loss<20% and moderate piloerection). Of note, regrowth of resected tumour might occur in the orthotopic site, and if that was the case, the clinical endpoint was 15mm in diameter. At clinical endpoint, lungs were harvested, kept in ice-cold PBS prior to further processing for generation of cell lines (described in 2.2.2.1). Analgesia was used prior and after all surgical procedures to minimise any pain/discomfort of the animals.

2.2.1.3 *Slc7a11* in situ hybridisation staining

Formalin fixed paraffin embedded (FFPE) tissues from MMTV-PyMT primary mammary tumours and matched metastatic lungs, from a cohort of mice in which tumour burden and metastatic index had already been assessed, were kindly provided by Karen Blyth's lab, CRUK Beatson Institute, Glasgow. All Haematoxylin & Eosin (H&E), and in-situ hybridisation (ISH) staining for Slc7a11 (xCT) were performed by Colin Nixon and the histology service, CRUK Beatson Institute, Glasgow. H&E and ISH staining were performed on 4µm formalin fixed paraffin embedded sections which had previously been ovened at 60˚C for 2 hours. H&E staining was performed on a Leica autostainer, where sections were dewaxed, taken through graded alcohols and stained with Haem Z (CellPath) for 13 minutes. Sections were then washed in tap water, differentiated in 1% acid alcohol, washed and the nuclei blued in scotts tap water substitute (in-house). After washing, the sections were placed in Putt's Eosin (in-house) for 3 minutes. ISH detection for Slc7a11 mRNA was performed using RNAScope 2.5 LSx (Brown) detection kit (Bio-Techne) on a Leica Bond Rx autostainer strictly according to the manufacturer's instructions. To complete H&E and ISH staining, sections were rinsed in tap water, dehydrated through graded ethanols and placed in xylene. The stained sections were coverslipped in xylene using DPX mountant (CellPath). Following staining, slides were scanned at 20x magnification using NanoZoomer NDP scanner (Hamamatsu), and HALO software (Indica Labs) was used to quantify the average optical density of the *Slc7a11* stain in sections of primary mammary tumours and corresponding lung metastases.

2.2.2 Cell culture

2.2.2.1 Generation of PyMT cell lines

Cell lines ('parental') from the MMTV-PyMT model were generated in-house by Nicola Ferrari and Nick Rooney, CRUK, Beatson Institute, as previously described (Ferrari, 2015). PyMT#1 and PyMT#2 cell lines were generated from two separate mice. To generate cell lines from the transplantation and resection model, we used a similar approach with slight modifications. Following surgical resection (as described in 2.2.1.2), single primary mammary tumours were minced using sterile surgical scalpels until a fine paste was achieved, and the finely chopped tissue was added to culture media (DMEM), followed by centrifugation at 1000rpm for 5

minutes at room temperature (RT). The cell pellet was resuspended in DMEM, filtered using a 70μm cell strainer (to eliminate remaining clumps) and added to a 10-cm dish. The media was supplemented with 10% FBS, 2mM glutamine, 100U/ml penicillin streptomycin, 20 ng/ml hEGF, 10 μg/ml insulin and 0.25μg/ml fungizone and cultured at 37°C/ 5% CO_2 in a humidified incubator. The cells were closely monitored during the first days of culture, PBS washes were performed in case there were too many red blood cells in the culture (as they might compromise mammary tumour cell growth), and media was changed every other day. To establish an immortalised mammary tumour cell line, cells were passaged (once reached around 90% confluence) for at least five generations and maintained in culture for a maximum of twenty passages. The same protocol was used for the generation of metastatic cells lines, with the exception that following centrifugation, the resuspended cell pellet was seeded in 6 well plates.

For cell culture growth and maintenance, cells were kept in the aforementioned conditions (without fungizone supplementation after the fifth passage; this is hereby referred to as full (culture) media) and passaged every two days. Following trypsinisation (0.25% trypsin) for 5 minutes at 37°C/ 5% CO_2, cells were resuspended in full media and plated at the appropriate number in new TC dishes. Long-term storage of our cell lines involved cryofreezing, where cells were trypsinised, centrifuged at 1000rpm for 5 minutes at RT and the pellet was resuspended in full culture media containing 10% DMSO. The cells were frozen at -80°C within cryovials that were placed in a Mr Frosty freezing container, according to the manufacturer's instructions, and eventually transferred to liquid nitrogen.

2.2.2.2 Cell lines

HEK293T cells (obtained from ATCC) and telomerase-immortalised human dermal fibroblasts (TIFs; generated in-house, CRUK Beatson Institute, Glasgow) were cultured in DMEM supplemented with 10% FBS, 2mM glutamine and 100U/ml penicillin streptomycin, and kept in a humidified incubator at 37°C/ 5% CO_2. For NMUMG (ATCC) cells, media were further supplemented with 10 μg/ml insulin. Cells were passaged and cryopreserved as described above (in 2.2.2.1).

All cell lines were tested for mycoplasma contamination on a regular basis using the in-house mycoplasma testing (qPCR based detection, Venor GeM qOneStep kit (ThermoFisher)) service (Jillian Murray, Molecular Technology Services, CRUK Beatson Institute, Glasgow).

2.2.2.3 Cell proliferation assay

PyMT#1- and PyMT#2-derived cell lines were seeded at $2x10^4$ and $3x10^4$ cells per well in 6-well culture plates and incubated at 37°C/ 5% CO_2 in a humidified incubator for 6 hours to adhere. Plates were transferred to a tissue culture incubator equipped with IncuCyte ZOOM live-cell imaging system, and images were acquired (10x objective) every 2 hours over a period of 120 hours (5 days). At the end of the incubation, images were analysed using the Incucyte Base Analysis Software, and confluence was measured using the same phase segmentation parameters across all PyMT-derived cell lines. Confluence was calculated as a % of the phase image area covered by cells (3 technical replicates or fields of view/condition) corresponding to individual time points, and these values (sixty time points) were plotted over the culture period to generate the growth curves for each cell line. The time elapsed ($t_{1/2}$) until half of the phase image area per field of view was covered by cells (50% confluence) was also plotted in these graphs.

2.2.2.4 Buthionine sulfoximine (BSO) treatment

PyMT#1-derived cells (parental, fat pad, micrometastatic) were plated at $3x10^3$ cells per well in 24-well culture plates, and incubated at 37°C/ 5% CO_2 for 24 hours. The following day, cells were treated with increasing concentrations (2.5μM, 5μM, 25μM, 50μM, and 100μM) of BSO or H_20 as control. For cell proliferation experiments, cells were incubated for 48 hours in the presence of the drug at 37°C/ 5% CO_2, and total cell number was counted at the end of the incubation time. To count cell number, cells were trypsinised in each well, resuspended in full media (as described in 2.2.2.1) and total number of cells was measured using a Casy Cell Counter according to the manufacturer's instructions. For metabolic or EV collection experiments, PyMT#1-derived parental cells were treated with BSO for 24 hours (0.625μM, 1.25μM, 1.875μM, and 2.5μM in full media)

or 48 hours (1.25μM or 1.88μM in EV-free media) respectively, and total cell number was measured.

2.2.2.5 Generation of nSMase deficient PyMT cells using the CRISPR/Cas9 technology

First, oligos were designed considering the target sequences (single guide RNA against non-targeting control(Wang et al., 2014), nSMase1 or nSMase2(Sanjana et al., 2014)), need to be flanked on the 3' end by a Protospacer Adjacent Motif (PAM sequence 5'- NGG-3'). The cloning of these sequences into a lentiCRISPR vector, formerly established by the Zhang lab(Shalem et al., 2014), was performed with slight modifications(O'Prey et al., 2017). 5μg of lentiCRISPR plasmid were digested with BsmBI for 2h at 37˚C, and the digested plasmid was run on an agarose gel followed by gel purification of the larger band (≈11 kb) using the QIAquick Gel Extraction Kit. Each pair of gRNA oligos (10μM) was phosphorylated and annealed with 5 units of T4 Polynucleotide kinase in T4 DNA ligase reaction buffer, for 30 minutes at 37˚C, followed by 5 minutes at 95˚C and ramped down to 25˚C at 5˚C/minute. After diluting the annealed gRNA oligos using ddH_2O (1:200), a ligation reaction was performed for 1h at 25˚C between the diluted oligo duplex and the digested lentiCRISPR plasmid (50ng) using the Quick Ligation kit.

To amplify clones of these lentiviral constructs, we transformed Stbl3 competent cells with 11μl of ligation reaction. After gentle mixing, cells were incubated on ice for 30 minutes, followed by brief heat-shock (45 seconds at 42˚C) and further placed on ice for 2 minutes. Then, 250μl of pre-warmed S.O.C. medium was added to the vials, which were shaken horizontally at 30˚C for 1 hour at 225 rpm in a shaking incubator. The entire transformation mix was spread onto ampicillin-containing agar plates and incubated overnight at 30˚C. Next day, several single colonies were picked for each gRNA cloning, and grown overnight in ampicillin (100 μg/ml) containing LB broth (10ml), at 30˚C in a shaking incubator (225rpm). To confirm successful gRNA cloning in these mini-cultures, plasmid purification and sequencing using the LKO.1 forward primer were performed by the Molecular Technology Service, CRUK Beatson Institute, Glasgow. CLC Genomics workbench software (7.5.2 version) was used for alignment of the desired gRNA sequences with the ones of the propagated clones. The positive clones for each of the gRNA

sequences were amplified in larger cultures and the plasmids were purified for long term storage (-20˚C) and use.

To produce the lentivirus encoding Cas9, along with the desired gRNAs, HEK 293T cells were used as the host packaging cell line. Prior to the transfection day, 1 x 10^6 HEK 293T cells were seeded in 10cm plates and cultured overnight at 37˚C/ 5% CO_2 in a humidified environment. Next day, cells were transfected using the calcium phosphate kit as follows: DNA (10μg plentiCRISPR for each of the gRNAs, 7.5μg pSPAX2, and 4μg pVSVG) is diluted in sterile H_2O (440μl), followed by addition of 2x HBS (500 μl) and thorough mixing. Then, 2M $CaCl_2$ (60μl) were added, immediately mixed up and down, and the mix was incubated for 30 minutes at 37˚C. At the end of this incubation time, the mixture was gently added to the cell media and left overnight at 37˚C. Next day, culture media was carefully discarded (CL 2 disposal), and replenished with the appropriate media containing 20% FBS. On the same day, 0.4 x 10^6 PyMT cells (primary tumour and metastatic lines) were seeded in 10cm plates (including an extra plate of cells to be used as a control for antibiotic selection), and left to adhere and grow overnight at 37˚C/ 5% CO_2 in a humidified incubator (so the cell confluence is <60% on the day of transduction).

To transduce our target cells with the lentivirus-containing media, HEK 293T supernatant was carefully collected 48 hours post transfection, and filtered through a 0.45μm PTFE filter membrane (to prevent cell line cross contamination). Then, polybrene was supplemented to the virus-containing media, to a final concentration of 4μg/ml, to enhance transduction efficiency. After removal of media from recipient PyMT cells, the lentivirus-containing media were added and the cells were infected overnight at 37˚C/ 5% CO_2. 24 hours post infection, the virus-containing media were removed from PyMT cells, which were further passaged into appropriate culture media containing puromycin (2μg/ml). The antibiotic selection media were replenished every 2 days, and the cells were passaged according to their confluence to generate stable cell lines. Almost 7 passages post infection, cells were harvested for qPRC analysis of nSMase deletion.

2.2.3 RNA extraction

Once reached ~80% confluence, PyMT-derived cells were washed twice with ice-cold PBS, lysed into Trizol (1ml per 10cm dish), and the lysate was pipetted up and down several times to achieve homogenisation, snap frozen on dry ice and stored at -80°C until further use. On the day of RNA extraction, samples were thawed and incubated for 5 minutes at RT to allow complete dissociation of the nucleoprotein complexes, which was followed by chloroform addition (0.2ml per 1ml Trizol used), thorough mixing by vortexing and incubation at RT for 3 minutes. Then, samples were centrifuged for 15 minutes at 12,000xg at 4°C, the upper aqueous phase (which contains the RNA) was transferred to a new tube, and an equal volume of isopropanol was added to precipitate the RNA. After brief vortexing, the samples were incubated for 10 minutes at RT, and further centrifuged at 12,000xg for 10 minutes at 4°C. The pellet was resuspended in 1ml of 75% ethanol (to wash the RNA), vortexed briefly and centrifuged for 5 minutes at 7600xg at 4°C. The supernatant was carefully aspirated, and the RNA pellet was left to air dry for 10 minutes prior to resuspension in 40µl of RNase-free water, which was pre-warmed to 55°C. Samples were pipetted up and down, incubated in a heat block set at 55°C for 15 minutes, and then transferred on ice. The RNA was stored at -80°C, and on the day of cDNA synthesis (described in 2.2.5) RNA yield was determined by calculating the A_{260}/A_{280} ratio using a NanoDrop spectrophotometer (Thermo) according to the manufacturer's instructions.

2.2.4 RNA-Sequencing

PyMT#1- and PyMT#2-derived cell lines were seeded at $0.5x10^6$ and $1x10^6$ cells respectively in 10cm dishes and incubated at 37°C/ 5% CO_2 in a humidified incubator for 24 hours prior to sample preparation for RNA sequencing (RNA-Seq).

2.2.4.1 Sample preparation and sequencing

RNA was extracted from the above cell lines (as described in 2.2.3). Ribodepletion of the samples and RNA-Seq were performed by Billy Clark, Molecular Technology Service, CRUK Beatson Institute, Glasgow. Briefly, a RiboZero magnetic kit was used per manufacturer's instructions, and removal of ribosomal RNA was determined by the lack of 18S and 28S rRNA peaks on the processed samples, which were analysed by the RNA 6000 Pico Kit and Bioanalyzer (Agilent

Technologies). Sample library preparation was, then, performed using the Illumina TruSeq RNA Library Prep kit v2, and sequencing was conducted on the NextSeq500 platform using a High Output 75 cycle kit.

2.2.4.2 Data analysis

Analysis of the RNA-Seq data was performed by Ann Hedley and Ryan Kwan, Bioinformatics, CRUK Beatson Institute, Glasgow. For RNA-Seq data analysis, the mouse genome version GRCm39v105 was used and gene count normalisation was performed using Deseq2 (which normalises gene counts after accounting for sequencing depth, gene length and RNA composition). Gene-set enrichment analysis (GSEA) of differentially expressed genes between primary tumour and metastatic PyMT-derived cell lines was performed using the Molecular Signatures Database (MSigDB) hallmark and/or curated gene sets. Following manual inspection of gene expression signatures in these groups (heat maps; not shown), normalised counts were extracted and plotted for the genes that contributed the most to the enrichment score (leading edge subset of the enrichment plot).

2.2.5 cDNA synthesis

Following RNA extraction and determination of RNA yield (described in 2.2.3), 1µg of RNA was used as template for cDNA synthesis using the Quantitech Reverse Transcription Kit according to the manufacturer's instructions. Genomic DNA (gDNA) was eliminated by adding gDNA wipeout buffer (2µl) to the template RNA in a total volume of 14µl per reaction. The samples were then incubated for 2 minutes at 42°C, and placed immediately on ice. Following preparation of a reverse transcription (RT) master mix containing 1µl Quantiscript reverse transcriptase, 4µl Quantiscript RT buffer, and 1µl RT primer mix, the mix was added to each sample, which was then incubated for 15 minutes at 42°C, followed by a 3 minute incubation at 95°C to inactivate the reverse transcriptase. To ensure the absence of gDNA contamination, a negative control (without reverse transcriptase) was also included in these reactions. The cDNA was used immediately for qPCR or stored at -20°C for later use.

2.2.6 RT-qPCR

Reverse transcription quantitative real-time PCR (RT-qPCR) reactions were performed in 96-well plates (BioRad CFX platform) by using SyBr green in a total reaction volume of 10µl per well. Each reaction contained a 1/20 dilution of cDNA template, 1X PerfeCTa SYBR Green Fast mix, 0.5µM forward primer and 0.5µM reverse primer (primer sequence details for the gene targets provided in 2.1.4), and samples were plated in duplicate. In each run, standard curves were generated using serially diluted cDNA from pooled samples to assess reaction efficiency, and no template controls (without cDNA) were also included for each target gene to check for potential primer dimer formation. Reactions were run on the BioRad C1000 thermal cycler using a 3 step protocol, during which cDNA was denatured for 3 minutes at 95°C, followed by 40 cycles of denaturation at 95°C for 20 seconds, annealing at 60°C for 20 seconds, and extension at 72°C for 20 seconds, with a final extension step of 72°C for 5 minutes and a melting curve from 65°C to 95°C in 0.5°C increments. Data acquisition and analysis were performed in CFX Manager Software, and the ΔΔCt method was used to compare gene expression levels between different cell lines.

2.2.7 Western blotting

Once PyMT-derived cells reached ~80% confluence, media was aspirated, cells were placed on ice, washed twice in ice-cold PBS and lysed into RIPA buffer supplemented with protease inhibitor cocktail (Fisher Scientific). 600µl of lysis buffer was added per 15cm dish, cells were scraped using a cell lifter, and lysate was transferred into a 1.5ml Eppendorf tube and centrifuged at 13,000rpm for 20 minutes at 4°C. The supernatant was carefully transferred into a new tube, and used immediately for protein quantification (BCA assay kit) or stored at -20°C.

Samples were reduced in 1x NuPAGE sample buffer containing 0.1M DTT at 95°C for 5 minutes. In the case of Western blotting for sEV markers, DTT was not added in the sample buffer (non-reducing conditions). To resolve proteins by SDS-PAGE electrophoresis, equal amounts of protein (15µg) were loaded onto 4-12% or 10% pre-cast NuPAGE Bis-Tris gels, along with a protein ladder, and were run using MOPs running buffer at 120V until separation of the all blue ladder was achieved. The proteins were then transferred from the gel to PVDF membrane (after being

activated with methanol) in NuPAGE transfer buffer at 120V for 90 minutes. The membrane was blocked using 4% non-fat milk in TBS-T for one hour at room temperature under gentle agitation. The membrane was incubated with primary antibodies diluted in 1% milk, overnight at 4˚C while gentle agitation was applied. Next day, the membrane was washed three times with TBS-T, every 10 minutes, under gentle rocking and after the final wash, the membrane was incubated with the appropriate secondary antibody for 1 hour at RT under gentle agitation. Following incubation, the membrane was washed three times for 10 minutes with TBS-T under gentle shaking, and was developed using the Licor Odyssey DLx imaging system. In the case of sEV markers, the secondary antibodies used were HRP-conjugated and the blots were incubated with ECL substrate (SuperSignal West Femto) for 1 minute and developed with Bio-Rad ChemiDoc imaging system. For band densitometry analysis of CD63, quantification was performed on blots at non-saturating exposures, while applying the same background settings across the samples, using the Image Lab software (Bio-Rad).

2.2.8 Recycling assay

$1x10^6$ PyMT cells (per 10cm dish) were cultured at 37˚C, 5% CO_2 (in a humidified incubator) for 16 hours to achieve a confluence of 80-90%. Cells were transferred to ice, washed twice with ice-cold PBS, and surface-labelled by adding 0.2mg/ml Sulfo-NHS-SS-Biotin (in PBS) and gentle rocking at 4˚C for 1 hour. To remove excess biotin, plates were washed twice with ice-cold PBS, and the ones required for measurement of total protein content and blank measurement were kept on ice until cell lysis and MesNa treatment respectively. The remaining plates were used to measure internalised biotinylated surface receptors recycled to the surface. Cells were incubated with pre-warmed growth media at 37˚C for 30 minutes to allow internalisation of tracer. Then, plates were returned to ice, washed once with ice-cold PBS, and once with biotin reduction buffer. After rocking the cells gently for 30 minutes at 4˚C in the presence of 20mM MesNa (in biotin reduction buffer) to remove biotin from proteins that remained in the cell surface, plates were transferred to ice and washed twice with ice cold PBS. The internalised biotin fraction was then chased by incubating the cells with pre-warmed media at 37 ˚C for the indicated time points. Following each point, plates were placed on ice, and a second reduction step with 20mM MesNa was performed (gentle rocking for 1 hour at 4˚C) to remove surface biotin from recycled

receptors. The reaction was quenched by adding 20mM IAA and incubating the cells at 4˚C with gentle rocking for 10 minutes. Cells were washed with ice-cold PBS and lysed in non-denaturing lysis buffer. Cell protein lysates were passaged though a 27-gauge needle three times, centrifuged at 13,000rpm for 10 minutes at 4˚C and supernatant was kept on ice until incubation with antibody-coated plates.

Recycled/biotinylated α_5, β_1 and TfnR were quantified by capture-ELISA as described below. One day prior to the recycling assay, 96-well Maxisorp plates were coated with antibodies recognising mouse α_5, β_1 or TfnR in Elisa coating buffer, and incubated overnight at 4˚C. Next day, plates were washed with PBS-T and blocked with 5% BSA (in 0.1% PBS-T) at room temperature for 1 hour. After removal of blocking buffer and two washes with PBS-T, plates were incubated with cell protein lysates overnight at 4˚C with gentle shaking. Plates were washed three times with PBS-T to remove unbound protein, and incubated with streptavidin-HRP (1/1000 dilution in 0.1% BSA/PBS-T) at 4˚C for 1 hour while gently shaking. Plates were thoroughly washed, three times with PBS-T and three times with PBS, and incubated with ELISA developing reagent at room temperature for 15 minutes. The reaction was stopped with 8M H_2SO_4 and absorbance at 490nm was determined on a plate reader (Tecan). The % of recycled receptor was calculated based on the following equation: $\frac{Abs\ (MesNa\ \#1) - Abs\ (MesNa\#2)}{Abs(MesNa\#1)}$, where Abs(Mesna#1) and Abs(MesNa#2) correspond to the absorbance obtained upon the first (internal pool) and second reduction steps with MesNa.

2.2.9 Metabolomics

2.2.9.1 Polar metabolite extraction

For polar metabolite extraction, a previously described method was used with slight modifications(Voorde et al., 2019). PyMT#1-derived parental, fat pad and micrometastatic cells were seeded in 6-well plates (3 technical replicates/cell line) in full culture media (2ml) at $1.5x10^4$ cells per well. After 24 hours (day 1), 2ml of culture medium was added to each well to prevent nutrient exhaustion. On day 2, culture media was changed to 2ml or 7ml for medium metabolite extractions (calculation of exchange rates) or intracellular metabolite extractions respectively. The volumes of culture media used enabled measurement of

exchange rates of nutrients with slow flux, while detecting intracellularly metabolites that are rapidly consumed. In parallel, at this time point (day 2) cells were harvested for determination of total cell number per condition. After 24 hours (day 3), media and intracellular metabolites were extracted. For media metabolic extractions, 20µl of medium was added to 980 µl of an ice-cold polar extraction solution (methanol, acetonitrile, and water in a 5:3:2 ratio), and the samples were then shaken in a thermomixer at 1400rpm for 10 minutes (4˚C). For cell extracts, cells were quickly washed three times with ice-cold PBS, followed by extraction with 600 µl of ice-cold extraction solution for 5 min at 4˚C, whilst gentle agitation was applied. To remove insoluble material, media and cell extracts were centrifuged at 16000g for 10 minutes, and the supernatant was transferred to glass vials, which were stored at -80 ˚C prior to LC-MS analysis.

All polar metabolite extraction experiments followed the aforementioned timeline with minor adjustments (as stated in the corresponding figure legends). In N-ethymaleimide (NEM) derivatisation experiments, additional steps were added to this protocol as denoted in Figure 4-2A. In every instance, the volume of extraction solution required was calculated from the total number cell count and was in the range 1-2 x 10^6 cells/ml.

To allow estimation of consumption/secretion rates of nutrients and metabolites, data normalisation was achieved by counting the total number (#) of cells on days 2 and 3, and the exchange rate per day for each metabolite was calculated according to the following equation: $x=\frac{\Delta\text{metabolite}}{(\#\text{ cell day2}+\#\text{cell day3})/2}$,where Δmetabolite= (detected peak area spent medium- detected peak area cell-free medium)(see 2.2.9.4 for detection and integration of peak areas), and whether the x value is positive or negative indicates that the metabolite is secreted or consumed by the cells respectively.

To generate calibration curves for both GSH, GSSH, increasing concentrations (0.5uM, 1uM, 5uM, 10uM, 25uM, 50uM) of each standard compound (Sigma) was added in the same volume of extraction solution and the samples were analysed by LC-MS.

2.2.9.2 Lipid extraction

For lipid extraction experiments, the same cell culture timeline was followed as the one described in 2.2.9.1. Briefly, $1.5x10^4$ PyMT#1-derived parental, fat pad and micrometastatic cells were seeded in 6-well plates in full culture media. On day 2 (see 2.2.9.1), culture media was changed to 2 ml and after 24 hours (day 3), lipids were extracted from cells using 600µl of an extraction solution composed of butanol and methanol (1:1), supplemented with Splash II standard. Lipid cell extracts were centrifuged at 16000g for 10 minutes to remove insoluble material, and the supernatant was transferred to glass vials, which were stored at -80 ˚C prior to LC-MS analysis.

2.2.9.3 Liquid chromatography-mass spectrometry

All polar metabolite and lipid extracts were analysed by Liquid chromatography-Mass Spectrometry (LC-MS). All analyses were conducted by David Sumpton and Engy Shokry Abd Shokry (Metabolomics, CRUK Beatson Institute, Glasgow) using a Q Exactive Plus Orbitrap Mass Spectrometer (Thermo Fisher Scientific), coupled with a Thermo Ultimate 3000 high-performance liquid chromatography (HPLC) system. All samples were run in both positive and negative ion mode.

2.2.9.4 Data analysis

Thermo Xcalibur was used for acquisition of raw data, which were stored on a dedicated server and available for analysis using the TraceFinder software (Thermo) in the case of polar metabolites. The peak areas of metabolites were determined by using the exact mass of the singly charged ions, while the retention time of metabolites was predetermined on the pHILIC column by analysing an in-house built mass spectrometry metabolite library. For identification and quantification of glutathione and other thiol-containing adducts of NEM, the chemical formulas were manually imported into the software. Integrated peak area values were then exported to excel files and plotted after normalisation to total cell number.

Both untargeted and targeted lipid analyses were conducted by Engy Shokry Abd Shokry, Metabolomics, CRUK Beatson Institute, Glasgow. Briefly, LC-MS raw data were searched against LipiDex for identification. For the untargeted analysis,

Perseus software was used for Principal Component Analysis (PCA) and generation of scatter plots, while the percentage of lipid classes per total lipids was manually calculated from the exported integrated areas of identified lipids. The targeted approach involved sequential steps of data filtering, as described in 4.2.8.

2.2.10 Immunofluorescence

For E-cadherin immunofluorescence experiments, glass bottom 6-well plates were coated with 0.2% gelatin and incubated at 37˚C/ 5% CO_2 for 1 hour. After two washes with PBS, plates were cross-linked with 1% glutaraldehyde at RT for 30 minutes, which was followed by two PBS washes and quenching in 1M glycine at RT for 20 minutes. Following two PBS washes, plates were incubated in the appropriate full culture media for each cell line at 37˚C/ 5% CO_2 for 30 minutes. $1.5x10^4$ PyMT#1-, $3x10^4$ PyMT#2-derived cells and $6x10^4$ NMuMG cells were seeded per well, and incubated at 37˚C/ 5% CO_2 for 48 hours before proceeding with the staining protocol. For ceramide staining experiments, glass bottom 35mm dishes were used, $3x10^4$ cells were seeded per dish, and incubated at 37˚C/ 5% CO_2 for 40 hours. In both cases, following the culture incubation period, media was aspirated, and cells were fixed with 4% PFA (in PBS) at RT for 15 minutes. After two PBS washes, cells were permeabilised with 0.1% Triton-X100 (in PBS) at RT for 15 minutes, followed by two PBS washes, and blocked in 1% BSA (in PBS) at RT for 1 hour. Cells were then incubated with primary antibody in blocking solution at 4˚C overnight. For E-cadherin staining experiments, cells were incubated with DAPI (1:1000) and CellMask (1:10,000) in PBS at RT for 90 minutes, followed by two PBS washes and stored (in PBS) at 4˚C prior to visualisation by an Opera Phenix Plus High-Content screening confocal microscope. In the case of ceramide staining experiments, after primary antibody incubation, cells were washed twice with PBS, and secondary antibody and phalloidin stain- 1:1000 dilution in PBS- were added in blocking solution at RT for 1 hour. Cells were then washed twice with PBS, mounted using Vectashield with DAPI and visualised by confocal microscopy using an Airyscan super resolution microscope.

Quantification of E-cadherin levels and cell morphological analysis are described in 2.2.11. For ceramide levels, ImageJ software was used to quantify the mean intensity of ceramide stain (sum of z-stacks, 10 stacks/field of view) as

determined by the default method. This method was developed in collaboration with David Novo, Francis Crick Institute, London.

2.2.11 High content image analysis

Quantification of cytoplasmic E-cadherin levels, and morphological analysis were performed using the Columbus Image Data Storage and Analysis System (PerkinElmer). Forty images per cell line were acquired at 20X magnification and individual cells were identified using an automated segmentation protocol. An unbiased automated analysis was then performed on a cell by cell basis to generate individual cell data. The mean cytoplasmic intensity levels for E-cadherin staining and the width to length ratio were calculated for each cell, in order to quantify E-cadherin protein levels and generate a readout for cell roundness respectively. Width and length measurements were taken at the widest and longest points of the cell. A decrease in this ratio indicates a decrease in cell roundness.

2.2.12 Cell-derived matrix (CDM) migration assay

Cell derived matrix (CDM) was generated from TIFs by Jillian Murray, Molecular Technology Services, CRUK Beatson Institute, Glasgow. Briefly, TIFs ($2x10^5$ cells/well) were seeded in 6-well plates coated with gelatin (as described in 2.2.10) and cells were incubated at 37°C/5% CO_2. Once cells reached confluence, the media was changed to full media supplemented with 50µg/ml ascorbic acid, which were refreshed every other day for seven days. Matrices were denuded by incubation with triton containing buffer (2 minutes at RT), residual DNA was digested with DNase I (10µg/ml in PBS containing calcium and magnesium; D-PBS), and CDMs were stored at 4°C. Before use, CDMs were washed twice in D-PBS and incubated with full media for 30 minutes at 37°C/5% CO_2. PyMT-derived cell lines were seeded at $0.8x10^5$ cells per well. After 4 hours, cells were imaged using a time-lapse phase-contrast microscope (Axiovert S100, Carl Zeiss, 10x objective), while kept at 37°C/ 5% CO_2 (6 fields of view per well were imaged every 10 minutes for 16 hours). After completion of image acquisition, images were analysed using ImageJ software and the length of protrusions that cells extend in the direction of migration (distance from the nucleus to cell front) was measured.

2.2.13 Collagen organotypic assay

Organotypic plugs were generated from rat tail-derived collagen I, as previously described in (Timpson et al., 2011). Briefly, $1x10^6$ confluent fibroblasts (TIFs) were mixed with collagen I (2mg/ml) under neutral or slightly acidic conditions (MEM, approximate pH=7.2 by using 0.22M NaOH) and the collagen/fibroblast matrix was allowed to contract for approximately 3 days, until it fitted in a 24-well culture dish. $3x10^3$ PyMT#1-derived parental, fat pad and micrometastatic cells or micrometastatic cells (NTC, nSMase1#2-KO, nSMase2#5-KO) were seeded on top of these plugs (in duplicates) and cultured for 2 days. Plugs were then transferred on top of a metal grid and cultured in full media by creating an air-liquid interface (invasion day 0) for 3 days. At the end of the incubation time, plugs were fixed in 4% paraformaldehyde before paraffin embedding (proper orientation of cross sections), and 4μm sections were then cut and stained (haematoxylin and eosin) by the histology service, CRUK Beatson Institute, Glasgow (as described in 2.2.1.3). Single cell tracking was performed manually using ImageJ software under enhanced brightness/contrast settings (black and white mode) and a distance value, along with an angle value (representing the orientation relative to the invasion baseline; negative angle: cell entering the plug, positive angle: cell residing on top of the plug) were assigned to each cell per field of view. Images were acquired using a brightfield microscope and raw data were exported in batches (.ome.tiff) using the Zeiss Zen lite software (blue edition).

2.2.14 Extracellular vesicle (EV) collection

EV-free media was prepared following overnight (16 hours) ultracentrifugation of 5% FBS-containing DMEM at 100,000g (4°C) and further filtration of the collected supernatant using a 0.2uM PES filter unit. For extracellular vesicle collection, $0.3x10^6$ PyMT#1- and $0.6x10^6$ PyMT#2-derived cells were seeded in 15cm dishes (three 15cm dishes/condition), and cultured in full media for 16 hours at 37°C/5% CO_2. Cells were then washed twice with PBS, media was changed to EV-free (15ml/dish), and cultured for 48 hours at 37°C/5% CO_2 prior to EV collection. After this incubation time, conditioned media (CM) was collected from ~80% confluent PyMT-derived cells and subjected to sequential centrifugation steps to remove live cells (300g for 10 minutes), dead cells (2,000g for 10 minutes) and finally to remove cell debris and larger lipid membrane particles, including the majority of

microvesicles (10,000g for 20 minutes). EVs were then pelleted in thinwall polypropylene tubes after ultracentrifugation at 100,000g for 70 minutes using a SW32 rotor (Beckman coulter). The EV pellet was then washed in filtered PBS (0.2uM PES) and subjected to a final ultracentrifugation step at 100,000g for 70 minutes. All centrifugation steps were performed at 4°C. At the end of the last spin, the supernatant was carefully aspirated by tilting the tube, EVs were re-suspended in 150µl PBS, which was previously filtered using a Whatman Anotop filter (0.02µM), and stored at 4°C until the next day.

2.2.15 Nanoparticle Tracking Analysis (NTA)

Nanoparticle tracking analysis (NTA) was performed using a NanoSight LM10 instrument (Malvern Panalytical) with a high sensitivity camera according to the manufacturer's instructions. Isolated EVs were diluted 1:50-1:200 in PBS (filtered through 0.02µM) depending on the donor cells. Diluted EV samples were then flushed through the chamber until vesicles were visible on the camera by using a 1ml syringe. The focus and gain settings were optimised for each run, and kept consistent across the samples, which were injected into the flow cell and 5 recordings of 60 seconds each were acquired. The chamber was washed with ethanol and deionised water between samples to ensure no residual particles remained. The data were analysed using the NTA3.1 analysis software and average of technical replicates were plotted per experiment following normalisation to the total number of EV-releasing cells and the dilution applied per condition.

2.2.16 Statistical analyses and schematics

Statistical analyses were performed with GraphPad Prism 9 on all relevant experiments using unpaired t-tests to compare two groups with normal data distribution. ANOVA tests (one-way, two- way or repeated measures) were used to compare more than two groups if the data were normally distributed, while a Kruskal-Wallis test was performed for not normally distributed datasets. A Friedman test (nonparametric repeated measures ANOVA) was used when no assumptions were made for the data distribution. Statistical significance is annotated in the figures (p–values are shown on the figures, with $p<0.05$ considered significant) and the associated tests are indicated in each figure legend.

All schematics were created with BioRender.com. Permission to use the BioRender content, including icons, templates and other original artwork, appearing in this thesis has been granted following BioRender's Academic License Terms. The schematics in Figure 3-7a (organotypic plugs), Figure 5-1a (EV collection centrifugation steps), and Figure 5-12 (organotypic plugs) were created and kindly provided by David Novo, Francis Crick Institute, London.

Chapter 3 Generation and characterisation of cells from MMTV-PyMT-driven mammary tumours and metastatic pulmonary lesions

3.1 Introduction

Despite ongoing efforts towards the development of early prognostic markers in breast cancer, and early identification and treatment of primary disease, metastasis to distant organs poses severe hurdles to disease eradication (Weigelt et al., 2005). Breast cancer subtypes can partially dictate metastatic spread patterns within various organs, including the bone, lungs, liver and brain (Kennecke et al., 2010). In a 15-year follow-up study of patients with early stage breast cancer, high rates (24-30%) of lung metastasis were observed in women with oestrogen receptor-positive subtype, and in almost half (47%) of patients with the HER2-positive, oestrogen receptor-negative subtype (Kennecke et al., 2010). The latter group (HER2-enriched) was associated with marked decrease in survival after relapse (Kennecke et al., 2010), indicating that lung metastases are a major contributor to breast cancer morbidity and mortality. With this in mind, the development of models to study metastatic recurrence and further understanding of the mechanisms that drive breast cancer metastasis to the lung are crucial to improve patient survival.

It remains technically challenging to study metastatic seeding in animal models (Francia et al., 2011), and this is due to tumour heterogeneity, limited metastatic tropism and scarcity of metastatic cells (Francia et al., 2011). Despite these challenges, some promising advances have been made to model metastatic breast cancer with the use of genetically engineered (transgenic) mouse models (GEMM) (Francia et al., 2011; Kim & Baek, 2010; Jonkers & Derksen, 2007). The MMTV-PyMT mouse is a well-characterised murine model of metastatic breast cancer in which Polyoma Middle T-Antigen is expressed specifically in the mammary epithelium leading to the development of tumours, and their ability to metastasise is heavily influenced by the mouse genetic background (Guy et al., 1992; Davie et al., 2007) (Figure 3-1, left panel). PyMT can be considered to be a constitutively active analogue of a growth factor receptor (Ichaso & Dilworth, 2001), and its insertion into membranes is an integral step of its transforming activity. It

subsequently associates with cellular proteins to promote cell growth via signal transduction pathways (ShcA, PI3K, PLCγ-1) activated by receptor tyrosine kinases (RTKs) (Ichaso & Dilworth, 2001). However, expression of PyMT in the mammary epithelium leads to the formation of multiple primary tumours which form in an asynchronous manner. This renders resection practically impossible, as is standard clinical procedure in breast cancer patients, thus modelling post-surgical metastatic recurrence is a challenge using the MMTV-PyMT model (Francia et al., 2011).

To overcome this challenge, we used a mammary fat pad transplantation and tumour resection model to study metastatic visceral disease (Figure 3-1, right panel). This approach leads to the formation of a single primary tumour, which can be cleanly resected, thus allowing sufficient time for manifestation of distant metastases (Francia et al., 2011; Fidler, 2006). Thus, following resection, mice do not succumb owing to primary tumour burden as observed in the autochthonous models, but to metastatic disease which arises later, thus more effectively modelling the manner in which breast cancer progresses, post-surgery, in humans (Wexler et al., 1965). We are interested in the very early stages of metastatic seeding, in particular how recently disseminated breast cancer cells adapt to metastatic microenvironments. To develop tools to study this, we established cell lines from resected mammary tumours that grew from MMTV-PyMT cells transplanted into the mammary fat pad, and from the spontaneous metastatic lesions that developed following resection of these primary tumours.

In this chapter, we have characterised the behaviour of cell lines derived from transplanted MMTV-PyMT primary mammary tumours and their corresponding lung metastases. In particular, we examined their morphological traits and growth rates, and explored whether the observed phenotypic shifts may be attributed to differences in transcriptomic profiles. Finally, we evaluated the migratory and invasive capacity of the primary and metastatic breast cancer cell lines both in 2D and 3D culture environments, and how this may be supported by trafficking of membrane receptors.

3.2 Results

3.2.1 Establishment of cell lines from transplanted MMTV-PyMT mammary tumours and their corresponding lung metastases

A number of studies have established organ-specific isogenic metastatic cell lines by using human breast cancer cell lines in either experimental models of metastasis (Kang et al., 2003; Minn et al., 2005) or orthotopic xenograft models (Winnard et al., 2017, 2020). As mentioned in the introduction to this chapter, we are interested in the early events that occur as recently disseminated primary tumour cells adapt to metastatic microenvironment. Moreover, we have a long-standing interest in how metabolic landscapes might sculpt the early metastatic microenvironment. Because we already have gathered a substantial body of data on the circulating metabolome of the MMTV-PyMT model in the FVB mouse strain (Cassie Clarke, personal communication), and we needed an immunocompetent model which allows us to consider the role of the immune system in early metastasis, we chose to establish organ-specific metastatic cell lines using a syngeneic MMTV-PyMT transplantation-resection approach. PyMT cell lines (hereafter referred to as 'parental') were established from spontaneous primary tumours arising in MMTV-PyMT female mice (FVB strain), as previously described (Ferrari et al., 2015) (Figure 3-1, left panel). This was performed in collaboration with Nicola Ferrari and Nick Rooney (CRUK Beatson Institute, Glasgow). We then transplanted these cells into the fourth mammary fat pad of wild-type recipient mice, from the same genetic background (FVB), and allowed tumours to grow to a defined size (8-9mm). Following surgical resection from the fat pad, these 'primary' tumours were used to establish PyMT positive cell lines (herein referred to as fat pad) (Figure 3-1, right panel). Following recovery from surgery, mice were monitored for signs of pulmonary metastases, which included weight loss, altered respiration and/or abdominal distension. Lungs were harvested at clinical endpoint, and metastatic cell lines (herein referred to as 'metastatic') were generated and cultured under standard conditions until spontaneous immortalisation occurred (>five serial passages) (Figure 3-1, right panel). We successfully established PyMT lung metastatic cells lines from two independent transplantation experiments (named PyMT#1 and PyMT#2 respectively, in collaboration with Emmanuel Dornier, CRUK Beatson Institute, Glasgow), using two independent parental PyMT cell lines. The majority of metastatic lines (5 out

of 8) were derived from lung micrometastases (named 'micrometastatic'); these were from the lungs of mice which displayed clinical signs of metastasis (normally weight loss), but in which no macroscopic metastases were visible. On the other hand, only one cell line (1 out of 8) was obtained from a visible and manually-dissected lesion (named 'macrometastatic', in collaboration with Anna Koessinger, CRUK Beatson Institute, Glasgow).

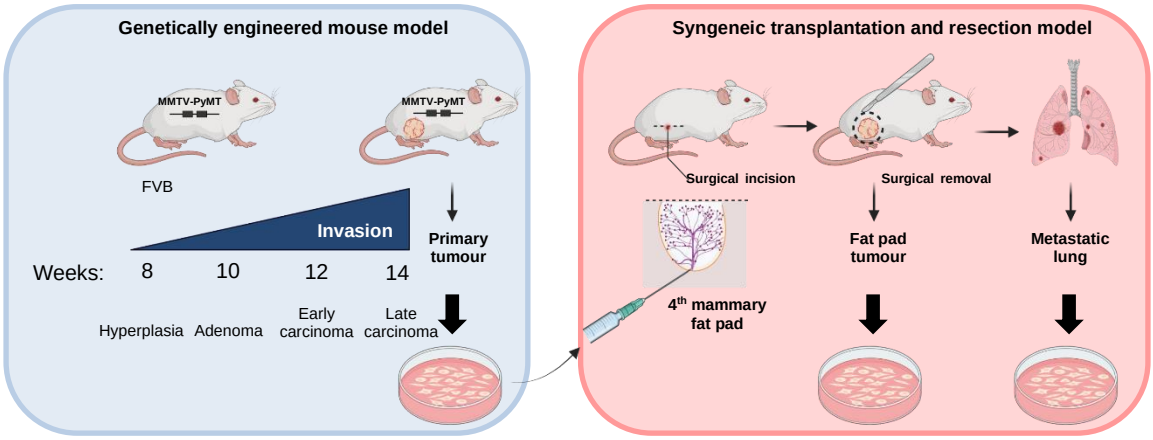

Figure 3-1 Schematic representation of the MMTV-PyMT model and the mammary fat pad transplantation and tumour resection model.
In blue: FVB/N mice carrying a polyoma virus middle T antigen (PyMT) transgene, the expression of which is restricted to the mammary epithelium under the control of mouse mammary tumour virus (MMTV) promoter. Four main stages of disease progression (time points at which the animals have these pathologies in weeks) can be identified in PyMT mice, ranging from premalignant lesions (hyperplasia) to late carcinoma, which can metastasise to the lungs. Parental tumour cell lines were established from spontaneous tumours arising in MMTV-PyMT female mice. *In pink*: These parental cells were transplanted into the fourth mammary fat pad of recipient mice, from the same genetic background (FVB/N), and tumours were allowed to grow to a defined size (8-9mm). Following surgical resection, tumours were used to establish fat pad cell lines, while mice were closely monitored for signs of metastasis (laboured breathing, weight loss, and/or abdominal distension). Metastatic lungs were harvested at clinical endpoint, and metastatic cell lines were generated and cultured under standard conditions.

3.2.2 PyMT cells derived from primary mammary tumours are morphologically distinct from their metastatic counterparts in the lung

A plethora of phenotypic characteristics have been reported for cell lines isolated from primary mammary tumours arising in the MMTV-PyMT model (Borowsky et al., 2005; Waldmeier et al., 2012; Saxena et al., 2018). The general consensus of these studies is that PyMT lines display an epithelial cell phenotype with varying degrees of differentiation. Inverted phase-contrast microscopy was used to compare the morphology between matched primary and metastatic cells grown *in vitro* on standard plastic TC surfaces (Figure 3-2). Parental cells from the PyMT GEMM exhibited a typical cobble stone-like epithelial morphology, as did cell lines

derived from resected (fat pad) tumours of the transplantation model. Interestingly, micrometastatic lines appeared to have a mesenchymal-like phenotype with numerous cells being elongated with spindle characteristics (PyMT#1, and to a lesser extent, PyMT#2), whilst the macrometastatic cells appeared to be relatively more epithelial-like with few spindle cells. Taken together, these data suggest that, when grown on plastic surfaces, micrometastatic cell lines are morphologically different from primary tumour cells, and these *in vitro* phenotypes are maintained over multiple successive passages.

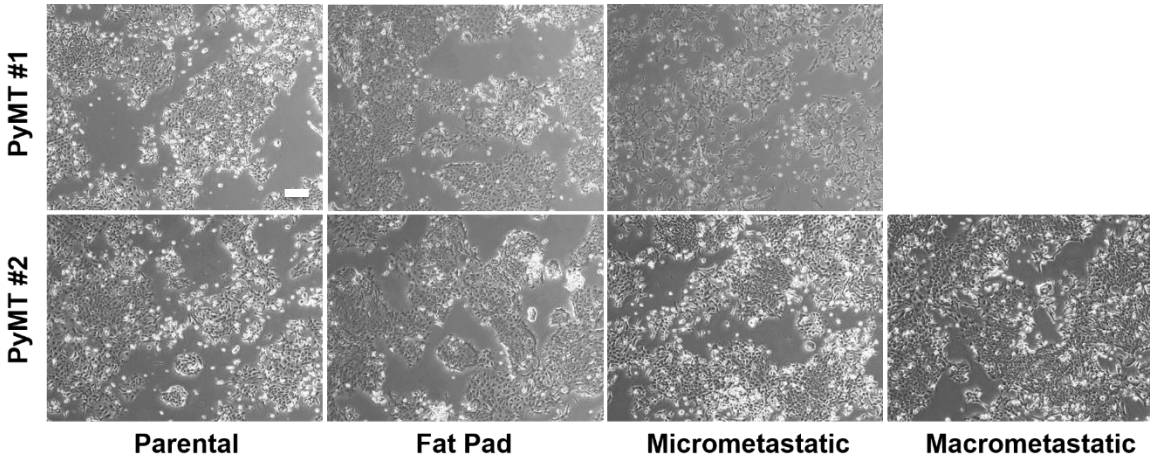

Figure 3-2 Phase contrast micrographs of PyMT cells derived from primary mammary tumours and matched lung metastases.
Phase contrast images of characteristic monolayer growth of PyMT-derived cell lines after 64 hours of culture, corresponding to cells reaching <80% confluence. PyMT#1 parental, fat pad and micrometastatic cells are shown on the top panel, while PyMT#2 parental, fat pad, micrometastatic and macrometastatic lines appear in the bottom panel. These images were taken using a 4x objective, scale bar 1mm.

3.2.3 Primary tumour cell lines proliferate at similar rates to their corresponding metastatic cells

Previous publications have, not only, highlighted morphological differences among established organ-specific isogenic metastatic breast cancer lines, but also shown differential growth rates of these cells (Winnard et al., 2017, 2020). Therefore, we sought to determine at which rate our established PyMT-derived cell lines proliferate. To achieve this, PyMT-derived cells were seeded on six-well plates, and their growth was monitored in real-time using the IncuCyte live-cell imaging system. After analysing the phase image area covered by cells (confluence mask) over the indicated time, we generated growth curves for each cell line, as shown in Figure 3-3. All PyMT-derived cells displayed a typical sigmoidal growth pattern consisting of lag, exponential and stationary phases. During the exponential

phases, cell lines coming from lung metastases proliferated only marginally faster (Figure 3-3, top panel, PyMT#1; $t_{1/2}$ = 58 hours) or at the same rate (Figure 3-3, bottom panel, PyMT#2; $t_{1/2}$ = 34 hours) than their matched counterparts from fat pad transplanted sites (PyMT#1; $t_{1/2}$ = 67 hours, PyMT#2; $t_{1/2}$ = 32 hours). Parental cells exhibited marginally slower growth rates compared with their metastatic derivatives. Our data reinforce previous findings in orthotopic xenografts (Winnard et al., 2017) that lung isogenic metastatic cells lines display similar proliferation rates to those observed for primary tumour-derived cells.

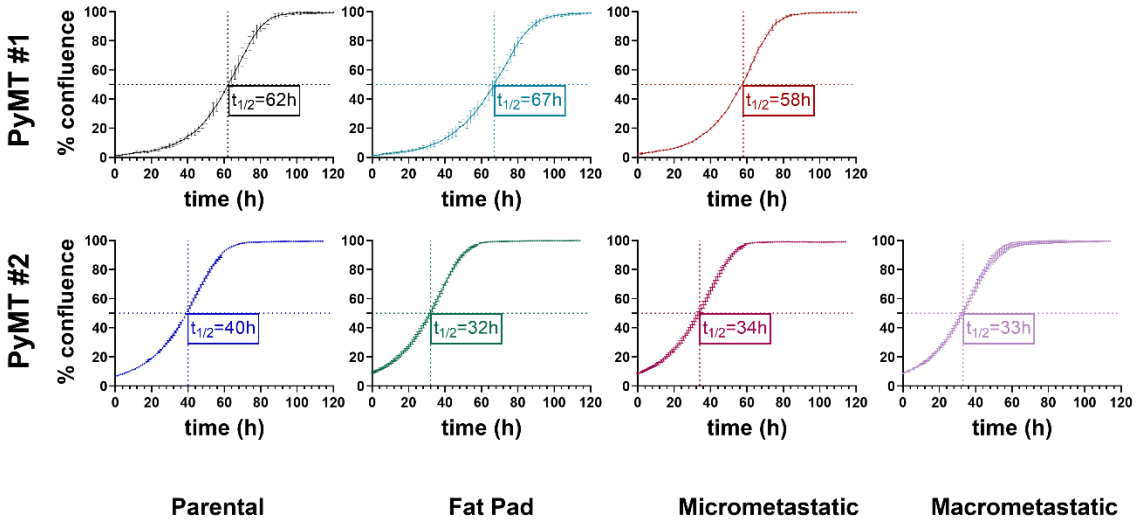

Figure 3-3 Growth curves of PyMT cells from primary tumour and lung metastatic sites. PyMT-derived cell lines were seeded on six-well plates, and proliferation was monitored by sequential image acquisition (once imaged every 2 hours over 5 days of culture) using the IncuCyte ZOOM live-cell imaging system. Growth curves were generated by utilising a segmentation algorithm (IncuCyte ZOOM Base analysis software) which calculates (as a %) the phase image area covered by cells (confluence mask). Values are mean ± SD, n=1 (3 technical replicates/cell line). The acquisition of these images was performed using a 10x objective. For each of the PyMT-derived lines, the time point (in hours), at which 50% of the area is covered by cells, is outlined in the graphs (coloured boxes; $t_{1/2}$ was generated following confluence mask analysis and corresponded to the time elapsed until cell confluence reached 50%).

3.2.4 Breast cancer-derived lung micrometastatic cells exhibit an EMT gene expression signature

In our genetically engineered mouse model, transformation of the mammary epithelium is driven by the expression of the polyomavirus middle T antigen, which is under the transcriptional control of the mouse mammary tumour virus promoter/enhancer (Guy et al., 1992). This means that only mammary epithelial cells specifically express PyMT, and display enhanced metastatic potential. Since the orthotopic transplantations were performed in wild-type syngeneic mice, we would expect to detect PyMT expression only in cancer cells. Indeed, PyMT expression was confirmed by qPCR in cell lines derived from primary mammary

tumours and metastatic lesions in the lung (Figure 3-4A). Quite surprisingly, we noticed that micrometastatic cells expressed lower levels of the oncogene (5-fold decrease) compared to parental cells in both sets of PyMT lines, whereas fat pad cells showed variable expression (either a 2.5-fold decrease in PyMT #1 or no change in PyMT #2). This observation was consistent over three consecutive cell culture passages, while extended culturing was avoided to prevent loss of transgene expression, as previously reported (Waldmeier et al., 2012). Therefore, the presence of PyMT oncogene in the genome of our established isogenic lines demonstrates their cancerous tissue-of-origin.

After observing the morphological differences between primary tumour and metastatic cells (as described in 3.2.2), we were interested in assessing whether changes at the transcriptional level could account for this phenotype. We used RNA sequencing (RNA-Seq) to analyse the transcriptome profiles of both sets of isogenic PyMT cell lines. Gene-set enrichment analysis (GSEA) of differentially expressed genes between primary tumour (parental or fat pad) and micrometastatic cells demonstrated enrichment (NES>2, FDR q<0.001) for epithelial-to-mesenchymal transition (EMT) genes (using either the MSigDB hallmark or curated gene sets) in the latter condition (in both sets of PyMT cell lines; Figure 3-4B). Furthermore, GSEA performed for the differentially expressed genes between micrometastatic and macrometastatic cells showed similar enrichment for EMT in the former (data not shown). To illustrate the EMT gene expression signature of micrometastatic cells, we extracted normalised counts of top hits (|FC|>1.5 with positive core enrichment) belonging to the leading edge subset of the enrichment plot (that is, the subset of genes that contribute most to the enrichment score) from our RNA-Seq data. This showed a 2-450 fold increase in expression of genes (Glipr1, Ddr2, Itga5) that have been shown to induce EMT (Tiu et al., 2022; Kim et al., 2017) or mediate metastasis (Pantano et al., 2021), in micrometastatic cells (by comparison with primary tumour derived lines) (Figure 3-4C). Interestingly, with the exception of ITGA5, these genes were less upregulated in macrometastatic cells, albeit their expression was considerably higher relative to parental and fat pad cells. Conversely, we noticed that genes regulating epithelial cell homeostasis and cytoskeleton remodelling (Cldn1, Ptprf, Rhpn2) (Zhou et al., 2015; Young et al., 2021; LeVea et al., 2000; Danussi et al., 2013) were expressed at lower levels (1.5-3 fold decrease) in micrometastastatic

cells compared to primary tumour (and macrometastatic) cells (Figure 3-4D). These data suggest that, despite controversy surrounding EMT during the metastatic cascade (Williams et al., 2019), cells derived from lung micrometastases display several EMT characteristics, while macrometastatic cells more closely resemble those from the primary tumour.

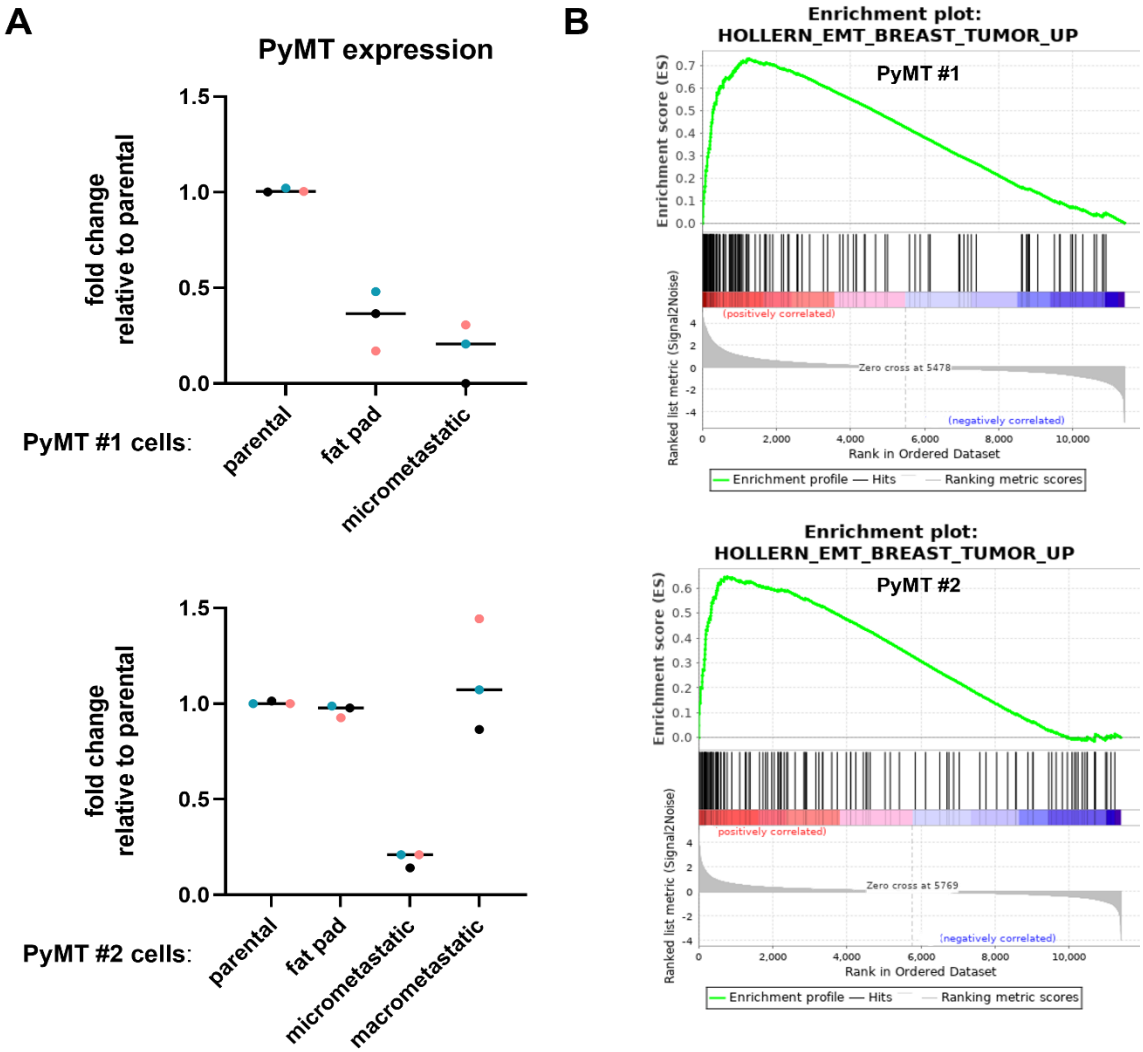
A
PyMT expression
fold change relative to parental
PyMT #1 cells:
parental
fat pad
micrometastatic
PyMT #2 cells:
macrometastatic
B
Enrichment plot:
HOLLERN_EMT_BREAST_TUMOR_UP
PyMT #1
PyMT #2
Enrichment score (ES)
Ranked list metric (Signal2Noise)
(positively correlated)
(negatively correlated)
Zero cross at 5478
Zero cross at 5769
Rank in Ordered Dataset
Enrichment profile — Hits
Ranking metric scores

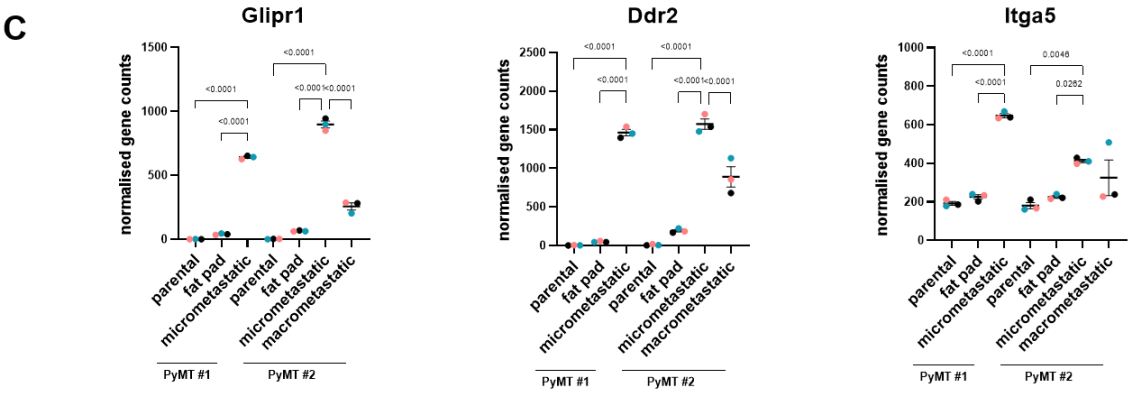
C
Glipr1
Ddr2
Itga5
normalised gene counts
parental
fat pad
micrometastatic
macrometastatic
PyMT #1
PyMT #2

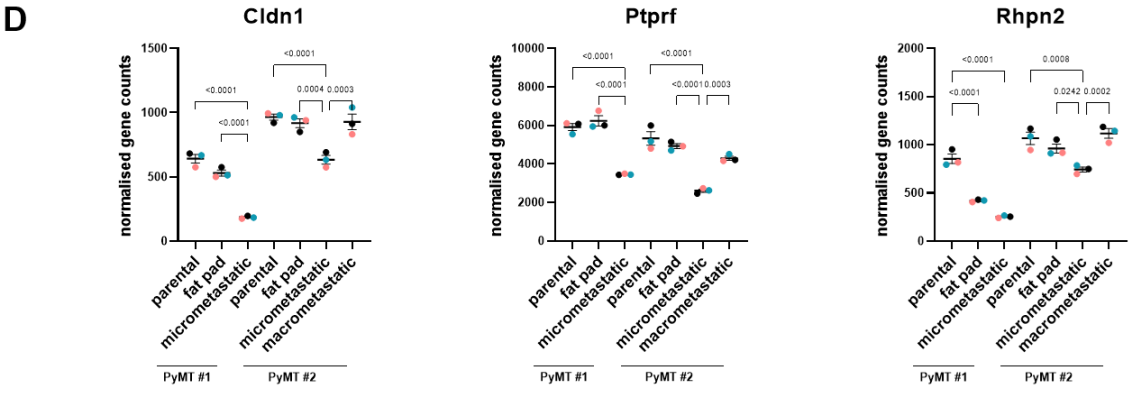
D
Cldn1
Ptprf
Rhpn2
normalised gene counts
parental
fat pad
micrometastatic
macrometastatic
PyMT #1
PyMT #2

Figure 3-4 PyMT-derived micrometastatic cells display an EMT phenotype.
(A) *Top panel*: Relative mRNA levels of PyMT (RT-qPCR) in PyMT#1-derived micrometastatic cells and primary tumour cells, all samples are normalised to ARPP P0 and are presented relative to parental, n=3 (coloured dots), mean ± SEM. *Bottom panel*: Relative mRNA levels of PyMT (RT-qPCR) in PyMT#2-derived micrometastatic, macrometastatic cells and primary tumour cells, all samples are normalised to ARPP P0 and are presented relative to parental, n=3 (coloured dots), mean ± SEM. (B) GSEA showing positive enrichment of Hallmark or curated gene set for EMT signature (HOLLERN_EMT_BREAST_TUMOR_UP gene set) in PyMT#1-derived (*top panel*) or PyMT#2-derived (*bottom panel*) micrometastatic cells as compared to primary tumour (parental, fat pad) lines. In both enrichment plots, the enrichment score demonstrates the degree to which genes upregulated in EMT are overrepresented at the top of the ranked list of genes present in our RNA-Seq data when we compare micrometastatic cells to primary tumour lines. (C) Normalised gene counts (RNA-Seq) of top hits (FC>1.5) belonging to the leading edge subset of the enrichment plot in (B), n=3 (coloured dots), values are mean ±SEM, one-way ANOVA, p-values are shown on the graph. (D) Normalised gene counts (RNA-Seq) of top hits (FC>1.5) belonging to the leading edge subset of the enrichment plot for genes downregulated in EMT (plots are not shown), n=3 (coloured dots), values are mean ±SEM, one-way ANOVA, p-values are shown on the graph.

3.2.5 Metastatic cells maintain E-cadherin expression, whilst displaying mesenchymal-like traits

Given the mesenchymal gene expression profiles we observed in the lung micrometastatic cell lines and the functional involvement of E-cadherin at multiple steps of metastasis (Na et al., 2020), we sought to examine its protein expression across the panel of PyMT-derived cell lines. To this end, we seeded cells onto gelatin-coated plates and used immunofluorescence to visualise E-cadherin. This indicated that the E-cadherin protein was expressed in both sets (PyMT#1 and PyMT#2) of our established lines (Figure 3-5A). Quantitative analysis of E-cadherin cytoplasmic levels showed that normal mammary epithelial cells (NMuMG) expressed higher levels compared to PyMT-derived cell lines (Figure 3-5B), which is consistent with its well-known tumour suppressor role (Behrens et al., 1989; Vleminckx et al., 1991). Micrometastatic cells maintained E-cadherin expression at significantly lower levels compared to that observed in parental cells (and marginally lower to the ones seen in fat pad derived cells). Intriguingly, macrometastatic and parental cells had similar expression levels of E-cadherin (Figure 3-5B). These observations reinforce the notion that lung micrometastatic cells acquire a mesenchymal-like phenotype (partial EMT), while maintaining some epithelial characteristics.

It has been recently shown that TGFβ-induced EMT morphological changes of PyMT-derived cells are accompanied by cadherin switching (Saxena et al., 2018). Hence, we were interested in assessing cell morphology in an unbiased automated manner. To achieve this, we stained our cells with HCS CellMask and found that all PyMT-derived cell lines were less round than NMuMG (Figure 3-5C), which

displayed a typical cobble stone-like epithelial morphology. In PyMT#1 cells, we found that both fat pad and micrometastatic cells were less round than parental cells, while both macro- and micro- metastatic PyMT#2 cells showed a reduction in roundness relative to primary tumour derived lines (Figure 3-5C). Although seemingly contradictory, these findings reflect the morphological heterogeneity of our PyMT-derived lines on a cell population level, and are in line with a previous report supporting that EMT related morphological changes precede downregulation of E-cadherin (Maeda et al., 2005).

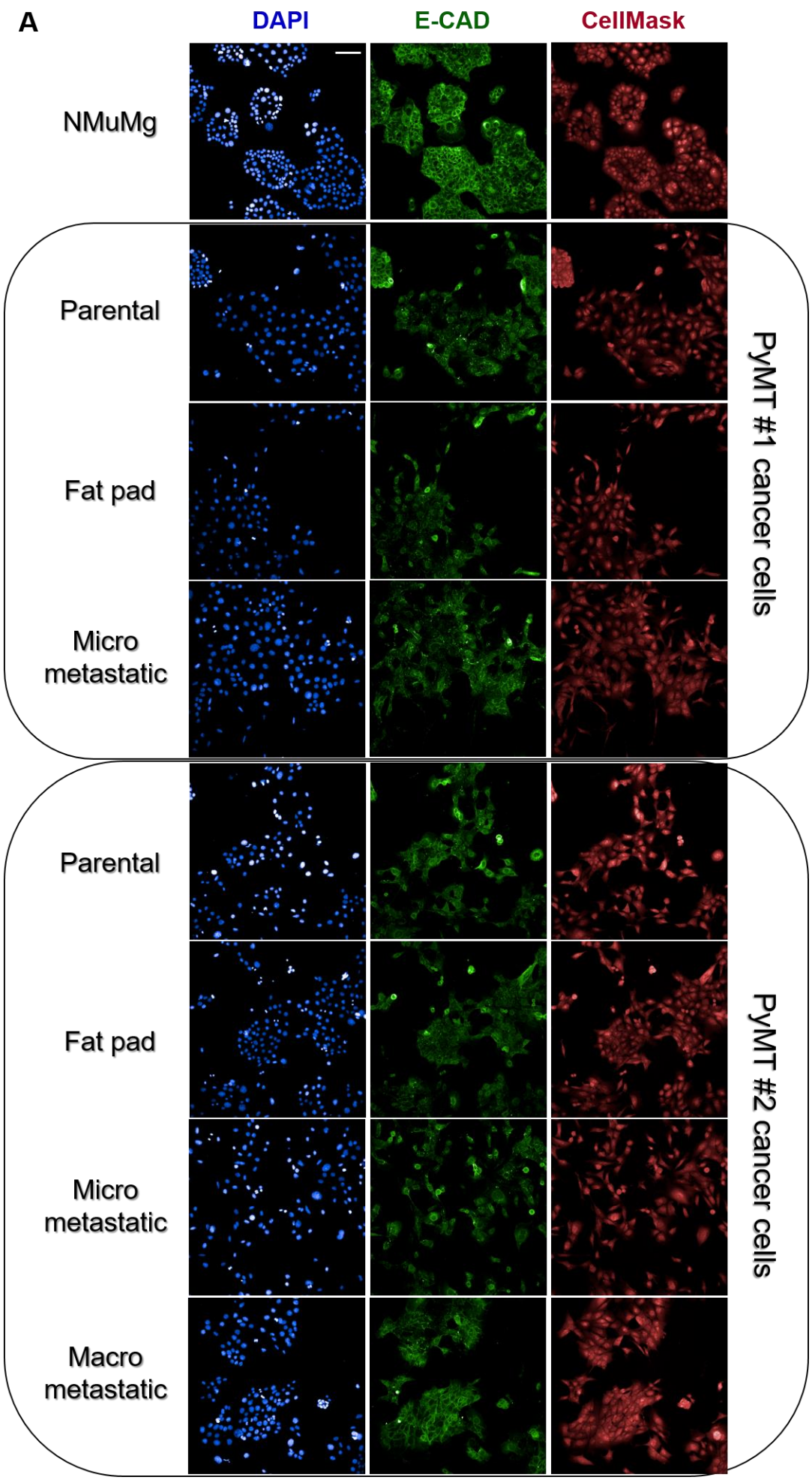
A
DAPI
E-CAD
CellMask
NMuMg
Parental
Fat pad
Micro metastatic
PyMT #1 cancer cells
Parental
Fat pad
Micro metastatic
Macro metastatic
PyMT #2 cancer cells

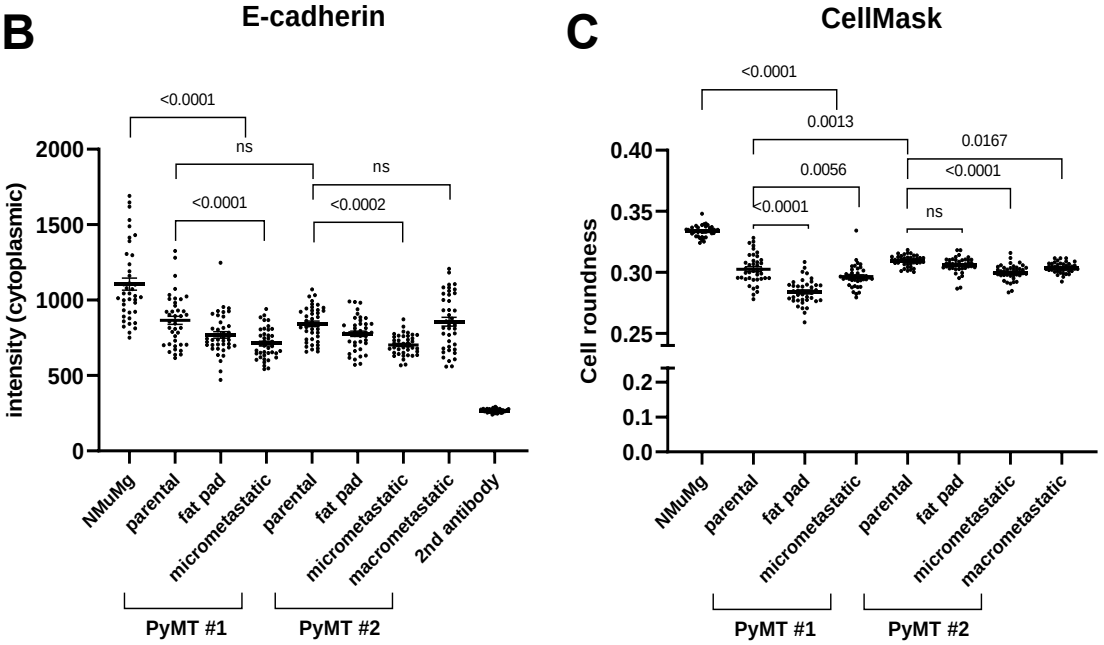

Figure 3-5 PyMT cells maintain E-cadherin expression, while exhibiting mesenchymal-like traits.
(A) NMuMg (normal mouse mammary epithelial cells), parental, fat pad, micro- and macro-metastatic cancer cell lines (PyMT#1 and PyMT#2) were seeded on gelatin-coated glass bottom dishes and fixed with 4% PFA following 48 hours of culture. E-cadherin (green) and CellMask (red) were visualised by immunofluorescence (20X magnification, Opera Phenix Plus High-Content screening confocal microscope). Scale bar, 100μm. Columbus Image Data Storage and Analysis System (PerkinElmer) was used to quantify (B) the mean cytoplasmic intensity levels for E-cadherin staining and (C) calculate the width to length ratio on a cell-by-cell basis. A decrease in this ratio indicates a decrease in cell roundness. Values are mean ± SEM, n=40 fields of view/cell line. Ordinary one-way ANOVA, p values are depicted on the graphs, ns; not significant. The acquisition and analysis of these images were performed in collaboration with Lynn McGarry and Madeleine Moore, CRUK Beatson Institute, Glasgow.

3.2.6 Metastatic cells extend long invasive protrusions when plated onto cell-derived matrices

The first crucial steps for metastatic dissemination are the breaching of the basement membrane followed by invasive migration cancer cells into the surrounding tissue, and this can be dictated by both cell-intrinsic and extrinsic factors present in the microenvironment (Sahai, 2005). Previous experiments focused on characterising intrinsic properties of our isogenic lines. To explore how primary and metastatic cells behave in a 3D microenvironment that recapitulates that of the fibrillar extracellular matrix (ECM) which surrounds tumours, we seeded PyMT-derived cells onto cell-derived matrices (CDM) (Cukierman et al., 2001) deposited by telomerase-immortalised fibroblasts (TIFs), and used time-lapse microscopy to assess their migratory capacity (Figure 3-6A). We found that, in both sets of PyMT-derived cells, those harvested from lungs extended longer invasive pseudopods (50-60μm) as they migrated through CDM than did cells from

primary PyMT tumours (35-40μm) (Figure 3-6B, C). Of note, we observed increased pseudopod length in PyMT#1 fat pad cells compared to parental, but still reduced length relative to their matched micrometastatic cells (Figure 3-6B). These data suggest that lung metastatic cells display enhanced migratory capacity on CDM compared to cells from primary mammary tumours.

So far, we have shown that PyMT-derived macrometastatic cells share some similarities with micrometastatic lines in regard to growth rate (Figure 3-3), maintenance of epithelial characteristics (E-cadherin expression, Figure 3-5) and enhanced migratory capacity (Figure 3-6), whereas they are transcriptionally distinct from each other, a phenotype which is associated with programs of epithelial-mesenchymal plasticity (Figure 3-4). We decided, though, to focus on the micrometastatic lines for the remainder of our study. This was, in part, dictated by the fact that we were only able to generate a single example of a macrometastatic line. Moreover, we believe that micrometastatic cells may possibly represent earlier events in the metastatic cascade that are important for the establishment of clinically overt metastases.

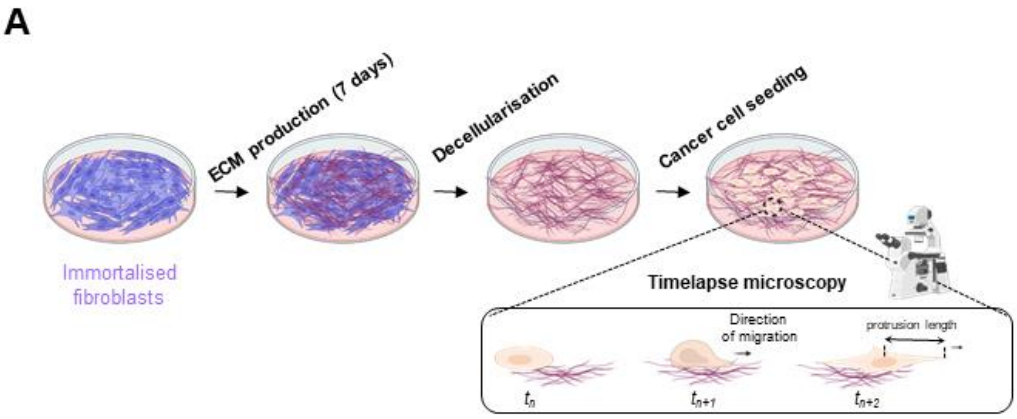
A
ECM production (7 days)
Decellularisation
Cancer cell seeding
Immortalised fibroblasts
Timelapse microscopy
Direction of migration
protrusion length
t_n
t_{n+1}
t_{n+2}

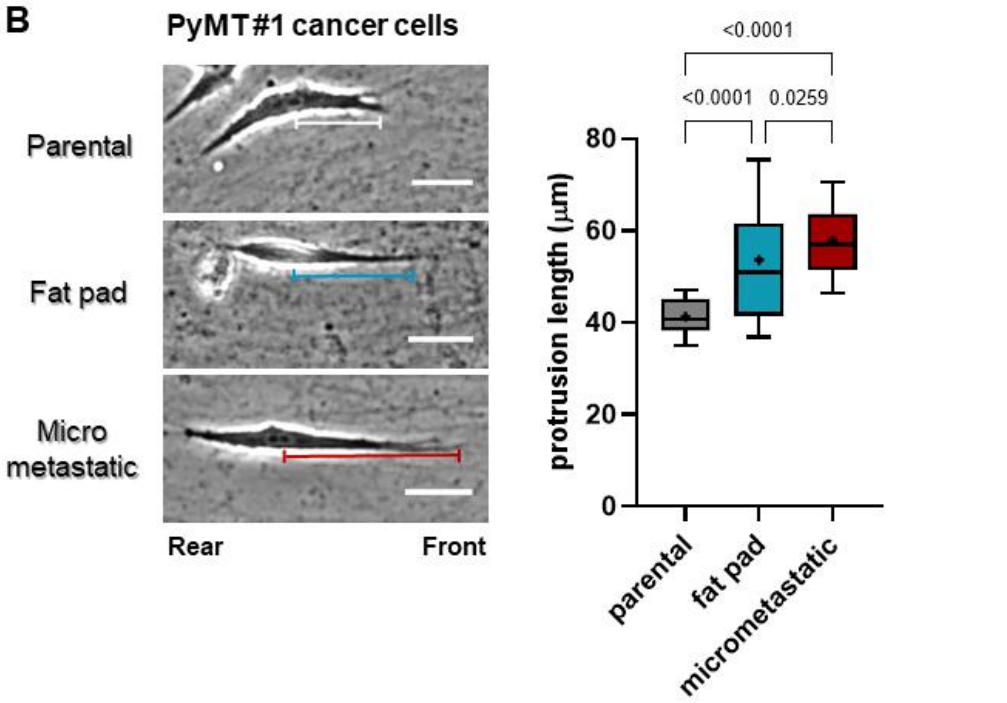
B
PyMT#1 cancer cells
Parental
Fat pad
Micro metastatic
Rear
Front
<0.0001
<0.0001
0.0259
protrusion length (μm)
0
20
40
60
80
parental
fat pad
micrometastatic

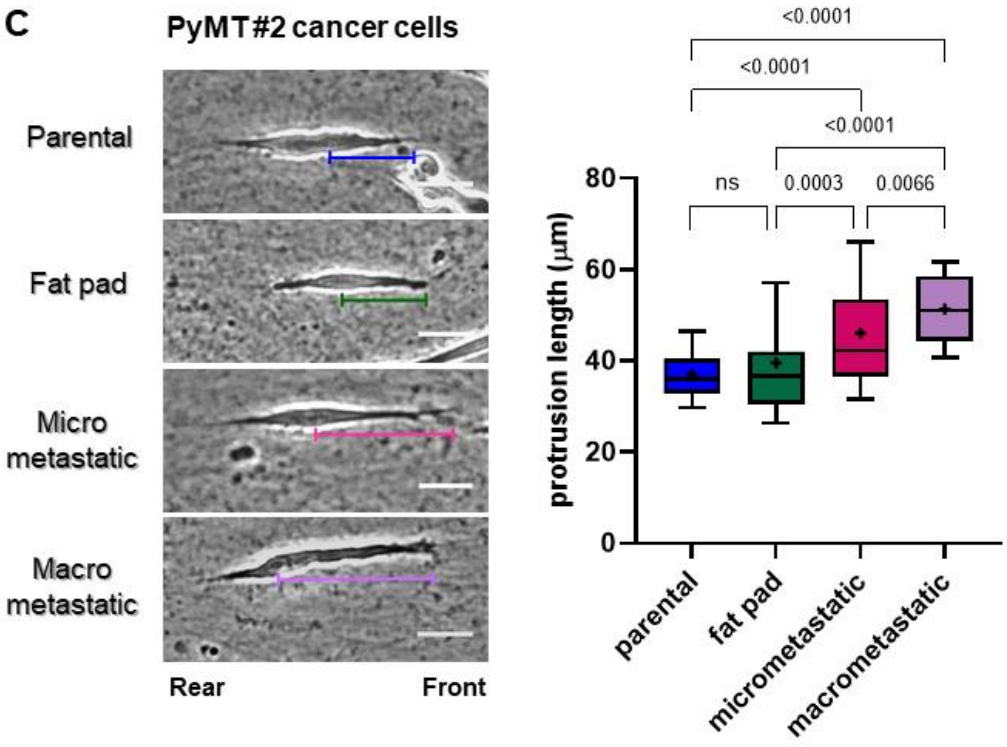
C
PyMT#2 cancer cells
Parental
Fat pad
Micro metastatic
Macro metastatic
Rear
Front
<0.0001
<0.0001
<0.0001
ns
0.0003
0.0066
protrusion length (μm)
0
20
40
60
80
parental
fat pad
micrometastatic
macrometastatic

Figure 3-6 Lung metastatic cells extend long protrusions while migrating on cell derived matrices.
(A) Schematic representation of the cell derived matrix (CDM) assay. Telomerase immortalised fibroblasts (TIFs) were plated to confluence on gelatin-coated plates, and then cultured for 7 days to produce ECM, followed by removal of cells using a triton containing buffer (CDM was generated by Jillian Murray, Molecular Technology Services, CRUK Beatson Institute, Glasgow). Parental, fat pad, micro- and macro-metastatic cells (PyMT#1 and PyMT#2) were seeded on CDM, which served as a substrate for cell migration. Time-lapse microscopy was used to assess the migratory capacity of these cancer cell lines, and ImageJ was used to measure the length of protrusions that cells extend in the direction of migration. (B) Left panel: Representative bright-field images (scale bar, 30μm) of PyMT#1-derived parental, fat pad and micrometastatic cells indicating the rear and front of cells according to the direction of movement. Right panel: The distance from the nucleus to cell front (protrusion length) was measured using ImageJ software. Whisker plots (10-90 percentile), + indicates the mean; n=96 cells assessed from 3-5 biological replicates (except fat pad cells where the length was assessed from one replicate), one-way ANOVA with Tukey's multiple comparison test, p-values are shown on the graph. (C) Left panel: Representative bright-field images (scale bar, 30μm) of PyMT#2-derived parental, fat pad, micro- and macro- metastatic cells indicating the rear and front of cells according to the direction of migration. Right panel: The distance from the nucleus to cell front (protrusion length) was measured using ImageJ. Whisker plots (10-90 percentile), + indicates the mean; n=96 cells assessed from 3 biological replicates (except fat pad and micrometastatic cells where the length was assessed from one replicate), one-way ANOVA with Tukey's multiple comparison test, p-values are shown on the graph, ns: not significant (p>0.05).

3.2.7 Micrometastatic cells are highly invasive in an organotypic microenvironment

An excellent way to assess cancer cell invasiveness in complex microenvironments is to use 'organotypic' plugs in which native type-I collagen has been conditioned for several days by fibroblasts (Timpson et al., 2011). We generated plugs of type-1 collagen containing telomerase-immortalised human fibroblasts (TIFs) and allowed these to pre-condition for 3-4 days. We then plated our PyMT#1 cell lines onto the top of these pre-conditioned plugs and allowed them to invade into the plug, as depicted in Figure 3-7A. This indicated that parental and fat pad cells were poorly and moderately invasive respectively, and largely remained on top, or near the top, of the plug. Conversely, micrometastatic cells invaded extensively into the plug 6 days post seeding (Figure 3-7B). We confirmed that the number of cells present either in, or on, the plug did not differ among conditions (Figure 3-7C) indicating that the growth rate of primary tumour and micrometastatic cells did not differ in these microenvironments. However, micrometastatic cells appeared to invade much further into the plug (attaining a mean invasion distance of 222μm) than did parental (184.3μm) or fat pad (202.6 μm) cell lines (Figure 3-7D). Consistently, the majority of parental (~57%) and fat pad (~40%) cells resided on the upper portion of the plug without being able to invade (distance from invasion baseline≤0), while this was not the case for micrometastatic (~27%) cells that very efficiently invaded throughout the collagen (Figure 3-7E). These

data indicate that lung micrometastatic cells are highly invasive into a collagen organotypic environment.

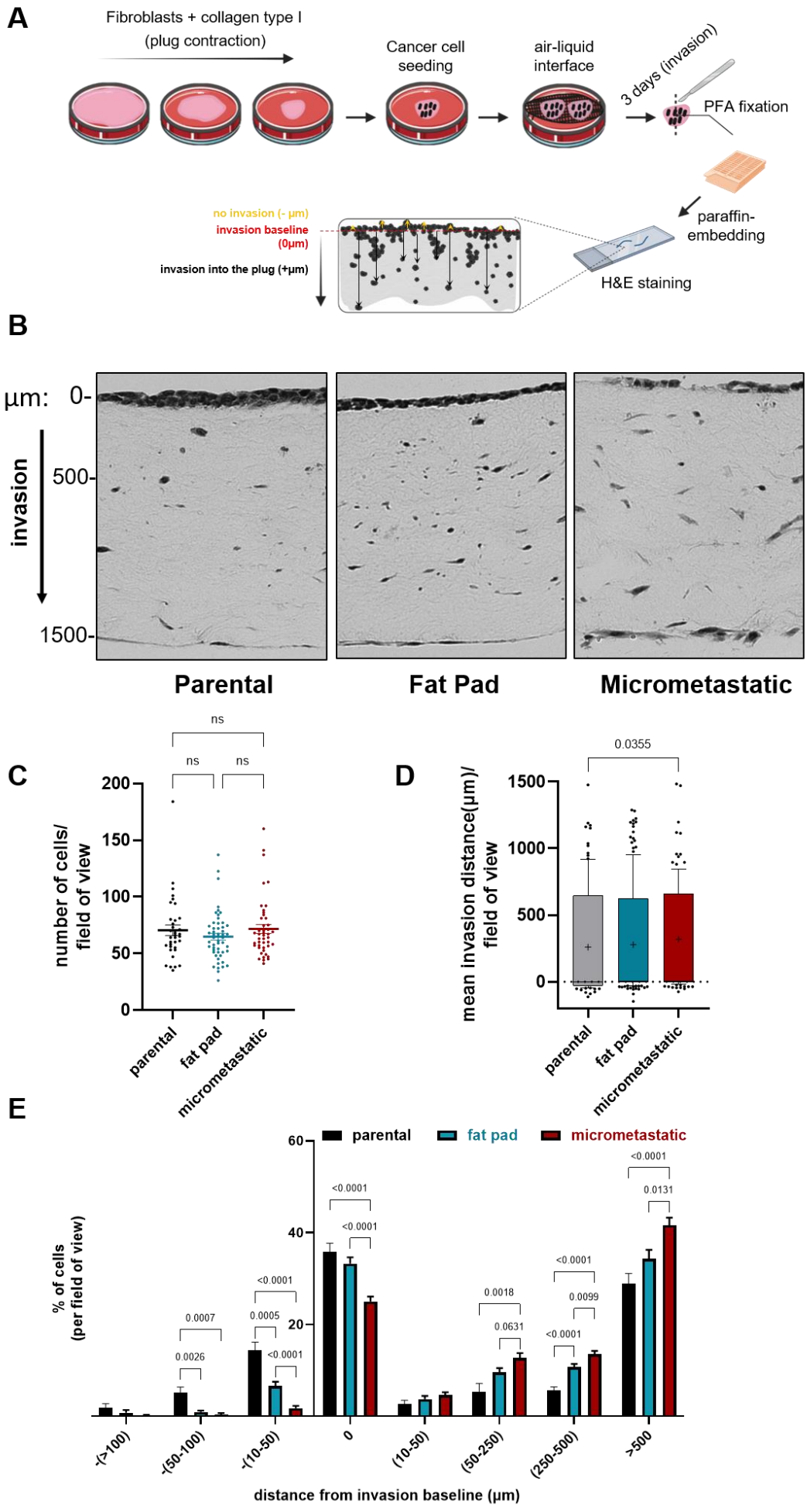
A
Fibroblasts + collagen type I
(plug contraction)
Cancer cell
seeding
air-liquid
interface
3 days (invasion)
PFA fixation
paraffin-
embedding
H&E staining
no invasion (- µm)
invasion baseline
(0µm)
invasion into the plug (+µm)
B
µm:
0-
500-
1500-
invasion
Parental
Fat Pad
Micrometastatic
C
number of cells/
field of view
ns
ns
ns
parental
fat pad
micrometastatic
D
mean invasion distance(µm)/
field of view
0.0355
parental
fat pad
micrometastatic
E
% of cells
(per field of view)
parental
fat pad
micrometastatic
0.0007
0.0026
0.0005
<0.0001
<0.0001
<0.0001
<0.0001
0.0018
0.0631
<0.0001
0.0099
<0.0001
<0.0001
0.0131
-(>100)
-(50-100)
-(10-50)
0
(10-50)
(50-250)
(250-500)
>500
distance from invasion baseline (µm)

Figure 3-7 Micrometastatic cells are highly invasive in a collagen organotypic environment. (A) Schematic representation of the collagen I organotypic invasion assay. Organotypic plugs were generated allowing polymerisation of collagen type I in the presence of TIFs. Once contracted well enough to fit 24-well plates, PyMT#1-derived parental, fat pad and micrometastatic cells were seeded on top of these plugs and cultured for 2 days. Plugs were then placed onto metallic grids to create an air-liquid interface that promotes invasion of cancer cells into the collagen plugs towards the FBS-containing media added below the grids. After 3 days of invasion, plugs were fixed in 4% PFA, paraffin-embedded and stained for haematoxylin and eosin (H&E). Images of stained plug cross-sections were acquired using a brightfield Leica microscope, and the distance between cancer cells and invasion baseline was measured for each cell per field of view (ImageJ). (B) Organotypic plugs overlaid with PyMT#1-derived parental (left panel), fat pad (middle panel) and micrometastatic (right panel) cell lines. Following 72 hours post seeding, plugs were placed onto grids in separate culture dishes containing full media (2 plugs/grid/condition). Tumour cells were allowed to invade for 3 days, followed by fixation and H&E staining. (C) Total number of cells tracked (H&E) per field of view for collagen plugs that were seeded with parental, fat pad and micrometastatic cells, n=36-52 fields of view/cell line, ANOVA Kruskal-Wallis test, ns; not significant. (D) The mean distance (μm) between each cancer cell and the invasion baseline (depicted as dotted line at y=0) per field of view was determined using ImageJ. Whisker plots (10-90 percentile), + indicates the mean; n=36-52 fields of view/cell line, ANOVA Kruskal-Wallis test, p value is shown on the graph. (E) Distribution (expressed as % of cells) of the distance between cancer cells and invasion baseline (0 μm) per field of view for collagen plugs overlaid with parental, fat pad and micrometastatic cells. A negative value in distance intervals indicates that cells do not invade into the plugs and lag behind the invasion baseline, while a positive value denotes the actual invasion distance into the plugs as measured by ImageJ. Values are mean ± SEM, n=36-52 fields of view/cell line (two biological replicates for fat pad and micrometastatic cells and one replicate for parental cells). Mixed effects ANOVA with Tukey's multiple comparison test, p values are depicted on the graphs.

3.2.8 Elevated rates of receptor recycling in metastatic cells

Receptor trafficking, including the internalisation and recycling of integrins, is central to the manifestation of migratory and invasive phenotypes in cancer cells (Jacquemet, Humphries, et al., 2013; Paul, Jacquemet, et al., 2015; Wilson et al., 2018; Hamidi & Ivaska, 2018). Numerous studies have reported that Rab GTPase dependent recycling of $\alpha_5\beta_1$ integrin promotes invasiveness via a number of mechanisms including its mobilisation to and/or retention in cell protrusions (Caswell et al., 2007; Rainero et al., 2012), altered growth factor signalling (Caswell et al., 2008), as well as increased RTK recycling (Muller et al., 2009). Transcriptional upregulation of ITGA5 in lung micrometastatic cells (in 3.2.4) led us to examine the expression of $\alpha_5\beta_1$ protein in PyMT#1 cell panel, and this confirmed higher total protein levels of α_5 in micrometastatic cells compared to parental, while there were no differences in total β_1 levels (Figure 3-8A). We further assessed the rates of recycling of a number of membrane receptors, and found the rates at which the internalised fraction of α_5, β_1 and TfnR returned to the plasma membrane in micrometastatic cells, were strongly increased compared to the rates observed in parental cells (Figure 3-8B, C, D). These data show that micrometastatic cells present enhanced receptor recycling, which is consistent with their enhanced migratory and invasive phenotype.

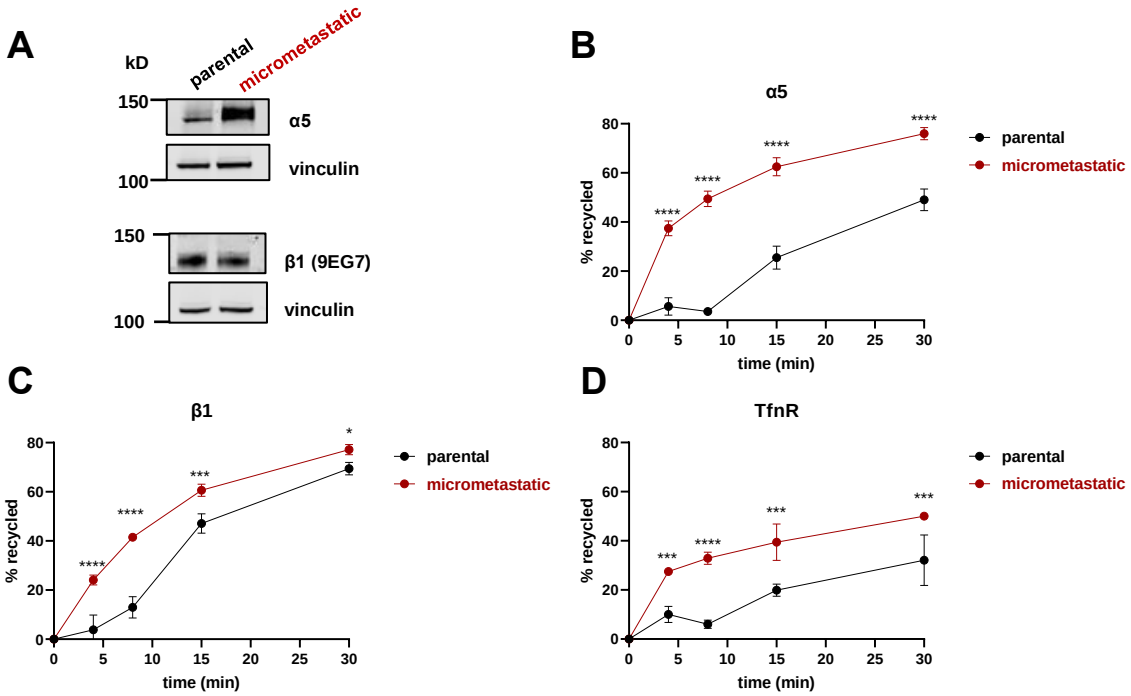

Figure 3-8 Breast cancer derived metastatic cells display increased rates of surface receptor recycling.

(A) Parental and micrometastatic cells were plated to 80-90% confluence, lysed into RIPA buffer, and subjected to western blotting to assess total protein levels of integrin α_5 and β_1(9EG7), and vinculin was used as loading control. (B) Parental and micrometastatic cells were seeded in 10cm dishes and cultured for 16 hours. Cells were then surface-labelled with Sulfo-NHS-SS-Biotin at 4˚C, warmed to 37˚C for 30 minutes to allow internalisation of the tracer, while the remaining label at the cell surface was reduced. The internalised biotin fraction was chased by incubating the cells at 37˚C for the indicated time points. The proportion of integrin α_5, (C) β_1 and (D) transferrin receptor (TfnR) were determined by ELISA. Values are mean ± SD, n=1 (3 technical replicates), ANOVA, * p-value<0.05, *** p-value<0.001, ****p-value<0.0001are shown on the graph.

3.3 Discussion

Although the 5-year relative survival of breast cancer patients with localised disease has drastically increased over the last four decades in the UK (Cancer Research UK, 2014), metastatic recurrence remains the main cause of cancer-related death (Eccles & Welch, 2007; Bray et al., 2018). Breast cancer subtypes not only dictate metastatic organotropism (Kennecke et al., 2010), but also predict the risk of relapse over time (Klein, 2020). If recurrence occurs, metastases are generally observed within 5 years post-surgery in young hormone receptor-negative breast cancer patients, and beyond 8 years after surgery in patients with hormone receptor-positive subtype (Copson et al., 2013). These findings, in combination with the previously reported (in 3.1) high incidence rates of lung metastasis in breast cancer patients, highlight the pressing need to study the mechanisms that mammary tumour cells employ to successfully colonise the lungs. Transcriptome profiling indicates that PyMT tumours group with the luminal B subtype (Pfefferle et al., 2013), while careful histopathological examination of PyMT tumours revealed overexpression of Her2 and loss of oestrogen (ER) and progesterone receptors (RP) during disease progression in the mice (Lin et al., 2003). Taken together, these studies indicate that the MMTV-PyMT model can faithfully recapitulate human mammary carcinoma progression analogous to luminal/HER2 and HER2-enriched subtypes, and also other traits (such as loss of steroid receptors) that have been attributed to human breast cancers with poor prognosis (Lapidus et al., 1998). Using PyMT-derived cancer cells in a syngeneic transplantation and resection model, we have established and characterised lung metastatic cell lines, and compared them with their isogenic counterparts from the primary tumours from which they were derived in order to understand cellular changes that may occur during the process of metastasis (Figure 3-1).

The successful use of adjuvant systemic therapies in targeting disseminated micrometastases (Klein, 2020) has led to substantial decrease in mortality from early breast cancer (Abe et al., 2005; Albain et al., 2012). However, after establishment of metastatic disease (macrometastases), these strategies usually fail, and the differential response of primary tumours and distant metastases has been partially attributed to a continuous evolution of heterogeneous cancer clones resistant to therapy (Greaves & Maley, 2012). However, many studies indicate little transcriptomic divergence between primary tumours and their metastases

(Lawson et al., 2015), so the resistance of disseminated cells to therapies may be owing to 'cytological' evolution that has been dictated by the microenvironments of metastatic target organs. Thus, several efforts have been made to generate organ-specific isogenic metastatic breast cancer cell lines and characterise these phenotypic intricacies (Kang et al., 2003; Minn et al., 2005; Winnard et al., 2017, 2020). In one of these studies, researchers identified differential morphologies, and similar growth rates for lung metastatic and primary tumour cell lines (MDA-MB-435 derived metastatic cells) (Winnard et al., 2017). Likewise, we were able to discern a morphological shift in micrometastatic cells towards a mesenchymal-like phenotype when compared to parental and fat pad derived cells that exhibited a more epithelial, cobblestone-like morphology (Figure 3-2). Also, we did not observe pronounced and maintained differences in proliferation rates of PyMT-derived lung metastatic cells compared to those derived from the primary tumour (Figure 3-3). However, all the aforementioned published studies established isogenic metastatic lines by using xenograft transplants, meaning that tumour cells were grown in immunocompromised hosts. It has become clear that primary tumours shape a favourable microenvironment, termed the pre-metastatic niche, for future metastatic seeding through a complex interplay between tumour, bone marrow-derived and lymphoid immune populations and stromal cells (Kaplan et al., 2005; Liu & Cao, 2016). We, therefore, believe, that our paired, isogenic primary tumour and micrometastatic cell lines generated using an aggressive tumour-type in immunocompetent FVB mice will be useful in identifying key adaptations to the early metastatic niche in which the immune system plays such an important role.

Controversy surrounds the role of EMT transition in metastasis (Williams et al., 2019). The first crucial step for metastatic dissemination is for cancer cells to acquire migratory and invasive properties that enable them to leave the primary site. These changes are usually accompanied by activation of transcriptional programmes akin to those invoked by cells undergoing EMT (Chaffer et al., 2016), although there is contradictory *in vivo* evidence depending on the cancer type and mouse model under investigation. Some studies have reported that the incidence of EMT-like events are very rare (0-5% of tumours) in tumours from MMTV-PyMT mice, and dispensable for the establishment of lung metastases (Trimboli et al., 2008; Fischer et al., 2015).Conversely, several studies have shown that MMTV-

PyMT luminal tumours present EMT-like features (Van Keymeulen et al., 2015; Ye et al., 2015, 2017; del Pozo Martin et al., 2015) associated with metastatic potential. Indeed, one of these studies underscores the importance of selecting appropriate Cre drivers for lineage tracing of carcinoma cells that have undergone EMT (Ye et al., 2017). Our data support the presence of EMT-like features in early metastasis, since GSEA analysis of differentially expressed genes identified an EMT signature in the micrometastatic cell lines (Figure 3-4B, C). In one of the studies that did not consider EMT-like phenotypes to contribute to metastases, authors reported that *ex vivo* expansion of PyMT cells resulted in progressive loss of E cadherin over ten consecutive passages, and shift into mesenchymal morphology due to TFG-β coming from the serum containing culture media (Fischer et al., 2015). However, we found that all our primary PyMT tumour and metastatic cell lines maintain E-cadherin expression over a prolonged period in culture (<20 passages), while displaying some mesenchymal-like traits (Figure 3-5). This observation is consistent with expression of E-cadherin in the distant metastases of breast cancer patients (Kowalski et al., 2003). It has been previously shown that morphological differences precede changes in expression of epithelial markers (Maeda et al., 2005), suggesting that differential expression/positivity of epithelial markers is feasible even if cancer cells have shifted towards a mesenchymal-like phenotype, further reinforcing the notion of epithelial-mesenchymal plasticity (Williams et al., 2019). Indeed, an independent study showed that lung metastases in the MMTV-PyMT display positivity for both epithelial and mesenchymal markers (Pastushenko et al., 2018).

One of the key characteristics of cancer cells is enhanced motility and invasion through the ECM (particularly the basement membrane), and dysregulation of genes modulating these processes correlates with metastasis (Sahai, 2005). Breast cancer cells migrate on and into fibroblast-derived 3D ECMs, that somewhat resemble the tumour stroma (Cukierman et al., 2001), by extending invasive protrusions (Dornier et al., 2017; Rabas et al., 2021). Interestingly, we found that metastatic lines from lung extended longer invasive protrusions, compared with cells derived from primary mammary tumours (Figure 3-6), indicating that metastatic cells generally display enhanced migratory traits. We further demonstrated the highly invasive behaviour of metastatic cells by establishing organotypic cultures in which native collagen I had been preconditioned by

fibroblasts (Figure 3-7). As previously described (Timpson et al., 2011), this 3D collagen plug assay closely resembles an *in vivo* ECM microenvironment, and examination of these plugs implies that tumour cells invade them both as groups and as single cells, perhaps reflecting continuous switching between more collective and mesenchymal modes of cell migration (Figure 3-7B,D). Taken together, all these findings suggest that micrometastatic cells have been selected throughout the steps of metastatic cascade to be more migratory and invasive compared to parental cells, and have acquired some more mesenchymal characteristics while retaining epithelial properties. Of note, cells derived from tumours resected from the fat pad tended to be slightly more invasive than parental cells(Figure 3-7E), which is consistent with previous reports showing that reintroduction of cancer cells into mice can render them more aggressive (Yano et al., 2016).

Since cells invading into 3D collagen matrices become dependent on a particular integrin receptor (adhesion-dependent ß1 clustering at the points of attachment with collagen fibres) (Friedl & Bröcker, 2000), we tested the hypothesis that altered integrin expression and trafficking might underlie the enhanced invasiveness of metastatic cells . Indeed, we found that metastatic cells expressed higher levels of ITGA5 mRNA and its product, α_5 protein. Although $ß_1$ integrin was not different (Figure 3-8A), this is consistent with increased expression of the $\alpha_5ß_1$ integrin heterodimer and in agreement with a previous study showing that elevated $\alpha_5ß_1$ integrin expression in MDA-MB-231 subclones enhanced invasiveness into a 3D collagen matrix through contractile forces (Mierke et al., 2011). We further demonstrated that metastatic cells display elevated recycling rates of $\alpha_5ß_1$ and TfnR compared to parental cells (Figure 3-8). This observation is consistent with the well documented role of $\alpha_5ß_1$ integrin and its recycling to promote cell migration and invasion in 3D microenvironments (Caswell et al., 2007, 2008).

In this chapter, we have phenotypically characterised a panel of isogenic matched primary tumour and metastatic PyMT-derived breast cancer cell lines which were established following resection of orthotopic mammary tumours and development of spontaneous pulmonary lesions respectively. Despite similar proliferation rates, lung metastatic cells display a range of mesenchymal-like characteristics by comparison with primary tumour-derived lines which exhibit a cobble stone-like epithelial morphology. Interestingly, this is predominantly evident in metastatic

cells derived from lung micrometastases, while macrometastatic cells more resemble their matched primary tumour-derived cells in epithelial characteristics. We have also shown that metastatic cells exhibit highly migratory and invasive phenotypes in physiologically relevant microenvironments (CDM and collagen-rich organotypic environment), which is also paralleled by increased recycling rates of integrin $\alpha_5\beta_1$ and other receptors. In addition to these processes that favour metastatic dissemination, cancer cells can acquire metabolic adaptations that further contribute to their invasive characteristics and/or help them counteract adverse environments on their way to metastasise distant organs. The next chapter will, therefore, explore whether lung micrometastatic cells have acquired such metabolic traits that could discern them from matched primary tumour-derived cell lines.

Chapter 4 Metabolic adaptations of cells from lung micrometastases of the MMTV-PyMT model of mammary cancer

4.1 Introduction

Cancer cells change their metabolism to overcome limitations imposed by (epi)genetic and microenvironmental cues during disease onset and progression (Cairns et al., 2011). Almost a century after the seminal observation of the 'Warburg effect', where tumour cells are able to switch their energy production from oxidative phosphorylation (OXPHOS) to aerobic glycolysis (Warburg, 1925; WARBURG, 1956), the role of glycolysis and glutaminolysis in providing metabolites to fuel tumour growth has now been well established. These processes not only shunt nutrients into metabolic pathways to support ATP generation and biosynthesis of macromolecules in the face of rapid cell growth, but also contribute to the fine tuning between redox status maintenance and replenishment of TCA intermediates (anaplerosis) (DeBerardinis et al., 2008). A growing body of evidence has revealed that cancer patients exhibit altered profiles of circulating and intratumoural metabolites (Asiago et al., 2010; Jobard et al., 2014; Terunuma et al., 2014; Dai et al., 2018), and this has led to intensive efforts to identify targetable metabolic dependencies of cancer cells (Vander Heiden, 2011). However, very little is known about the mechanisms linking these observations to altered primary tumour metabolism (Dornier et al., 2017), and how these metabolic changes could possibly affect cellular processes that drive invasion and early metastatic events.

Only recently, systematic studies have helped us appreciate that metastasising cancer cells continuously undergo metabolic adaptations to counteract adverse environments along the various steps of the metastatic cascade (Bergers & Fendt, 2021). These adaptations are shaped by the tumour type and cancer cell-of-origin, but also by differences in the metabolic microenvironments between primary and metastatic sites; especially by factors that influence nutrient and oxygen availability (Faubert et al., 2020). Moreover, the metabolic re-wiring acquired by metastasising cells can influence invasive and metastatic behaviour in a number of ways. For instance, glutamate derived from glutaminolysis of glutamine can be secreted by primary breast cancer cells via the cystine antiporter xCT, leading to

auto- and para- crine activation of the GRM3 metabotropic glutamate receptor which, in turn, upregulates Rab27-dependent recycling of the transmembrane matrix metalloproteinase (MT1-MMP) to promote invasiveness of breast cancer cells (Dornier et al., 2017). On the other hand, when metastasising cells detach from the ECM and enter the circulation, they encounter a more oxidative environment, and they can counteract oxidative stress by clustering together. This clustering behaviour is thought to generate a more hypoxic microenvironment and assist with the clearance of damaged mitochondria (Labuschagne et al., 2019). The ability of some cancer cells to cope with altering oxidative microenvironments on the road to metastasis can increase their need to depend on glycolysis for energy production, and this can limit their capacity to metastasise to the lungs (Blomme et al., 2017; Labuschagne et al., 2019). Then, when cells leave the circulation and reach their metabolic target organ, nutrient availability at this site can dictate further metabolic re-wiring. In the lung, pyruvate availability is increased whereas glutamine concentrations tend to be less than those found in the circulation. Thus when metastasising breast cancer cells leave the circulation for the lung, they have been found to deploy a pyruvate carboxylase-dependent mode of TCA cycle function to efficiently perform anaplerosis (Christen et al., 2016). Furthermore, increased pyruvate levels in the lung have been shown to stimulate the activity of collagen prolyl-4-hydroxylase – an enzyme which is essential for type-I collagen production - via transamination reactions to generate α-ketoglutarate (Elia et al., 2019). Lastly, the availability of non-essential amino acids, such as serine, glycine and proline, in the microenvironment can shape the permissiveness of the metastatic niche. In particular, the scarcity of serine and glycine in the brain environment has been shown to create a serine synthesis pathway dependence for breast cancer-derived brain metastases, which can be treated by targeting the rate limiting enzyme (PHGDH) of serine biosynthesis (Ngo et al., 2020).

In chapter 3 we generated isogenic lines derived from primary mammary tumours and matched lung metastases and demonstrated that they have different invasive behaviour. In this chapter, we seek to determine whether cells from metastases are metabolically distinct from those from the matched primary tumours, with the aim of understanding whether the altered metabolism and invasive behaviour of cells from metastases might be mechanistically linked.

4.2 Results

4.2.1 Mapping the metabolic landscapes of cells from micrometastases and primary tumours

To determine whether micrometastatic cells are metabolically different from PyMT-derived primary tumour cells, we employed a targeted analysis of the steady-state metabolome using liquid chromatography-mass spectrometry (LC-MS) (method as previously described (Voorde et al., 2019)). A ranked heatmap of differences in the intracellular metabolite abundances of primary tumour (parental, fat pad) and micrometastatic cells indicated that a number of metabolites significantly differed between the two (Figure 4-1A, B). Intracellular levels of proline were substantially elevated in micrometastatic cells (Figure 4-1B), in line with a previous report showing that proline catabolism supports metastatic outgrowth *in vitro* and *in vivo* (Elia et al., 2017). Most interestingly, however, we found that glutathione levels (both the reduced - GSH - and oxidised – GSSG - forms) were downregulated (by almost 40%) in metastatic cells (Figure 4-1B). At first glance, this was seemingly contradictory to published data reporting that elevated glutathione promotes metastasis in melanoma and liver cancer (Carretero et al., 1999; Huang et al., 2001). However, in the MMTV-PyMT model the glutathione pathway has been shown to be essential only for tumour initiation, and becomes dispensable after tumour establishment due to alternative antioxidant pathways (Harris et al., 2015). We further noticed that the levels of urea cycle intermediates (citrulline, ornithine, arginine, arginosuccinate) were also consistently decreased in metastatic cells, a finding that is consistent with the well-documented reprogramming of urea cycle in different types of cancer to support anabolic needs (Keshet et al., 2018). Taken together, these data reveal that lung micrometastatic cells have rewired their metabolism compared to the cells derived from primary mammary PyMT tumours, and that two key feature of this are reduced intracellular glutathione and increased proline concentrations.

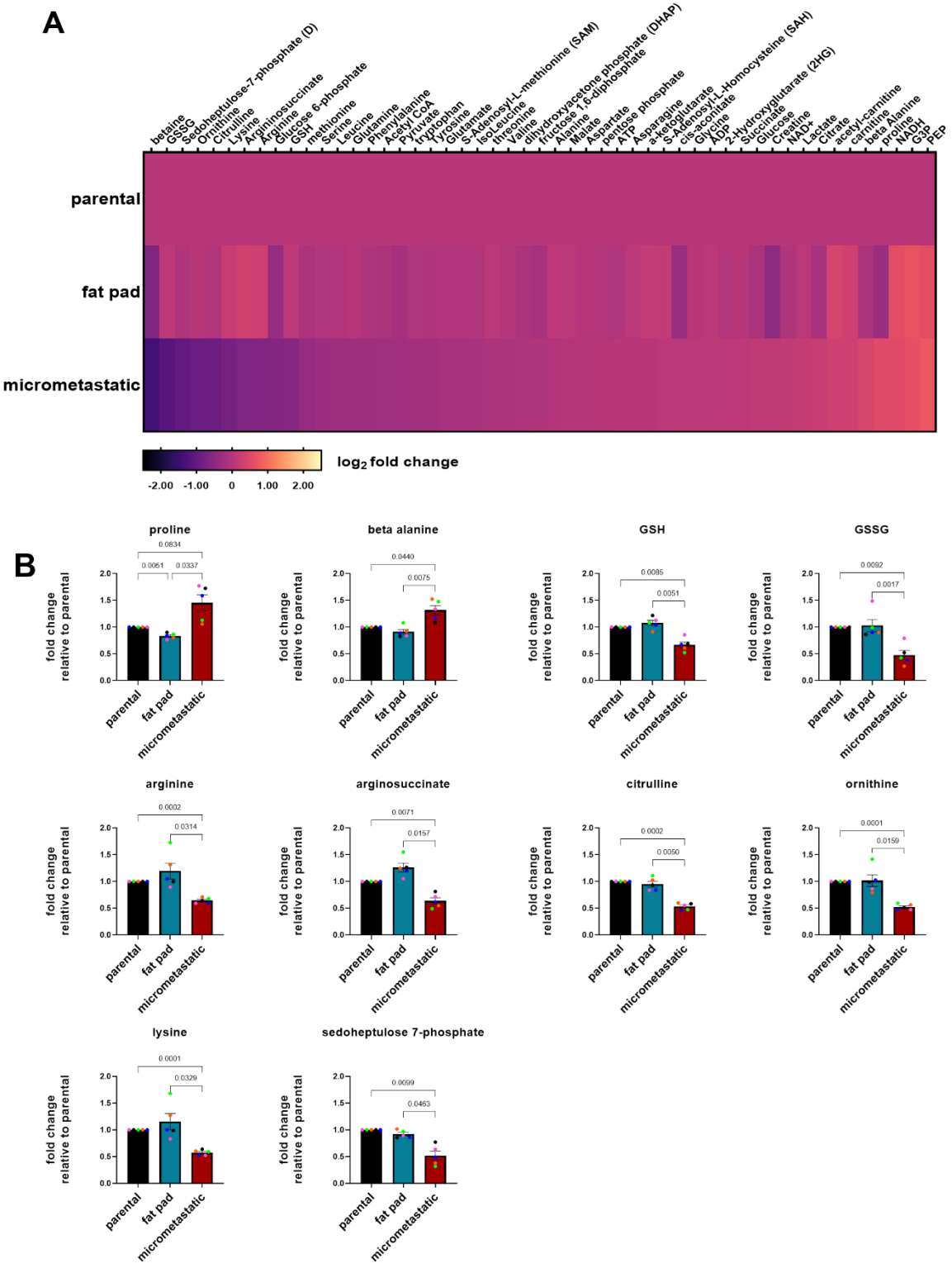

Figure 4-1 Targeted analysis of polar metabolites to compare the metabolic landscapes of matched primary tumour and micrometastatic cells.
(A) Targeted metabolomics of intracellular metabolites in PyMT#1 cell lines derived from primary mammary tumours (parental, fat pad cells) and lung metastases (micrometastatic cells). The heatmap displays ranked log_2 fold change values of metabolite intensities (normalised to cell number) relative to parental cells, n=5 biological replicates. (B) Abundance of polar metabolites (normalised to cell number and expressed as a fold change relative to parental cells) significantly different in micrometastatic cells and primary tumour derived cell lines, n=5 (coloured dots), values are mean ±SEM, repeated measures one-way ANOVA, p-values are shown on the graph.

4.2.2 Reduced and oxidised glutathione levels are downregulated in metastatic cells

Glutathione is an abundant antioxidant in the cytosol, with its reduced form (GSH) being 10- to 100-fold higher in concentration than its oxidised form (GSSG) under physiological conditions (Bansal & Celeste Simon, 2018). The ratio of GSH to GSSG is widely used as an indicator of cellular redox state and is tightly regulated by glutathione reductase (Townsend et al., 2003). In our targeted metabolomics approach (described in 4.2.1), we found that total glutathione levels decreased in metastatic cells. However, determination of glutathione levels is challenging as it suffers from autoxidation of GSH at the sulfhydryl group leading to disulphide bond formation and a consequent overestimation of GSSG (Sun et al., 2020). To circumvent this problem, and further validate our findings, we added the thiol alkylating agent N-ethylmaleimide (NEM) (Figure 4-2A), a highly cell-permeable agent that reacts with GSH (but not GSSG), prior to metabolite extraction (Giustarini et al., 2013; Sun et al., 2020). From this we found that GS-NEM (the glutathione adduct of NEM) levels were lower in NEM-treated micrometastatic cells, indicating that these cells likely display genuinely reduced levels of GSH. (Figure 4-2B, right graph).

De novo glutathione biosynthesis involves two ATP-dependent enzymatic steps, where ligation of cysteine to glutamate is catalysed by glutamate cysteine ligase (GCL) the rate-limiting enzyme for glutathione biosynthesis to form γ-glutamylcysteine. Subsequently, glycine is added to this dipeptide by glutathione synthetase (GSS) to form the tripeptide, GSH (Bansal & Celeste Simon, 2018). Although cysteine levels remained unchanged (Figure 4-2B, left graph), we found that the levels of γ-glutamylcysteine were reduced in metastatic cells (Figure 4-2B, middle graph). To determine whether expression of glutathione biosynthetic enzymes might explain these reductions in GSH and GSSG levels, we used qPCR to quantify the expression of Gclc, the catalytic subunit of Gcl (Lu, 2009). Gclc expression was suppressed in micrometastatic cells, by comparison with cells from primary tumours (fat pad) (Figure 4-2C), indicating that suppression of Gcl activity may be one reason underlying reduced glutathione levels in micrometastatic cells.

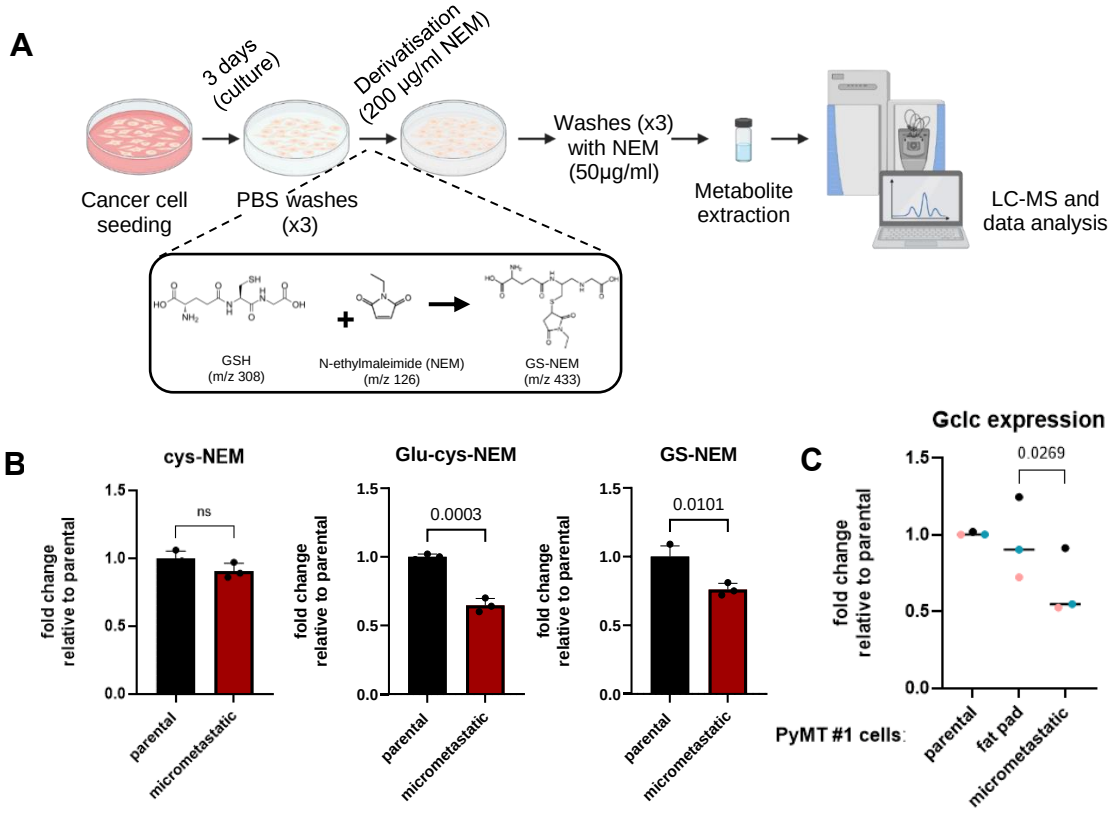

Figure 4-2 Glutathione levels are downregulated in lung micrometastatic cells.
(A) Schematic representation of polar metabolite extracted from PyMT#1 derived cells following derivatisation with NEM. Parental and micrometastatic cells were seeded in 6-well plates and cultured for 64 hours at 37˚C/ 5% CO_2. At the end of the incubation, cells were quickly washed three times with ice-cold phosphate buffered saline (PBS), derivatised with NEM (200µg/ml) at 4˚C, followed by three sequential washes with NEM (50µg/ml). After the final wash step, excess derivatisation solution was aspirated, and metabolites were extracted using LC-MS grade methanol, acetonitrile and water in a 5:3:2 ratio. The samples were analysed using LC-MS, and identification and quantification of metabolites was performed using the TraceFinder (Thermo Fisher Scientific) software. The chemical reaction of GSH with NEM to form glutathione adduct of NEM (GS-NEM) is depicted in the graph. (B) Abundance of intracellular thiol-containing metabolites, which were derivatised with NEM, was normalised to cell number and expressed as fold change relative to parental cells. Cysteine (left graph), glutathione (middle graph) and γ-glutamylcysteine (right graph) adducts of NEM were identified based on their retention time and m/z, n=1, values are mean ±SD (technical replicates), unpaired t-test, p-values are shown on the graph. (C) Relative mRNA levels of Gclc (RT-qPCR) in PyMT#1-derived micrometastatic cells and primary tumour cells (parental, fat pad). All samples were normalised to ARPP P0 and expressed as fold change relative to parental, n=3 (coloured dots), mean ± SEM, paired t-test between parental-micrometastatic, fat-pad-micrometastatic test, p-value is shown on the graph.

As we were interested in further pursuing the cell biological consequences of altered GSH and GSSG, we needed to be confident that our estimates of the incremental changes in these metabolites were precise. Therefore, we assessed the linearity of the response of our assay to various dilutions of GSH and GSSG. Calibration curves for standards of each metabolite were generated by plotting the peak area of the detected analytes versus the corresponding nominal concentration (Figure 4-3, left panels), and this indicated that the assay responded linearly to GSH and GSSG within the range of 0.5µM to 50µM (r^2=0.9858

and r^2=0.9878, respectively). We analysed the peak areas of GSH and GSSG detected in samples coming from primary and metastatic PyMT cell lines, and found that they fell within the linear range of detection (Figure 4-3, right panels). Thus, these data indicate that the proportional reduction of both GSH and GSSG levels in micrometastatic cells is 40% and 50% respectively, giving us confidence in our ability to explore pharmacological strategies for recapitulating these changes in MMTV-PyMT cells and determining how they influence their behaviour.

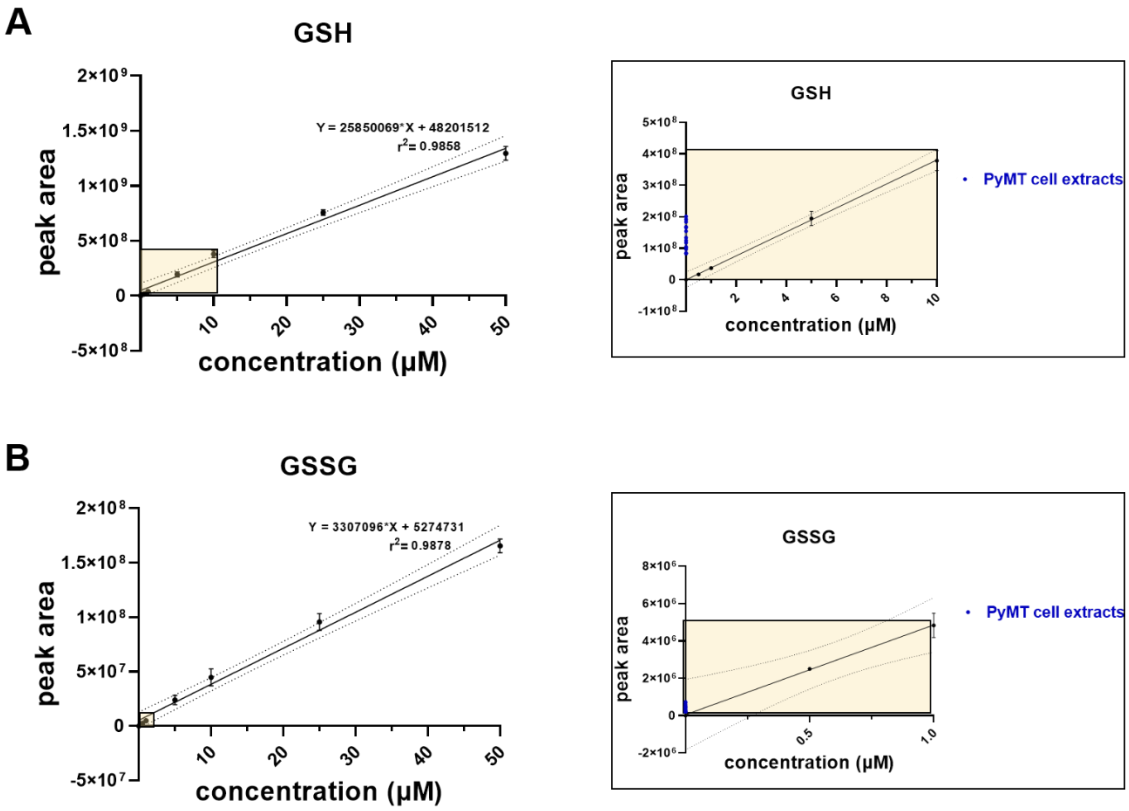

Figure 4-3 Glutathione levels in MMTV-PyMT cells fall within the linear response of detection by LC-MS.
(A) Left panel: A seven-point GSH calibration curve was generated over a concentration range 0-50μM, after plotting the peak area of the detected metabolite versus the corresponding nominal concentration. Right panel: zoom-in (in yellow) of calibration curve (0-10μM) depicting the peak areas of GSH detected in extracts coming from PyMT-derived cell lines. (B) Left panel: A seven-point GSSG calibration curve was generated over a concentration range 0- 50μM, after plotting the peak area of the detected metabolite versus the corresponding nominal concentration. Right panel: zoom-in (in yellow) of calibration curve (0-1μM) depicting the peak areas of GSSG detected in extracts coming from PyMT-derived cell lines.

4.2.3 xCT is downregulated in lung micrometastases compared to matched primary PyMT tumours

Cysteine and glutamate are critical precursors for glutathione biosynthesis, and xCT, the functional subunit of the cystine/glutamate antiporter system x_c^-, is responsible for equimolar antiport of cystine and glutamate across the plasma

membrane (Bansal & Celeste Simon, 2018). xCT is upregulated in various human cancers (Timmerman et al., 2013; Koppula et al., 2018) and previously published work has highlighted the ability of PyMT-derived primary tumour cells to release glutamate via increased xCT expression (Dornier et al., 2017). To assess whether reduced glutathione levels in micrometastatic cells might be due to altered xCT, we checked its expression by qPCR. This indicated that micrometastatic cells express almost 50% less xCT than parental or fat pad cells (Figure 4-4A). To further assess the (patho)-physiological relevance of our finding, we used RNAScope to compare xCT expression in primary tumours and matched metastatic lungs of MMTV-PyMT mice. RNAScope is a commercially available RNA in situ hybridization (ISH) assay used for detecting and visualising gene expression (single RNA molecules) within individual cells in samples including formalin fixed paraffin-embedded tissue (Duncan et al., 2019). This indicated that primary tumours express substantial amounts of xCT, whereas this was significantly reduced in lung micrometastases from the same animals (Figure 4-4B, C). Importantly, the surrounding lung parenchyma expressed more xCT than the micrometastases indicating that RNAScope detection was effective in this tissue (Figure 4-4B, C). These data indicate that xCT is specifically downregulated in lung micrometastases and that this is maintained in cell lines cultured from these.

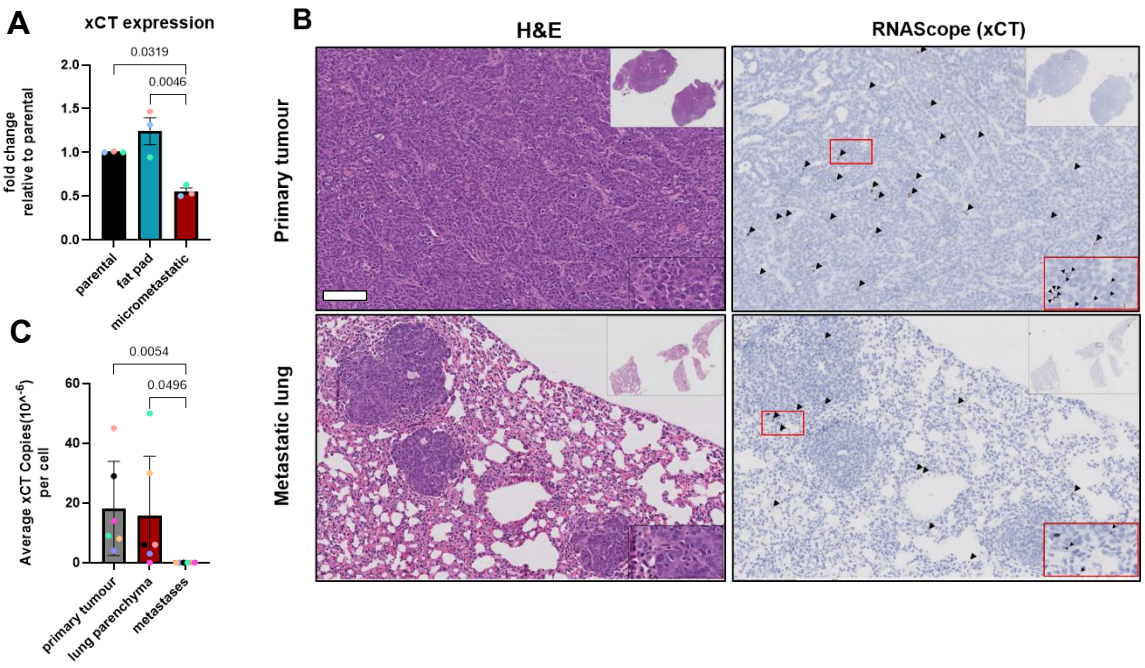

Figure 4-4 Lung micrometastases in the MMTV-PyMT mouse exhibit decreased xCT expression.
(A) Relative mRNA levels of xCT (RT-qPCR) in micrometastatic cells and primary tumour cells, all samples were normalised to ARPP P0 and presented relative to parental, n=3, ± SEM, one-way

ANOVA, p-values are shown on the graph. (B) Representative H&E staining and RNAScope (xCT probe) in MMTV-PyMT primary mammary tumours and matched metastatic lung tissues (>10 metastases) of PyMT mice. Each brown dot is highlighted with small arrowheads in these images (boxed regions outlined in red on the bottom right represent zoom-in areas of primary tumour and lung parenchyma) and represents copies of the xCT probe, bar 100μm. (C) Quantification of xCT probe (RNAScope) in primary mammary tumours (whole tissue), matched metastatic lungs (whole tissue) and micrometastases (alone) using the HALO software (Indica Labs), Kruskal-wallis with Dunn's multiple comparisons test, n=6 mice/group (colour-coded).

4.2.4 Micrometastatic cells display increased sensitivity to glutathione depletion

Several studies have reported that increased expression of GSH biosynthetic enzymes, or elevated GSH production, in different types of cancer can confer resistance to oxidative stress and chemotherapeutic drugs to promote disease progression (Lien et al., 2016; Fujimori et al., 2004; LI et al., 2014; Lu, 2009). For example, oncogenic PI3K mutant breast cancer cells upregulate glutathione biosynthesis by activating and stabilising NRF2 to cope with cellular stress (Lien et al., 2016). Thus, modulation of GSH levels, by inhibiting its biosynthetic enzymes, may enhance sensitivity to targeted therapies (Bansal & Celeste Simon, 2018). Depletion of glutathione by the use of buthionine sulfoximine (BSO), an irreversible inhibitor of GCL, promotes ferroptosis in breast cancer cells upon glucose deprivation (Andringa et al., 2006). We were therefore interested in assessing how sensitive our PyMT-derived isogenic cell lines were to glutathione depletion. To this end, we cultured PyMT-derived cells in increasing concentrations of BSO and counted the total cell number after 48 hours of incubation. We found that micrometastatic cells were the most sensitive in high doses of BSO (50μM, 100μM), which is in agreement with their basal low levels of glutathione, while parental and fat pad cells were more tolerant (Figure 4-5). In particular, parental cells seemed to tolerate glutathione depletion better than those derived from the fat pad in high BSO concentrations (50μM, 100μM), while this was not the case in lower amounts (5μM) (Figure 4-5).

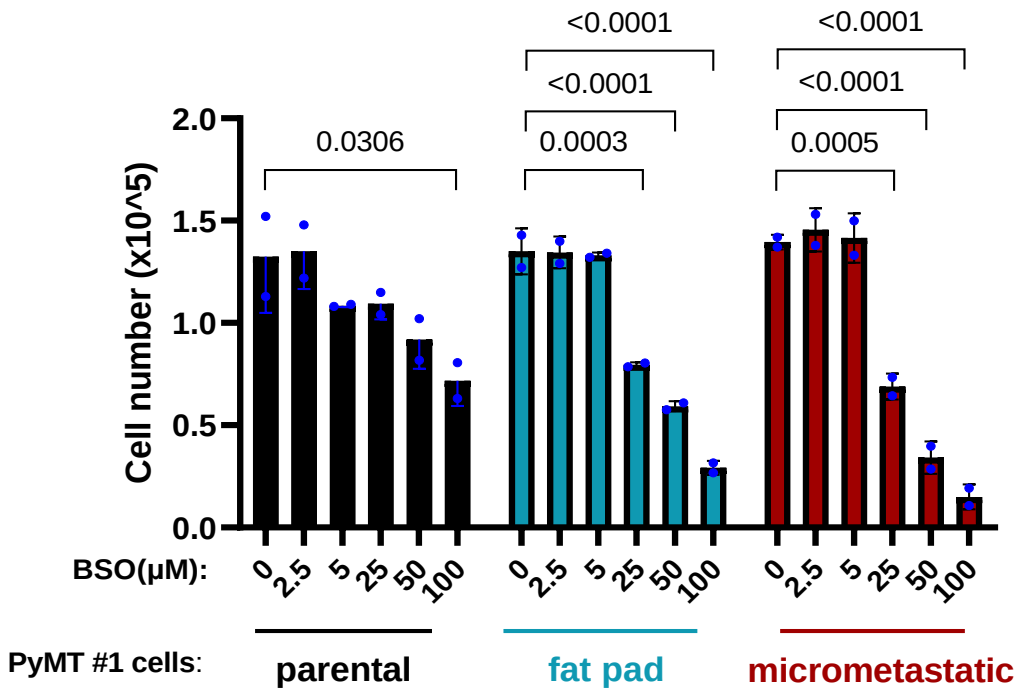

Figure 4-5 BSO treatment reduces cell number of PyMT-derived cell lines.
(A) Parental, fat pad and micrometastatic PyMT#1-derived cells were seeded in 24-well plates and treated with the indicated concentrations of BSO for 48 hours. At the end of the incubation, total cell number was counted using a Casy Cell Counter, n=1, values are mean ± SD (technical replicates, blue dots), one-way ANOVA, p-values are shown on the graph.

4.2.5 Use of BSO to manipulate glutathione levels

BSO has been extensively used in experiments to extensively deplete GSH reserves leading to severe oxidative stress (Wang et al., 2021; Lushchak, 2012). However, we wished to determine whether it was possible to identify a dosing regimen for BSO that would reduce GSH and GSSG levels in parental cells to recapitulate those identified in micrometastatic ones, and to do so without catastrophically disturbing redox balance and the overall cellular metabolic landscape. To explore this, we used LC-MS to characterise metabolic changes in parental cells following treatment for 24 hours with increasing concentrations of BSO, remaining within a range (between 0.0 and 2.5 μM) that did not compromise cell viability, as previously determined (in 4.2.4). We were able to confirm that both GSH and GSSG levels proportionally decreased in a dose dependent manner with increasing doses of BSO, with 1.25 and 1.88μM yielding reductions in GSH levels akin to that observed in micrometastatic cells (Figure 4-6B). Despite the reduction in glutathione levels, a ranked heatmap of $\log_2$ fold change of intracellular metabolite abundance between untreated and BSO treated cells (0.625μM, 1.25μM, 1.88μM and 2.5μM) showed that BSO treatment did not result in any

dramatic shifts of intracellular metabolites (Figure 4-6A). Indeed, none of the metabolic differences we reported previously (in 4.2.1) to exist between micrometastatic and primary tumour derived cells were observed, suggesting the previous metabolic changes (such as altered proline levels) were not specifically attributed to glutathione depletion. However, we did find that that lactate and PEP decreased in a way similar to glutathione (Figure 4-6A), which might suggest an increased flux towards the pentose phosphate pathway to meet NADPH requirements for GSH reductase, as previously reported (Zhang et al., 2016). Taken together, these data emphasise that treatment of primary tumour cells with defined concentrations of BSO leads to moderate glutathione depletion without precipitating substantial metabolic changes, noticeable redox stress or cell death.

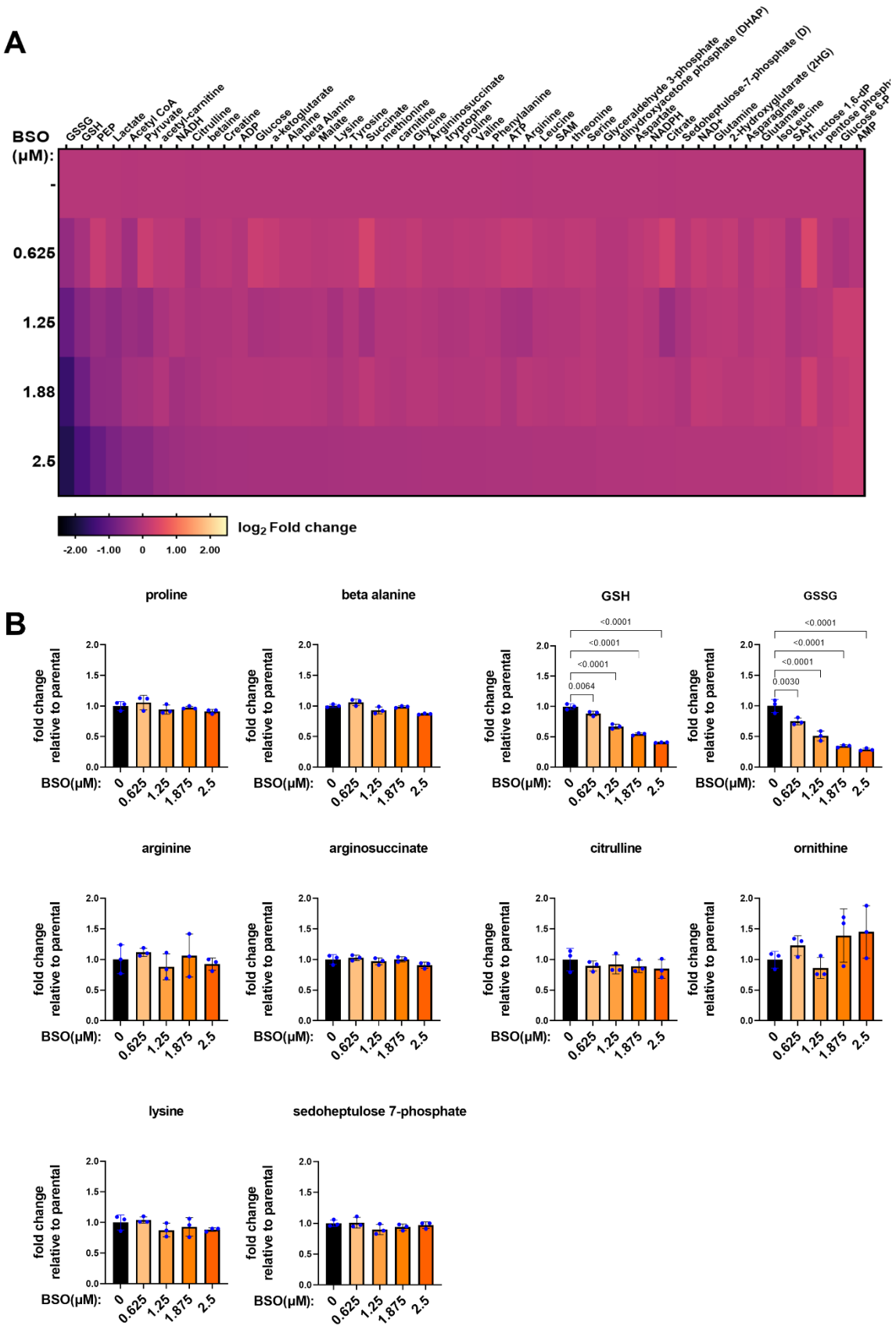
A
BSO (μM):
-
0.625
1.25
1.88
2.5
GSSG
GSH
PEP
Lactate
Acetyl CoA
Pyruvate
acetyl-carnitine
NADH
Citrulline
betaine
Creatine
ADP
Glucose
a-ketoglutarate
Alanine
beta Alanine
Malate
Lysine
Tyrosine
Succinate
methionine
carnitine
Glycine
Argininosuccinate
tryptophan
proline
Valine
Phenylalanine
ATP
Arginine
Leucine
SAM
threonine
Serine
Glyceraldehyde 3-phosphate
dihydroxyacetone phosphate (DHAP)
Aspartate
NADPH
Citrate
Sedoheptulose-7-phosphate (D)
NADx
Glutamine
2-Hydroxyglutarate (2HG)
Asparagine
Glutamate
IsoLeucine
SAH
fructose 1,6-dP
pentose phosph
Glucose 6-P
AMP
log2 Fold change
-2.00 -1.00 0 1.00 2.00
B
proline
beta alanine
GSH
GSSG
arginine
arginosuccinate
citrulline
ornithine
lysine
sedoheptulose 7-phosphate
fold change relative to parental
BSO(μM): 0 0.625 1.25 1.875 2.5
<0.0001
0.0064
0.0030

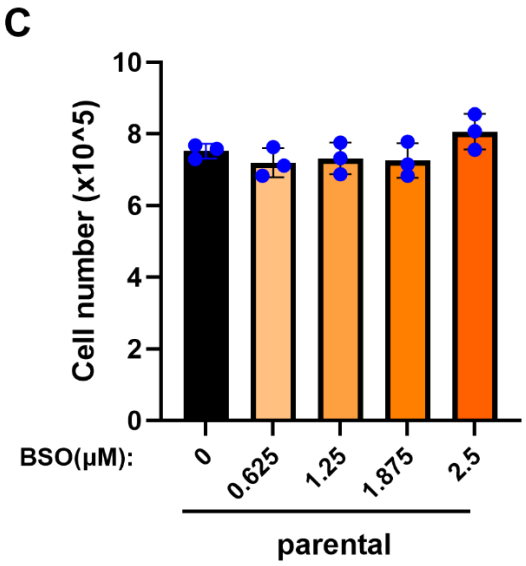

Figure 4-6 Acute BSO treatment of primary tumour cells leads to glutathione depletion, and does not depict the altered metabolism in metastatic cells.
(A) Targeted metabolomics of intracellular metabolites in PyMT#1-derived parental cells either left untreated or treated with the indicated concentrations of BSO. Heatmap of ranked log_2 fold change values of different metabolite intensities (normalised to cell number) relative to parental cells, 3 technical replicates/ condition. (B) The abundance of polar metabolites was normalised to total number of cells and expressed as fold change relative to untreated cells, 3 technical replicates/condition, values are mean ±SD (technical replicates, blue dots); one-way ANOVA with Dunnett's post hoc test, p-values are shown on the graph. (C) Parental PyMT#1-derived cells were treated with the indicated concentrations of BSO for 24 hours. At the end of the incubation, total cell number was counted using a Casy Cell Counter, 3 technical replicates/condition, values are mean ± SD (technical replicates, blue dots).

4.2.6 Micrometastatic cells secrete proline, while primary tumour cells consume it

Having characterised the landscape of cellular metabolites in primary tumour and micrometastatic PyMT cells and highlighted the significant differences between these (as described in 4.2.1), we were interested in building on this body of data by determining the nutrient and metabolite exchange rates between cells and the media (Voorde et al., 2019). Calculation of the exchange rate per day for each metabolite showed that glutamine was one of the most consumed, whilst lactate was consistently the most released, metabolites in the PyMT-derived cell lines, (Figure 4-7A). Interestingly, the only metabolite whose exchange differed between metastatic and non-metastatic cells was proline (Figure 4-7A). Indeed, proline was consumed by cells derived from primary mammary tumours (i.e. the parental and fat pad lines), but was released by micrometastatic cells (Figure 4-7B), and this is interesting given previous reports highlighting the importance of *de novo* proline synthesis in the metastasis of mammary cancer to the lung (Elia et al., 2017). Given the now well-documented association between proline

metabolism and redox homeostasis (Vettore et al., 2021; Zhu et al., 2021; Schwörer et al., 2020; Westbrook et al., 2022), we considered whether modulation of glutathione levels in parental cells could affect proline exchange rates. However, treatment of parental cells with BSO (1.88μM) for 48 hours did not affect proline exchange rates, with primary tumour cells consuming proline from their media, which was still evident 24 hours post BSO incubation (Figure 4-7C). Taken, together, these data indicate that micrometastatic cells secrete proline, while primary tumour cells consume it, and the use of BSO to moderately reduce GSH levels in cells from primary tumours does not affect this.

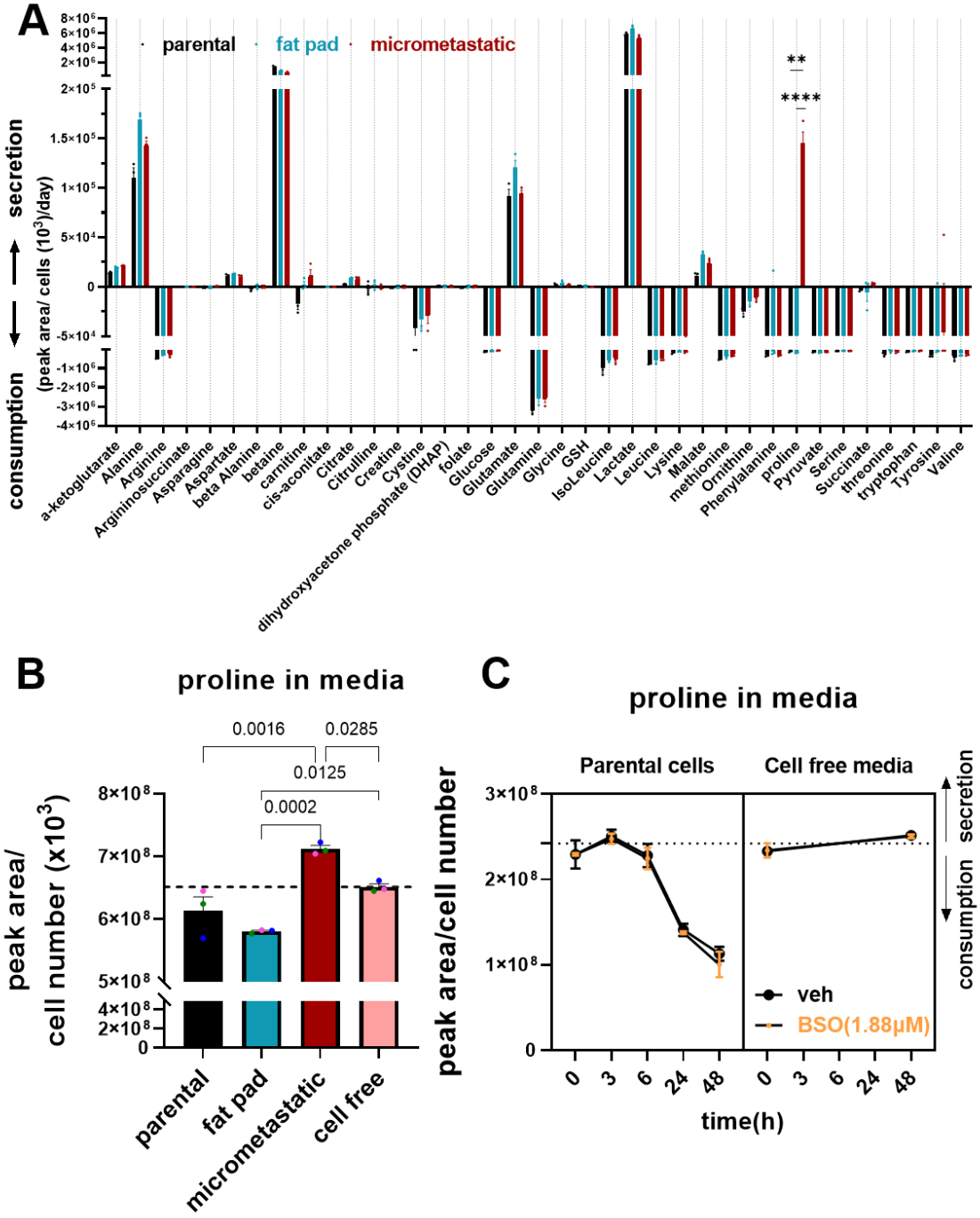

Figure 4-7 Micrometastatic cells secrete proline whilst primary tumour cells consume it.
(A) Secretion and consumption rates of amino acids and metabolites in parental, fat pad and micrometastatic PyMT#1-derived cell lines cultured under standard conditions (DMEM, 10%FBS), n= 3 biological replicates, values represent mean ±SEM, two-way ANOVA, **p-value <0.005, **** p-value <0.0001. (B) Proline abundance (normalised to cell number) in conditioned media from PyMT#1-derived primary tumour and metastatic cell lines cultured under standard conditions. For the same culture period, cell-free conditioned media were used as control to assess the secretion/consumption of proline levels by PyMT-derived cell lines, n= 3, values represent mean ±SEM, one-way ANOVA with Tukey's multiple comparison test, p-values are shown on the graph. (C) Parental cells were either left untreated (black line) or treated with BSO (1.88µM) (orange line) for 48 hours, and proline levels were quantified in their conditioned media. In parallel, cell-free conditioned media were used as control (t=0, t=48 hours) for the secretion/consumption of proline levels in the presence of BSO.

4.2.7 Micrometastatic cells exhibit a distinct lipidomic profile

Altered lipid metabolism is being increasingly recognised as an acquired feature of cancer cells which enables them to meet anabolic and catabolic needs in the face of rapid cell growth (Cairns et al., 2011). Accumulation of lipids, increased uptake of fatty acids and upregulation of genes encoding fatty acid biosynthesis or fatty acid transporters have been shown to enhance migratory and invasive traits of cancer cells and to be associated with metastatic progression in many cancers (Antalis et al., 2011; Pascual et al., 2017; Nath & Chan, 2016). Thus, we performed a single-phase lipid extraction and employed untargeted and targeted LC-MS approaches to compare the lipid profiles of PyMT-derived cancer cell lines. Principal component analysis (PCA) of normalised $\log_2$ peak areas of identified total lipids clearly showed that PC component 1 (x-axis) is able to separate micrometastatic cells from the parental and fat pad cells, suggesting that the lipidome profile of lung micrometastatic cells has features that discriminates it from that of the cells from the primary tumour site (Figure 4-8A). Comparison of lipid classes expressed as a percentage of total lipids did not reveal differences among the three cell groups (Figure 4-8B), with the majority of lipids detected (>75%) representing major structural lipid classes; phosphatidylcholine (PC), phosphatidylethanolamine (PE), phosphatidylinositol (PI) and phosphatidylserine (PS). This is in agreement with the well-documented lipid composition of cell membranes in most eukaryotes, where PC accounts for >50% of the membranous phospholipids (Van Meer et al., 2008). To look in more detail at what might explain the distinct lipidome of micrometastatic cells, we generated a scatter plot showing the mean difference of peak areas for all detected lipid classes between micrometastatic and parental (x-axis) and fat pad and parental (y-axis) (Figure 4-8C). From this plot, we were able to see that, besides the aforementioned lipid classes, sphingomyelin (SM) and ceramide (Cer) were upregulated in micrometastatic cells by comparison with parental cells (t-test difference >1.2, q value<0.05, black circles). Our untargeted lipidomic approach therefore suggests that micrometastatic cells do differ in lipid composition when compared to primary tumour cell lines and that increased levels of SM and Cer lipid classes make a key contribution to this difference.

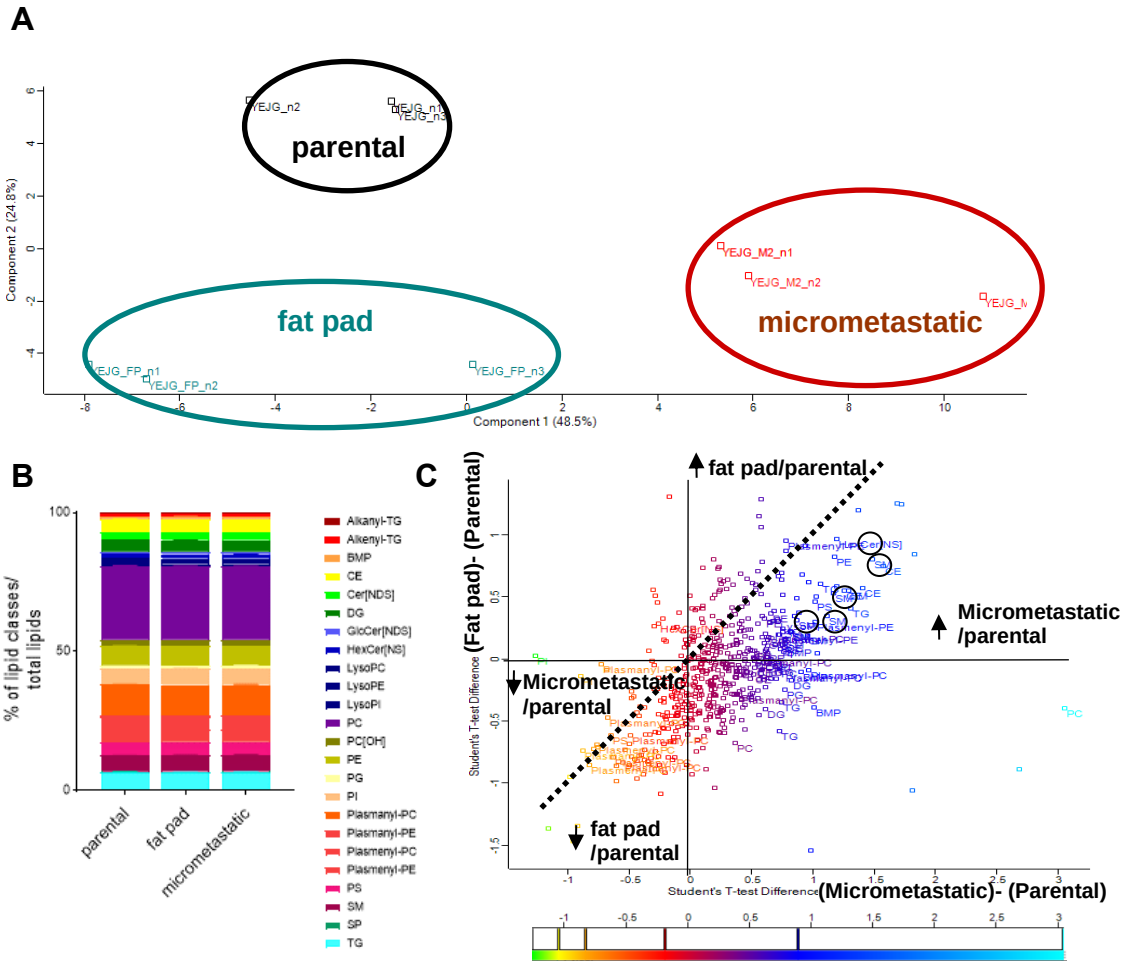

Figure 4-8 Micrometastatic cells are lipidomically distinct from primary mammary tumour cells.
(A) Principal component analysis (PCA) of normalised log_2 peak areas of identified total lipids among PyMT-derived cell lines. Each point represents a biological repeat and samples corresponding to parental, fat pad and micrometastatic cells are coloured in black, blue and red, respectively. (B) Percentage of lipid classes per total lipids (peak area) was calculated in parental, fat pad and micrometastatic cells, n=3 biological repeats. (C) Scatter plot showing the relationship between the mean differences of peak areas (lipid classes) when we compare fat pad cells to parental (y axis) and micrometastatic cells to parental (x axis). The dotted line represents all the lipid classes that display no difference across the conditions, while the t-test difference between micrometastatic and parental cells is colour coded (SM and Cer lipid classes are shown in black circles, t-test diff >1.2, q value<0.05), n=3 biological replicates. These graphs were generated in collaboration with Engy Shokry Abd Shokry, CRUK Beatson Institute, Glasgow.

4.2.8 Targeted lipidomic analysis reveals enrichment of sphingolipids in metastatic cells

As our untargeted lipidomic analysis indicated that sphingolipids are upregulated in micrometastatic cells, we sought to develop a targeted approach to further interrogate alterations to these lipid species. To this end, raw data files were imported to LipiDex, an open-source software for automated lipid identification utilising *in silico* libraries (fragmentation data and MS/MS spectral matching) (Hutchins et al., 2018). This process yielded considerable number of sphingolipid

species, namely ceramide (Cer), ceramide phosphate (CerP), hexosylceramide (HexCer) and sphingomyelin (SM), as shown in Figure 4-9 (top row). At this stage, we applied sequential steps of data filtering by first removing lipid species that were present in the 'blank' samples (cell-free samples that were taken through the extraction protocol) that we included in LC-MS runs with our samples of interest. Of the remaining species, we removed ones that were missing in ≥ 40% across biological repeats (3 technical replicates/repeat) or those whose peak area was at or near the detection limit (≤ 10^3), thus proceeding only with robustly identified species. Lastly, we retained the species with the highest sum or means (unless their retention time≤2 min), removed outliers after manual inspection, and filtered-out species with a relative standard error ≥20%. Collectively, these cut-off criteria resulted in a small number of sphingolipid species (0.75%- 3% relatively to the initial number of identified species) that we were able to identify with sufficient confidence to determine which ones were specifically enriched in micrometastatic cells.

No of species in each step	**Cer**	**CerP**	**HexCer**	**SM**
Species Measured	**1579**	**1654**	**1092**	**904**
After removal of IDs in blanks	776	950	764	553
After removing IDs ≥ 40% missingness	133	151	214	177
Removing duplicates, keeping only IDs with the highest sum or means of all samples	62	140	127	102
RSE (<20%) filter	20	80	28	58
$FC_{M2\ vs\ P}$ >1.2 or <0.8	**12**	**46**	**16**	**28**

Figure 4-9 Number of sphingolipid species detected following targeted lipidomic analysis in isogenic PyMT-derived cell lines.
Each row indicates the number of sphingolipid species remaining after each step of data filtering. This analysis was performed in collaboration with Engy Shokry Abd Shokry, CRUK Beatson Institute, Glasgow.

It has been recently shown that increased sphingolipid metabolism enhances metastatic potential of colorectal cancer cells by promoting their proliferative, migratory and invasive behaviour (Jafari et al., 2019). Although the bioactive sphingolipid ceramide has been predominantly studied in the context of growth arrest and cell death (Hannun & Obeid, 2008), it is now clear that various ceramide species at different (sub-) cellular compartments are involved in diverse biological processes (Hannun & Obeid, 2011). We thus took advantage of our targeted

lipidomics approach to focus on ceramide species that displayed differential abundance (fold change >1.2 or <0.8) in metastatic cells (Fig. 4-9). We found that four C16- and C18- ceramide species were enriched by at least 1.7-fold in micrometastatic cells compared to parental (but not fat pad-derived) cells (highlighted in red; Figure 4-10A, B). These findings not only reinforce the suitability of our targeted method to examine lipid changes across our cell lines, but also show that certain C16-, C18- ceramide species are specifically enriched in metastatic cells. Moreover, it was notable that we were unable to detect any ceramide species that were specifically depleted in micrometastatic cells.

A

Ceramide species	Fold change Fat pad vs parental	log2(FC) FP	Fold change Micrometastatic vs parental	log2(FC)_ M2
Cer.16.1.2.20.3.1Cer.18.0.2.18.4.1	1.8524	0.8894	1.5853	0.66478
Cer.16.1.2.22.4.1Cer.18.0.2.20.5.1	**1.0202**	**0.028894**	**1.8699**	**0.90293**
Cer.16.1.2.24.2.1Cer.18.0.2.22.3.1	0.71119	-0.49168	1.222	0.2892
Cer.18.0.2.16.0	0.94182	-0.086476	1.3154	0.39549
Cer.18.0.2.17.2	**1.6965**	**0.76255**	**4.346**	**2.1197**
Cer.18.0.2.21.2	0.86631	-0.20704	0.75186	-0.41146
Cer.18.0.2.24.0	0.96306	-0.054304	1.2545	0.32713
Cer.18.0.2.24.1	1.1844	0.24413	1.3906	0.47575
Cer.18.1.2.17.2	**1.1011**	**0.13899**	**2.0343**	**1.0245**
Cer.18.1.2.21.2	1.0573	0.080423	1.2347	0.30413
Cer.18.1.2.22.3	**0.86309**	**-0.21241**	**1.6731**	**0.74256**
Cer.18.1.2.23.3	1.0611	0.085512	1.327	0.4082

B

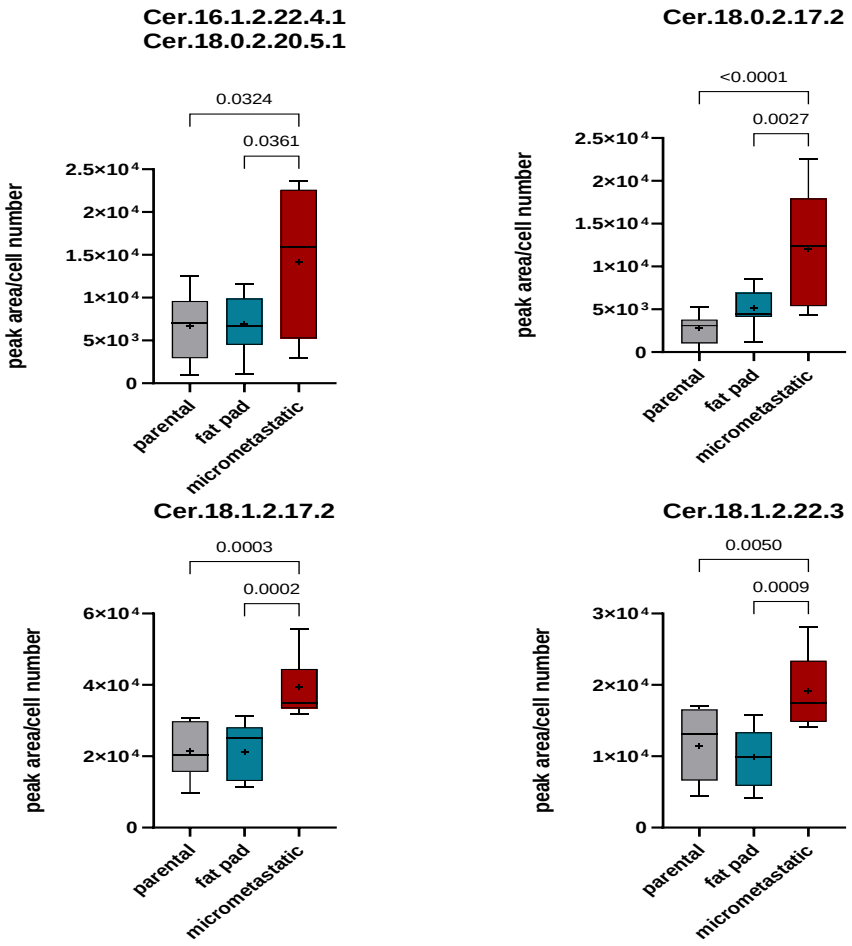

Figure 4-10 C16- and C18- ceramide species which are specifically enriched in micrometastatic cells.
(A) Differentially abundant ceramide species showing a fold change of >1.2 or <0.8 when we compare micrometastatic cells to parental cells. The species significantly changing in abundance in metastatic cells compared to parental (but not fat pad) cells are highlighted in red. (B) Normalised (to cell number) peak areas of ceramide species that are significantly enriched in metastatic cells. Whiskers are the 10th-90th percentiles; + represents the mean. P-values are shown on the graphs, one-way ANOVA with Tukey's comparison test, n=3 independent experiments. This analysis was performed in collaboration with Engy Shokry Abd Shokry, CRUK Beatson Institute, Glasgow.

We next sought to visualise ceramide in PyMT-derived cell lines using an anti-ceramide antibody, monoclonal antibody MID 15B4, a mouse IgM previously used

for studies of sphingomyelin metabolism and ceramide signalling (Parashuraman & D'Angelo, 2019; Vielhaber et al., 2001; Choezom & Gross, 2022). Airyscan super resolution confocal microscopy of cells stained with the anti-ceramide antibody (counterstained with phalloidin to visualise the actin cytoskeleton) revealed a punctate distribution of ceramide which was localised both in the cytoplasm and at the plasma membrane, with the staining appearing brighter in micrometastatic cells (Figure 4-11A). Indeed, quantitative analysis of mean fluorescence intensity revealed significantly higher ceramide levels in micrometastatic cells compared to the primary tumour ones (Figure 4-11B). In agreement with our targeted lipidomic approach, these data confirm that metastatic cells show enrichment for ceramide species compared to parental and fat pad cells.

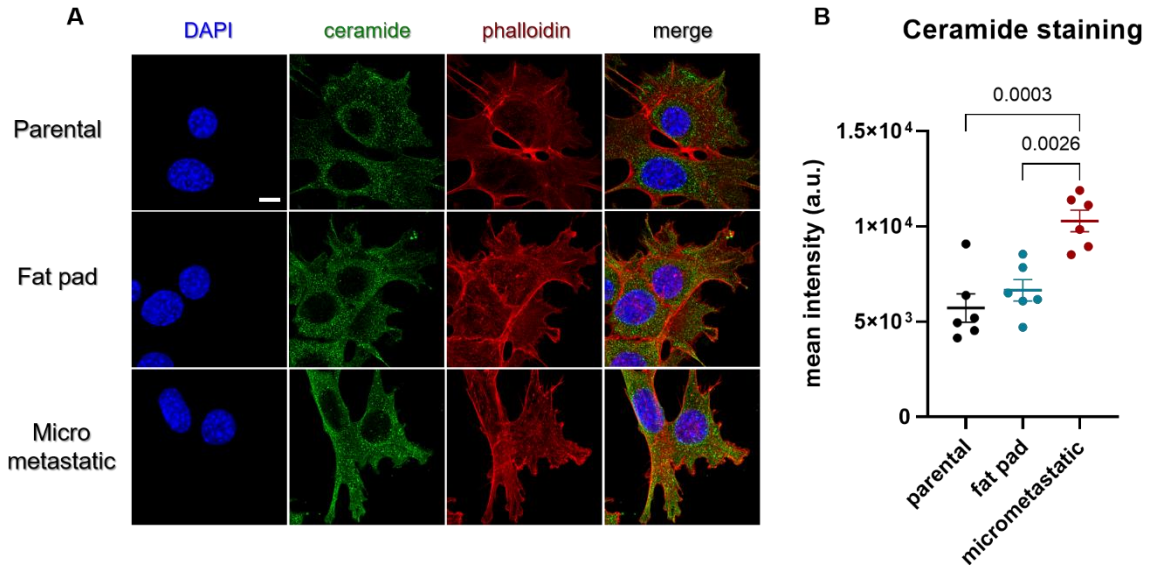

Figure 4-11 Immunofluorescence reveals increased levels of ceramide in micrometastatic cells.
(A) Parental, fat pad and micrometastatic cells were seeded on glass bottom dishes and fixed following 48h of culture. Ceramide (green) and phalloidin (red) were visualised by immunofluorescence (63X magnification, Zeiss LSM 880 Airyscan confocal microscope). Bar, 10μm. (B) ImageJ was used to quantify the mean intensity of ceramide (sum of z-stacks, 10 stacks/field of view) as determined by the default method. Values are mean ± SEM. n=6 fields of view. P values are depicted on the graph, ordinary one-way ANOVA. The acquisition of these images were performed in collaboration with Luis Pardo, CRUK Beatson Institute, Glasgow.

A key metabolite of ceramide is ceramide-1-phosphate, which is formed following phosphorylation of ceramide by ceramide kinase (CerK) (Morad & Cabot, 2012), and has been recently shown to promote migration and invasion of cancer cells (Rivera et al., 2016; Schwalm et al., 2020). To determine its levels in PyMT-derived cells, we focussed-on the ceramide phosphate species that displayed different abundances (fold change >1.2 or <0.8) in metastatic cells (Figure 4-12A). This yielded a considerable number of species, and although only four were

significantly upregulated in metastatic cells relative to parental and fat pad cells (Figure 4-12B), the data strongly identify an enrichment of specific ceramide phosphate species (C20-) in the metastatic cell lines.

A

Ceramide phosphate species	Fold change Fat pad vs parental	log2(FC)_FP	Fold change Micrometastatic vs parental	log2(FC)_M2
CerP.16.1.2.18.1.1	0.95203	-0.070921	0.76525	-0.386
CerP.16.1.3.16.0.1	0.92633	-0.11041	1.2241	0.29178
CerP.16.1.3.18.1.1	1.2724	0.34759	1.6119	0.68874
CerP.16.1.3.22.3.1	1.5851	0.66461	1.3268	0.40793
CerP.18.0.2.16.3	0.84258	-0.24712	1.3644	0.44823
CerP.18.0.2.17.1	0.93867	-0.091307	1.3677	0.45171
CerP.18.0.2.17.5	0.73191	-0.45027	1.3833	0.46815
CerP.18.0.2.18.1.1CerP.18.0.2.19.0	0.83117	-0.26678	0.76194	-0.39226
CerP.18.0.2.20.5.1	1.6952	0.76144	1.2762	0.35181
CerP.18.0.2.21.4	1.5681	0.64903	1.2928	0.3705
CerP.18.0.2.22.2	1.3417	0.42407	0.76659	-0.38346
CerP.18.0.2.24.0	1.1598	0.21385	1.2291	0.29756
CerP.18.0.2.26.5.1	1.2244	0.29202	1.4522	0.53821
CerP.18.0.3.26.4.1	1.349	0.43192	1.2857	0.36251
CerP.18.1.2.16.1	1.094	0.12967	1.2653	0.33949
CerP.18.1.2.16.1.1CerP.18.1.2.17.0	0.97849	-0.03137	1.2897	0.36705
CerP.18.1.2.16.4	0.98908	-0.015835	1.3306	0.41209
CerP.18.1.2.17.3	1.2166	0.28287	1.2997	0.37819
CerP.18.1.2.18.5	0.93425	-0.098114	0.78311	-0.35271
CerP.18.1.2.20.3.1CerP.18.1.2.21.2	1.5429	0.62562	1.3369	0.41891
CerP.18.1.2.20.4	1.2519	0.3241	1.2548	0.32744
CerP.18.1.2.20.4.1CerP.18.1.2.21.3	1.2456	0.3168	1.2533	0.32579
CerP.18.1.2.21.5	1.2633	0.33718	1.2006	0.2637
CerP.18.1.2.22.0	1.6738	0.7431	1.3024	0.38112
CerP.18.1.2.22.1	1.6908	0.75773	1.4471	0.53321
CerP.18.1.2.22.3	1.7363	0.79605	1.5669	0.64789
CerP.18.1.2.22.3.1CerP.18.1.2.23.2	1.3882	0.47317	1.2146	0.28049
CerP.18.1.2.22.4	1.4278	0.51384	1.2131	0.27869
CerP.18.1.2.22.4.1CerP.18.1.2.23.3	1.7682	0.82231	1.8901	0.91843
CerP.18.1.2.23.2.1CerP.18.1.2.24.1	2.0618	1.0439	2.0651	1.0462
CerP.18.1.2.24.3.1CerP.18.1.2.25.2	1.8598	0.89513	1.4715	0.5573
CerP.18.1.2.24.4.1CerP.18.1.2.25.3	1.8957	0.92275	1.4846	0.57007
CerP.18.1.2.24.5.1CerP.18.1.2.25.4	1.4364	0.52244	1.6362	0.71039
CerP.18.1.2.26.1	1.9304	0.94889	1.7051	0.76981
CerP.18.1.2.26.2.1	1.6069	0.68432	1.8902	0.91856
CerP.18.1.2.26.3.1	1.221	0.28806	1.2427	0.31349
CerP.18.1.2.26.4.1	0.99335	-0.0096284	1.2478	0.31938
CerP.18.1.2.26.5.1	1.8834	0.91336	1.5195	0.60363
CerP.18.1.3.26.0.1	0.95216	-0.070721	0.55789	-0.84196
CerP.20.0.2.21.2.1	1.3401	0.42234	1.5761	0.65633
CerP.20.0.2.23.5.1	**1.4677**	**0.55351**	**2.0594**	**1.0422**
CerP.20.0.2.24.0.1	**0.81433**	**-0.29632**	**1.4613**	**0.54728**
CerP.20.0.3.24.0.1	**1.1561**	**0.20928**	**1.5484**	**0.63078**
CerP.20.1.2.21.2.1	1.1732	0.23046	1.4958	0.58091
CerP.20.1.2.23.5.1	**1.2651**	**0.33921**	**1.6476**	**0.72036**
CerP.20.1.2.24.0.1	0.82445	-0.27849	1.4142	0.49995

B

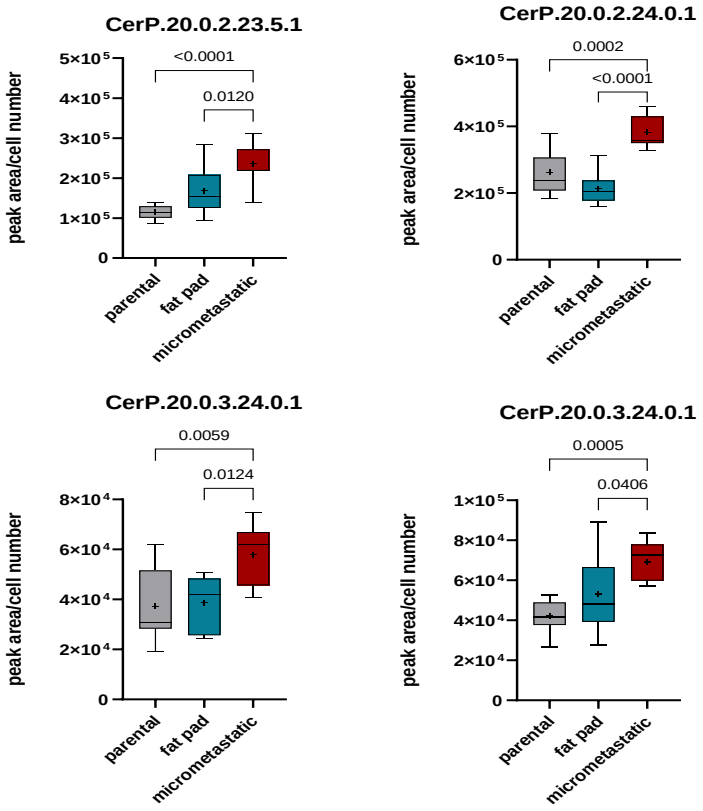

Figure 4-12 (C20-) Ceramide phosphate species are enriched in micrometastatic cells.
(A) Differentially abundant ceramide phosphate species showing a fold change of >1.2 or <0.8 when we compare micrometastatic cells to parental cells. The species significantly changing in abundance in metastatic cells compared to parental and fat pad cells are highlighted in red. (B) Normalised (to cell number) peak areas of ceramide phosphate species that are significantly enriched in metastatic cells. Whiskers are the 10th-90th percentiles; + represents the mean. P-values are shown on the graphs, one-way ANOVA with Tukey's comparison test, n=3 independent experiments. This analysis was performed in collaboration with Engy Shokry Abd Shokry, CRUK Beatson Institute, Glasgow.

Sphingomyelin is one of the major sphingolipids in mammalian cells, mostly found on the plasma membrane (outer leaflet), in the Golgi (luminal side) and endosomes (luminal leaflet) (Van Meer et al., 2008). Ceramide can be catabolised from sphingomyelin following hydrolytic removal of its phosphocholine moiety by sphingomyelinase enzymes, which are characterised according to their subcellular localisation and optimum pH activity (acid, neutral, alkaline) (Morad & Cabot, 2012). To test whether sphingomyelin levels were altered in metastatic cells, we focussed-on these species in the same way as previous (fold change >1.2 or <0.8) (Figure 4-13A). Indeed, we were able to detect four sphingomyelin species (C18-, C20-) that were specifically enriched in micrometastatic cells (but not fat pad cells) by comparison with primary tumour cells. Taken together, our data from untargeted lipidomic analysis indicate that metastatic cells are lipidomically distinct from parental and fat pad cells, with certain ceramide and sphingomyelin lipid classes being upregulated. When we specifically looked into these classes in a targeted way, we found an enrichment for distinct species of ceramide, ceramide-1-phosphate and sphingomyelin in metastatic cells compared to their matched primary tumour lines.

A

Sphingomyelin species	Fold change Fat pad vs parental	log2(FC)_FP	Fold change Micrometastatic vs parental	log2(FC)_M2
SM.16.0.2.20.4.1.....SM.16.1.2.20.3.1....SM.18.1.2.18.3.1....SM.16.0.2.21.3....SM.16.1.2.21.2....SM.18.0.2.19.3	1.5171	0.60134	1.6797	0.74823
SM.16.0.3.25.3.1SM.16.1.3.25.2.1SM.18.0.3.23.3.1SM.18.1.3.23.2.1SM.20.0.3.21.3.1SM.20.1.3.21.2.1SM.16.0.2.26.2.1SM.16.1.2.26.1.1SM.18.0.2.24.2.1SM.18.1.2.24.1.1SM.20.0.2.22.2.1SM.20.1.2.22.1.1SM.18.0.2.25.1SM.18.1.2.25.0SM.20.0.2.23.1SM.20.1.2.23.0	0.93109	-0.10301	1.3949	0.48012
SM.16.0.3.26.3.1SM.16.1.3.26.2.1SM.18.0.3.24.3.1SM.18.1.3.24.2.1SM.20.0.3.22.3.1SM.20.1.3.22.2.1SM.18.0.2.25.2.1SM.18.1.2.25.1.1SM.20.0.2.23.2.1SM.20.1.2.23.1.1SM.18.0.2.26.1SM.18.1.2.26.0SM.20.0.2.24.1SM.20.1.2.24.0	0.94218	-0.08592	1.453	0.53906
SM.16.1.2.18.3.1	1.8152	0.8601	2.399	1.2624
SM.16.1.2.21.5.1SM.16.0.2.22.5SM.16.1.2.22.4SM.18.0.2.20.5SM.18.1.2.20.4SM.16.0.3.19.0.1SM.18.0.3.17.0.1	0.88213	-0.18094	1.2329	0.30204
SM.16.1.2.22.5.1SM.18.1.2.20.5.1SM.16.0.2.23.5SM.16.1.2.23.4SM.18.1.2.21.4SM.16.0.3.20.0.1SM.18.0.3.18.0.1SM.20.0.3.16.0.1	0.58557	-0.77209	0.67284	-0.57166
SM.16.1.2.24.5SM.18.1.2.22.5SM.20.1.2.20.5SM.16.0.3.21.1.1SM.16.1.3.21.0.1SM.18.0.3.19.1.1SM.18.1.3.19.0.1SM.20.0.3.17.1.1SM.20.1.3.17.0.1SM.16.0.2.22.0.1SM.18.0.2.20.0.1SM.20.0.2.18.0.1	0.89659	-0.15748	1.2588	0.3321
SM.16.1.3.25.5.1SM.18.1.3.23.5.1SM.20.1.3.21.5.1SM.16.0.2.26.5.1SM.16.1.2.26.4.1SM.18.0.2.24.5.1SM.18.1.2.24.4.1SM.20.0.2.22.5.1SM.20.1.2.22.4.1SM.18.0.2.25.4SM.18.1.2.25.3SM.20.0.2.23.4SM.20.1.2.23.3	1.325	0.40603	1.2197	0.28656
SM.18.0.2.18.0.1	0.76163	-0.39283	0.68102	-0.55424
SM.18.0.2.20.4.1	1.379	0.46366	1.4147	0.50051
SM.18.0.2.21.0.1	0.86617	-0.20728	1.2848	0.36155
SM.18.0.3.26.3.1SM.18.1.3.26.2.1SM.20.0.3.24.3.1SM.20.1.3.24.2.1SM.20.0.2.25.2.1SM.20.1.2.25.1.1SM.20.0.2.26.1SM.20.1.2.26.0	0.98751	-0.01813	1.2836	0.36018
SM.18.0.3.26.4.1SM.18.1.3.26.3.1SM.20.0.3.24.4.1SM.20.1.3.24.3.1SM.20.0.2.25.3.1SM.20.1.2.25.2.1SM.20.0.2.26.2SM.20.1.2.26.1	0.94576	-0.08045	1.2912	0.36872
SM.18.1.2.16.1.SM.16.1.2.18.1	1.5202	0.60429	1.401	0.48645
SM.18.1.2.18.4.1	1.4273	0.51326	1.5278	0.61141
SM.18.1.2.20.4.1..SM.18.1.2.21.3	1.4787	0.56434	1.316	0.39615
SM.18.1.2.20.5.1	2.0774	1.0548	1.8427	0.8818
SM.18.1.2.22.4.1..SM.18.1.2.23.3	1.7013	0.76665	1.24	0.31037
SM.18.1.2.23.2.1.M.18.1.2.24.1	0.96438	-0.05233	1.2845	0.36121
SM.18.1.2.23.2.SM.18.1.2.22.3.1	**1.339**	**0.42121**	**1.7138**	**0.77719**
SM.18.1.2.23.4..SM.18.1.2.22.5.1	1.7823	0.83373	1.3135	0.39337
SM.20.0.3.25.1.1SM.20.1.3.25.0.1SM.20.0.2.26.0.1	0.77518	-0.36739	1.2203	0.28718
SM.20.0.3.25.3.1SM.20.1.3.25.2.1SM.20.0.2.26.2.1SM.20.1.2.26.1.1	0.65564	-0.60901	1.2238	0.29134
SM.20.0.3.26.1.1SM.20.1.3.26.0.1	**1.0723**	**0.10069**	**1.5606**	**0.64207**
SM.20.0.3.26.2.1SM.20.1.3.26.1.1	**1.3767**	**0.46118**	**2.0248**	**1.0178**
SM.20.0.3.26.3.1SM.20.1.3.26.2.1	**1.2592**	**0.33248**	**1.7844**	**0.83543**
SM.20.1.2.26.5.1SM.18.0.3.26.0.1SM.20.0.3.24.0.1	1.0906	0.12513	1.2759	0.35155
SM.20.1.3.25.5.1SM.20.0.2.26.5.1SM.20.1.2.26.4.1	0.50574	-0.98353	0.69763	-0.51947

B

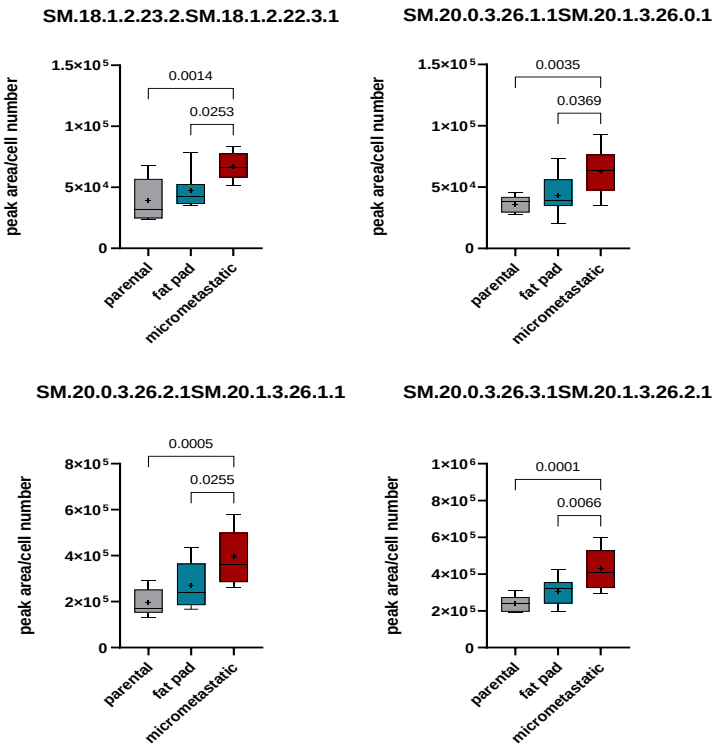

Figure 4-13 Metastatic cells are more enriched in sphingomyelin species compared to their matched primary tumour lines.
(A) Differentially abundant sphingomyelin species showing a fold change of >1.2 or <0.8 when we compare micrometastatic cells to parental cells. The species significantly changing in abundance in metastatic cells compared to parental and fat pad cells are highlighted in red. (B) Normalised (to cell number) peak areas of sphingomyelin species that are significantly enriched in metastatic cells. Whiskers are the 10th-90th percentiles; + represents the mean. P-values are shown on the graphs, one-way ANOVA with Tukey's comparison test, n=3 independent experiments. This analysis was performed in collaboration with Engy Shokry Abd Shokry, CRUK Beatson Institute, Glasgow.

4.3 Discussion

Disseminated cancer cells dynamically re-wire their metabolism to survive throughout the course of the metastatic cascade (Bergers & Fendt, 2021). As our understanding of the biology of tumour recurrence continues to grow we are beginning to appreciate the intricate processes that confer metastasis-initiating properties to cancer cells which allow them to seed distant organs (Oskarsson et al., 2014). However, metastatic dissemination is a highly inefficient process, mainly due to the programmed death of cancer cells after entering the circulation, in addition to the transition into a quiescent state (dormancy) following subsequent extravasation (Lyon et al., 2006). Understanding the metabolic changes that cancer cells acquire to overcome these bottlenecks could be key to developing approaches that sensitise metastases to therapies by targeting these adaptations (Klein, 2020). Using isogenic PyMT-derived cancer cells, which were phenotypically characterised in the previous chapter, we aimed to investigate the metabolic differences between primary mammary tumour and lung metastatic cell lines. Principally, we show that glutathione (reduced and oxidised) is reduced, and proline is increased in micrometastatic cells. Reduced glutathione is consistent with the reduced expression of xCT cystine-glutamate antiporter system that we detect in these cells and in lung metastases from these mice. Sensitivity of PyMT-derived cell lines to pharmacological inhibition of glutathione biosynthesis is increased in metastatic cells relative to primary tumour-derived cells, and this correlates with their reduced levels of GSH. Furthermore, modulation of glutathione levels in parental cells to mimic that observed in metastatic lines cannot solely account for the full gamut of metabolic differences found in the latter. Notably, artificially reducing glutathione levels to the same extent as found in micrometastatic cells does not lead to increased proline synthesis or secretion. In addition to these alterations in polar metabolites, we find that metastatic and primary tumour cells also differ in lipid composition such that certain sphingolipid species are enriched in micrometastatic cells. These findings are compelling since several of the metabolic changes we observe in metastatic cells have been closely linked to the metastatic potential of breast cancer cells, as discussed below.

In the face of increased proliferation rates, cancer cells depend on the availability of nutrients and amino acids to support cell growth, while employing redox

cytoprotective programs, such as glutathione biosynthesis, to cope with metabolically stressful microenvironments (Zhu & Thompson, 2019). Glutathione is a tripeptide that consists of glutamate, cysteine and glycine, and cysteine availability can be limiting for glutathione production in normal tissues. The requirement for glutathione for survival and proliferation of cancer cells depends on the surrounding microenvironment (Combs & Denicola, 2019). Indeed, a recent study has reported that the glutathione pathway is required for MMTV-PyMT tumour initiation, but becomes dispensable following tumour establishment and disease progression due to the activation of other antioxidant pathways, such as those dependent on thioredoxin (Harris et al., 2015). Consistent with this, we find that primary mammary tumour cells have higher GSH and GSSG levels than matched cells from lung micrometastases (Figure 4-1& Figure 4-2), suggesting that glutathione biosynthesis may be downregulated to allow other antioxidant pathways to protect the metastasising cells.

Outside the cells, the oxidising environment promotes the formation of disulphide bonds between two cysteine residues leading to generation of cystine, a dipeptide which is the predominant form of cysteine taken up by the tissues (Combs & Denicola, 2019). The xCT cystine-glutamate antiporter (SLC7A11) system is key to glutathione synthesis since it allows import of cystine and equimolar export of glutamate from the cells (Bansal & Celeste Simon, 2018). This is of special interest as several studies have reported that many cancer cells need to overexpress xCT to cope with oxidative stress (Gu et al., 2017; Sayin et al., 2017; Lanzardo et al., 2016) and promote invasive programs (Dornier et al., 2017), rendering xCT a promising pharmacological target for the treatment of multiple cancer types (Lanzardo et al., 2016; Conti et al., 2020). However, we show that lung micrometastases and the micrometastatic cells that we have generated from these downregulate xCT expression (Figure 4-4). Consistently, glutathione levels are downregulated in micrometastatic cells. Although our finding initially appears contradictory to the published literature, the aforementioned studies describe upregulation of xCT in the context of oxidative insults at the primary site without addressing xCT expression status in established metastatic lesions. Recently, an insightful study revealed that breast cancer cells bearing oncogenic phosphatidylinositol 3-kinase (PI3KCA) mutations (E545K or H1047R) can suppress xCT activity via protein kinase B (AKT)-mediated phosphorylation at xCT's serine-

26 (Lien et al., 2017). Two independent groups have further validated this posttranslational regulatory site in other types of cancer (glioblastoma and pancreatic cancer) showing that suppression of xCT activity through phosphorylation involves mTORC2 signalling (Gu et al., 2017) and its subcellular localisation is controlled by basal autophagy (Mukhopadhyay et al., 2021). Thus, xCT expression and activity can be modulated by multiple metabolic and posttranslational inputs. Indeed, pharmacological inhibition of xCT by sulfasalazine, which induces ferroptosis (Bansal & Celeste Simon, 2018), had to be terminated early in a clinical trial of patients with malignant gliomas due to detrimental effects on survival (Robe et al., 2009), highlighting the pressing need for further mechanistic dissection of xCT role in cancer progression (Li et al., 2022).

Our studies indicate that maintenance of redox homeostasis in lung metastatic cells is finely tuned. Marked depletion of total glutathione levels by pharmacological inhibition of its rate limiting biosynthetic enzyme (glutamate-cysteine ligase) using BSO results in reduced cell number (likely owing to inhibition of cell growth and/or increased cell death by ferroptosis (see below)) (Figure 4-5) in a way that is dictated by their basal glutathione levels. Reduced xCT and glutathione levels have been previously reported to induce the non-apoptotic cell death mechanism, ferroptosis (Stockwell et al., 2017). It has been highlighted that glutathione depletion leads to ferroptosis, even though BSO treatment does not necessarily induce this form of death (Combs & Denicola, 2019). This discrepancy has been attributed to the differential rate of GSH exhaustion by Gpx4 which is dictated by mitochondrial activity (Gao et al., 2019). Indeed, we have previously seen that micrometastatic cells have higher basal and maximal oxygen consumption rates than parental cells (data not shown), an observation that supports the notion of rapid GSH exhaustion in the former leading to ferroptosis and increased sensitivity to BSO treatment. Conversely, increasing concentrations of the inhibitor (up to 2.5μM) can be well-tolerated by parental cells without compromising cell viability or evoking further metabolic changes (Figure 4-6), akin to that which we observe in metastatic cells under similar glutathione depleted conditions.

A recent study has described a novel role for oxidative TCA cycle activity and mitochondrial respiration in thiol redox homeostasis which affects *de novo* proline biosynthesis (Ryan et al., 2021). In particular, inhibition of TCA cycle and respiration led to increased glutathione synthesis and impairment of proline synthesis (by triggering an Atf4-dependent integrated stress response) (Ryan et al., 2021). However, we find that micrometastatic cells produce increased quantities of proline (Figure 4-1) and secrete it in into the medium (Figure 4-7), whilst decreasing total glutathione levels. Nevertheless, our findings do not necessarily contradict the involvement of TCA cycle and oxidative phosphorylation, which are both functional in primary tumour and metastatic cells (as assessed by targeted metabolomics, Figure 4-1, and Seahorse flux analysis, data not shown), in proline biosynthesis. In fact, glutaminolysis is crucial for cancer cells to utilise glutamine-derived glutamate into several metabolic pathways, including TCA cycle (anaplerosis), and GSH and proline biosynthesis (Zhu&thompson, 2019). Previous work has shown that breast cancer cells rely on proline metabolism to sustain ATP production allowing them to efficiently colonise the lungs in the orthotopic 4T1 and EMT6.5 mouse models (Elia et al., 2017). Thus, it would be interesting to characterise the rewiring of glutamine metabolism associated with glutathione depletion by employing stable isotope tracing of U-^{13}C-glutamine with LC-MS analysis of our PyMT-derived panel of cell lines. Indeed, one possibility that could be addressed is that the selection pressures imposed by the lung microenvironment has forced micrometastatic cells to use so much of their glutamate pool to synthesise proline that there is insufficient remaining for glutathione production.

In addition to the altered polar metabolite profiles, we also show that micrometastatic cells differ in lipid metabolism and are enriched in certain sphingolipid species (ceramide, ceramide-1-phosphate and sphingomyelin) (Figure 4-10 - Figure 4-13). This finding is of importance as differences in sphingolipid composition can affect the physicochemical properties of cellular membranes, such as fluidity and subcellular organisation and this is likely to be mediated via the generation of lipid microdomains or ‘rafts’ (Van Meer et al., 2008). These properties, in turn, influence signal transduction pathways, and the sorting and transport of membrane cargoes within different subcellular compartments (Van Meer & Lisman, 2002). Recently, a mechanistic study showed that fatty acid

synthase (FASN)-mediated upregulation of sphingolipid metabolism-dependent signalling was involved in migration and invasion in colorectal cancer cells. Moreover, expression of FASN was higher in cells from liver metastases than those from patient-matched colorectal primary tumours (Jafari et al., 2019), and this is consistent with our observations that sphingolipid species are enriched in cells from lung micrometastases.

Taken together, here we provide evidence indicating that cells from the lung micrometastases of MMTV-PyMT driven mammary tumours downregulate glutathione production (Figure 4-14). We propose that, through reduced expression of the xCT cystine-glutamate antiporter system, micrometastatic cells cannot support so much γ-glutamyl-cysteine synthesis leading to decreased levels of both reduced and oxidised forms of glutathione. In addition, sphingolipid metabolism, and particularly ceramide, is altered in metastatic cells relative to primary tumour lines, a finding that can influence the biogenesis of small extracellular vesicles (sEVs), as previously reported (Trajkovic et al., 2008). Previous work from our lab has shown that metabolic stress can activate release of sEVs that transfer invasive characteristics to recipient cells (Rabas et al., 2021). The next chapter will, therefore, explore whether cells from primary tumours and lung micrometastases differentially release sEVs, and investigate the effects of glutathione and sphingomyelin metabolism on these processes.

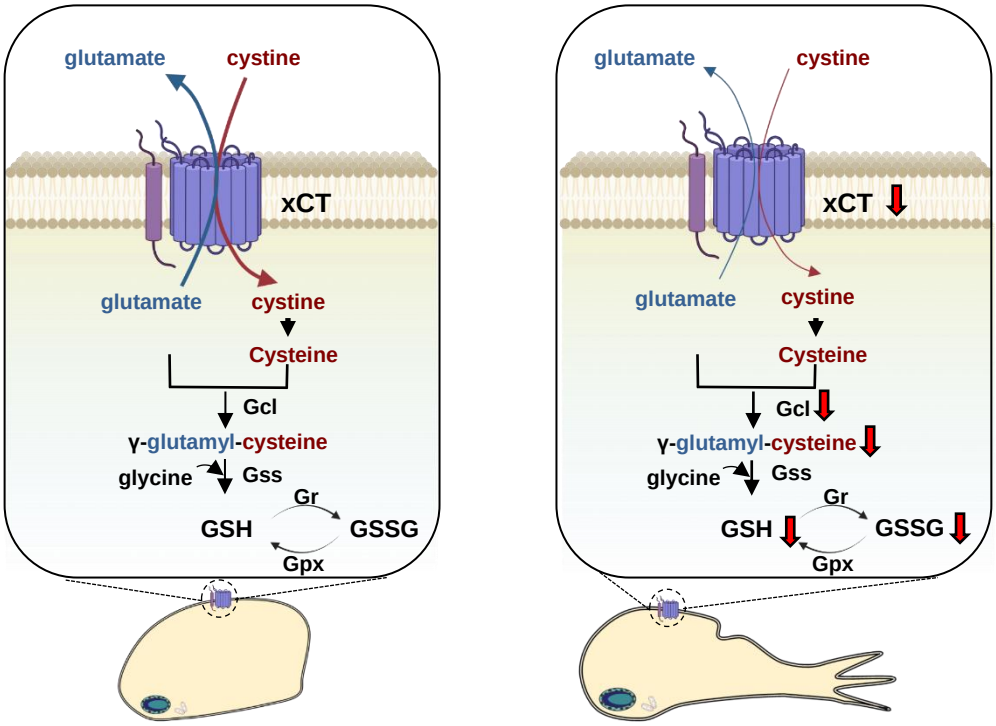

Figure 4-14 Schematic representation of altered glutathione metabolism in lung micrometastatic cells.
Reduced expression of the cystine-glutamate antiporter, xCT, leads to decreased γ-glutamyl-cysteine levels in micrometastatic cells. This, in turn, lowers total glutathione levels affecting both reduced (GSH) and oxidised form (GSSG) without affecting the ratio of GSH to GSSG.

Chapter 5 Glutathione and sphingomyelin metabolism influence small extracellular vesicle release

5.1 Introduction

Extracellular vesicle (EV) release is an evolutionarily conserved process (Margolis & Sadovsky, 2019). EVs are lipid-bilayered vesicles that can be of endocytic (exosomes, subset of small EVs or sEVs) or plasma membrane origin (microvesicles, apoptotic bodies), and transfer cargoes mediating cell-to-cell or cell-to-stroma communication within or between tissues (Tkach & Théry, 2016). Indeed, EVs have emerged as pivotal mediators of intercellular communication that regulate tissue homeostasis. EVs mediate communication between organs, such as between the liver and adipose tissue, in a way that influences the ability of these tissues to maintain metabolic homeostasis at a systemic level (Zhao et al., 2020). The capacity to mediate long-distance communication between tissues ideally places EV-mediated communication to be subverted by cancers to influence local and systemic microenvironments in a way that favours metastasis. Several independent studies have reported correlations between circulating levels of tumour derived EVs and cancer progression (Kim et al., 2003; Baran et al., 2010; Galindo-Hernandez et al., 2013; Nanou et al., 2020). Importantly, tumour-derived sEV cargoes have been shown to contribute to the generation of pre-metastatic niches either by influencing extracellular matrix deposition (Novo et al., 2018) or by modulating metabolism of resident cells in metastatic target organs (Fong et al., 2015; La Shu et al., 2018). However, thus far there are no studies, to our knowledge, comparing the sEV biogenesis/release pathways in primary tumour and matched metastatic cells.

Although the cellular and molecular mechanisms for the generation of EVs at the plasma membrane are still not clear, the machineries governing the biogenesis of sEVs within the endosomal pathway are well-studied (Van Niel et al., 2018). Indeed, sEVs are formed as intraluminal vesicles (ILVs) within the endosomal lumen during endosome maturation into late or multivesicular endosomes (MVEs) and this involves fine-tuning of intracellular membrane trafficking and cytoskeletal rearrangements. Furthermore, the cellular machineries controlling these processes dictate the cargo composition of sEVs, and govern the fate of MVEs

towards lysosomal degradation or transport to cell periphery for fusion with the plasma membrane (Van Niel et al., 2018). Recently, two independent studies have shown that sphingolipid metabolites are important both for maturation and trafficking of MVEs affecting cargo sorting (Kajimoto et al., 2013) and sEV production (Choezom & Gross, 2022) respectively.

Published work from our lab has recently established a link between cancer metabolism and upregulation of sEV release from breast cancer cells (Rabas et al., 2021). Indeed, depolarisation of mitochondria activates the PINK1 kinase to promote physical interaction of endosomes with late endosomes/MVEs. This leads to production of mitochondrial DNA (mtDNA)-containing sEVs that can, in turn, influence pro-invasive endosomal trafficking in recipient cells (Rabas et al., 2021). In the previous chapter, we found that lung micrometastatic and primary mammary tumour-derived cells have metabolomes which indicate that their glutathione and sphingolipid metabolism are distinct. This therefore raised the possibility that the metabolic re-wiring in micrometastatic cells might influence sEV release, and if this were to occur, it may involve cellular machineries influenced by glutathione and/or sphingolipid levels.

In this chapter, we have characterised the effect of cellular metabolism on the release of sEVs from PyMT-derived cells, with a particular focus on the sEV biogenesis pathway that discerns metastatic cells from matched primary tumour lines. We have interrogated the extent to which modulation of glutathione levels affects sEV release from primary tumour cells, and whether this is linked to altered sphingolipid metabolism. Finally, we have used CDM and organotypic collagen assays to assess whether disrupting the sEV biogenesis pathway in metastatic cells could affect their migratory capacity and invasiveness in complex microenvironments.

5.2 Results

5.2.1 Cells derived from lung micrometastases display increased sEV release

To test whether EV release differs in primary tumour derived and matched metastatic cell lines, we used differential centrifugation to isolate EVs from the conditioned media of PyMT-derived cells (Figure 5-1A, top panel). The isolated EVs were further processed by nanoparticle tracking analysis (NTA) to define the concentration and size of these extracellular vesicles (Figure 5-1A, bottom panel).

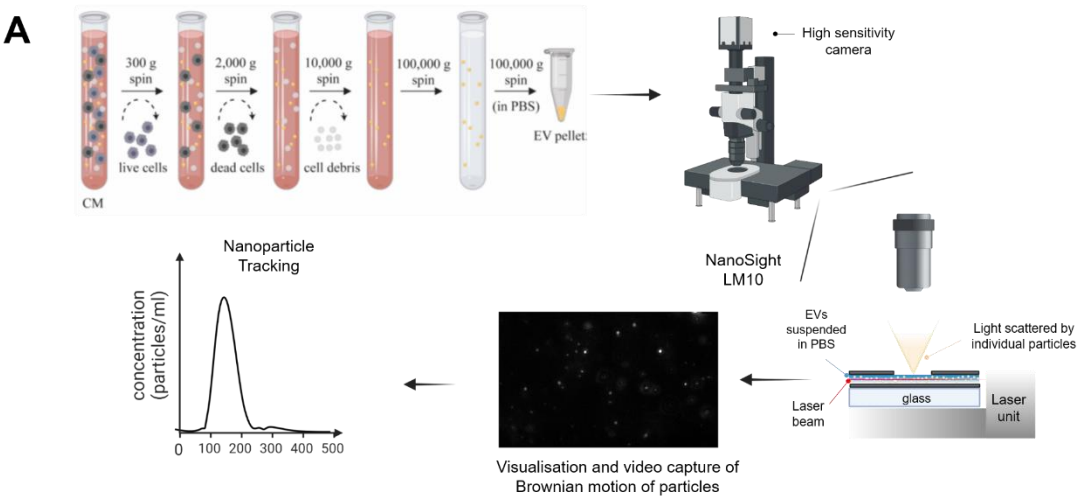

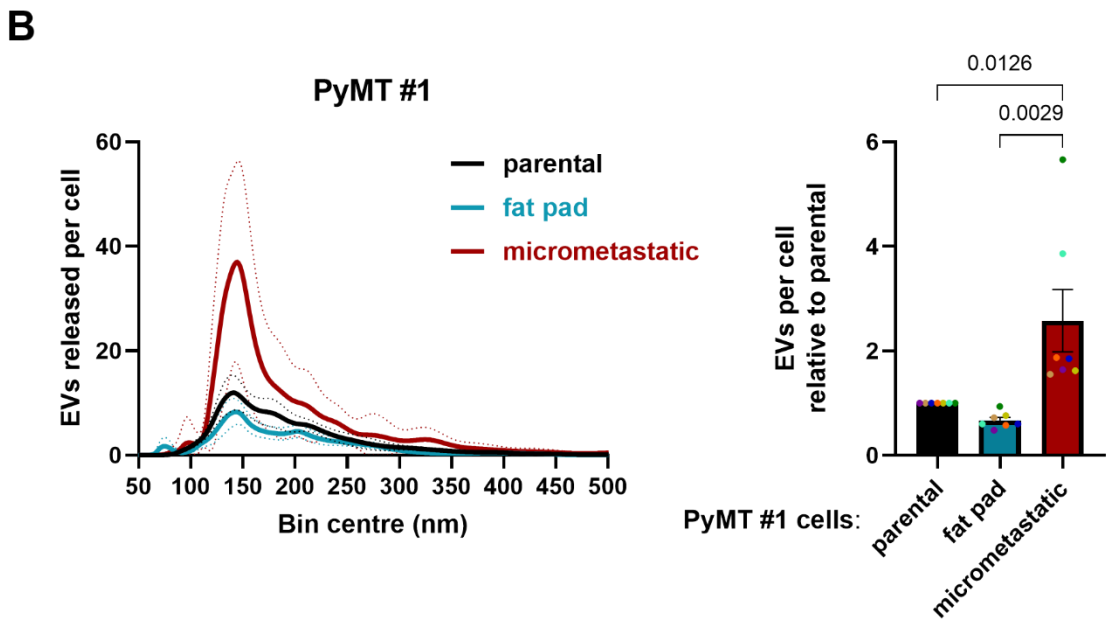

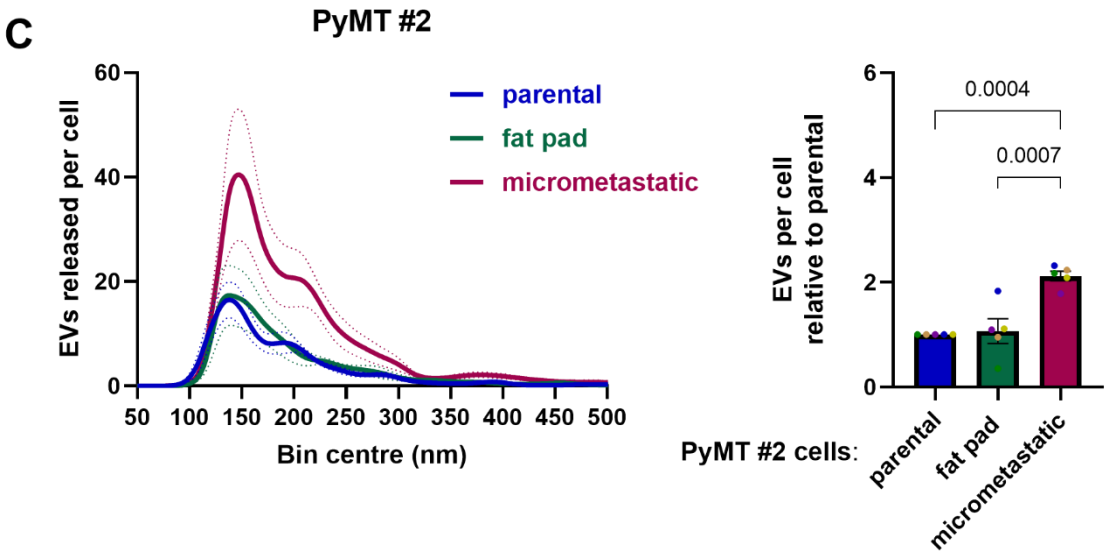

Figure 5-1 Cells from micrometastases release more sEVs than their counterparts from matched primary tumour cells.
(A) Schematic representation of sEV collection protocol and downstream NTA analysis. Conditioned media were collected from PyMT-derived cell lines and differentially centrifuged to remove live cells (300g), dead cells (2000g) and cell debris and larger lipid membrane fragments (10,000g). Then sEVs were pelleted at 100,000g, the pellet was washed in PBS before a final pelleting centrifugation at 100,000g, after which sEVs were re-suspended in PBS. Concentration and size distribution of these particles were determined using a NanoSight LM10 microscope. The sEV pellet was further diluted in PBS, and the light scattered by individual particles was collected, allowing direct visualisation and video capture of their Brownian motion. NTA software was used to track these movements and measure the particle size and concentration. (B, C) NTA analysis of particle number and size distribution of sEVs purified from PyMT#1 (B) or PyMT#2 (C) parental, fat pad and micrometastatic cells (left panels). Total particle concentration was normalised to the number of secreting cells and then expressed as fold change relative to the appropriate parental cells (right panels). Values are mean ± SEM, n=7 (PyMT#1 series (B)) or n=5 (PyMT#2 series (C)) independent experiments (coloured dots), one-way ANOVA, p-values are shown on the graph.

Strikingly, NTA showed that micrometastatic cells (PyMT#1 and PyMT#2) consistently secrete more EVs than their matched primary tumour lines (1.5-3-fold increase in metastatic/primary tumour-derived EVs, Figure 5-1B, C-right panel). Of note, this analysis revealed that more than 60% of EVs in all preparations were smaller than 200nm in particle diameter (Figure 5-1B, C-left panel), which is consistent with the size that is canonically attributed to exosomes (Van Niel et al., 2018). According to the recent ISEV guidelines (Théry et al., 2018) and appreciating the limitations of the EV isolation protocol used in our studies, we hereafter refer to exosomes as small extracellular vesicles (sEVs, size <200nm).

5.2.2 EV pellets from micrometastatic cells have increased tetraspanin and ESCRT-I protein content

Although exosomes and microvesicles originate from different cellular compartments (MVEs and plasma membrane respectively) and differ in size, their

overlapping range of EV cargoes makes the identification of proteins specifically enriched in sEVs challenging (Van Niel et al., 2018). For instance, several members of the tetraspanin family, including CD63, CD81 and CD9, have been extensively used as markers of exosomes, but with the latter two also being described to be present in microvesicles (Zhang et al., 2018; Mathieu et al., 2021). However, accumulation of CD63 in MVEs, and its strong enrichment in exosomes (Escola et al., 1998), renders it a reliable marker for sEVs (Mathieu et al., 2021). We therefore used western blotting to evaluate the expression of a panel of *bona fide* sEV markers in our preparations. We were able to detect the presence of the membrane-associated tetraspanins CD63, CD81, as well as the ESCRT-I associated protein TSG101 in sEVs pellets isolated from the conditioned media of PyMT-derived lines (Figure 5-2A, B-left panel). Quantitative analysis of protein levels revealed that the CD63 content of EV pellets from micrometastatic cells was 6-fold higher than that found in EV pellets from the corresponding primary tumour cells (Figure 5-2A, B-right panel). Taken together, these data indicate that metastatic cells release more CD63-containing sEVs than primary tumour derived lines.

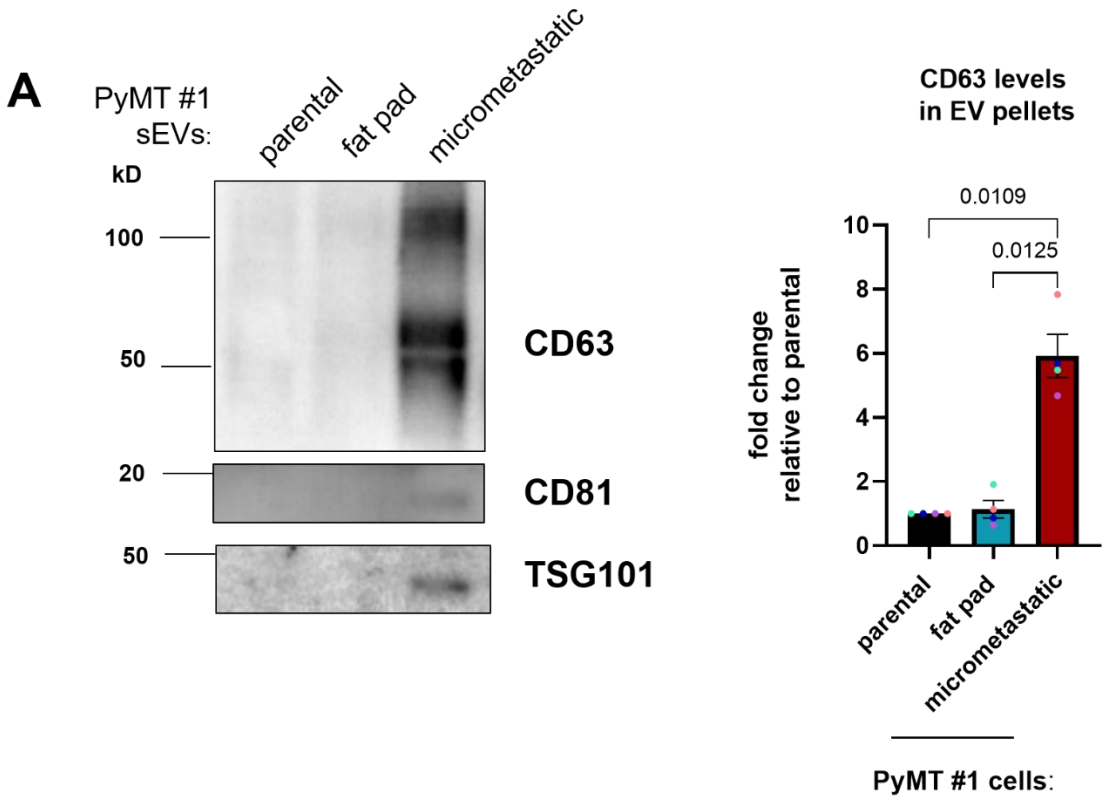

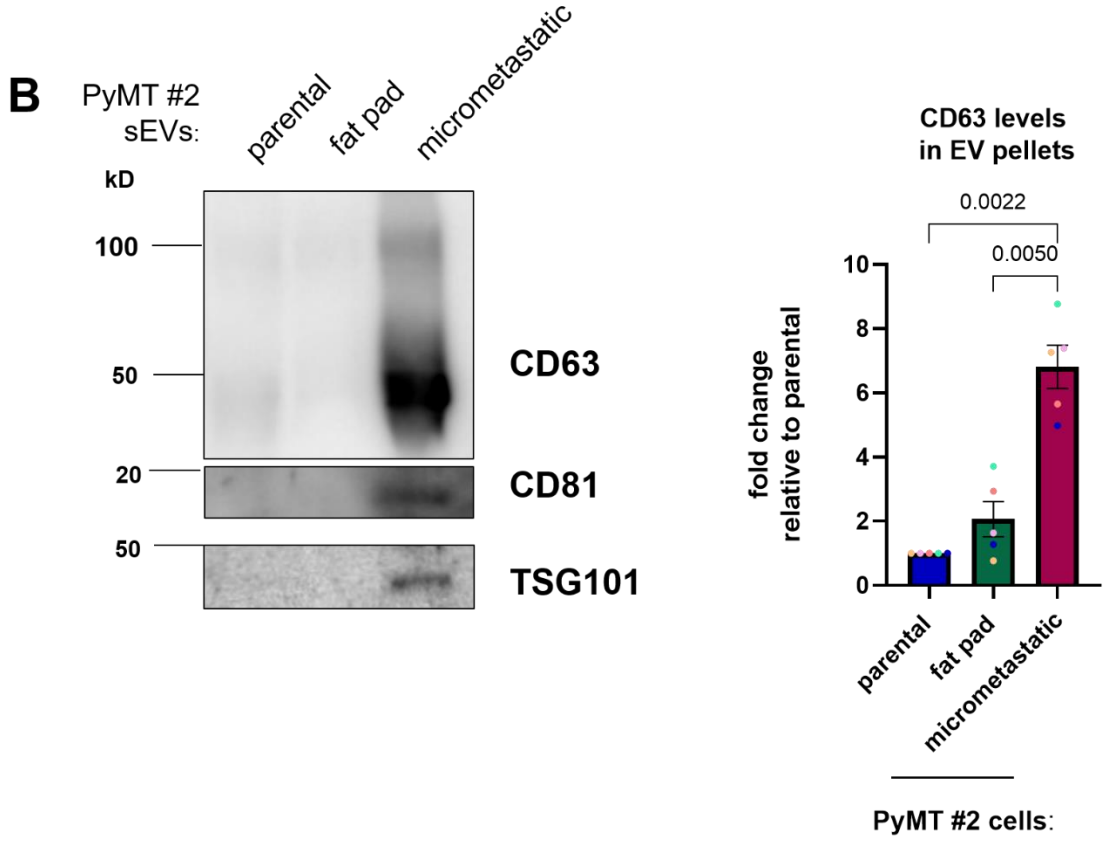

Figure 5-2 EV pellets from micrometastatic cells have increased tetraspanin (CD63, CD81) and ESCRT-I protein (TSG101) content.
sEV pellets were purified by differential centrifugation from parental, fat pad and micrometastatic cells from the PyMT#1 (A) and PyMT#2 (B) series and analysed by western blotting for the presence of EV markers (CD63, CD81 and TSG101). Sample loading was normalised to the number of sEV donor cells (left panels). Quantification of western blots for CD63 pellets was performed using the Image Lab software (Bio-Rad) (right panels). Values are mean ± SEM, n=4 (A) or n=5 (B) independent experiments (coloured dots), one-way ANOVA, p-values are shown on the graph.

5.2.3 Generation of nSMase CRISPR-KO PyMT-derived cell lines

EV biogenesis is tightly linked to cellular membrane dynamics, and the sphingomyelin pathway has been previously shown to regulate sEV biogenesis independently of the endosomal sorting complex required for transport (ESCRT) machinery (Trajkovic et al., 2008). Ceramide, the catabolic product of sphingomyelin following hydrolytic removal of phosphocholine moiety by neutral sphingomyelinases (nSMases), promotes inward budding into the lumen of endosomes (MVEs) and is enriched in sEVs (Trajkovic et al., 2008). Lipidome profiling revealed pronounced differences in ceramide and sphingomyelin levels between metastatic and primary tumour cell derived lines (see chapter 4). We, therefore, generated parental, fat pad and micrometastatic cells (from the PyMT#1 series) deficient for nSMase isoforms previously reported to contribute to the formation of sEVs (Trajkovic et al., 2008; Menck et al., 2017). We used the

CRISPR-Cas9 system to delete regions of the *Smpd2* gene, which encodes nSMase1, and this was achieved by designing three sets of single guide RNAs (sgRNA) against the target sequences (Figure 5-3A), as previously described (Sanjana et al., 2014). Following lentiviral infection and positive selection of Cas9-expressing cells, we determined nSMase1 expression by qPCR using primer pairs that were specifically designed to anneal outside of the deleted regions (in collaboration with Louise Mitchell, CRUK Beatson Institute, Glasgow). Although nSMase1 was the first identified and cloned mammalian nSMase, both its functional role and enzymatic specificity in sphingolipid metabolism remain ambiguous (Airola & Hannun, 2013). However, by mapping its sequence onto the *Smpd2* gene (NCBI primer blast) and extracting the encoded peptide sequence (UniProt blast) we were able to show that the region of nSMase1 which is deleted by sgRNA#2 is part of the catalytic domain of the enzyme, as previously reported (Airola et al., 2017) (Figure 5-3B). Indeed, we found that sgRNA #2 resulted in 95% deletion of nSMase1 (but not nSMase2; Figure 5-3C, right panel) expression (Figure 5-3C, left panel) across all three cell lines (without any further clonal selection) compared to their respective controls (NTC). On the other hand, sgRNAs #1 and #3 led to less efficient cleavage (65%, 75% deletion) of the target sequences (data not shown). Thus, we proceeded with the set of CRISPR-knockout (CRISPR-KO) cell lines derived from sgRNA #2, named hereafter as nSMase1#2, to study the effect of nSMase1 on sEV biogenesis and sphingolipid metabolism.

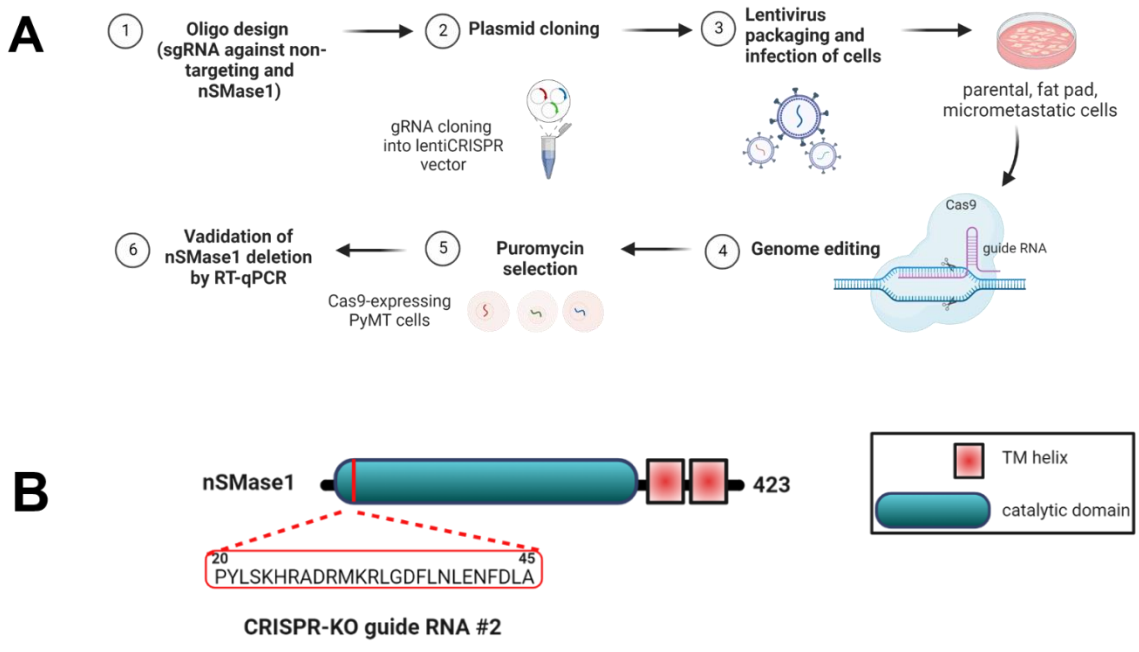

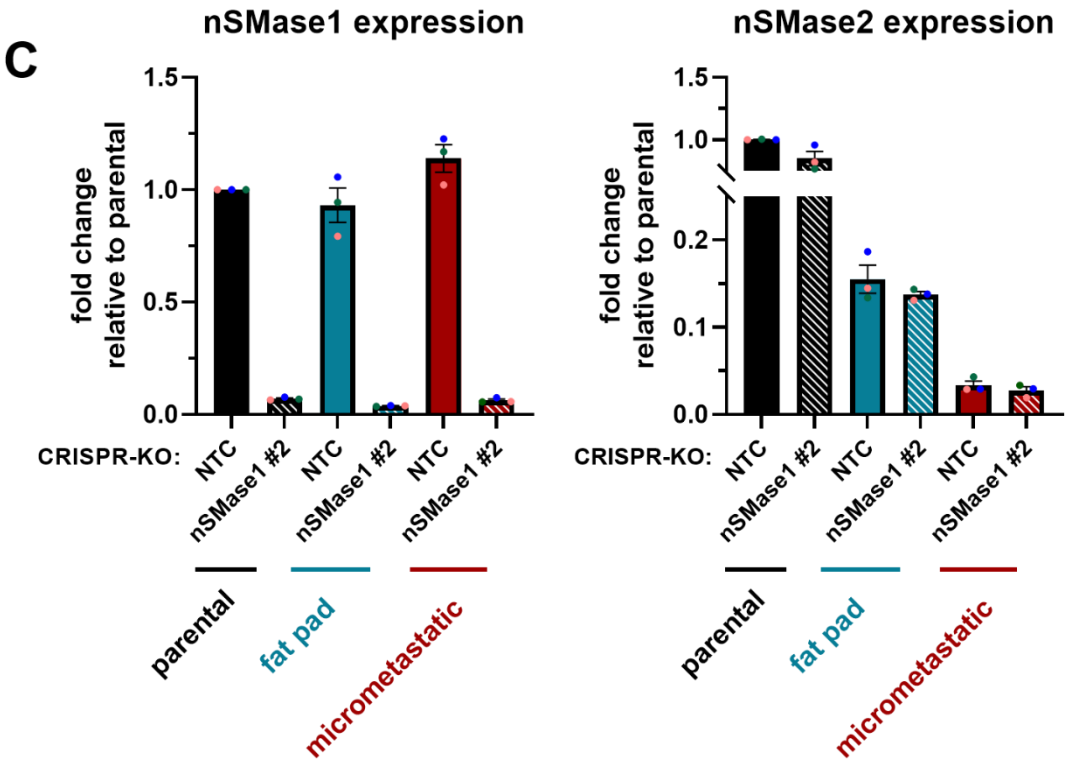

Figure 5-3 Generation and validation of nSMase1 CRISPR-KO cells.
(A) Schematic workflow for generating nSMase1 CRISPR-KO parental, fat pad and micrometastatic cells. First, oligos were designed based on the target sequences, and then cloned into a lentiCRISPR vector. HEK293T cells were used as the host packaging cell line, and target PyMT-derived cells were transduced with the lentivirus-containing media. 24 hours post infection, cells were cultured in puromycin-containing (2µg/ml) medium and were selected for seven consecutive passages. (B) Domain architecture, as previously reported in (Airola et al., 2017), of nSMase1 (*Smpd2*) highlighting in red the sequence and position of the peptide fragment encoded by part of the gene, the deletion of which was validated in (C) using a specific pair of primers.(C) qPCR was used to validate the Cas9-mediated deletion of nSMase1 (left graph) and assess nSMase2 expression (right graph). All data were normalised to ARPP P0 and presented relative to expression in parental NTC cells, values are mean ± SEM, n=3 independent repeats (coloured dots). These cell lines were generated in collaboration with Louise Mitchell, CRUK Beatson Institute, Glasgow.

In a similar manner as Figure 5-3A, genomic deletion of *Smpd3*, which encodes nSMase2, regions were also accomplished following infection with lentivirus encoding Cas9, along with gRNAs against the target sequences. We again used qPCR to validate the lack of nSMase2 mRNA expression by designing primers that specifically annealed outside of the regions designed to be deleted (in collaboration with Louise Mitchell, CRUK Beatson Institute, Glasgow). We confirmed that sgRNA #5 generated 95% cleavage of the target sequence (Figure 5-4B, right panel), while the efficiency of sgRNA (#1, #3)-mediated deletions were not consistent across the PyMT-derived cells (data not shown). Surprisingly, we noticed that metastatic cells, and to a lesser extent fat pad cells, showed decreased levels of mRNA encoding nSMase2 compared to parental cells (Figure 5-4B, right panel). Consistent with this, a number of studies have reported hyper

methylation of *Smpd3* gene leading to suppression of its expression in aggressive breast cancer cells (Demircan et al., 2009; Clarke et al., 2016). RT-qPCR showed that there were no significant differences in the levels of mRNA encoding nSMase1 following nSMase2 deletion in PyMT-derived cells (Figure 5-4B, left panel). After aligning the sequence of the deleted region with the *Smpd3* gene and extracting the encoded peptide sequence, we found that sgRNA #5 disrupted nSMase2 close to its C-terminal domain that encompasses the catalytic domain of the enzyme (Figure 5-4A). Collectively these data indicate the successful generation and establishment of nSMase2 deficient PyMT-derived lines, named hereafter as nSMase2#5.

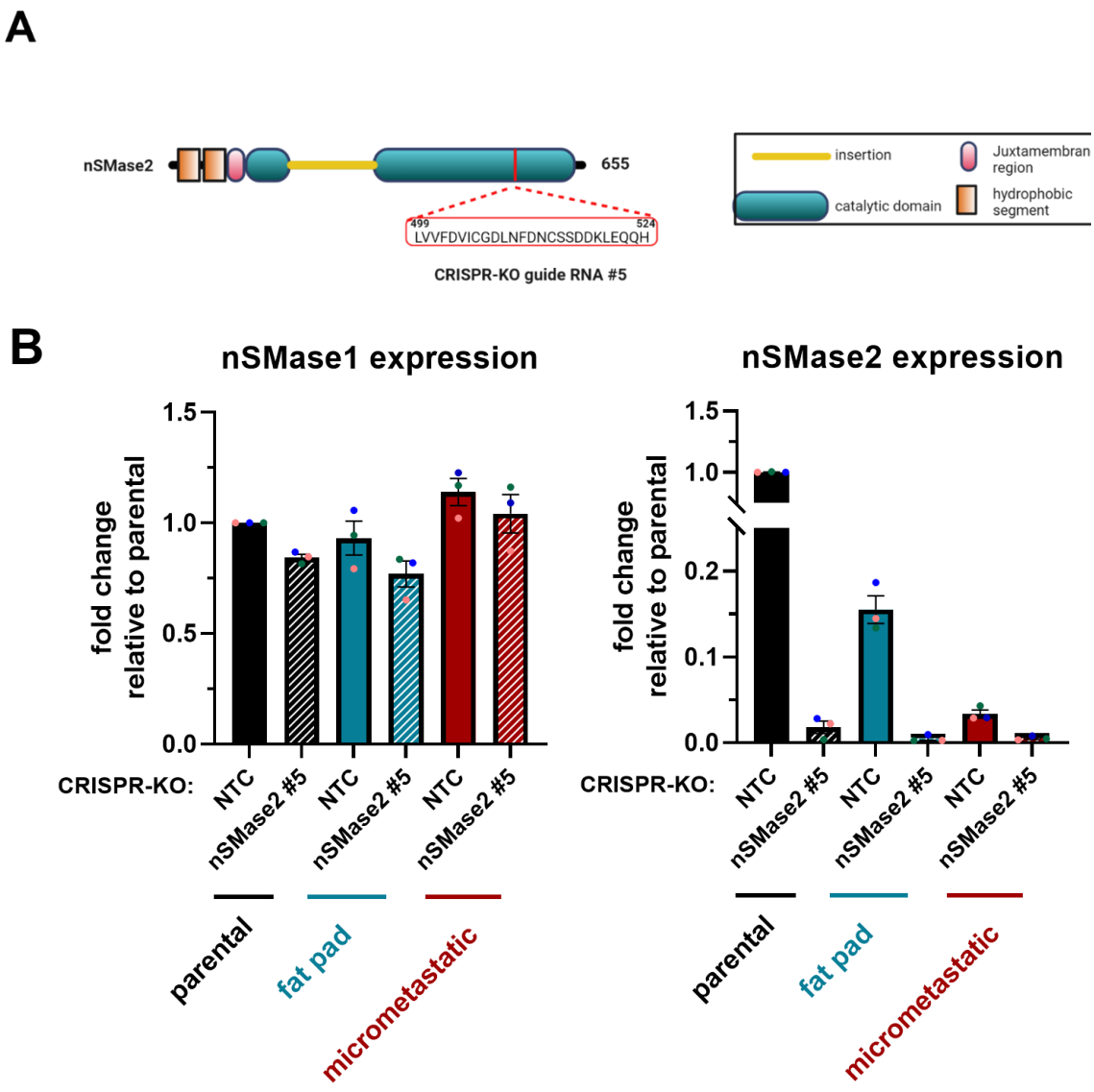

Figure 5-4 Generation and validation of nSMase2 CRISPR-KO cells.
(A) Domain architecture, as previously reported in (Airola et al., 2017), of nSMase2 (*Smpd3*) highlighting in red the sequence and position of the peptide fragment encoded by part of the gene, the deletion of which was validated in (B) using a specific pair of primers. (B) qPCR was used to assess nSMase1 expression (left graph) and validate the Cas9-mediated deletion of nSMase2 (right

graph) in PyMT-derived cell lines. All data were normalised to ARPP P0 and presented relative to expression in parental NTC cells, values are mean ± SEM, n=3 independent repeats (coloured dots). These cell lines were generated in collaboration with Louise Mitchell, CRUK Beatson Institute, Glasgow.

5.2.4 nSMase2 deletion leads to decreased ceramide levels in metastatic cells

Since data presented in Chapter 4 specifically suggest an enrichment of ceramide species in micrometastatic cells, we proceeded to assess whether deletion of nSMase1 or nSMase2 affects ceramide subcellular localisation and/or levels. To do this, we performed immunofluorescence staining of ceramide in control (NTC), nSMase1#2 and nSMase2#5 CRISPR-KO micrometastatic cells and visualisation using Airyscan super-resolution confocal microscopy. We detected punctate staining of ceramide both at the cytoplasm and plasma membrane in control (NTC) metastatic cells and quantitative analysis of mean fluorescence intensity indicated that nSMase2 depletion significantly reduced cellular ceramide levels, whilst CRISPR-KO of nSMase1 was less effective in this regard (Figure 5-5). These findings indicate that nSMase2 is the isoform of neutral sphingomyelinase which is primarily responsible for regulating ceramide levels in metastatic cells.

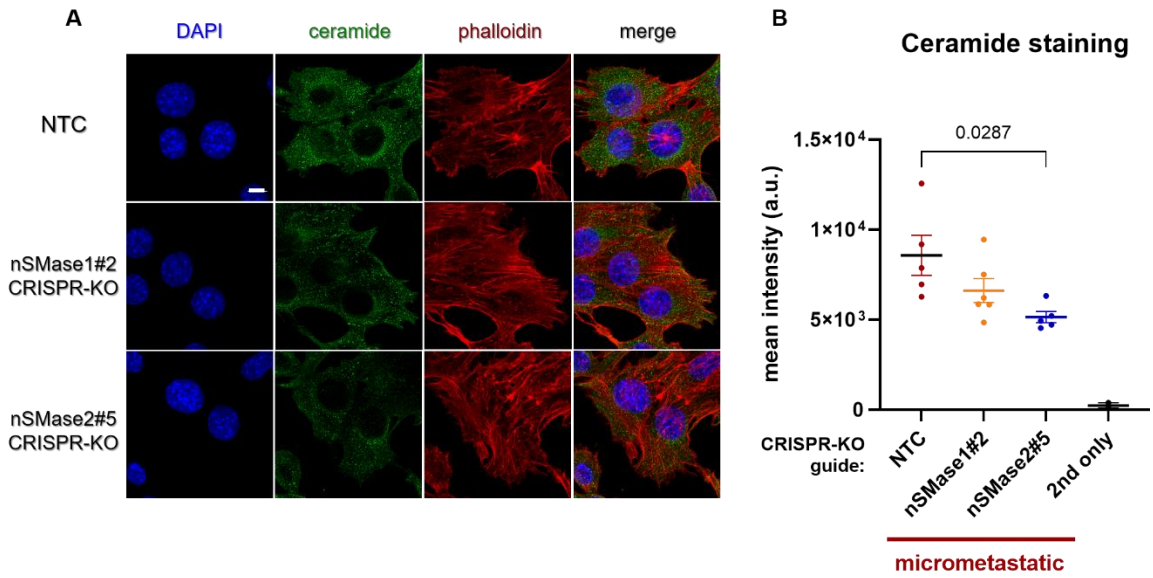

Figure 5-5 Immunofluorescence reveals decreased cellular ceramide levels following CRISPR-KO of nSMase2.
(A) Control (NTC), nSMase1#2 and nSMase2#5 CRISPR-KO micrometastatic cells were seeded on glass bottom dishes and fixed with 4% PFA following 48h of culture. Representative z-stack projections of confocal images showing ceramide (green) and phalloidin (red) that were visualised by immunofluorescence (63X magnification, Zeiss LSM 880 Airyscan confocal microscope). Scale bar, 10µm. (B) ImageJ was used to quantify the mean intensity of ceramide (sum of z-stacks, 10 stacks/field of view). Values represent mean ± SEM. n=5 fields of view, p values are shown on the graph, ordinary one-way ANOVA. The acquisition of these images was performed in collaboration with Luis Pardo, CRUK Beatson Institute, Glasgow.

5.2.5 CRISPR-KO of nSMase1 does not affect sEV release

A recent study has shown that depletion of nSMase1 has differential effects on the secretion of sEVs and larger EVs from breast cancer cells (SK-BR-3, Her2 amplified) (Menck et al., 2017). Though lacking a comprehensive characterisation of EV markers upon transient knockdown of nSMase1, the authors reported a decrease in sEV (<100nm) concentration, while the number of larger EVs (>100nm) was increased (Menck et al., 2017). First, we confirmed that nSMase1 knockout did not affect cell number across our panel of isogenic cell lines indicating that it does not play a significant role in cell proliferation (Figure 5-6A). To investigate whether nSMase1 affects sEV release in PyMT-derived mammary cancer cell lines, we collected conditioned media from control (NTC) and nSMase1#2 CRISPR-KO cells, and isolated EVs by differential centrifugation. NTA and western blotting of EV pellets indicated that nSMase knockout did not significantly alter the size (Figure 5-6B), number (Figure 5-6C) or CD63 (and other EV markers, including CD81 and TSG101) content (Figure 5-6D, E) of EVs released by parental, fat pad and micrometastatic cells.

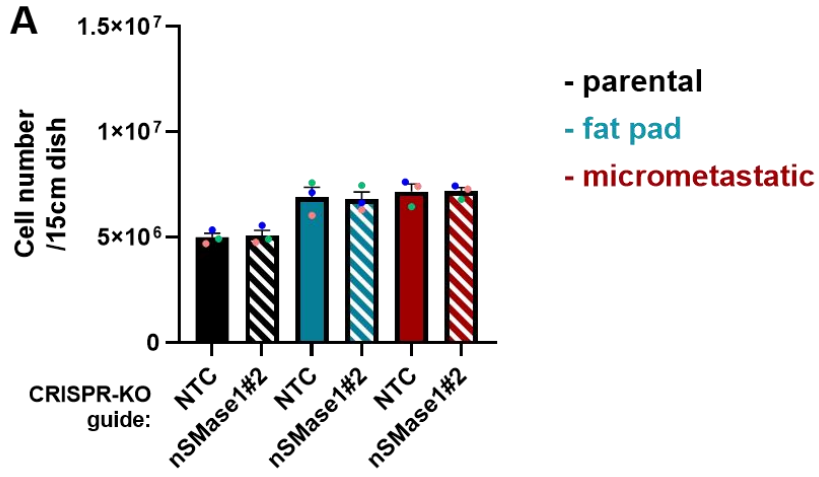
A
Cell number /15cm dish
1.5×10⁷
1×10⁷
5×10⁶
0
CRISPR-KO guide:
NTC
nSMase1#2
- parental
- fat pad
- micrometastatic

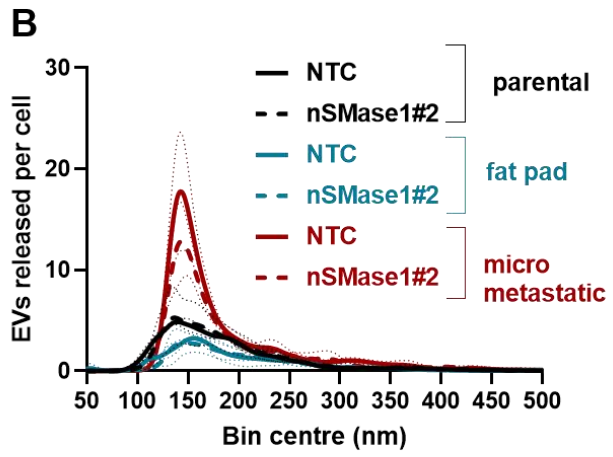
B
EVs released per cell
Bin centre (nm)
NTC
nSMase1#2
parental
fat pad
micro metastatic

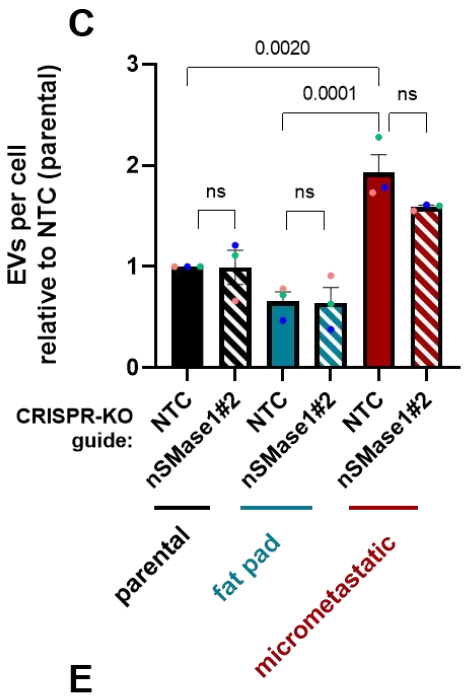
C
EVs per cell relative to NTC (parental)
0.0020
0.0001
ns
CRISPR-KO guide:
parental
fat pad
micrometastatic

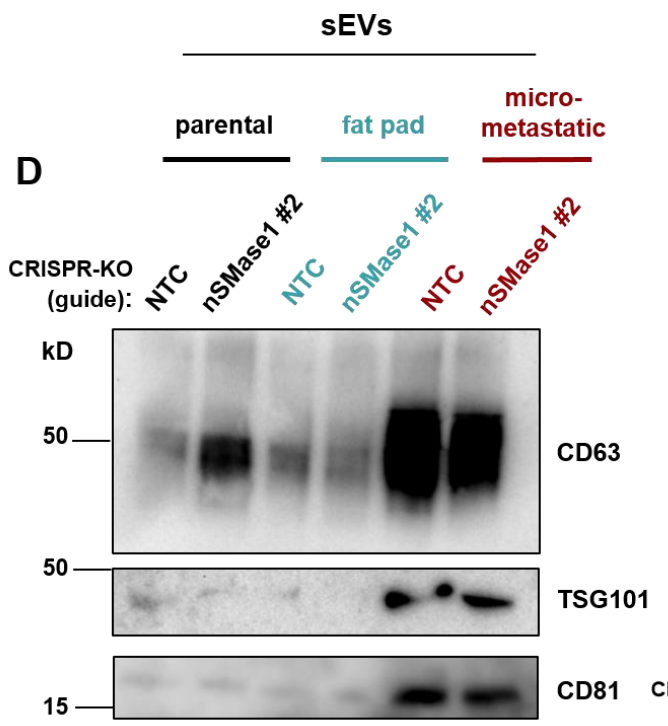
sEVs
parental
fat pad
micro-metastatic
D
CRISPR-KO (guide):
NTC
nSMase1 #2
kD
50
CD63
TSG101
CD81
15

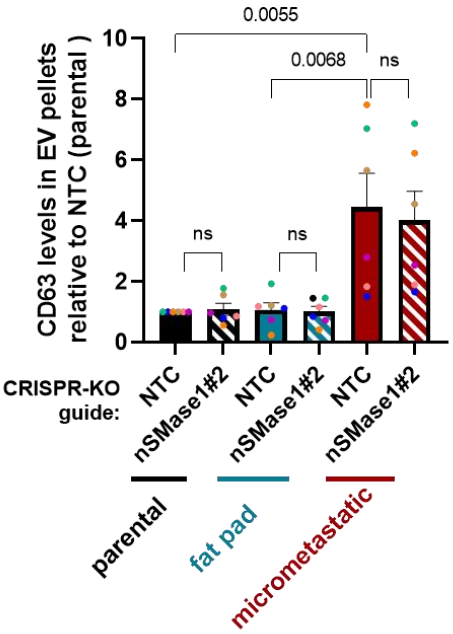
E
CD63 levels in EV pellets relative to NTC (parental)
0.0055
0.0068
ns
CRISPR-KO guide:
parental
fat pad
micrometastatic

Figure 5-6 nSMase1 knockout does not influence sEV release.
(A) Control (NTC) and nSMase1#2 CRISPR-KO PyMT-derived cells (parental, fat pad, and micrometastatic) were seeded in 15cm culture dishes and cell number counted 72 hours post seeding (day of EV collection), corresponding to cells reaching <80% confluence. Values are mean ± SEM, n=3 independent experiments (coloured dots). NTA analysis of (B) size distribution and (C) particle concentration of sEVs purified from NTC and nSMase1#2 KO parental, fat pad and micrometastatic cells. Total particle concentration was expressed as fold change relative to parental NTC cells. Values are mean ± SEM, n=3 independent experiments (coloured dots), one-way ANOVA, p-values are shown on the graph, ns; not significant. (D) sEVs were purified from NTC and nSMase1#2 KO cells and analysed by western blotting for the presence of established EV markers (CD63, CD81, and TSG101). Sample loading was normalised to the number of sEV donor cells. (E) Quantification of CD63 levels in sEV pellets was performed using the Image Lab software (Bio-Rad). Values are mean ± SEM, n=6 independent experiments (coloured dots), one-way ANOVA, p-values are shown on the graph, ns; not significant.

5.2.6 nSMase2 knockout reduces sEV release from micrometastatic cells

nSMase2 is one of the most studied mammalian neutral sphingomyelinases and has been established to be a critical regulator of cellular stress-induced generation of ceramide and secretion of sEVs (Airola & Hannun, 2013). Unlike nSMase1 whose role in sphingolipid metabolism is unclear, nSMase2 has been readily shown to hydrolyse sphingomyelin to ceramide, which promotes sEV biogenesis (Trajkovic et al., 2008) either via generation of membrane subdomains (Goñi & Alonso, 2009) and/or receptor mediated cargo-sorting into ILVs (Kajimoto et al., 2013). To study whether nSMase2 affects release of sEVs, we used differential centrifugation to isolate sEVs from the conditioned media of control (NTC) and nSMase2#5 CRISPR-KO PyMT-derived cells. Since intracellular ceramide levels may influence programmed cell death (Airola & Hannun, 2013), we assessed total cell numbers and showed that nSMase2 depletion did not compromise cell viability in any of our cell lines (Figure 5-7A). Strikingly, NTA revealed that nSMase2 deletion specifically inhibited secretion of sEVs from metastatic cells, whilst it did not oppose sEV release from primary tumour-derived lines (fat pad or parental) (Figure 5-7B, C). We further validated this by western blotting and found that nSMase2 deletion reduced the level of sEV markers in EV pellets from conditioned medium of micrometastatic (but not parental or fat pad) cells (Figure 5-7D). Indeed, quantitative analysis of western blots revealed an almost 2-fold decrease in CD63 content of EV pellets from micrometastatic cells following CRISPR-KO of nSMase2 (Figure 5-7E). Taken together, these data indicate that nSMase2 (and not nSMase1) controls EV release from micrometastatic cells, but not from cells derived from primary tumours.

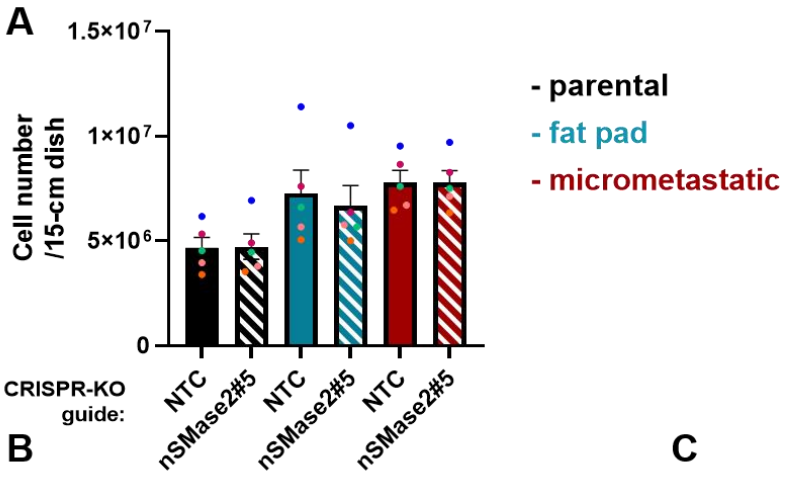
A
Cell number /15-cm dish
1.5×10^7
1×10^7
5×10^6
0
- parental
- fat pad
- micrometastatic
CRISPR-KO guide:
NTC
nSMase2#5
NTC
nSMase2#5
NTC
nSMase2#5

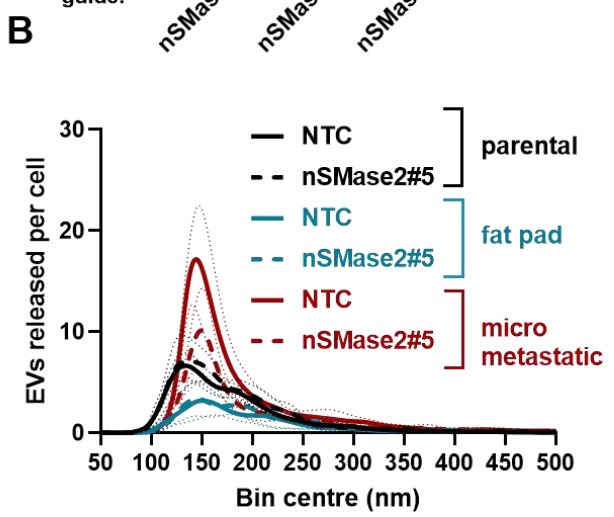
B
EVs released per cell
30
20
10
0
50 100 150 200 250 300 350 400 450 500
Bin centre (nm)
NTC
nSMase2#5
parental
NTC
nSMase2#5
fat pad
NTC
nSMase2#5
micro metastatic

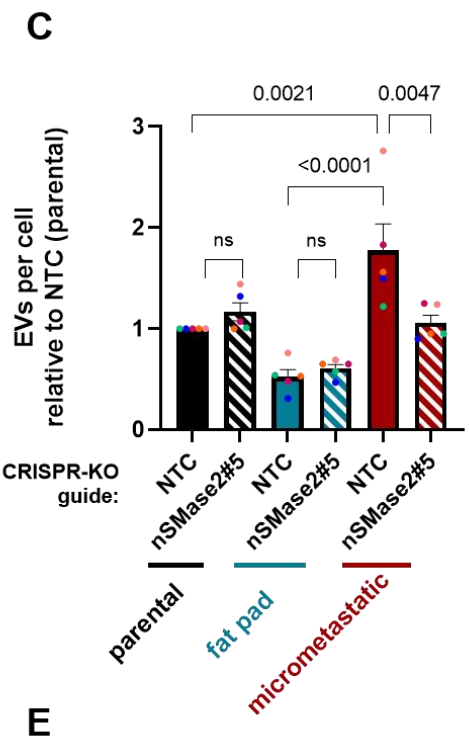
C
EVs per cell relative to NTC (parental)
0.0021
0.0047
<0.0001
ns
ns
3
2
1
0
CRISPR-KO guide:
NTC
nSMase2#5
NTC
nSMase2#5
NTC
nSMase2#5
parental
fat pad
micrometastatic

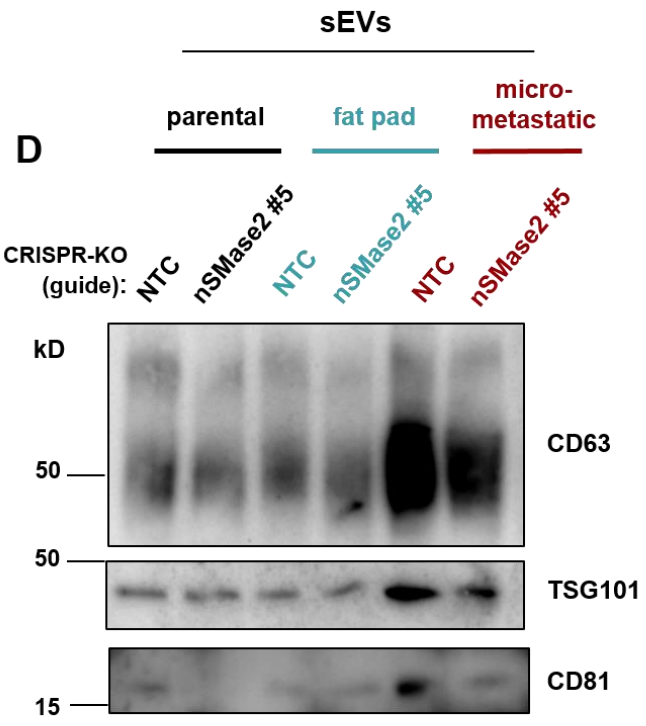
D
sEVs
parental
fat pad
micro-metastatic
CRISPR-KO (guide):
NTC
nSMase2 #5
NTC
nSMase2 #5
NTC
nSMase2 #5
kD
50
50
15
CD63
TSG101
CD81

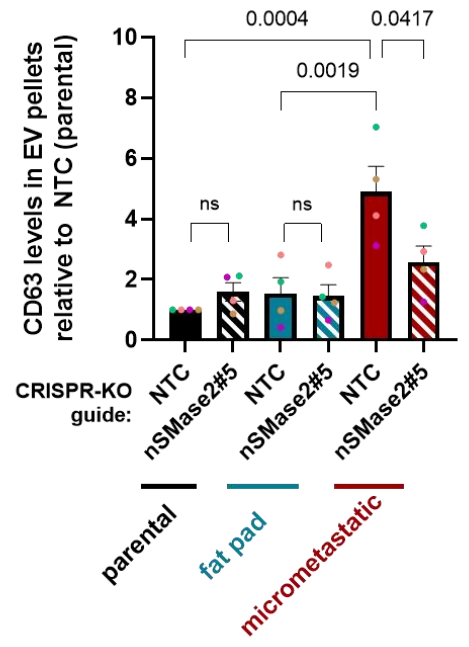
E
CD63 levels in EV pellets relative to NTC (parental)
0.0004
0.0417
0.0019
ns
ns
10
8
6
4
2
0
CRISPR-KO guide:
NTC
nSMase2#5
NTC
nSMase2#5
NTC
nSMase2#5
parental
fat pad
micrometastatic

Figure 5-7 nSMase2 knockout decreases sEV release from micrometastatic, but not primary tumour cells.
(A) Control (NTC) and nSMase2#5 CRISPR-KO PyMT-derived cells (parental, fat pad, and micro metastatic) were seeded in 15cm culture dishes and total cell number was counted 72 hours post seeding (day of EV collection), corresponding to cells reaching <80% confluence. Values are mean ± SEM, n=5 independent experiments (coloured dots). NTA analysis of (B) size distribution and (C) particle concentration of sEVs purified from NTC and nSMase2#5 KO parental, fat pad and micrometastatic cells. Total particle concentration was expressed as fold change relative to parental NTC cells. Values are mean ± SEM, n=5 independent experiments (coloured dots), one-way ANOVA, p-values are shown on the graph, ns; not significant. (D) sEVs were purified from NTC and nSMase2#5 KO PyMT-derived cells and analysed by western blotting for the presence of established EV markers (CD63, CD81, TSG101). Sample loading was normalised to the number of sEV donor cells. (E) Quantification of CD63 levels in sEVs was performed using the Image Lab software (Bio-Rad). Values represent mean ± SEM, n=4 independent experiments (coloured dots), one-way ANOVA, p-values are shown on the graph, ns; not significant.

5.2.7 Assessing the use of BSO to stably suppress cellular glutathione levels

A growing number of studies have focused on the effect of redox status (mainly oxidative stress) on EV release, but very few of them have provided mechanistic insights into the link between redox homeostasis and EV biogenesis pathways (Chiaradia et al., 2021). Recently, a study reported that sEVs possess antioxidant activity that mediates amelioration of senescence-associated phenotypes, including increased glutathione levels in recipient cells, without examining/targeting the underlying EV secretion routes (Fafiá N-Labora et al., 2020). In micrometastatic PyMT cells, glutathione levels are approximately 50-60% of those in PyMT cells derived from primary tumours, and we were interested in understanding whether this reduced glutathione could be linked to increased sEV release. We collect sEVs by allowing PyMT cells to condition EV-free medium over a 48-hour period. We, therefore, needed to determine whether reductions in cellular glutathione observed following incubation with BSO were maintained during this EV collection period. We treated parental PyMT cells with two concentrations of BSO (1.25μM and 1.88μM) that were previously (in Chapter 4) shown to reduce glutathione levels by approximately 40-50%. We then employed LC-MS to analyse the levels of reduced and oxidised glutathione over a 48-hour timecourse, thus mimicking the protocol used for EV collection (Figure 5-8A-schematic). This revealed that BSO treatment decreased GSH levels in parental cells as early as 3 hours (1.88 μM) and 6 hours (1.25 μM) post treatment respectively (Figure 5-8B, top graphs) and that these reductions were maintained for 48hr following addition of the inhibitor. GSSG levels were reduced with similar dynamics, but to a slightly greater extent than GSH levels (Figure 5-8B, middle graphs).

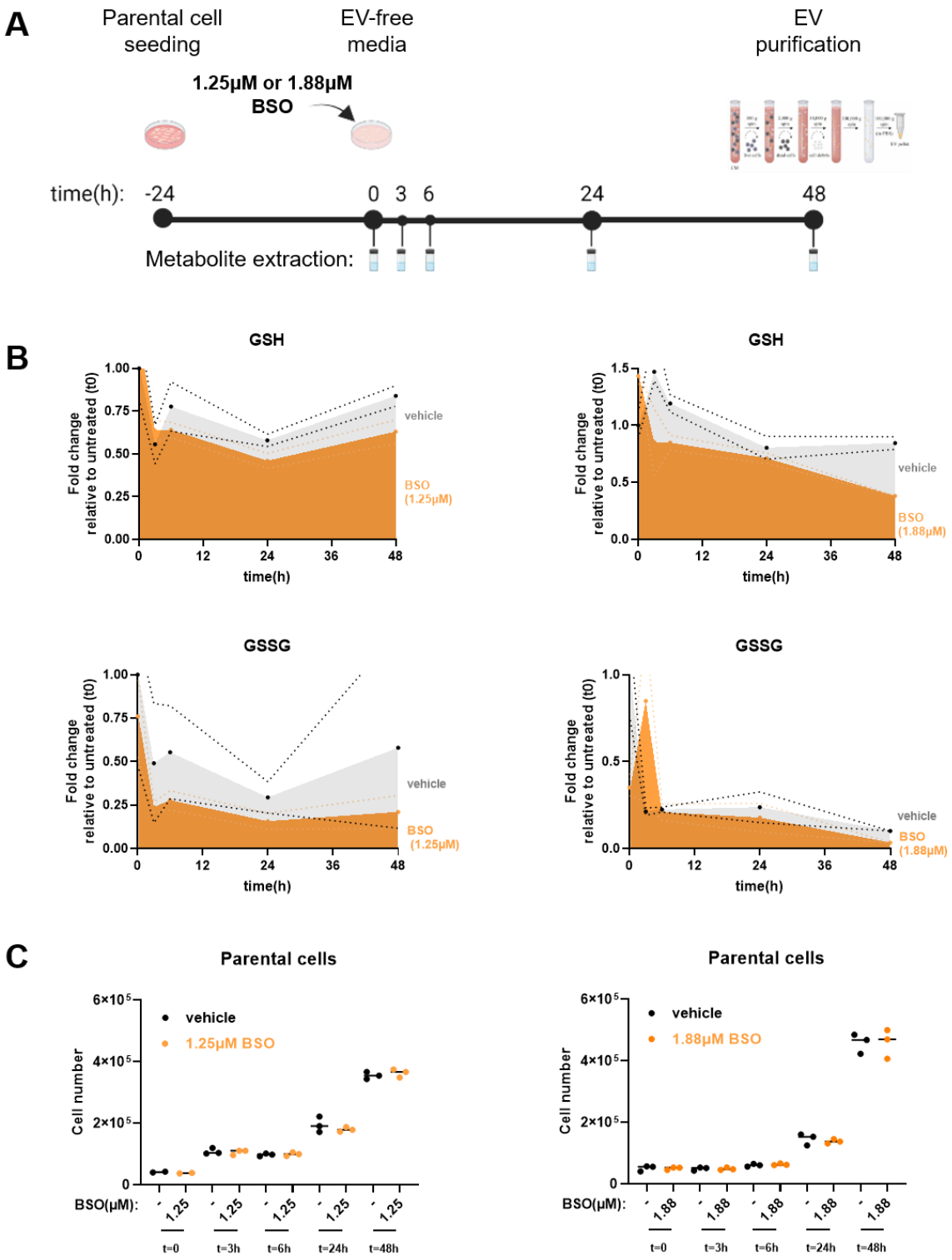

Figure 5-8 Dynamics of glutathione depletion following BSO treatment.
(A) Schematic representation of the time-course used for BSO treatment (1.25 or 1.88μM) of PyMT-derived parental cells which corresponds to the one used in our EV purification protocol. (B) Intracellular abundance (normalised to cell number) of GSH (top graphs) and GSSG (middle graphs) in parental cells treated with BSO (1.25 (left graphs) or 1.88 (right graphs) μM) or left untreated (vehicle) for the indicated times. (C) Parental PyMT cells were seeded in 6 well plates. After 24 hours, media were changed to EV-free media, treated with BSO (1.25 (left graph) or 1.88 (right graph) μM) or left untreated (vehicle) for the indicated time. Total cell number was counted at the indicated time points following BSO treatment. Values are mean ± SD, n=1 (3 technical replicates/condition).

We also counted the total number of parental cells (untreated and treated with BSO) for the indicated time points (Figure 5-8C, bottom graphs), and confirmed that inhibition of GSH synthesis did not compromise cell viability, and cells were able to grow exponentially up to the day of EV collection. Taken together, these data indicate that moderate and sustained depletion of glutathione may be evoked by treatment with BSO (at 1.25 or 1.88μM) thus allowing us to study its effect on EV release from PyMT-derived cells without compromising cell viability.

5.2.8 Glutathione depletion leads to upregulation of CD63 positive sEV release

To determine whether glutathione depletion affects sEV release, we treated primary tumour cells with various concentrations of BSO and collected EVs by differential centrifugation. We confirmed that, as before, pharmacological inhibition of GSH did not affect total number of sEV releasing cells (Figure 5-9A). NTA of EV preparations showed that there were no significant changes in the size (Figure 5-9B) or number (Figure 5-9C) of sEVs released following BSO treatment. However, western blotting revealed that the EVs pellets collected from cells treated with BSO contained increased levels of the EV markers, CD63 and TSG101 (Figure 5-9D). Quantification of these western blots indicated that the 48-hour treatment with 1.88μM BSO led to an approximately 4-fold increase in the CD63 content of EV pellets collected from parental PyMT cells (Figure 5-9E). These data imply that glutathione depletion does not influence the quantity of sEVs released by primary tumour cells, but it is sufficient to upregulate the release of CD63 positive sEVs from primary tumour cells.

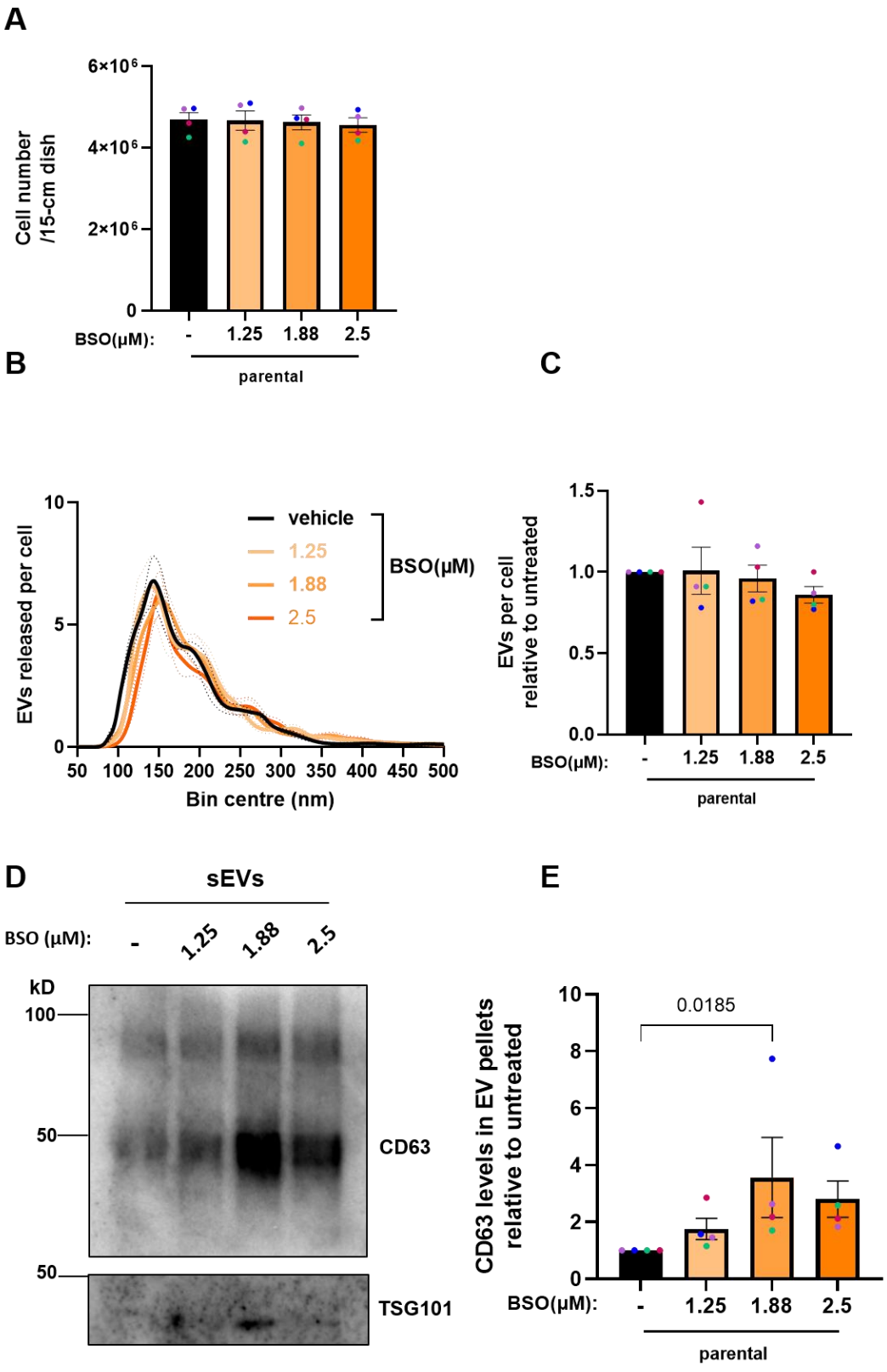

Figure 5-9 BSO treatment upregulates release of CD63-positive sEVs.
PyMT-derived parental cells were seeded in 15cm culture dishes and cultured for 24 hours in complete media. Following PBS washes, media were changed to EV-free, and cells were either left untreated (vehicle) or treated with increasing concentrations of BSO (1.25μM, 1.88μM, 2.5μM). (A) Total cell number was counted 72 hours post seeding (day of EV collection), corresponding to cells reaching <80% confluence. Values represent mean ± SEM, n=4 independent experiments (coloured dots). NTA analysis of (B) size distribution and (C) particle concentration of sEVs isolated from parental cells cultured in EV-free media without or with the indicated concentrations of BSO. Total particle concentration was expressed as fold change relative to untreated cells. Values are mean ± SEM, n=4 independent experiments (coloured dots). (D) sEVs were purified from untreated or BSO

treated (1.25μM, 1.88μM, 2.5μM) PyMT-derived parental cells and analysed by western blotting for the presence of established EV markers (CD63 and TSG101). Sample loading was normalised to the number of sEV donor cells. (E) Quantification of CD63 levels in EV pellets was performed using the Image Lab software (Bio-Rad). Values represent mean ± SEM, n=4 independent experiments (coloured dots), Friedman ANOVA with Dunn's multiple comparison, p-values are shown on the graph.

5.2.9 BSO-driven release of CD63-positive sEVs is nSMase-dependent

Earlier in this chapter, we showed that nSMase2 regulates ceramide production (5.2.4) and is required for sEV release (5.2.6) by micrometastatic cells. It has been reported that nSMase2 activity can be reversibly inhibited by GSH (Rutkute et al., 2007; Liu & Hannun, 1997), whereas reducing agents, like dithiothreitol and ß-mercaptoethanol do not, suggesting that reduction of disulphide(s) might not play a role in nSMase2 inhibition by GSH (Liu & Hannun, 1997). We reasoned that nSMase2 activity could act as a potential link between downregulated GSH levels and upregulated sEV release in metastatic cells. We were therefore interested in understanding whether nSMase activity is required for upregulation of CD63 positive sEVs in primary tumour cells upon glutathione depletion. To test this, we used differential centrifugation to isolate sEVs from the conditioned media of control (NTC), nSMase1#2 and nSMase2#5 CRISPR-KO parental cells, which were either treated with BSO (1.88uM) or left untreated. As modulation of glutathione and ceramide levels might affect cell viability, we confirmed that there were no changes in total cell number between untreated and BSO-treated cells when using this concentration of BSO (Figure 5-10A). nSMase2 (and, to a lesser extent, nSMase1) deletion opposed the BSO-driven increase in the CD63 content of EV pellets purified from the medium conditioned by PyMT-derived parental cells (Figure 5-10B). Consistent with our previous observations, NTA did not reveal any differences in the number (Figure 5-10C) or size distribution (Figure 5-10D) of sEVs secreted from NTC, nSMase1#2 and nSMase2-KO parental cells following treatment with BSO. Collectively, these preliminary findings support the notion that GSH exerts an effect on sEV release via regulation of nSMase2 activity, indicating a novel regulatory axis (GSH/nSMase2/ceramide) for the release of CD63-positive sEVs.

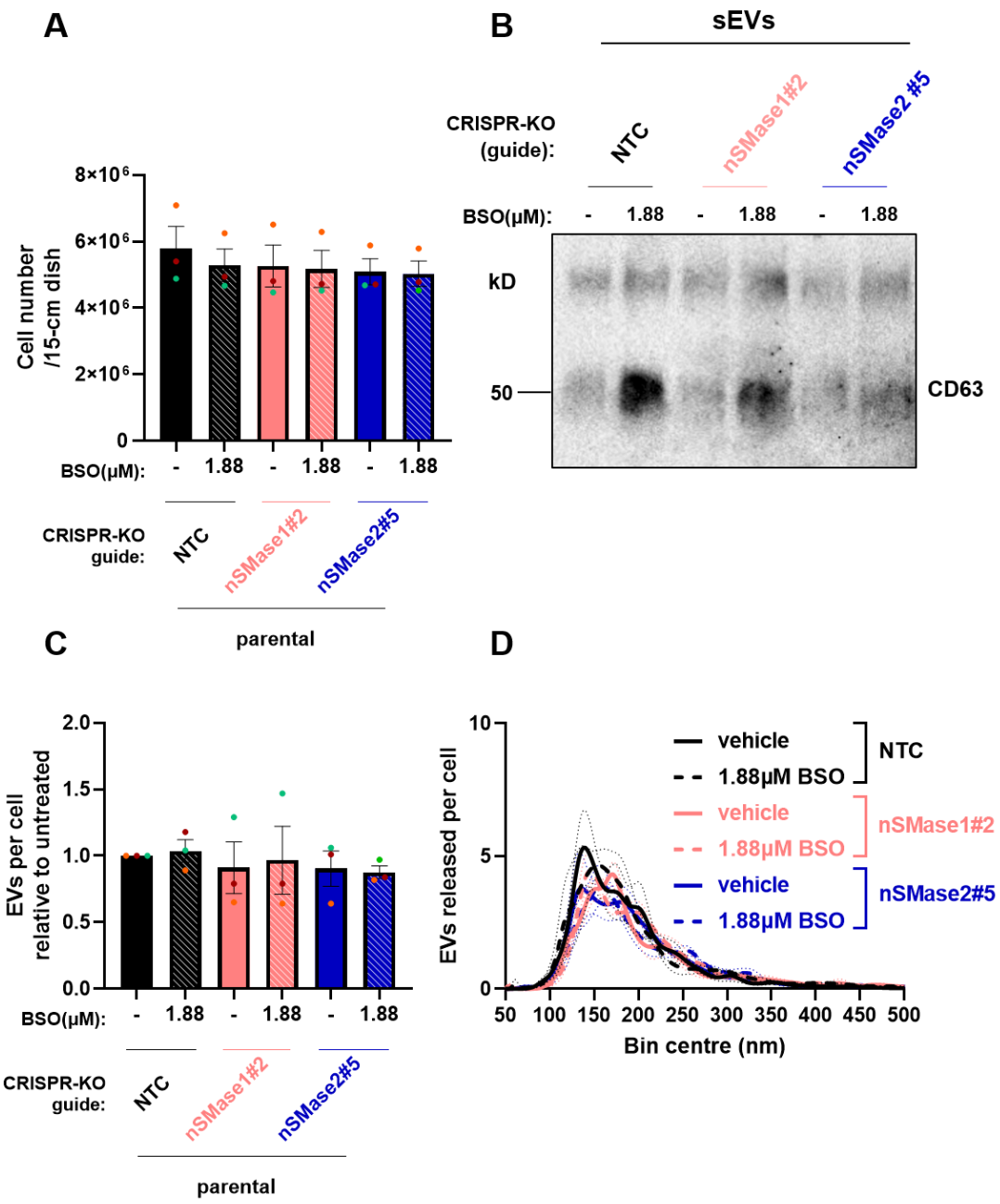

Figure 5-10 Deletion of nSMase2 opposes the BSO-driven increase in the CD63 content of EV pellets from primary tumour cells.
(A) Control (NTC), nSMase1#2 and nSMase2#5 CRISPR-KO PyMT-derived parental cells were seeded in 15cm culture dishes and grown for 24 hours in complete media. Following PBS washes, media were changed to EV-free medium, and cells were either left untreated (vehicle) or treated with BSO (1.88μM). Total cell number was counted 72 hours post seeding (day of EV collection), corresponding to cells reaching <80% confluence. Values represent mean ± SEM, n=3 independent experiments (coloured dots). (B) sEVs were purified from untreated or BSO treated (1.88μM) PyMT-derived parental cells (NTC, nSMase1#2 and nSMase2#5 CRIPSR-KO) and analysed by western blotting for the presence of CD63. Sample loading was normalised to the number of sEV-releasing cells. NTA analysis of (C) particle concentration and (D) size distribution of sEVs isolated from parental cells (NTC, nSMase1#2 and nSMase2#5 CRIPSR-KO) cultured in EV-free media without or with the indicated concentration of BSO. Total particle concentration was expressed as fold change relative to untreated cells. Values are mean ± SEM, n=3 independent experiments (coloured dots).

5.2.10 nSMase deletion does not affect the protrusion length of metastatic cells as they migrate on CDM

Recently published work has highlighted the ability of a specific ceramide pool (C16, C18, C24, C24:1) at the plasma membrane, which is generated via nSMase2, to influence cancer cell adhesion and migration (Canals et al., 2020). Interestingly, the effects of ceramide on loss of cell adhesion and increased migration of cancer cells were observed only upon chemotherapeutic drug-mediated activation of nSMase2 activity (Canals et al., 2020). To address whether the enhanced invasive behaviour of PyMT-derived metastatic cells (described in chapter 3) might be associated with nSMase expression, we seeded NTC, nSMase1#2 and nSMase2#5-CRISPR KO metastatic cells on CDM and assessed their subsequent ability to extend invasive protrusions into this physiologically-relevant matrix (Cukierman et al., 2001). Using time-lapse microscopy, we found that deletion of neither nSMase1 nor nSMase2 was sufficient to decrease the extension of invasive protrusions by metastatic cells (Figure 5-11). We confirmed that metastatic CRISPR control cells extended longer invasive protrusions (50-60μm) than their matched primary tumour counterparts (35-40μm) (Figure 5-11), indicating that selection of Cas9-expressing cells did not affect the original migratory phenotype we previously observed (in chapter 3). Our findings demonstrate that expression of neutral sphingomyelinases is not required for metastatic cells to extend invasive protrusions while migrating on CDM.

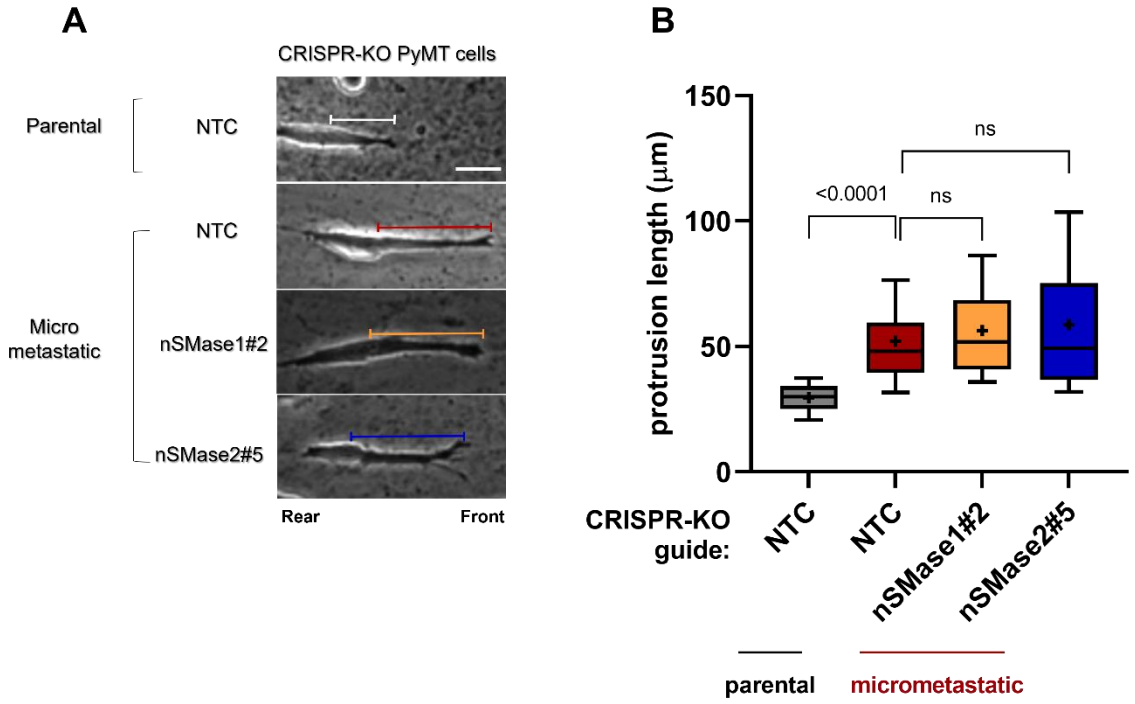

Figure 5-11 The extension of invasive protrusions by cells from lung micrometastases is not affected by deletion of nSMase1 or nSMase2.
(A) PyMT-derived parental (NTC) and micrometastatic cells (NTC, nSMase1#2 and nSMase2#5 CRISPR-KO) were plated onto fibroblast (TIF)-derived ECM and imaged using time-lapse video microscopy. Representative bright-field images (bar, 30μm) indicating the rear and front of cells according to the direction of movement. (B) The length of protrusions that cells extend in the direction of migration (distance from the nucleus to cell front) was measured using ImageJ. Whisker plots (10-90 percentile). The cross indicates the mean; n=96 cells assessed from 1 biological replicate, p-value is shown on the graph, ns: no significant ($p>0.05$), two-way ANOVA with Dunn's multiple comparison test.

5.2.11 nSMase2 deletion reduces invasion of micrometastatic cells into collagen plugs

In addition to cell autonomous mechanisms that foster tumour progression, the release of diffusible factors between cancer cells and other non-tumour cell types is critical for metastatic dissemination. Among these factors, sEVs have been shown to transfer cargoes through which they are able to influence the tumour stroma (Kosaka et al., 2013) or educate other cells in distant tissues (Peinado et al., 2012; Costa-Silva et al., 2015; Zhang et al., 2017; Novo et al., 2018) towards phenotypes that favour the formation of premetastatic niches (PMNs). As previously described (in chapter 3), organotypic collagen I plugs provide an excellent model of such complex microenvironments where ECM has been conditioned by fibroblasts for several days (Timpson et al., 2011). We were therefore interested in understanding whether deletion of nSMases could affect invasiveness of PyMT-derived metastatic cells when plated on organotypic plugs. We found that NTC and nSMase1#2-CRISPR KO metastatic lines were highly

invasive, with most cells invading into the plug and few of them residing on the upper portion (Figure 5-12, left, middle panels). Despite their ability to extend invasive protrusions whilst migrating on CDMs (Figure 5-11), nSMase2#5 CRISPR-KO metastatic cells were poorly invasive when plated onto fibroblast-conditioned collagen plugs. Indeed, barely any nSMase2-KO cells invaded into the collagen, with the majority of cells forming a thick layer on top of the plug (Figure 5-12, right panel). One possibility for the discrepancy between the requirements for nSMase2 in invasiveness in CDM (Figure 5-11) and organotypic assays (Figure 5-12) is that EVs (released by micrometastatic cells) can influence the microenvironment of the collagen by altering the behaviour of the fibroblasts in the plug.

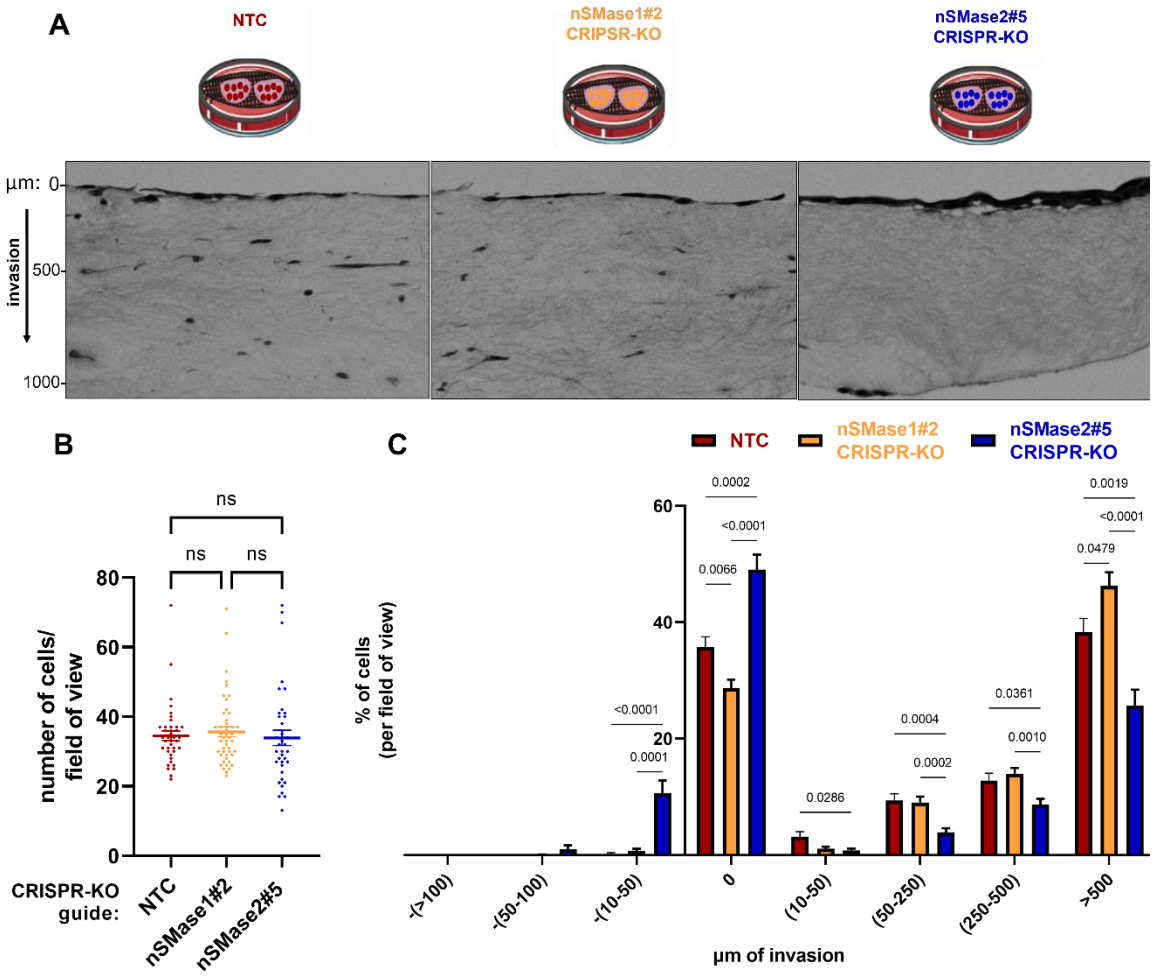

Figure 5-12 nSMase2 deletion opposes invasion of cells from lung micrometastases in an organotypic microenvironment.
(A) Organotypic plugs overlaid with NTC (left panel; red), nSMase1#2 CRISPR-KO (middle panel; orange) and nSMase2#5 CRISPR-KO PyMT#1-derived micrometastatic cell lines. Following 72 hours post seeding, plugs were placed onto grids in separate culture dishes containing full media (2 plugs/grid/condition). Tumour cells were allowed to invade for 3 days, followed by fixation and H&E staining. (B) Total number of cells tracked (H&E) per field of view for collagen plugs that were seeded with NTC, nSMase1#2 CRISPR-KO and nSMase2#5 CRISPR-KO PyMT#1-derived micrometastatic cells, n=39-47 fields of view/cell line, ANOVA Kruskal-Wallis test, ns; not significant. (C) Distribution

(expressed as % of cells) of the distance between cancer cells and invasion baseline (0 μm) per field of view for collagen plugs overlaid with NTC, nSMase1#2 CRISPR-KO and nSMase2#5 CRISPR-KO PyMT#1-derived micrometastatic cells. A negative value in distance intervals indicates that cells do not invade into the plugs and lag behind the invasion baseline, while a positive value denotes the actual invasion distance into the plugs as measured by ImageJ. Values are mean ± SEM, n=39-47 fields of view/cell line (one biological replicate for each cell line). Mixed effects ANOVA with Tukey's multiple comparison test, p values are depicted on the graphs.

5.3 Discussion

Cellular membrane dynamics coordinate cargo-shuttling between the cell surface and intracellular endosomal compartments, thus allowing communication of cancer cells with surrounding microenvironment and contributing to acquisition of highly invasive characteristics. Trafficking (endocytosis, exocytosis/recycling) of ECM receptors of the integrin family has proved fundamental in dictating their roles in different steps of the metastatic cascade (Caswell et al., 2009; Hamidi & Ivaska, 2018). Consistent with this, we previously showed (in chapter 3) that cells derived from lung micrometastases, which are highly invasive, display increased $\alpha_5\beta_1$ and TfnR recycling rates compared to cells derived from the primary tumour that engendered them. As early endosomes mature into MVEs, disruption of endosomal recycling regulators and retrograde transport from endosomes to the Golgi can affect cargo sorting into ILVs and the composition of sEVs released from cells (Van Niel et al., 2018). For instance, it was recently shown that deletion of caveolin-1, which regulates endomembrane trafficking, increases sEV release and affects cargo sorting (ECM components) across several cell types by acting as a cholesterol rheostat in MVEs (Albacete-Albacete et al., 2020). However, in this case, sEVs can be transferred to distant organs mediating stroma-tumour communication and priming of PMNs for subsequent colonisation and metastatic outgrowth (Peinado et al., 2012; Costa-Silva et al., 2015; Albacete-Albacete et al., 2020). Understanding the molecular mechanisms for sEV biogenesis could shed light on their pathophysiological relevance to disease progression, and help develop strategies to specifically interfere with machineries regulating cargo sorting and vesicle release. In this chapter, we report that cells derived from lung micrometastases release more sEVs by comparison with cells from their corresponding primary mammary tumour (Figure 5-1), and these vesicles are highly enriched in sEV markers (CD63, CD81, and TSG101) (Figure 5-2). We now discuss compelling evidence suggesting that metastatic cells derived from primary breast tumours rewire their metabolism in a way that influences the cellular machinery controlling sEV production.

Initial proof of ESCRT-independent mechanisms for MVE biogenesis, and thus sEV formation, came after showing that MVEs, highly enriched in CD63-positive ILVs, are still formed followed depletion of components of all four ESCRT complexes (Stuffers et al., 2009). This finding was corroborated by the seminal study showing

that ceramide formation generated by nSMase2 activity, promotes inward budding of endosomes to produce ILVs, which are subsequently secreted as sEVs (Trajkovic et al., 2008). In agreement with this, we found that increased release of sEVs by cells from lung micrometastases (but not from their corresponding primary tumour cells) was opposed following deletion of nSMase2 (Figure 5-7B, C). Similarly, expression of CD63 protein levels were significantly downregulated in these metastatic-derived sEVs upon nSMase2 loss (Figure 5-7D, E), which strongly supports their endocytic rather than plasma membrane origin (Escola et al., 1998; Mathieu et al., 2021). Certain studies have also reported a role for nSMase1 in EV biogenesis and cargo sorting (Guo et al., 2015; Albacete-Albacete et al., 2020; Menck et al., 2017). However, we were not able to find any significant differences in the size, number or composition of sEVs released from PyMT-derived cell lines following nSMase1 deletion (Figure 5-6). Intriguingly, the differential effect of nSMase expression on sEV biogenesis correlated with the intracellular levels of ceramide. Indeed, both ceramide levels and the CD63 content of EV pellets were reduced by nSMase2-KO, but nSMase1-KO was ineffective in both these regards (Figure 5-5). Moreover, data presented in the previous chapter revealed that metastatic cells are enriched for certain ceramide and sphingomyelin species. These findings are of interest for three reasons: Firstly, because they show that sphingolipid metabolism, and specifically ceramide generation, is altered in cells from lung micrometastases; Secondly, they suggest that ceramide levels are tightly linked to the biogenesis of CD63-positive sEVs released from micrometastatic cells; Thirdly, they provide the first evidence that mammary cancer cells switch-on a nSMase2-dependent mechanism of sEV release when they relocate from the mammary gland to the lung.

Although we cannot rule out that deletion of other regions of nSMase1 might be involved in ceramide formation and EV biogenesis in PyMT-derived cells, our data strongly suggest that the mechanism by which metastatic cells upregulate their sEV release requires ceramide generated by basal expression levels of nSMase2. Thus, it would be tempting to speculate that modulation of nSMase2 activity, besides its expression, in primary tumour cells could have an impact on the profile of sEVs secreted from these cells.

Although nSMase2 was cloned and identified almost 20 years ago (Hofmann et al., 2000; Marchesini et al., 2003), only recently a structural study deciphered its complete catalytic domain revealing an interdomain allosteric activation mechanism for ceramide formation. The proposed mechanism entails conformational change of a highly conserved structural element, the DK switch (named after two conserved aspartate (D) and lysine (K) residues), due to interdomain interactions promoting sphingomyelin hydrolysis to ceramide (Airola et al., 2017). Interestingly, the same research group has previously shown that nSMase2 activity can be reversibly inhibited by GSH (Liu & Hannun, 1997), a finding that was further supported by an independent study reporting an inverse correlation between GSH levels and nSMase activity *in cellulo* (Rutkute et al., 2007). Given the reduced glutathione levels in lung metastatic cells (as described in chapter 4), and their switch to nSMase2-dependent mechanism of sEV release, we hypothesised that there may be a link between these two phenotypes. With this in mind, we treated primary tumour cells with concentrations of BSO that we found to mimic (Figure 5-8) the alterations in GSH levels previously detected in micrometastatic cells. Indeed, we were able to show that glutathione depletion in parental cells leads to upregulation of CD63 positive sEVs (Figure 5-9), supporting our hypothesis that altered GSH metabolism can influence sEV secretion. Strikingly, preliminary data revealed that loss of nSMase2 was sufficient to oppose the increase in CD63 positive sEVs released from primary tumour cells upon glutathione depletion (Figure 5-10), further implying that GSH levels affect the secretion of CD63 positive sEVs in a nSMase2-dependent manner. Interestingly, neither glutathione depletion nor loss of nSMase2 expression influenced the number or size of sEVs released from primary tumour cells (Figure 5-9 & Figure 5-10). These observations point to the possibility of there being a sEV subpopulation with distinct composition (CD63 positive) that reflects the action of specific sorting machineries on the MVE compartment (van Niel et al., 2011; Van Niel et al., 2018). Another possible explanation for CD63 enrichment in parental-derived sEVs upon GSH depletion could also be the nSMase2-induced generation of ceramide, which could be further catabolised to sphingosine 1-phosphate promoting the maturation of MVEs and CD63 cargo sorting via receptor-mediated signalling, as previously reported (Kajimoto et al., 2013). Furthermore, stimulation of nSMase2 activity has been recently demonstrated to increase sEV secretion by decreasing vacuolar H^+-ATPase (V-ATPase)-mediated endosome

acidification (Choezom & Gross, 2022), and thus these additional mechanisms could be further investigated by studying the relationship between nSMase2 activity (modulation of intracellular GSH levels using BSO and validation of its effect on ceramide levels) and the dynamics of CD63 (fluorescently labelled) sorting into ILVs (using fluorescence recovery after photobleaching, FRAP, as previously described in (Kajimoto et al., 2013)).

With regard to invasive characteristics, we found that depletion of nSMase1 or nSMase2 did not affect the ability of metastatic cells to extend invasive protrusions as they migrate on CDM (Figure 5-11). This is in contrast with the recently reported role for ceramide in regulating cell adhesion and migration in HeLa cells (Canals et al., 2020). In this study, sublethal doses of chemotherapy drugs (doxorubicin and vorinostat) led to nSMase2-dependent generation of specific pool of ceramide at the plasma membrane, which was sufficient to drive cell migration by regulating acute signalling programs. However, because we have not examined the effects of chemotherapy drugs, these findings cannot be extrapolated to our experimental conditions. Another study has reported that modulation of nSMase2 levels in 4T1 cells (mouse mammary tumour cells with high metastatic ability) did not affect migration and invasion *in vitro* (Kosaka et al., 2013), which is in agreement with our observations. Interestingly, these researchers found that, following orthotopic transplantation of these cells into the mammary fat pad, nSMase2 overexpression or silencing respectively led to increased and decreased lung metastatic burden by influencing angiogenesis in the transplanted tumours via release of microRNA (miRNA)-containing sEVs (Kosaka et al., 2013). Similarly, we noticed that loss of nSMase2 prevented metastatic cells from invading into collagen I organotypic plugs, while control or nSMase1-depleted cells were highly invasive with most cells entering the plug (Figure 5-12). This exciting finding cannot be explained by a cell autonomous mechanism by which nSMase2 expression promotes the invasive capacity of metastatic cells, raising the possibility that cancer cell invasion might be indirectly mediated by the effect of EVs on fibroblasts that are also present in the organotypic environment. This hypothesis could be further tested by pre-treating fibroblasts with sEVs from nSMase2-depleted and control metastatic cells, allowing them to generate ECM, which could then be decellularised and parental

cells then plated onto these ECM to assess their migration, as previously reported in (Novo et al., 2018).

In conclusion, we have found compelling evidence indicating that altered glutathione levels in mammary cancer-derived lung metastatic cells influence the cellular machinery controlling sEV production (Figure 5-13). Through downregulating cellular glutathione levels, lung micrometastatic cells are able to upregulate the release of CD63 positive sEVs in a nSMase2-dependent manner. And finally, we have shown preliminary data suggesting a requirement of nSMase2 for metastatic cells to exhibit invasive phenotypes in a collagen-rich organotypic environment, a phenomenon which appears to be mediated via a non-cell autonomous mechanism and warrants further mechanistic investigation.

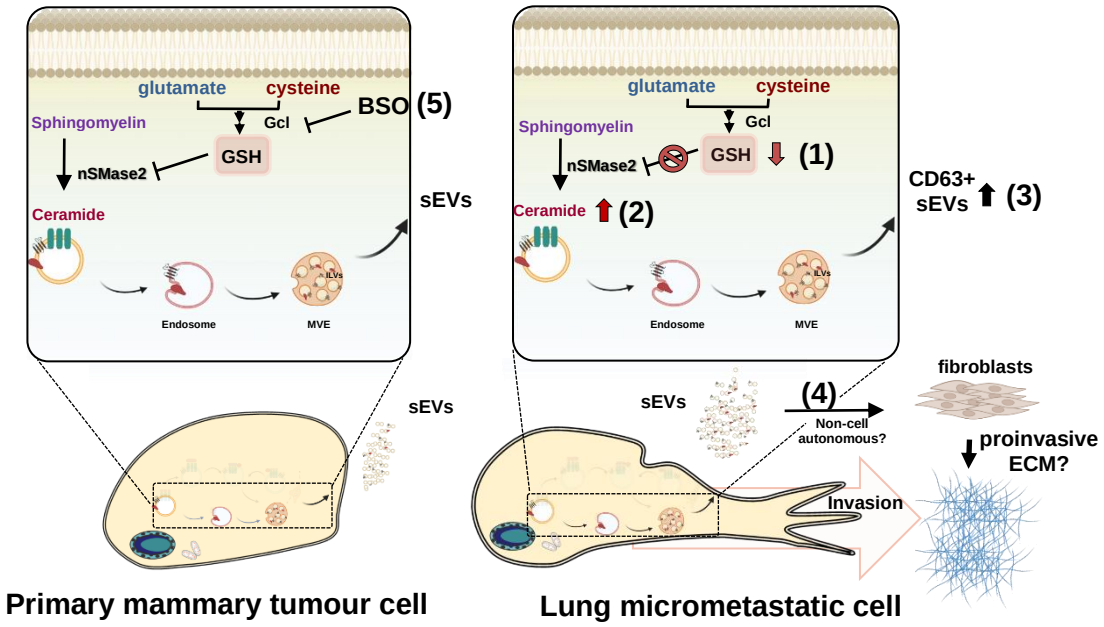

Figure 5-13 Schematic representation of the effects of glutathione levels and neutral sphingomyelinase 2 activity on sEV production.
(1) Metastatic cells with downregulated levels of GSH, which has been previously shown to inhibit nSMase2 activity(Liu & Hannun, 1997; Rutkute et al., 2007), increase production of ceramide (2) which is mediated by nSMase2. (3) In turn, they switch to a nSMase2-dependent EV biogenesis pathway leading to the upregulation of CD63 positive sEV release. (4) nSMase2 promotes invasiveness of metastatic cells in an organotypic environment. It is currently unknown whether this is due to effects of metastatic-derived sEVs on fibroblasts present in this complex microenvironment, and/or whether it is related to the ability of the fibroblasts to influence ECM deposition/remodelling to support invasion. (5) GSH depletion (BSO treatment) in primary tumour cells (to levels that mimic those detected in metastatic cells) can promote upregulation of CD63 positive sEV release in a nSMase2-dependent manner.

Chapter 6 Final Discussion

Metabolic reprogramming enables cancer cells to overcome challenges encountered on the path to metastasis and drives their potential to seed distant organs. We show here that cells from mammary cancer lung metastases display increased invasive behaviour, and rewire their metabolism, possibly to adapt to the microenvironment of the lung. These metabolic adaptations are manifest in reduced cellular glutathione - which we show leads to upregulation of sEV release - and increased levels of sphingolipids, particularly ceramide. Moreover, both sEV release and invasiveness of micrometastatic cells is dependent on the action of neutral sphingomyelinase 2, a key enzyme for generation of ceramide. (Figure 6-1).

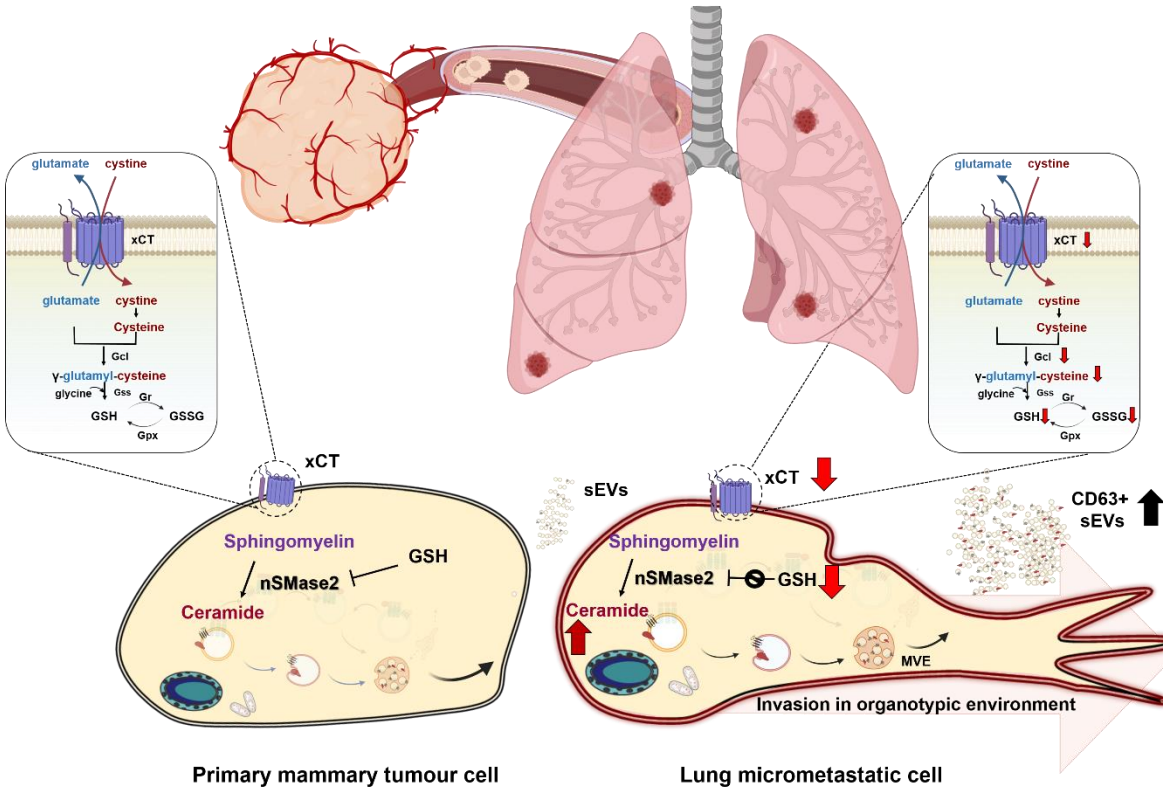

Figure 6-1 Proposed model for metabolic control of sEV production in cells from primary tumours and lung micrometastases.
Lung micrometastases and cells derived from these, have reduced levels of the xCT antiporter system. This reduces synthesis of γ-glutamyl-cysteine and, in turn, glutathione. nSMase2 is inhibited by glutathione. Therefore, we propose that reduced glutathione levels lead to activation of nSMase2. Increased nSMase2 activity then generates ceramide which drives the biogenesis and release of CD63-containing sEVs. We propose that increased sEV release contributes to the generation of a more invasive microenvironment.

A recent study demonstrated that although glutathione production is required for tumour initiation in mammary carcinogenesis, it becomes dispensable later in

disease progression (Harris et al., 2015). These authors showed that both genetic depletion of Gclm - the modifier subunit of glutamate-cysteine ligase (Gcl; Figure 6-1) that supports Gclc (catalytic subunit) in *de novo* GSH synthesis - and administration of BSO, decrease tumour burden. Moreover, BSO treatment only decreases tumour burden when administered prior to tumour onset. Gclm-knockout (which leads to an 80% decrease in GSH levels) in primary mammary epithelial cells evokes Nrf2-mediated antioxidant response leading to upregulation of the thioredoxin pathway which enables GSH-depleted cells to scavenge ROS. Thus, it is clear that cells may need to adjust the amount of glutathione they make to overcome various hurdles encountered throughout disease progression – indeed, high glutathione levels are likely key for tumour initiating cells to overcome oncogene-induced senescence (Nogueira et al., 2008; Harris et al., 2015) during very early tumorigenesis, and our study indicates that low glutathione levels might be necessary during the early stages of metastatic seeding. It is interesting to speculate what selection pressures might lead to establishment of a micrometastatic cell population with reduced glutathione levels. We are currently considering two possible factors that might contribute to this:

1. **The role of ROS in acquisition of reversible senescence-like states.** Senescence-like states are driven by cellular damage and stresses, including oncogenic mutations, and are thought to play a role in tumour suppression by taking damaged cells out of the cell cycle (Takasugi et al., 2022). However, it is now clear that in some cancers, such as hepatocellular carcinoma (HCC), senescence-like states contribute to establishment of fibrotic microenvironments which favour tumour initiation. This is because the secretome associated with senescence-like states, the senescence-associated secretory phenotype (SASP) is highly pro-inflammatory and rich in ECM proteins (Takasugi et al., 2022). Oxidative stress and ROS play a key role in the establishment/maintenance of senescence (Reczek & Chandel, 2017). Indeed, it is the antioxidant properties of certain senolytic drugs that imbues them with the capacity to reverse senescence (Zhu et al., 2020). Given its association with inflammation and ECM deposition, it is possible that assumption of a senescence-like state is also important in metastatic seeding. If so, then it may be advantageous for micrometastatic cells to reduce their glutathione levels to permit ROS levels to be sufficient

to support the acquisition of senescence and the generation of a SASP-like secretome. Indeed, increased EV production, which we show here that is a key characteristic of lung micrometastatic cells, has previously been reported following induction of senescence phenotypes, with EVs not only mediating the transfer of SASP components to recipient cells, but also being a part of the SASP themselves (Wallis et al., 2020).

2. **Competition between proline and glutathione synthesis pathways for glutamate.** We know that micrometastatic cells synthesise more proline than their primary tumour counterparts, and glutamate is an important precursor for both proline and glutathione synthesis. Moreover, as discussed in chapter 4, large amounts of proline are required for collagen production and this ECM component is known to be important for generating the appropriate microenvironment for metastatic colonisation (Elia et al., 2017). Thus, it may be that the demand for glutamate to synthesise proline for collagen production, may reduce the amount available for glutathione synthesis.

Another factor that needs to be considered is the possibility that, if scenario 2 (above) is applicable, then cells which have reduced their glutathione levels to maintain proline synthesis may need to invoke alternative antioxidant/cytoprotective strategies, and EV production may contribute to this. Reduced glutathione can provoke a form of non-apoptotic cell death, termed ferroptosis. This is due to accumulation of reactive hydroperoxides in polyunsaturated fatty acid (PUFA)-containing phospholipids, which can generate toxic alkoxy radicals, ultimately compromising the integral properties of cellular membranes (Dixon et al., 2012; Agmon et al., 2018). Glutathione peroxidase 4 (GPX4) can convert these potentially toxic hydroperoxides to non-reactive lipid alcohols by utilising glutathione. However, when GPX4-mediated lipid peroxide detoxification (which occurs when glutathione levels are low) is compromised, ferroptotic cell death can be triggered (Stockwell et al., 2017). Ferroptosis is iron-dependent and cellular uptake of iron is mediated by transferrin and its receptor. It is, therefore, of interest that lung micrometastatic cells have increased transferrin receptor recycling which, in combination with reduced glutathione, may sensitise metastatic cells to ferroptosis. Indeed, we have shown that

micrometastatic cells have increased sensitivity to BSO-mediated glutathione depletion and it will be interesting to determine whether this could be reversed by treatment with inhibitors of ferroptosis, such as the ferristatin-1 inhibitor or the iron chelator deferoxamine. Interestingly, sEVs have been recently shown to increase ferroptosis-resistance following ECM detachment by controlling the secretion of iron-containing ferritin to reduce intracellular iron overload (Brown et al., 2019). Therefore, it is tempting to speculate that increased sEV release by lung micrometastatic cells could reflect an adaptation mechanism which counters pro-ferroptotic stimuli.

Although the relevance of nSMase2-dependent sEV release in cancer progression is only beginning to be appreciated, there are several studies reporting altered expression of nSMase2 in different types of cancer. Notably, the association of nSMase2 with carcinogenesis was implicated by its chromosomal localisation at 16q22.1, which is a common site of loss of heterozygosity (LOH) in breast cancer, and this suggested that nSMase2 might have tumour suppressor function (Driouch et al., 1997). Indeed, hyper methylation of the *Smpd3* gene, which encodes nSMase2, has been reported in aggressive breast cancer (Demircan et al., 2009; Clarke et al., 2016), clear cell renal carcinoma (Wang et al., 2015), and HCC (Revill et al., 2013), whilst low nSMase2 expression has been associated with high tumour grade and early recurrence (Revill et al., 2013; Wang et al., 2015). We find low mRNA expression levels of nSMase2 in cells from lung micrometastases, consistent with their more invasive behaviour compared to cells derived from primary tumours, although EV release by these cells is still nSMase2-dependent. Conversely, nSMase2 has also been shown to promote metastasis of mouse and human mammary carcinoma cells though release of miRNA-containing sEVs which induce angiogenesis in the tumour microenvironment (Kosaka et al., 2013). It is clear from our data that only a subset of ceramide species (particularly C16- and C18-) are increased in micrometastatic cells. Particular ceramide species have been shown to partition into distinct subcellular compartments depending on the cellular context (Hannun & Obeid, 2011). Thus, it would be interesting to examine the lipid composition, both intracellular and sEV specific, of lung micrometastatic cells upon nSMase2 depletion, to not only shed light on their biological function, but also help uncover characteristics that may be unique to metastatic cells, potentially yielding biomarkers for metastatic disease.

We have shown that treating cells from primary tumours with BSO, to recapitulate the decrease in glutathione levels displayed by micrometastatic cells, upregulates nSMase2-dependent release of CD63 positive sEVs. However, we know that sEV release from cells derived from primary tumours is not nSMase2-dependent, and it is interesting to consider how the pathways that control release from primary and metastatic cells might differ. Rab27 has a well-established role in controlling the plasma membrane-delivery and exocytosis of MVEs and, therefore, sEV release (Bobrie et al., 2012; Ostrowski et al., 2010). Indeed, previously published work from our lab has shown that Rab27 knockdown reduces plasma membrane delivery of late endosomal cargoes and release of mtDNA/CD63-positive sEVs from breast cancer cells (Dornier et al., 2017; Rabas et al., 2021). Moreover, we have recently generated cells from primary tumours of MMTV-PyMT; Rab27a knockout mice and find that these have markedly reduced ability to release CD63 positive sEVs (J. Peters, personal communication). It will be interesting to determine whether the nSMase2-dependent sEV release from micrometastatic cells is also dependent on Rab27s (Rab27a and/or Rab27b), and whether PyMT cells switch to a nSMase2-dependent/Rab27-independent mode of sEV release when they are colonising the lung.

The deletion of nSMase2 in lung micrometastatic cells impaired their ability to invade into a collagen-rich organotypic environment, but did not influence their invasive migration on CDM. The difference between these two approaches in assessing invasive cell behaviour is the presence of fibroblasts in the organotypic environment, as opposed to the absence of them within the denuded CDM. This points to the possibility that sEVs released from micrometastatic cells might influence fibroblast behaviour to alter the collagen microenvironment and promote invasiveness. A non-cancer cell autonomous role for nSMase2 in metastasis has previously been described (Kosaka et al., 2013). Indeed, this study reported that nSMase2-depleted mammary cancer cells displayed reduced ability to metastasise to the lung following orthotopic transplantation into the mammary fat pad, and that the metastatic capacity of these cells could be restored following administration of sEVs from nSMase2-expressing cells. Importantly, this study indicated that sEVs from nSMase2-expressing cells likely promote metastasis by influencing the behaviour of endothelial cells (Kosaka et al., 2013). This indicates that nSMase2's contribution to invasive phenotypes extends beyond cell

autonomous processes, and it would be interesting to determine whether sEVs from nSMase2-expressing cells are able to restore the invasive behaviour of nSMase2-knockout cells in organotypic plugs and, if so, whether this is mediated via influencing the behaviour of fibroblasts in the plugs.

On the journey to metastasis, cancer cells need to undergo reversible and dynamic transitions between cellular states. Maintaining such phenotypic plasticity is crucial for adaptation in target organs and efficient metastatic outgrowth (Jehanno et al., 2022). The degree to which these transitions are reversible, and how this reversibility can depend on the tissue microenvironment, has just begun to be investigated. Recent studies have shown that complete transition to a mesenchymal phenotype with concomitant loss of epithelial traits renders cancer cells unable to form primary tumours or support metastatic colonisation (Ocaña et al., 2012; Padmanaban et al., 2019). Consistent with this, preliminary *in vivo* studies in our lab indicate that cells from lung micrometastases, which exhibit primarily mesenchymal characteristics, display low efficiency in forming tumours following orthotopic transplantation (data not shown). Also, when injected into the tail vein, micrometastatic cells grow slowly and form small 'metastases' in the lung (data not shown). Interestingly, however, we found that mice bearing these small 'metastases' experience a degree of weight loss (>10% of body weight) that would normally be associated with a much larger metastatic burden in the lung. Cancer-associated weight loss, or cachexia, is a poorly-understood process, but it is now known to be driven, at least in part, by the systemic inflammation associated with cancer; In particular, by increased levels of inflammatory cytokines, such as TNFα (Biswas & Acharyya, 2020). It is likely, therefore, that micrometastatic cells are particularly potent in evoking systemic inflammatory responses and this may be EV-mediated. We plan to further investigate this by injecting control and nSMase2-knockout micrometastatic cells into the tail vein of mice and deploying immunophenotyping approaches to characterise how they influence the immune landscapes of the lung and various other organs, including the bone marrow and spleen.

Taken together, the data presented in this thesis highlight how metabolic reprogramming of lung micrometastatic cells in mammary cancer influences the cellular machinery controlling sEV production. Both altered metabolism and sEVs

can contribute to cancer progression and acquisition of invasive behaviours to drive metastatic dissemination and outgrowth in distant organs. Here, we provide mechanistic insights that further our understanding of how changes in cellular metabolic programs can coordinate membrane trafficking processes to influence cancer progression, and a deeper appreciation of these links may uncover cancer cell dependencies that could be targeted therapeutically.

References

Abe, O., Abe, R., Enomoto, K., Kikuchi, K., Koyama, H., Masuda, H., Nomura, Y., Sakai, K., Sugimachi, K., Tominaga, T., Uchino, J., Yoshida, M., Haybittle, J.L., Davies, C., Harvey, V.J., Holdaway, T.M., Kay, R.G., Mason, B.H., Forbes, J.F., et al. (2005) 'Effects of chemotherapy and hormonal therapy for early breast cancer on recurrence and 15-year survival: an overview of the randomised trials', *Lancet (London, England)*, 365(9472), pp. 1687–1717.

Aceto, N., Bardia, A., Miyamoto, D.T., Donaldson, M.C., Wittner, B.S., Spencer, J.A., Yu, M., Pely, A., Engstrom, A., Zhu, H., Brannigan, B.W., Kapur, R., Stott, S.L., Shioda, T., Ramaswamy, S., Ting, D.T., Lin, C.P., Toner, M., Haber, D.A., et al. (2014) 'Circulating tumor cell clusters are oligoclonal precursors of breast cancer metastasis', *Cell*, 158(5), pp. 1110–1122.

Agmon, E., Solon, J., Bassereau, P. & Stockwell, B.R. (2018) 'Modeling the effects of lipid peroxidation during ferroptosis on membrane properties', *Scientific Reports*, 8(1), pp. 1–11.

Aguirre-Ghiso, J.A. (2007) 'Models, mechanisms and clinical evidence for cancer dormancy'. Nature Reviews Cancer 7 (11) p.pp. 834–846.

Airola, M. V. & Hannun, Y.A. (2013) 'Sphingolipid metabolism and neutral sphingomyelinases', *Handbook of Experimental Pharmacology*, 215pp. 57–76.

Airola, M. V., Shanbhogue, P., Shamseddine, A.A., Guja, K.E., Senkal, C.E., Maini, R., Bartke, N., Wu, B.X., Obeid, L.M., Garcia-Diaz, M., Hannun, Y.A. & Russell, D.W. (2017) 'Structure of human nSMase2 reveals an interdomain allosteric activation mechanism for ceramide generation', *Proceedings of the National Academy of Sciences of the United States of America*, 114(28), pp. E5549–E5558.

Al-Mehdi, A.B., Tozawa, K., Fisher, A.B., Shientag, L., Lee, A. & Muschel, R.J. (2000) 'Intravascular origin of metastasis from the proliferation of endothelium-attached tumor cells: A new model for metastasis', *Nature Medicine*, 6(1), pp. 100–102.

Albacete-Albacete, L., Navarro-Lérida, I., López, J.A., Martín-Padura, I., Astudillo, A.M., Ferrarini, A., Van-Der-Heyden, M., Balsinde, J., Orend, G., Vázquez, J. & del Pozo, M.Á. (2020) 'ECM deposition is driven by caveolin-1–dependent regulation of exosomal biogenesis and cargo sorting', *Journal of Cell Biology*, 219(11), .

Albain, K., Anderson, S., Arriagada, R., Barlow, W., Bergh, J., Bliss, J., Buyse, M., Cameron, D., Carrasco, E., Clarke, M., Correa, C., Coates, A., Collins, R., Costantino, J., Cutter, D., Cuzick, J., Darby, S., Davidson, N., Davies, C., et al. (2012) 'Comparisons between different polychemotherapy regimens for early breast cancer: Meta-analyses of long-term outcome among 100 000 women in 123 randomised trials', *The Lancet*, 379(9814), pp. 432–444.

Albrengues, J., Shields, M.A., Ng, D., Park, C.G., Ambrico, A., Poindexter, M.E., Upadhyay, P., Uyeminami, D.L., Pommier, A., Küttner, V., Bružas, E., Maiorino, L., Bautista, C., Carmona, E.M., Gimotty, P.A., Fearon, D.T., Chang, K., Lyons, S.K., Pinkerton, K.E., et al. (2018) 'Neutrophil extracellular traps produced during inflammation awakendormant cancer cells in mice', *Science (New York, N.Y.)*, 361(6409), .

Andringa, K.K., Coleman, M.C., Aykin-Burns, N., Hitchler, M.J., Walsh, S.A., Domann, F.E. & Spitz, D.R. (2006) 'Inhibition of glutamate cysteine ligase activity sensitizes human breast cancer cells to the toxicity of 2-deoxy-D-glucose', *Cancer research*, 66(3), pp. 1605–1610.

Antalis, C.J., Uchida, A., Buhman, K.K. & Siddiqui, R.A. (2011) 'Migration of MDA-

MB-231 breast cancer cells depends on the availability of exogenous lipids and cholesterol esterification', *Clinical and Experimental Metastasis*, 28(8), pp. 733–741.

Antonescu, C.N., McGraw, T.E. & Klip, A. (2014) 'Reciprocal regulation of endocytosis and metabolism', *Cold Spring Harbor Perspectives in Biology*, 6(7), .

Asiago, V.M., Alvarado, L.Z., Shanaiah, N., Gowda, G.A.N., Owusu-Sarfo, K., Ballas, R.A. & Raftery, D. (2010) 'Early detection of recurrent breast cancer using metabolite profiling.', *Cancer research*, 70(21), pp. 8309–8318.

Baietti, M.F., Zhang, Z., Mortier, E., Melchior, A., Degeest, G., Geeraerts, A., Ivarsson, Y., Depoortere, F., Coomans, C., Vermeiren, E., Zimmermann, P. & David, G. (2012) 'Syndecan-syntenin-ALIX regulates the biogenesis of exosomes', *Nature Cell Biology*, 14(7), pp. 677–685.

Ballabio, A. & Bonifacino, J.S. (2020) 'Lysosomes as dynamic regulators of cell and organismal homeostasis'. Nature Reviews Molecular Cell Biology 21 (2) p.pp. 101–118.

Bansal, A. & Celeste Simon, M. (2018) 'Glutathione metabolism in cancer progression and treatment resistance', *Journal of Cell Biology*, 217(7), pp. 2291–2298.

Bar-Peled, L., Chantranupong, L., Cherniack, A.D., Chen, W.W., Ottina, K.A., Grabiner, B.C., Spear, E.D., Carter, S.L., Meyerson, M. & Sabatini, D.M. (2013) 'A tumor suppressor complex with GAP activity for the Rag GTPases that signal amino acid sufficiency to mTORC1', *Science*, 340(6136), pp. 1100–1106.

Baran, J., Baj-Krzyworzeka, M., Weglarczyk, K., Szatanek, R., Zembela, M., Barbasz, J., Czupryna, A., Szczepanik, A. & Zembala, M. (2010) 'Circulating tumour-derived microvesicles in plasma of gastric cancer patients', *Cancer Immunology, Immunotherapy*, 59(6), pp. 841–850.

Barthel, A., Okino, S.T., Liao, J., Nakatani, K., Li, J., Whitlock, J.P. & Roth, R.A. (1999) 'Regulation of GLUT1 gene transcription by the serine/threonine kinase Akt1', *Journal of Biological Chemistry*, 274(29), pp. 20281–20286.

Behrens, J., Mareel, M.M., Roy, F.M. Van & Birchmeier, W. (1989) 'Dissecting tumor cell invasion: epithelial cells acquire invasive properties after the loss of uvomorulin-mediated cell-cell adhesion', *The Journal of cell biology*, 108(6), pp. 2435–2447.

Bergers, G. & Fendt, S.M. (2021) 'The metabolism of cancer cells during metastasis', *Nature reviews. Cancer*, 21(3), p. 162.

Bissell, M.J., Hall, H.G. & Parry, G. (1982) 'How does the extracellular matrix direct gene expression?', *Journal of Theoretical Biology*, 99(1), pp. 31–68.

Biswas, A.K. & Acharyya, S. (2020) 'Understanding cachexia in the context of metastatic progression'. Nature Reviews Cancer 20 (5) p.pp. 274–284.

Blomme, A., Costanza, B., De Tullio, P., Thiry, M., Van Simaeys, G., Boutry, S., Doumont, G., Di Valentin, E., Hirano, T., Yokobori, T., Gofflot, S., Peulen, O., Bellahcène, A., Sherer, F., Le Goff, C., Cavalier, E., Mouithys-Mickalad, A., Jouret, F., Cusumano, P.G., et al. (2017) 'Myoferlin regulates cellular lipid metabolism and promotes metastases in triple-negative breast cancer', *Oncogene*, 36(15), pp. 2116–2130.

Bobrie, A., Krumeich, S., Reyal, F., Recchi, C., Moita, L.F., Seabra, M.C., Ostrowski, M. & Théry, C. (2012) 'Rab27a supports exosome-dependent and -independent mechanisms that modify the tumor microenvironment and can promote tumor progression', *Cancer Research*, 72(19), pp. 4920–4930.

De Boer, M., Van Dijck, J.A.A.M., Bult, P., Borm, G.F. & Tjan-Heijnen, V.C.G.

(2010) ‘Breast cancer prognosis and occult lymph node metastases, isolated tumor cells, and micrometastases’, *Journal of the National Cancer Institute*, 102(6), pp. 410–425.

Borowsky, A.D., Namba, R., Young, L.J.T., Hunter, K.W., Hodgson, J.G., Tepper, C.G., McGoldrick, E.T., Muller, W.J., Cardiff, R.D. & Gregg, J.P. (2005) ‘Syngeneic mouse mammary carcinoma cell lines: Two closely related cell lines with divergent metastatic behavior’, *Clinical and Experimental Metastasis*, 22(1), pp. 47–59.

Braun, S., Vogl, F.D., Naume, B., Janni, W., Osborne, M.P., Coombes, R.C., Schlimok, G., Diel, I.J., Gerber, B., Gebauer, G., Pierga, J.-Y., Marth, C., Oruzio, D., Wiedswang, G., Solomayer, E.-F., Kundt, G., Strobl, B., Fehm, T., Wong, G.Y.C., et al. (2005) ‘A Pooled Analysis of Bone Marrow Micrometastasis in Breast Cancer’, *New England Journal of Medicine*, 353(8), pp. 793–802.

Bray, F., Ferlay, J., Soerjomataram, I., Siegel, R.L., Torre, L.A. & Jemal, A. (2018) ‘Global cancer statistics 2018: GLOBOCAN estimates of incidence and mortality worldwide for 36 cancers in 185 countries’, *CA: A Cancer Journal for Clinicians*, 68(6), pp. 394–424.

Bridgewater, R.E., Norman, J.C. & Caswell, P.T. (2012) ‘Integrin trafficking at a glance’. Journal of Cell Science 125 (16) p.pp. 3695–3701.

Brown, C.W., Amante, J.J., Chhoy, P., Elaimy, A.L., Liu, H., Zhu, L.J., Baer, C.E., Dixon, S.J. & Mercurio, A.M. (2019) ‘Prominin2 Drives Ferroptosis Resistance by Stimulating Multivesicular Body/Exosome-Mediated Iron Export’, *Developmental cell*, 51(5), p. 575.

Buschow, S.I., Nolte-’t Hoen, E.N.M., van Niel, G., Pols, M.S., ten Broeke, T., Lauwen, M., Ossendorp, F., Melief, C.J.M., Raposo, G., Wubbolts, R., Wauben, M.H.M. & Stoorvogel, W. (2009) ‘MHC II In dendritic cells is targeted to lysosomes or t cell-induced exosomes via distinct multivesicular body pathways’, *Traffic*, 10(10), pp. 1528–1542.

Cairns, R.A., Harris, I.S. & Mak, T.W. (2011) ‘Regulation of cancer cell metabolism.’, *Nature reviews. Cancer*, 11(2), pp. 85–95.

Canals, D., Salamone, S., Santacreu, B.J., Nemeth, E., Aguilar, D., Hernandez-Corbacho, M.J., Adada, M., Staquicini, D.I., Arap, W., Pasqualini, R., Haley, J., Obeid, L.M. & Hannun, Y.A. (2020) ‘Ceramide launches an acute anti-adhesion pro-migration cell signaling program in response to chemotherapy’, *FASEB Journal*, 34(6), pp. 7610–7630.

Cancer Research UK (2014) *Breast cancer statistics | Cancer Research UK*. [Online] [online]. Available from: https://www.cancerresearchuk.org/health-professional/cancer-statistics/statistics-by-cancer-type/breast-cancer#heading-Three (Accessed 1 August 2022).

Carmeliet, P. & Jain, R.K. (2011) ‘Principles and mechanisms of vessel normalization for cancer and other angiogenic diseases’. Nature Reviews Drug Discovery 10 (6) p.pp. 417–427.

Carretero, J., Obrador, E., Anasagasti, M.J., Martin, J.J., Vidal-Vanaclocha, F. & Estrela, J.M. (1999) ‘Growth-associated changes in glutathione content correlate with liver metastatic activity of B16 melanoma cells’, *Clinical & experimental metastasis*, 17(7), pp. 567–574.

Caswell, P.T., Chan, M., Lindsay, A.J., McCaffrey, M.W., Boettiger, D. & Norman, J.C. (2008) ‘Rab-coupling protein coordinates recycling of α5β1 integrin and EGFR1 to promote cell migration in 3D microenvironments’, *Journal of Cell Biology*, 183(1), pp. 143–155.

Caswell, P.T. & Norman, J.C. (2006) ‘Integrin trafficking and the control of cell

migration'. Traffic 7 (1) p.pp. 14–21.
Caswell, P.T., Spence, H.J., Parsons, M., White, D.P., Clark, K., Cheng, K.W., Mills, G.B., Humphries, M.J., Messent, A.J., Anderson, K.I., McCaffrey, M.W., Ozanne, B.W. & Norman, J.C. (2007) 'Rab25 Associates with α5β1 Integrin to Promote Invasive Migration in 3D Microenvironments', *Developmental Cell*, 13(4), pp. 496–510.
Caswell, P.T., Vadrevu, S. & Norman, J.C. (2009) 'Integrins: masters and slaves of endocytic transport', *Nature Reviews Molecular Cell Biology 2009 10:12*, 10(12), pp. 843–853.
Chaffer, C.L., San Juan, B.P., Lim, E. & Weinberg, R.A. (2016) 'EMT, cell plasticity and metastasis', *Cancer and Metastasis Reviews*, 35(4), pp. 645–654.
Chambers, A.F., Groom, A.C. & MacDonald, I.C. (2002) 'Dissemination and growth of cancer cells in metastatic sites', *Nature Reviews Cancer 2002 2:8*, 2(8), pp. 563–572.
Charrin, S., Jouannet, S., Boucheix, C. & Rubinstein, E. (2014) 'Tetraspanins at a glance', *Journal of Cell Science*, 127(17), pp. 3641–3648.
Chen, Q., Zhang, X.H.F. & Massagué, J. (2011) 'Macrophage Binding to Receptor VCAM-1 Transmits Survival Signals in Breast Cancer Cells that Invade the Lungs', *Cancer Cell*, 20(4), pp. 538–549.
Cheng, K.W., Lahad, J.P., Kuo, W.L., Lapuk, A., Yamada, K., Auersperg, N., Liu, J., Smith-McCune, K., Lu, K.H., Fishman, D., Gray, J.W. & Mills, G.B. (2004) 'The RAB25 small GTPase determines aggressiveness of ovarian and breast cancers', *Nature Medicine*, 10(11), pp. 1251–1256.
Chiaradia, E., Tancini, B., Emiliani, C., Delo, F., Pellegrino, R.M., Tognoloni, A., Urbanelli, L. & Buratta, S. (2021) 'Extracellular Vesicles under Oxidative Stress Conditions: Biological Properties and Physiological Roles', *Cells*, 10(7), p. 1763.
Choezom, D. & Gross, J.C. (2022) 'Neutral sphingomyelinase 2 controls exosome secretion by counteracting V-ATPase-mediated endosome acidification', *Journal of Cell Science*, 135(5), .
Christen, S., Lorendeau, D., Schmieder, R., Broekaert, D., Metzger, K., Veys, K., Elia, I., Buescher, J.M., Orth, M.F., Davidson, S.M., Grünewald, T.G.P., De Bock, K. & Fendt, S.M. (2016) 'Breast Cancer-Derived Lung Metastases Show Increased Pyruvate Carboxylase-Dependent Anaplerosis', *Cell Reports*, 17(3), pp. 837–848.
Christoforides, C., Rainero, E., Brown, K.K., Norman, J.C. & Toker, A. (2012) 'PKD Controls αvβ3 Integrin Recycling and Tumor Cell Invasive Migration through Its Substrate Rabaptin-5', *Developmental Cell*, 23(3), pp. 560–572.
Clarke, C.J., Shamseddine, A.A., Jacob, J.J., Khalife, G., Burns, T.A. & Hannun, Y.A. (2016) 'ATRA transcriptionally induces nSMase2 through CBP/p300-mediated histone acetylation', *Journal of Lipid Research*, 57(5), pp. 868–881.
Coffelt, S.B., Kersten, K., Doornebal, C.W., Weiden, J., Vrijland, K., Hau, C.S., Verstegen, N.J.M., Ciampricotti, M., Hawinkels, L.J.A.C., Jonkers, J. & De Visser, K.E. (2015) 'IL-17-producing γδ T cells and neutrophils conspire to promote breast cancer metastasis', *Nature*, 522(7556), pp. 345–348.
Colombo, M., Moita, C., Van Niel, G., Kowal, J., Vigneron, J., Benaroch, P., Manel, N., Moita, L.F., Théry, C. & Raposo, G. (2013) 'Analysis of ESCRT functions in exosome biogenesis, composition and secretion highlights the heterogeneity of extracellular vesicles', *Journal of Cell Science*, 126(24), pp. 5553–5565.
Combs, J.A. & Denicola, G.M. (2019) 'The Non-Essential Amino Acid Cysteine Becomes Essential for Tumor Proliferation and Survival', *Cancers 2019, Vol. 11, Page 678*, 11(5), p. 678.

Conti, L., Bolli, E., Di Lorenzo, A., Franceschi, V., MacChi, F., Riccardo, F., Ruiu, R., Russo, L., Quaglino, E., Donofrio, G. & Cavallo, F. (2020) 'Immunotargeting of the xCT cystine/glutamate antiporter potentiates the efficacy of HER2-targeted immunotherapies in breast cancer', *Cancer Immunology Research*, 8(8), pp. 1039–1053.

Copson, E., Eccles, B., Maishman, T., Gerty, S., Stanton, L., Cutress, R.I., Altman, D.G., Durcan, L., Simmonds, P., Lawrence, G., Jones, L., Bliss, J. & Eccles, D. (2013) 'Prospective Observational Study of Breast Cancer Treatment Outcomes for UK Women Aged 18–40 Years at Diagnosis: The POSH Study', *JNCI: Journal of the National Cancer Institute*, 105(13), pp. 978–988.

Costa-Silva, B., Aiello, N.M., Ocean, A.J., Singh, S., Zhang, H., Thakur, B.K., Becker, A., Hoshino, A., Mark, M.T., Molina, H., Xiang, J., Zhang, T., Theilen, T.M., García-Santos, G., Williams, C., Ararso, Y., Huang, Y., Rodrigues, G., Shen, T.L., et al. (2015) 'Pancreatic cancer exosomes initiate pre-metastatic niche formation in the liver', *Nature cell biology*, 17(6), pp. 816–826.

Cruys, B., Wong, B.W., Kuchnio, A., Verdegem, D., Cantelmo, A.R., Conradi, L.C., Vandekeere, S., Bouche, A., Cornelissen, I., Vinckier, S., Merks, R.M.H., Dejana, E., Gerhardt, H., Dewerchin, M., Bentley, K. & Carmeliet, P. (2016) 'Glycolytic regulation of cell rearrangement in angiogenesis', *Nature Communications*, 7(1), pp. 1–15.

Cukierman, E., Pankov, R., Stevens, D.R. & Yamada, K.M. (2001) 'Taking cell-matrix adhesions to the third dimension', *Science (New York, N.Y.)*, 294(5547), pp. 1708–1712.

Cullen, P.J. & Steinberg, F. (2018) 'To degrade or not to degrade: mechanisms and significance of endocytic recycling'. Nature Reviews Molecular Cell Biology 19 (11) p.pp. 679–696.

Dai, C., Arceo, J., Arnold, J., Sreekumar, A., Dovichi, N.J., Li, J. & Littlepage, L.E. (2018) 'Metabolomics of oncogene-specific metabolic reprogramming during breast cancer', *Cancer & Metabolism*, 6(1), p. 5.

Danen, E.H.J., Van Rheenen, J., Franken, W., Huveneers, S., Sonneveld, P., Jalink, K. & Sonnenberg, A. (2005) 'Integrins control motile strategy through a Rho-cofilin pathway', *Journal of Cell Biology*, 169(3), pp. 515–526.

Danussi, C., Akavia, U.D., Niola, F., Jovic, A., Lasorella, A., Pe'Er, D. & Iavarone, A. (2013) 'RHPN2 drives mesenchymal transformation in malignant glioma by triggering RhoA activation', *Cancer Research*, 73(16), pp. 5140–5150.

Davie, S.A., Maglione, J.E., Manner, C.K., Young, D., Cardiff, R.D., MacLeod, C.L. & Ellies, L.G. (2007) 'Effects of FVB/NJ and C57Bl/6J strain backgrounds on mammary tumor phenotype in inducible nitric oxide synthase deficient mice', *Transgenic Research*, 16(2), pp. 193–201.

Davis, R.T., Blake, K., Ma, D., Gabra, M.B.I., Hernandez, G.A., Phung, A.T., Yang, Y., Maurer, D., Lefebvre, A.E.Y.T., Alshetaiwi, H., Xiao, Z., Liu, J., Locasale, J.W., Digman, M.A., Mjolsness, E., Kong, M., Werb, Z. & Lawson, D.A. (2020) 'Transcriptional diversity and bioenergetic shift in human breast cancer metastasis revealed by single-cell RNA sequencing', *Nature Cell Biology*, 22(3), pp. 310–320.

Deatheragea, B.L. & Cooksona, B.T. (2012) 'Membrane Vesicle Release in Bacteria, Eukaryotes, and Archaea: a Conserved yet Underappreciated Aspect of Microbial Life', *Infection and Immunity*, 80(6), p. 1948.

DeBerardinis, R.J., Lum, J.J., Hatzivassiliou, G. & Thompson, C.B. (2008) 'The Biology of Cancer: Metabolic Reprogramming Fuels Cell Growth and Proliferation', *Cell Metabolism*, 7(1), pp. 11–20.

Demers, M., Krause, D.S., Schatzberg, D., Martinod, K., Voorhees, J.R., Fuchs,

T.A., Scadden, D.T. & Wagner, D.D. (2012) 'Cancers predispose neutrophils to release extracellular DNA traps that contribute to cancer-associated thrombosis', *Proceedings of the National Academy of Sciences of the United States of America*, 109(32), pp. 13076–13081.

Demircan, B., Dyer, L.M., Gerace, M., Lobenhofer, E.K., Robertson, K.D. & Brown, K.D. (2009) 'Comparative epigenomics of human and mouse mammary tumors', *Genes Chromosomes and Cancer*, 48(1), pp. 83–97.

Deng, M., Cai, X., Long, L., Xie, L., Ma, H., Zhou, Y., Liu, S. & Zeng, C. (2019) 'CD36 promotes the epithelial-mesenchymal transition and metastasis in cervical cancer by interacting with TGF-β', *Journal of Translational Medicine*, 17(1), .

van Deventer, H.W., Palmieri, D.A., Wu, Q.P., McCook, E.C. & Serody, J.S. (2013) 'Circulating Fibrocytes Prepare the Lung for Cancer Metastasis by Recruiting Ly-6C + Monocytes Via CCL2', *The Journal of Immunology*, 190(9), pp. 4861–4867.

Dias, M.V.S., Teixeira, B.L., Rodrigues, B.R., Sinigaglia-Coimbra, R., Porto-Carreiro, I., Roffé, M., Hajj, G.N.M. & Martins, V.R. (2016) 'PRNP/prion protein regulates the secretion of exosomes modulating CAV1/caveolin-1-suppressed autophagy', *Autophagy*, 12(11), pp. 2113–2128.

Dixon, S.J., Lemberg, K.M., Lamprecht, M.R., Skouta, R., Zaitsev, E.M., Gleason, C.E., Patel, D.N., Bauer, A.J., Cantley, A.M., Yang, W.S., Morrison, B. & Stockwell, B.R. (2012) 'Ferroptosis: An iron-dependent form of nonapoptotic cell death', *Cell*, 149(5), pp. 1060–1072.

Donato, C., Kunz, L., Castro-Giner, F., Paasinen-Sohns, A., Strittmatter, K., Szczerba, B.M., Scherrer, R., Di Maggio, N., Heusermann, W., Biehlmaier, O., Beisel, C., Vetter, M., Rochlitz, C., Weber, W.P., Banfi, A., Schroeder, T. & Aceto, N. (2020) 'Hypoxia Triggers the Intravasation of Clustered Circulating Tumor Cells', *Cell Reports*, 32(10), p. 108105.

Dornier, E., Rabas, N., Mitchell, L., Novo, D., Dhayade, S., Marco, S., MacKay, G., Sumpton, D., Pallares, M., Nixon, C., Blyth, K., MacPherson, I.R., Rainero, E. & Norman, J.C. (2017) 'Glutaminolysis drives membrane trafficking to promote invasiveness of breast cancer cells', *Nature Communications 2017 8:1*, 8(1), pp. 1–14.

Douen, A.G., Ramlal, T., Rastogi, S., Bilan, P.J., Cartee, G.D., Vranic, M., Holloszy, J.O. & Klip, A. (1990) 'Exercise induces recruitment of the "insulin-responsive glucose transporter". Evidence for distinct intracellular insulin- and exercise-recruitable transporter pools in skeletal muscle', *Journal of Biological Chemistry*, 265(23), pp. 13427–13430.

Dozynkiewicz, M.A., Jamieson, N.B., MacPherson, I., Grindlay, J., VandenBerghe, P.V.E., VonThun, A., Morton, J.P., Gourley, C., Timpson, P., Nixon, C., McKay, C.J., Carter, R., Strachan, D., Anderson, K., Sansom, O.J., Caswell, P.T. & Norman, J.C. (2012) 'Rab25 and CLIC3 Collaborate to Promote Integrin Recycling from Late Endosomes/Lysosomes and Drive Cancer Progression', *Developmental Cell*, 22(1), pp. 131–145.

Driouch, K., Dorion-Bonnet, F., Briffod, M., Champème, M.H., Longy, M. & Lidereau, R. (1997) 'Loss of heterozygosity on chromosome arm 16q in breast cancer metastases', *Genes Chromosomes and Cancer*, 19(3), pp. 185–191.

Duleh, S.N. & Welch, M.D. (2012) 'Regulation of integrin trafficking, cell adhesion, and cell migration by WASH and the Arp2/3 complex', *Cytoskeleton*, 69(12), pp. 1047–1058.

Duncan, D.J., Scott, M., Scorer, P. & Barker, C. (2019) 'Assessment of PD-L1 mRNA and protein expression in non-small cell lung cancer, head and neck squamous

cell carcinoma and urothelial carcinoma tissue specimens using RNAScope and immunohistochemistry', *PloS one*, 14(4), .

Durcin, M., Fleury, A., Taillebois, E., Hilairet, G., Krupova, Z., Henry, C., Truchet, S., Trötzmüller, M., Köfeler, H., Mabilleau, G., Hue, O., Andriantsitohaina, R., Martin, P. & Lay, S. Le (2017) 'Characterisation of adipocyte-derived extracellular vesicle subtypes identifies distinct protein and lipid signatures for large and small extracellular vesicles', *Journal of Extracellular Vesicles*, 6(1), .

Eccles, S.A. & Welch, D.R. (2007) 'Metastasis: recent discoveries and novel treatment strategies'. Lancet 369 (9574) p.pp. 1742–1757.

Eisenblaetter, M., Flores-Borja, F., Lee, J.J., Wefers, C., Smith, H., Hueting, R., Cooper, M.S., Blower, P.J., Patel, D., Rodriguez-Justo, M., Milewicz, H., Vogl, T., Roth, J., Tutt, A., Schaeffter, T. & Ng, T. (2017) 'Visualization of Tumor-Immune Interaction - Target-Specific Imaging of S100A8/A9 Reveals Pre-Metastatic Niche Establishment', *Theranostics*, 7(9), p. 2392.

Elia, I., Broekaert, D., Christen, S., Boon, R., Radaelli, E., Orth, M.F., Verfaillie, C., Grünewald, T.G.P. & Fendt, S.M. (2017) 'Proline metabolism supports metastasis formation and could be inhibited to selectively target metastasizing cancer cells', *Nature Communications*, 8(1), pp. 1–11.

Elia, I., Doglioni, G. & Fendt, S.M. (2018) 'Metabolic Hallmarks of Metastasis Formation'. Trends in Cell Biology 28 (8) p.pp. 673–684.

Elia, I., Rossi, M., Stegen, S., Broekaert, D., Doglioni, G., van Gorsel, M., Boon, R., Escalona-Noguero, C., Torrekens, S., Verfaillie, C., Verbeken, E., Carmeliet, G. & Fendt, S.M. (2019) 'Breast cancer cells rely on environmental pyruvate to shape the metastatic niche', *Nature*, 568(7750), pp. 117–121.

Erler, J.T., Bennewith, K.L., Cox, T.R., Lang, G., Bird, D., Koong, A., Le, Q.T. & Giaccia, A.J. (2009) 'Hypoxia-Induced Lysyl Oxidase Is a Critical Mediator of Bone Marrow Cell Recruitment to Form the Premetastatic Niche', *Cancer Cell*, 15(1), pp. 35–44.

Escola, J.M., Kleijmeer, M.J., Stoorvogel, W., Griffith, J.M., Yoshie, O. & Geuze, H.J. (1998) 'Selective enrichment of tetraspan proteins on the internal vesicles of multivesicular endosomes and on exosomes secreted by human B-lymphocytes', *Journal of Biological Chemistry*, 273(32), pp. 20121–20127.

Ewing, J. (1928) *Neoplastic diseases : a treatise on tumors*. W. B. Saunders, Philadelphia, 1928.

Fader, C.M., Sánchez, D.G., Mestre, M.B. & Colombo, M.I. (2009) 'TI-VAMP/VAMP7 and VAMP3/cellubrevin: two v-SNARE proteins involved in specific steps of the autophagy/multivesicular body pathways', *Biochimica et Biophysica Acta - Molecular Cell Research*, 1793(12), pp. 1901–1916.

Fafiá N-Labora, J.A., Antonio Rodríguez-Navarro, J. & O'loghlen, A. (2020) 'll Small Extracellular Vesicles Have GST Activity and Ameliorate Senescence-Related Tissue Damage', *Cell Metabolism*, 32pp. 71–86.

Faubert, B., Solmonson, A. & DeBerardinis, R.J. (2020) 'Metabolic reprogramming and cancer progression'. Science 368 (6487).

Ferrari, N., Riggio, A.I., Mason, S., McDonald, L., King, A., Higgins, T., Rosewell, I., Neil, J.C., Smalley, M.J., Sansom, O.J., Morris, J., Cameron, E.R. & Blyth, K. (2015) 'Runx2 contributes to the regenerative potential of the mammary epithelium', *Scientific Reports 2015 5:1*, 5(1), pp. 1–16.

Fidler, I.J. (2006) 'Models for spontaneous metastasis [3]'. Cancer Research 66 (19) p.p. 9787.

Fischer, K.R., Durrans, A., Lee, S., Sheng, J., Li, F., Wong, S.T.C., Choi, H., El Rayes, T., Ryu, S., Troeger, J., Schwabe, R.F., Vahdat, L.T., Altorki, N.K.,

Mittal, V. & Gao, D. (2015) ‘EMT is not required for lung metastasis but contributes to chemoresistance’, *Nature*, 527(7579), p. 472.

Foley, K., Boguslavsky, S. & Klip, A. (2011) ‘Endocytosis, recycling, and regulated exocytosis of glucose transporter 4’, *Biochemistry*, 50(15), pp. 3048–3061.

Fong, M.Y., Zhou, W., Liu, L., Alontaga, A.Y., Chandra, M., Ashby, J., Chow, A., O’Connor, S.T.F., Li, S., Chin, A.R., Somlo, G., Palomares, M., Li, Z., Tremblay, J.R., Tsuyada, A., Sun, G., Reid, M.A., Wu, X., Swiderski, P., et al. (2015) ‘Breast-cancer-secreted miR-122 reprograms glucose metabolism in premetastatic niche to promote metastasis’, *Nature Cell Biology*, 17(2), pp. 183–194.

Font-Clos, F., Zapperi, S. & La Porta, C.A.M. (2020) ‘Blood Flow Contributions to Cancer Metastasis’, *iScience*, 23(5), .

de Franceschi, N., Hamidi, H., Alanko, J., Sahgal, P. & Ivaska, J. (2015) ‘Integrin traffic-the update’. Journal of Cell Science 128 (5) p.pp. 839–852.

Francia, G., Cruz-Munoz, W., Man, S., Xu, P. & Kerbel, R.S. (2011) ‘Mouse models of advanced spontaneous metastasis for experimental therapeutics’. Nature Reviews Cancer 11 (2) p.pp. 135–141.

Friedl, P. & Bröcker, E.B. (2000) ‘The biology of cell locomotion within three-dimensional extracellular matrix’. Cellular and Molecular Life Sciences 57 (1) p.pp. 41–64.

Fujimori, S., Abe, Y., Nishi, M., Hamamoto, A., Inoue, Y., Ohnishi, Y., Nishime, C., Matsumoto, H., Yamazaki, H., Kijima, H., Ueyama, Y., Inoue, H. & Nakamura, M. (2004) ‘The subunits of glutamate cysteine ligase enhance cisplatin resistance in human non-small cell lung cancer xenografts in vivo.’, *International journal of oncology*, 25(2), pp. 413–418.

Gal, K. Le, Ibrahim, M.X., Wiel, C., Sayin, V.I., Akula, M.K., Karlsson, C., Dalin, M.G., Akyürek, L.M., Lindahl, P., Nilsson, J. & Bergo, M.O. (2015) ‘Antioxidants can increase melanoma metastasis in mice’, *Science Translational Medicine*, 7(308), .

Galindo-Hernandez, O., Villegas-Comonfort, S., Candanedo, F., González-Vázquez, M.C., Chavez-Ocaña, S., Jimenez-Villanueva, X., Sierra-Martinez, M. & Salazar, E.P. (2013) ‘Elevated concentration of microvesicles isolated from peripheral blood in breast cancer patients’, *Archives of Medical Research*, 44(3), pp. 208–214.

Gao, H., Chakraborty, G., Lee-Lim, A.P., Mo, Q., Decker, M., Vonica, A., Shen, R., Brogi, E., Brivanlou, A.H. & Giancotti, F.G. (2012) ‘The BMP inhibitor Coco reactivates breast cancer cells at lung metastatic sites’, *Cell*, 150(4), pp. 764–779.

Gao, M., Yi, J., Zhu, J., Minikes, A.M., Monian, P., Thompson, C.B. & Jiang, X. (2019) ‘Role of Mitochondria in Ferroptosis’, *Molecular Cell*, 73(2), pp. 354-363.e3.

Gasic, G.J., Gasic, T.B. & Stewart, C.C. (1968) ‘Antimetastatic effects associated with platelet reduction.’, *Proceedings of the National Academy of Sciences of the United States of America*, 61(1), pp. 46–52.

Gay, L.J. & Felding-Habermann, B. (2011) ‘Contribution of platelets to tumour metastasis’. Nature Reviews Cancer 11 (2) p.pp. 123–134.

Georgiadou, M., Lilja, J., Jacquemet, G., Guzmán, C., Rafaeva, M., Alibert, C., Yan, Y., Sahgal, P., Lerche, M., Manneville, J.B., Mäkelä, T.P. & Ivaska, J. (2017) ‘AMPK negatively regulates tensin-dependent integrin activity’, *Journal of Cell Biology*, 216(4), pp. 1107–1121.

Gerull, W.D., Puri, V. & Kozower, B.D. (2021) ‘The epidemiology and biology of pulmonary metastases’. Journal of Thoracic Disease 13 (4) p.pp. 2585–2589.

Ghajar, C.M. (2015) ‘Metastasis prevention by targeting the dormant niche’. Nature Reviews Cancer 15 (4) p.pp. 238–247.

Ghajar, C.M., Peinado, H., Mori, H., Matei, I.R., Evason, K.J., Brazier, H., Almeida, D., Koller, A., Hajjar, K.A., Stainier, D.Y.R., Chen, E.I., Lyden, D. & Bissell, M.J. (2013) ‘The perivascular niche regulates breast tumour dormancy’, *Nature Cell Biology 2013 15:7*, 15(7), pp. 807–817.

Giampieri, S., Manning, C., Hooper, S., Jones, L., Hill, C.S. & Sahai, E. (2009) ‘Localized and reversible TGFß signalling switches breast cancer cells from cohesive to single cell motility’, *Nature Cell Biology*, 11(11), pp. 1287–1296.

Gil-Bernabé, A.M., Ferjančič, Š., Tlalka, M., Zhao, L., Allen, P.D., Im, J.H., Watson, K., Hill, S.A., Amirkhosravi, A., Francis, J.L., Pollard, J.W., Ruf, W. & Muschel, R.J. (2012) ‘Recruitment of monocytes/macrophages by tissue factor-mediated coagulation is essential for metastatic cell survival and premetastatic niche establishment in mice’, *Blood*, 119(13), pp. 3164–3175.

Gilkes, D.M., Chaturvedi, P., Bajpai, S., Wong, C.C., Wei, H., Pitcairn, S., Hubbi, M.E., Wirtz, D. & Semenza, G.L. (2013) ‘Collagen prolyl hydroxylases are essential for breast cancer metastasis’, *Cancer Research*, 73(11), pp. 3285–3296.

Gilleron, J., Gerdes, J.M. & Zeigerer, A. (2019) ‘Metabolic regulation through the endosomal system’. Traffic 20 (8) p.pp. 552–570.

Ginter, P.S., Karagiannis, G.S., Entenberg, D., Lin, Y., Condeelis, J., Jones, J.G. & Oktay, M.H. (2019) ‘Tumor microenvironment of metastasis (TMEM) doorways are restricted to the blood vessel endothelium in both primary breast cancers and their lymph node metastases’, *Cancers*, 11(10), .

Giustarini, D., Dalle-Donne, I., Milzani, A., Fanti, P. & Rossi, R. (2013) ‘Analysis of GSH and GSSG after derivatization with N-ethylmaleimide’, *Nature Protocols 2013 8:9*, 8(9), pp. 1660–1669.

Goldenring, J.R., Shen, K.R., Vaughan, H.D. & Modlin, I.M. (1993) ‘Identification of a small GTP-binding protein, Rab25, expressed in the gastrointestinal mucosa, kidney, and lung’, *Journal of Biological Chemistry*, 268(25), pp. 18419–18422.

Goñi, F.M. & Alonso, A. (2009) ‘Effects of ceramide and other simple sphingolipids on membrane lateral structure’, *Biochimica et Biophysica Acta (BBA) - Biomembranes*, 1788(1), pp. 169–177.

Goodyear, L.J., Hirshman, M.F. & Horton, E.S. (1991) ‘Exercise-induced translocation of skeletal muscle glucose transporters’, *American Journal of Physiology - Endocrinology and Metabolism*, 261(6 24-6), .

Greaves, M. & Maley, C.C. (2012) ‘CLONAL EVOLUTION IN CANCER’, *Nature*, 481(7381), p. 306.

Gu, Y., Albuquerque, C.P., Braas, D., Zhang, W., Villa, G.R., Bi, J., Ikegami, S., Masui, K., Gini, B., Yang, H., Gahman, T.C., Shiau, A.K., Cloughesy, T.F., Christofk, H.R., Zhou, H., Guan, K.L. & Mischel, P.S. (2017) ‘mTORC2 Regulates Amino Acid Metabolism in Cancer by Phosphorylation of the Cystine-Glutamate Antiporter xCT’, *Molecular Cell*, 67(1), pp. 128-138.e7.

Gu, Z., Noss, E.H., Hsu, V.W. & Brenner, M.B. (2011) ‘Integrins traffic rapidly via circular dorsal ruffles and macropinocytosis during stimulated cell migration’, *Journal of Cell Biology*, 193(1), pp. 61–70.

Guix, F.X., Sannerud, R., Berditchevski, F., Arranz, A.M., Horré, K., Snellinx, A., Thathiah, A., Saido, T., Saito, T., Rajesh, S., Overduin, M., Kumar-Singh, S., Radaelli, E., Corthout, N., Colombelli, J., Tosi, S., Munck, S., Salas, I.H., Annaert, W., et al. (2017) ‘Tetraspanin 6: A pivotal protein of the multiple vesicular body determining exosome release and lysosomal degradation of

amyloid precursor protein fragments', *Molecular Neurodegeneration*, 12(1), .

Guo, B.B., Bellingham, S.A. & Hill, A.F. (2015) 'The Neutral Sphingomyelinase Pathway Regulates Packaging of the Prion Protein into Exosomes', *The Journal of Biological Chemistry*, 290(6), p. 3455.

Gupta, G.P., Nguyen, D.X., Chiang, A.C., Bos, P.D., Kim, J.Y., Nadal, C., Gomis, R.R., Manova-Todorova, K. & Massagué, J. (2007) 'Mediators of vascular remodelling co-opted for sequential steps in lung metastasis', *Nature*, 446(7137), pp. 765–770.

Gupta, S., Yano, J., Mercier, V., Htwe, H.H., Shin, H.R., Rademaker, G., Cakir, Z., Ituarte, T., Wen, K.W., Kim, G.E., Zoncu, R., Roux, A., Dawson, D.W. & Perera, R.M. (2021) 'Lysosomal retargeting of Myoferlin mitigates membrane stress to enable pancreatic cancer growth', *Nature Cell Biology*, 23(3), pp. 232–242.

Guy, C.T., Cardiff, R.D. & Muller, W.J. (1992) 'Induction of mammary tumors by expression of polyomavirus middle T oncogene: a transgenic mouse model for metastatic disease.', *Molecular and Cellular Biology*, 12(3), pp. 954–961.

Gwinn, D.M., Shackelford, D.B., Egan, D.F., Mihaylova, M.M., Mery, A., Vasquez, D.S., Turk, B.E. & Shaw, R.J. (2008) 'AMPK Phosphorylation of Raptor Mediates a Metabolic Checkpoint', *Molecular Cell*, 30(2), pp. 214–226.

Haeger, A., Krause, M., Wolf, K. & Friedl, P. (2014) 'Cell jamming: Collective invasion of mesenchymal tumor cells imposed by tissue confinement', *Biochimica et Biophysica Acta - General Subjects*, 1840(8), pp. 2386–2395.

Hamidi, H. & Ivaska, J. (2018) 'Every step of the way: Integrins in cancer progression and metastasis'. Nature Reviews Cancer 18 (9) p.pp. 533–548.

Hanna, R.N., Cekic, C., Sag, D., Tacke, R., Thomas, G.D., Nowyhed, H., Herrley, E., Rasquinha, N., McArdle, S., Wu, R., Peluso, E., Metzger, D., Ichinose, H., Shaked, I., Chodaczek, G., Biswas, S.K. & Hedrick, C.C. (2015) 'Patrolling monocytes control tumor metastasis to the lung', *Science*, 350(6263), pp. 985–990.

Hannun, Y.A. & Obeid, L.M. (2011) 'Many Ceramides', *The Journal of Biological Chemistry*, 286(32), p. 27855.

Hannun, Y.A. & Obeid, L.M. (2008) 'Principles of bioactive lipid signalling: lessons from sphingolipids', *Nature Reviews Molecular Cell Biology 2008 9:2*, 9(2), pp. 139–150.

Hara, K., Maruki, Y., Long, X., Yoshino, K. ichi, Oshiro, N., Hidayat, S., Tokunaga, C., Avruch, J. & Yonezawa, K. (2002) 'Raptor, a binding partner of target of rapamycin (TOR), mediates TOR action', *Cell*, 110(2), pp. 177–189.

Harney, A.S., Arwert, E.N., Entenberg, D., Wang, Y., Guo, P., Qian, B.Z., Oktay, M.H., Pollard, J.W., Jones, J.G. & Condeelis, J.S. (2015) 'Real-time imaging reveals local, transient vascular permeability, and tumor cell intravasation stimulated by TIE2hi macrophage–derived VEGFA', *Cancer Discovery*, 5(9), pp. 932–943.

Harris, I.S., Treloar, A.E., Inoue, S., Sasaki, M., Gorrini, C., Lee, K.C., Yung, K.Y., Brenner, D., Knobbe-Thomsen, C.B., Cox, M.A., Elia, A., Berger, T., Cescon, D.W., Adeoye, A., Brüstle, A., Molyneux, S.D., Mason, J.M., Li, W.Y., Yamamoto, K., et al. (2015) 'Glutathione and Thioredoxin Antioxidant Pathways Synergize to Drive Cancer Initiation and Progression', *Cancer Cell*, 27(2), pp. 211–222.

Hartkopf, A.D., Taran, F.A., Wallwiener, M., Hagenbeck, C., Melcher, C., Krawczyk, N., Hahn, M., Wallwiener, D. & Fehm, T. (2013) 'The presence and prognostic impact of apoptotic and nonapoptotic disseminated tumor cells in

the bone marrow of primary breast cancer patients after neoadjuvant chemotherapy', *Breast Cancer Research*, 15(5), .

Havas, K.M., Milchevskaya, V., Radic, K., Alladin, A., Kafkia, E., Garcia, M., Stolte, J., Klaus, B., Rotmensz, N., Gibson, T.J., Burwinkel, B., Schneeweiss, A., Pruneri, G., Patil, K.R., Sotillo, R. & Jechlinger, M. (2017) 'Metabolic shifts in residual breast cancer drive tumor recurrence', *Journal of Clinical Investigation*, 127(6), pp. 2091–2105.

Hayman, J., Naidoo, J. & Ettinger, D.S. (2020) 'Lung Metastases', *Abeloff's Clinical Oncology*, pp. 831-845.e6.

Vander Heiden, M.G. (2011) 'Targeting cancer metabolism: a therapeutic window opens', *Nature Reviews Drug Discovery*, 10p. 671.

Helmlinger, G., Sckell, A., Dellian, M., Forbes, N.S. & Jain, R.K. (2002) 'Acid production in glycolysis-impaired tumors provides new insights into tumor metabolism', *Clinical Cancer Research*, 8(4), pp. 1284–1291.

Hessvik, N.P., Øverbye, A., Brech, A., Torgersen, M.L., Jakobsen, I.S., Sandvig, K. & Llorente, A. (2016) 'PIKfyve inhibition increases exosome release and induces secretory autophagy', *Cellular and Molecular Life Sciences*, 73(24), pp. 4717–4737.

Hetmanski, J.H.R., Zindy, E., Schwartz, J.M. & Caswell, P.T. (2016) 'A MAPK-Driven Feedback Loop Suppresses Rac Activity to Promote RhoA-Driven Cancer Cell Invasion', *PLoS Computational Biology*, 12(5), .

Hofmann, K., Tomiuk, S., Wolff, G. & Stoffel, W. (2000) 'Cloning and characterization of the mammalian brain-specific, Mg2+-dependent neutral sphingomyelinase', *Proceedings of the National Academy of Sciences of the United States of America*, 97(11), pp. 5895–5900.

Hoshino, A., Costa-Silva, B., Shen, T.L., Rodrigues, G., Hashimoto, A., Tesic Mark, M., Molina, H., Kohsaka, S., Di Giannatale, A., Ceder, S., Singh, S., Williams, C., Soplop, N., Uryu, K., Pharmer, L., King, T., Bojmar, L., Davies, A.E., Ararso, Y., et al. (2015) 'Tumour exosome integrins determine organotropic metastasis', *Nature*, 527(7578), pp. 329–335.

Hosokawa, N., Hara, T., Kaizuka, T., Kishi, C., Takamura, A., Miura, Y., Iemura, S.I., Natsume, T., Takehana, K., Yamada, N., Guan, J.L., Oshiro, N. & Mizushima, N. (2009) 'Nutrient-dependent mTORCl association with the ULK1-Atg13-FIP200 complex required for autophagy', *Molecular Biology of the Cell*, 20(7), pp. 1981–1991.

Hosseini, H., Obradovic, M.M.S., Hoffmann, M., Harper, K.L., Sosa, M.S., Werner-Klein, M., Nanduri, L.K., Werno, C., Ehrl, C., Maneck, M., Patwary, N., Haunschild, G., Guzvic, M., Reimelt, C., Grauvogl, M., Eichner, N., Weber, F., Hartkopf, A.D., Taran, F.A., et al. (2016) 'Early dissemination seeds metastasis in breast cancer', *Nature*, 540(7634), pp. 552–558.

Hsu, C., Morohashi, Y., Yoshimura, S.I., Manrique-Hoyos, N., Jung, S.Y., Lauterbach, M.A., Bakhti, M., Grønborg, M., Möbius, W., Rhee, J.S., Barr, F.A. & Simons, M. (2010) 'Regulation of exosome secretion by Rab35 and its GTPase-activating proteins TBC1D10A-C', *Journal of Cell Biology*, 189(2), pp. 223–232.

Huang, Z.Z., Chen, C., Zeng, Z., Yang, H., Oh, J., Chen, L. & Lu, S.C. (2001) 'Mechanism and significance of increased glutathione level in human hepatocellular carcinoma and liver regeneration', *FASEB journal : official publication of the Federation of American Societies for Experimental Biology*, 15(1), pp. 19–21.

Hugel, B., Martínez, M.C., Kunzelmann, C. & Freyssinet, J.M. (2005) 'Membrane microparticles: Two sides of the coin'. Physiology 20 (1) p.pp. 22–27.

Hurley, J.H. & Hanson, P.I. (2010) 'Membrane budding and scission by the ESCRT machinery: It's all in the neck'. Nature Reviews Molecular Cell Biology 11 (8) p.pp. 556–566.

Hüsemann, Y., Geigl, J.B., Schubert, F., Musiani, P., Meyer, M., Burghart, E., Forni, G., Eils, R., Fehm, T., Riethmüller, G. & Klein, C.A. (2008) 'Systemic Spread Is an Early Step in Breast Cancer', *Cancer Cell*, 13(1), pp. 58–68.

Hutchins, P.D., Russell, J.D. & Coon, J.J. (2018) 'LipiDex: An Integrated Software Package for High-Confidence Lipid Identification', *Cell Systems*, 6(5), pp. 621-625.e5.

Hynes, R.O. (2002) 'Integrins: Bidirectional, allosteric signaling machines', *Cell*, 110(6), pp. 673–687.

Ichaso, N. & Dilworth, S.M. (2001) 'Cell transformation by the middle T-antigen of polyoma virus'. Oncogene 20 (54) p.pp. 7908–7916.

Ishikawa, K., Takenaga, K., Akimoto, M., Koshikawa, N., Yamaguchi, A., Imanishi, H., Nakada, K., Honma, Y. & Hayashi, J.I. (2008) 'ROS-generating mitochondrial DNA mutations can regulate tumor cell metastasis', *Science*, 320(5876), pp. 661–664.

Ivaska, J., Vuoriluoto, K., Huovinen, T., Izawa, I., Inagaki, M. & Parker, P.J. (2005) 'PKCε-mediated phosphorylation of vimentin controls integrin recycling and motility', *EMBO Journal*, 24(22), pp. 3834–3845.

Jacquemet, G., Green, D.M., Bridgewater, R.E., Kriegsheim, A. von, Humphries, M.J., Norman, J.C. & Caswell, P.T. (2013) 'Rcp-driven α5β1 recycling suppresses rac and promotes rhoa activity via the racgap1-iqgap1 complex', *Journal of Cell Biology*, 202(6), pp. 917–935.

Jacquemet, G., Humphries, M.J. & Caswell, P.T. (2013) 'Role of adhesion receptor trafficking in 3D cell migration'. Current Opinion in Cell Biology 25 (5) p.pp. 627–632.

Jafari, N., Drury, J., Morris, A.J., Onono, F.O., Stevens, P.D., Gao, T., Liu, J., Wang, C., Lee, E.Y., Weiss, H.L., Mark Evers, B. & Zaytseva, Y.Y. (2019) 'De novo fatty acid synthesis-driven sphingolipid metabolism promotes metastatic potential of colorectal cancer', *Molecular Cancer Research*, 17(1), pp. 140–152.

Jamil, A. & Kasi, A. (2022) *Lung Metastasis.*, in [Online]. Treasure Island (FL): .

Jehanno, C., Vulin, M., Richina, V., Richina, F. & Bentires-Alj, M. (2022) 'Phenotypic plasticity during metastatic colonization'. Trends in Cell Biology

Jiang, L., Shestov, A.A., Swain, P., Yang, C., Parker, S.J., Wang, Q.A., Terada, L.S., Adams, N.D., McCabe, M.T., Pietrak, B., Schmidt, S., Metallo, C.M., Dranka, B.P., Schwartz, B. & Deberardinis, R.J. (2016) 'Reductive carboxylation supports redox homeostasis during anchorage-independent growth', *Nature*, 532(7598), pp. 255–258.

Jin, L., Chun, J., Pan, C., Alesi, G.N., Li, D., Magliocca, K.R., Kang, Y., Chen, Z.G., Shin, D.M., Khuri, F.R., Fan, J. & Kang, S. (2017) 'Phosphorylation-mediated activation of LDHA promotes cancer cell invasion and tumour metastasis', *Oncogene*, 36(27), pp. 3797–3806.

Jobard, E., Pontoizeau, C., Blaise, B.J., Bachelot, T., Elena-Herrmann, B. & Tredan, O. (2014) 'A serum nuclear magnetic resonance-based metabolomic signature of advanced metastatic human breast cancer.', *Cancer letters*, 343(1), pp. 33–41.

Johnstone, R.M., Adam, M., Hammond, J.R., Orr, L. & Turbide, C. (1987) 'Vesicle formation during reticulocyte maturation. Association of plasma membrane activities with released vesicles (exosomes).', *Journal of Biological Chemistry*, 262(19), pp. 9412–9420.

Jonkers, J. & Derksen, P.W.B. (2007) 'Modeling metastatic breast cancer in mice', *Journal of Mammary Gland Biology and Neoplasia*, 12(2–3), pp. 191–203.

Joyce, J.A. & Pollard, J.W. (2009) 'Microenvironmental regulation of metastasis'. Nature Reviews Cancer 9 (4) p.pp. 239–252.

Kaczanowska, S., Beury, D.W., Gopalan, V., Tycko, A.K., Qin, H., Clements, M.E., Drake, J., Nwanze, C., Murgai, M., Rae, Z., Ju, W., Alexander, K.A., Kline, J., Contreras, C.F., Wessel, K.M., Patel, S., Hannenhalli, S., Kelly, M.C. & Kaplan, R.N. (2021) 'Genetically engineered myeloid cells rebalance the core immune suppression program in metastasis', *Cell*, 184(8), pp. 2033-2052.e21.

Kajimoto, T., Okada, T., Miya, S., Zhang, L. & Nakamura, S.I. (2013) 'Ongoing activation of sphingosine 1-phosphate receptors mediates maturation of exosomal multivesicular endosomes', *Nature Communications 2013 4:1*, 4(1), pp. 1–13.

Kang, Y., Siegel, P.M., Shu, W., Drobnjak, M., Kakonen, S.M., Cordón-Cardo, C., Guise, T.A. & Massagué, J. (2003) 'A multigenic program mediating breast cancer metastasis to bone', *Cancer Cell*, 3(6), pp. 537–549.

Kaplan, R.N., Riba, R.D., Zacharoulis, S., Bramley, A.H., Vincent, L., Costa, C., MacDonald, D.D., Jin, D.K., Shido, K., Kerns, S.A., Zhu, Z., Hicklin, D., Wu, Y., Port, J.L., Altorki, N., Port, E.R., Ruggero, D., Shmelkov, S. V., Jensen, K.K., et al. (2005) 'VEGFR1-positive haematopoietic bone marrow progenitors initiate the pre-metastatic niche', *Nature*, 438(7069), pp. 820–827.

Kennecke, H., Yerushalmi, R., Woods, R., Cheang, M.C.U., Voduc, D., Speers, C.H., Nielsen, T.O. & Gelmon, K. (2010) 'Metastatic behavior of breast cancer subtypes', *Journal of Clinical Oncology*, 28(20), pp. 3271–3277.

Kersten, K., Coffelt, S.B., Hoogstraat, M., Verstegen, N.J.M., Vrijland, K., Ciampricotti, M., Doornebal, C.W., Hau, C.S., Wellenstein, M.D., Salvagno, C., Doshi, P., Lips, E.H., Wessels, L.F.A. & de Visser, K.E. (2017) 'Mammary tumor-derived CCL2 enhances pro-metastatic systemic inflammation through upregulation of IL1ß in tumor-associated macrophages', *OncoImmunology*, 6(8), .

Keshet, R., Szlosarek, P., Carracedo, A. & Erez, A. (2018) 'Rewiring urea cycle metabolism in cancer to support anabolism', *Nature Reviews Cancer 2018 18:10*, 18(10), pp. 634–645.

Van Keymeulen, A., Lee, M.Y., Ousset, M., Brohée, S., Rorive, S., Giraddi, R.R., Wuidart, A., Bouvencourt, G., Dubois, C., Salmon, I., Sotiriou, C., Phillips, W.A. & Blanpain, C. (2015) 'Reactivation of multipotency by oncogenic PIK3CA induces breast tumour heterogeneity', *Nature*, 525(7567), pp. 119–123.

Kim, D., You, E., Jeong, J., Ko, P., Kim, J.W. & Rhee, S. (2017) 'DDR2 controls the epithelial-mesenchymal-transition-related gene expression via c-Myb acetylation upon matrix stiffening', *Scientific Reports 2017 7:1*, 7(1), pp. 1–15.

Kim, D.H., Sarbassov, D.D., Ali, S.M., King, J.E., Latek, R.R., Erdjument-Bromage, H., Tempst, P. & Sabatini, D.M. (2002) 'mTOR interacts with raptor to form a nutrient-sensitive complex that signals to the cell growth machinery', *Cell*, 110(2), pp. 163–175.

Kim, E., Goraksha-Hicks, P., Li, L., Neufeld, T.P. & Guan, K.L. (2008) 'Regulation of TORC1 by Rag GTPases in nutrient response', *Nature Cell Biology*, 10(8), pp. 935–945.

Kim, H.K., Song, K.S., Park, Y.S., Kang, Y.H., Lee, Y.J., Lee, K.R., Kim, H.K., Ryu, K.W., Bae, J.M. & Kim, S. (2003) 'Elevated levels of circulating platelet microparticles, VEGF, IL-6 and RANTES in patients with gastric cancer:

Possible role of a metastasis predictor', *European Journal of Cancer*, 39(2), pp. 184–191.

Kim, H.M., Jung, W.H. & Koo, J.S. (2014) 'Site-specific metabolic phenotypes in metastatic breast cancer', *Journal of Translational Medicine*, 12(1), .

Kim, I.S. & Baek, S.H. (2010) 'Mouse models for breast cancer metastasis', *Biochemical and Biophysical Research Communications*, 394(3), pp. 443–447.

Kitamura, T., Qian, B.Z., Soong, D., Cassetta, L., Noy, R., Sugano, G., Kato, Y., Li, J. & Pollard, J.W. (2015) 'CCL2-induced chemokine cascade promotes breast cancer metastasis by enhancing retention of metastasis-associated macrophages', *Journal of Experimental Medicine*, 212(7), pp. 1043–1059.

Klein, C.A. (2020) 'Cancer progression and the invisible phase of metastatic colonization', *Nature Reviews Cancer 2020 20:11*, 20(11), pp. 681–694.

Knott, S.R.V., Wagenblast, E., Khan, S., Kim, S.Y., Soto, M., Wagner, M., Turgeon, M.O., Fish, L., Erard, N., Gable, A.L., MacEli, A.R., DIckopf, S., Papachristou, E.K., D'Santos, C.S., Carey, L.A., Wilkinson, J.E., Harrell, J.C., Perou, C.M., Goodarzi, H., et al. (2018) 'Asparagine bioavailability governs metastasis in a model of breast cancer', *Nature*, 554(7692), pp. 378–381.

Koppula, P., Zhang, Y., Zhuang, L. & Gan, B. (2018) 'Amino acid transporter SLC7A11/xCT at the crossroads of regulating redox homeostasis and nutrient dependency of cancer.', *Cancer communications (London, England)*, 38(1), p. 12.

Kosaka, N., Iguchi, H., Hagiwara, K., Yoshioka, Y., Takeshita, F. & Ochiya, T. (2013) 'Neutral Sphingomyelinase 2 (nSMase2)-dependent Exosomal Transfer of Angiogenic MicroRNAs Regulate Cancer Cell Metastasis', *The Journal of Biological Chemistry*, 288(15), p. 10849.

Kowalski, P.J., Rubin, M.A. & Kleer, C.G. (2003) 'E-cadherin expression in primary carcinomas of the breast and its distant metastases', *Breast Cancer Research*, 5(6), .

Kvainickas, A., Orgaz, A.J., Nägele, H., Diedrich, B., Heesom, K.J., Dengjel, J., Cullen, P.J. & Steinberg, F. (2017) 'Retromer- and WASH-dependent sorting of nutrient transporters requires a multivalent interaction network with ANKRD50', *Journal of Cell Science*, 130(2), pp. 382–395.

Labelle, M., Begum, S. & Hynes, R.O. (2011) 'Direct Signaling between Platelets and Cancer Cells Induces an Epithelial-Mesenchymal-Like Transition and Promotes Metastasis', *Cancer Cell*, 20(5), pp. 576–590.

Labelle, M. & Hynes, R.O. (2012) 'The initial hours of metastasis: The importance of cooperative host-tumor cell interactions during hematogenous dissemination'. Cancer Discovery 2 (12) p.pp. 1091–1099.

Labuschagne, C.F., Cheung, E.C., Blagih, J., Domart, M.C. & Vousden, K.H. (2019) 'Cell Clustering Promotes a Metabolic Switch that Supports Metastatic Colonization', *Cell Metabolism*, 30(4), pp. 720-734.e5.

Lambert, A.W., Pattabiraman, D.R. & Weinberg, R.A. (2017) 'Emerging Biological Principles of Metastasis'. Cell 168 (4) p.pp. 670–691.

Lambert, A.W. & Weinberg, R.A. (2021) 'Linking EMT programmes to normal and neoplastic epithelial stem cells', *Nature Reviews Cancer*, 21(5), pp. 325–338.

Lanzardo, S., Conti, L., Rooke, R., Ruiu, R., Accart, N., Bolli, E., Arigoni, M., Macagno, M., Barrera, G., Pizzimenti, S., Aurisicchio, L., Calogero, R.A. & Cavallo, F. (2016) 'Immunotargeting of antigen xCT attenuates stem-like cell behavior and metastatic progression in breast cancer', *Cancer Research*, 76(1), pp. 62–72.

Lapidus, R.G., Nass, S.J. & Davidson, N.E. (1998) 'The Loss of Estrogen and Progesterone Receptor Gene Expression in Human Breast Cancer', *Journal of*

Mammary Gland Biology and Neoplasia, 3(1), pp. 85–94.
Lawrence, R.E. & Zoncu, R. (2019) 'The lysosome as a cellular centre for signalling, metabolism and quality control'. Nature Cell Biology 21 (2) p.pp. 133–142.
Lawson, D.A., Bhakta, N.R., Kessenbrock, K., Prummel, K.D., Yu, Y., Takai, K., Zhou, A., Eyob, H., Balakrishnan, S., Wang, C.Y., Yaswen, P., Goga, A. & Werb, Z. (2015) 'Single-cell analysis reveals a stem-cell program in human metastatic breast cancer cells', *Nature*, 526(7571), pp. 131–135.
LeBleu, V.S. & Kalluri, R. (2018) 'A peek into cancer-associated fibroblasts: Origins, functions and translational impact', *DMM Disease Models and Mechanisms*, 11(4), .
LeVea, C.M., McGary, C.T., Symons, J.R. & Mooney, R.A. (2000) 'PTP LAR expression compared to prognostic indices in metastatic and non-metastatic breast cancer', *Breast Cancer Research and Treatment*, 64(2), pp. 221–228.
Li, A.M., Ducker, G.S., Li, Y., Seoane, J.A., Xiao, Y., Melemenidis, S., Zhou, Y., Liu, L., Vanharanta, S., Graves, E.E., Rankin, E.B., Curtis, C., Massague, J., Rabinowitz, J.D., Thompson, C.B. & Ye, J. (2020) 'Metabolic profiling reveals a dependency of human metastatic breast cancer on mitochondrial serine and one-carbon unit metabolism', *Molecular Cancer Research*, 18(4), pp. 599–611.
Li, I. & Nabet, B.Y. (2019) 'Exosomes in the tumor microenvironment as mediators of cancer therapy resistance'. Molecular Cancer 18 (1) p.pp. 1–10.
LI, M., ZHANG, Z., YUAN, J., ZHANG, Y. & JIN, X. (2014) 'Altered glutamate cysteine ligase expression and activity in renal cell carcinoma', *Biomedical reports*, 2(6), pp. 831–834.
Li, S., Lu, Z., Sun, R., Guo, S., Gao, F., Cao, B. & Aa, J. (2022) 'The Role of SLC7A11 in Cancer: Friend or Foe?', *Cancers*, 14(13), p. 3059.
Li, S.C. & Kane, P.M. (2009) 'The yeast lysosome-like vacuole: Endpoint and crossroads'. Biochimica et Biophysica Acta - Molecular Cell Research 1793 (4) p.pp. 650–663.
Lien, E.C., Ghisolfi, L., Geck, R.C., Asara, J.M. & Toker, A. (2017) 'Oncogenic PI3K Promotes Methionine Dependency in Breast Cancer Cells Through the Cystine-Glutamate Antiporter xCT', *Science signaling*, 10(510), .
Lien, E.C., Lyssiotis, C.A., Juvekar, A., Hu, H., Asara, J.M., Cantley, L.C. & Toker, A. (2016) 'Glutathione biosynthesis is a metabolic vulnerability in PI(3)K/Akt-driven breast cancer', *Nature Cell Biology*, 18(5), pp. 572–578.
Lignitto, L., LeBoeuf, S.E., Homer, H., Jiang, S., Askenazi, M., Karakousi, T.R., Pass, H.I., Bhutkar, A.J., Tsirigos, A., Ueberheide, B., Sayin, V.I., Papagiannakopoulos, T. & Pagano, M. (2019) 'Nrf2 Activation Promotes Lung Cancer Metastasis by Inhibiting the Degradation of Bach1', *Cell*, 178(2), pp. 316-329.e18.
Lin, E.Y., Jones, J.G., Li, P., Zhu, L., Whitney, K.D., Muller, W.J. & Pollard, J.W. (2003) 'Progression to Malignancy in the Polyoma Middle T Oncoprotein Mouse Breast Cancer Model Provides a Reliable Model for Human Diseases', *American Journal of Pathology*, 163(5), pp. 2113–2126.
Liu, B. & Hannun, Y.A. (1997) 'Inhibition of the neutral magnesium-dependent sphingomyelinase by glutathione', *Journal of Biological Chemistry*, 272(26), pp. 16281–16287.
Liu, Y. & Cao, X. (2016) 'Characteristics and Significance of the Pre-metastatic Niche'. Cancer Cell 30 (5) p.pp. 668–681.
Lizunov, V.A., Lee, J.P., Skarulis, M.C., Zimmerberg, J., Cushman, S.W. & Stenkula, K.G. (2013) 'Impaired tethering and fusion of GLUT4 vesicles in insulin-resistant human adipose cells', *Diabetes*, 62(9), pp. 3114–3119.

Loayza-Puch, F., Rooijers, K., Buil, L.C.M., Zijlstra, J., Oude Vrielink, J.F., Lopes, R., Ugalde, A.P., Van Breugel, P., Hofland, I., Wesseling, J., Van Tellingen, O., Bex, A. & Agami, R. (2016) 'Tumour-specific proline vulnerability uncovered by differential ribosome codon reading', *Nature*, 530(7591), pp. 490–494.

Lu, S.C. (2009) 'Regulation of glutathione synthesis'. Molecular Aspects of Medicine 30 (1–2) p.pp. 42–59.

Lucotti, S., Kenific, C.M., Zhang, H. & Lyden, D.C. (2022) 'Extracellular vesicles and particles impact the systemic landscape of cancer', *EMBO Journal*, 41(18), p. e109288.

Lüönd, F., Sugiyama, N., Bill, R., Bornes, L., Hager, C., Tang, F., Santacroce, N., Beisel, C., Ivanek, R., Bürglin, T., Tiede, S., van Rheenen, J. & Christofori, G. (2021) 'Distinct contributions of partial and full EMT to breast cancer malignancy', *Developmental Cell*, 56(23), pp. 3203-3221.e11.

Lushchak, V.I. (2012) 'Glutathione Homeostasis and Functions: Potential Targets for Medical Interventions', *Journal of Amino Acids*, 2012pp. 1–26.

Luzzi, K.J., MacDonald, I.C., Schmidt, E.E., Kerkvliet, N., Morris, V.L., Chambers, A.F. & Groom, A.C. (1998) 'Multistep nature of metastatic inefficiency: Dormancy of solitary cells after successful extravasation and limited survival of early micrometastases', *American Journal of Pathology*, 153(3), pp. 865–873.

Lyon, B., Lyon, F., Mehlen, P. & Puisieux, A. (2006) 'Metastasis: a question of life or death', *NATURE REVIEWS | CANCER*, 6p. 449.

Macpherson, I.R., Rainero, E., Mitchell, L.E., van den Berghe, P.V.E., Speirs, C., Dozynkiewicz, M.A., Chaudhary, S., Kalna, G., Edwards, J., Timpson, P. & Norman, J.C. (2014) 'CLIC3 controls recycling of late endosomal MT1-MMP and dictates invasion and metastasis in breast cancer', *Journal of cell science*, 127(Pt 18), pp. 3893–3901.

Maeda, M., Johnson, K.R. & Wheelock, M.J. (2005) 'Cadherin switching: essential for behavioral but not morphological changes during an epithelium-to-mesenchyme transition', *Journal of Cell Science*, 118(5), pp. 873–887.

Maianu, L., Keller, S.R. & Garvey, W.T. (2001) 'Adipocytes exhibit abnormal subcellular distribution and translocation of vesicles containing glucose transporter 4 and insulin-regulated aminopeptidase in type 2 diabetes mellitus: Implications regarding defects in vesicle trafficking', *Journal of Clinical Endocrinology and Metabolism*, 86(11), pp. 5450–5456.

Malanchi, I., Santamaria-Martínez, A., Susanto, E., Peng, H., Lehr, H.A., Delaloye, J.F. & Huelsken, J. (2012) 'Interactions between cancer stem cells and their niche govern metastatic colonization', *Nature*, 481(7379), pp. 85–91.

Malladi, S., MacAlinao, D.G., Jin, X., He, L., Basnet, H., Zou, Y., De Stanchina, E. & Massagué, J. (2016) 'Metastatic Latency and Immune Evasion through Autocrine Inhibition of WNT', *Cell*, 165(1), pp. 45–60.

Marchesini, N., Luberto, C. & Hannun, Y.A. (2003) 'Biochemical properties of mammalian neutral sphingomyelinase2 and its role in sphingolipid metabolism', *Journal of Biological Chemistry*, 278(16), pp. 13775–13783.

Margolis, L. & Sadovsky, Y. (2019) 'The biology of extracellular vesicles: The known unknowns', *PLoS Biology*, 17(7), .

Massagué, J. & Obenauf, A.C. (2016) 'Metastatic colonization by circulating tumour cells'. Nature 529 (7586) p.pp. 298–306.

Massberg, S., Konrad, I., Schürzinger, K., Lorenz, M., Schneider, S., Zohlnhoefer, D., Hoppe, K., Schiemann, M., Kennerknecht, E., Sauer, S., Schulz, C., Kerstan, S., Rudelius, M., Seidl, S., Sorge, F., Langer, H., Peluso, M., Goyal,

P., Vestweber, D., et al. (2006) 'Platelets secrete stromal cell-derived factor 1α and recruit bone marrow-derived progenitor cells to arterial thrombi in vivo', *Journal of Experimental Medicine*, 203(5), pp. 1221–1233.

Mathieu, M., Martin-Jaular, L., Lavieu, G. & Théry, C. (2019) 'Specificities of secretion and uptake of exosomes and other extracellular vesicles for cell-to-cell communication'. Nature Cell Biology 21 (1) p.pp. 9–17.

Mathieu, M., Névo, N., Jouve, M., Valenzuela, J.I., Maurin, M., Verweij, F.J., Palmulli, R., Lankar, D., Dingli, F., Loew, D., Rubinstein, E., Boncompain, G., Perez, F. & Théry, C. (2021) 'Specificities of exosome versus small ectosome secretion revealed by live intracellular tracking of CD63 and CD9', *Nature Communications 2021 12:1*, 12(1), pp. 1–18.

McAllister, S.S. & Weinberg, R.A. (2014) 'The tumour-induced systemic environment as a critical regulator of cancer progression and metastasis'. Nature Cell Biology 16 (8) p.pp. 717–727.

Medina, D.L., Fraldi, A., Bouche, V., Annunziata, F., Mansueto, G., Spampanato, C., Puri, C., Pignata, A., Martina, J.A., Sardiello, M., Palmieri, M., Polishchuk, R., Puertollano, R. & Ballabio, A. (2011) 'Transcriptional activation of lysosomal exocytosis promotes cellular clearance', *Developmental Cell*, 21(3), pp. 421–430.

Van Meer, G. & Lisman, Q. (2002) 'Sphingolipid transport: Rafts and translocators', *Journal of Biological Chemistry*, 277(29), pp. 25855–25858.

Van Meer, G., Voelker, D.R. & Feigenson, G.W. (2008) 'Membrane lipids: where they are and how they behave', *Nature reviews. Molecular cell biology*, 9(2), p. 112.

Menck, K., Sönmezer, C., Worst, T.S., Schulz, M., Dihazi, G.H., Streit, F., Erdmann, G., Kling, S., Boutros, M., Binder, C. & Gross, J.C. (2017) 'Neutral sphingomyelinases control extracellular vesicles budding from the plasma membrane', *Journal of Extracellular Vesicles*, 6(1), .

Menon, S., Dibble, C.C., Talbott, G., Hoxhaj, G., Valvezan, A.J., Takahashi, H., Cantley, L.C. & Manning, B.D. (2014) 'Spatial control of the TSC complex integrates insulin and nutrient regulation of mTORC1 at the lysosome', *Cell*, 156(4), pp. 771–785.

Mierke, C.T., Frey, B., Fellner, M., Herrmann, M. & Fabry, B. (2011) 'Integrin α5β1 facilitates cancer cell invasion through enhanced contractile forces', *Journal of Cell Science*, 124(3), pp. 369–383.

Minciacchi, V.R., Freeman, M.R. & Di Vizio, D. (2015) 'Extracellular Vesicles in Cancer: Exosomes, Microvesicles and the Emerging Role of Large Oncosomes'. Seminars in Cell and Developmental Biology 40 p.pp. 41–51.

Minn, A.J., Gupta, G.P., Siegel, P.M., Bos, P.D., Shu, W., Giri, D.D., Viale, A., Olshen, A.B., Gerald, W.L. & Massagué, J. (2005) 'Genes that mediate breast cancer metastasis to lung', *Nature 2005 436:7050*, 436(7050), pp. 518–524.

Morad, S.A.F. & Cabot, M.C. (2012) 'Ceramide-orchestrated signalling in cancer cells', *Nature Reviews Cancer 2012 13:1*, 13(1), pp. 51–65.

Mukhopadhyay, S., Biancur, D.E., Parker, S.J., Yamamoto, K., Banh, R.S., Paulo, J.A., Mancias, J.D. & Kimmelman, A.C. (2021) 'Autophagy is required for proper cysteine homeostasis in pancreatic cancer through regulation of SLC7A11', *Proceedings of the National Academy of Sciences of the United States of America*, 118(6), p. e2021475118.

Muller, P.A.J., Caswell, P.T., Doyle, B., Iwanicki, M.P., Tan, E.H., Karim, S., Lukashchuk, N., Gillespie, D.A., Ludwig, R.L., Gosselin, P., Cromer, A., Brugge, J.S., Sansom, O.J., Norman, J.C. & Vousden, K.H. (2009) 'Mutant p53 drives invasion by promoting integrin recycling', *Cell*, 139(7), pp. 1327–1341.

Muller, P.A.J., Trinidad, A.G., Caswell, P.T., Norman, J.C. & Vousden, K.H. (2014) 'Mutant p53 Regulates Dicer through p63-dependent and -independent Mechanisms to Promote an Invasive Phenotype', *The Journal of Biological Chemistry*, 289(1), p. 122.

Muranen, T., Iwanicki, M.P., Curry, N.L., Hwang, J., DuBois, C.D., Coloff, J.L., Hitchcock, D.S., Clish, C.B., Brugge, J.S. & Kalaany, N.Y. (2017) 'Starved epithelial cells uptake extracellular matrix for survival', *Nature Communications*, 8(1), pp. 1–12.

Na, T.Y., Schecterson, L., Mendonsa, A.M. & Gumbiner, B.M. (2020) 'The functional activity of E-cadherin controls tumor cell metastasis at multiple steps', *Proceedings of the National Academy of Sciences of the United States of America*, 117(11), pp. 5931–5937.

Nabhan, J.F., Hu, R., Oh, R.S., Cohen, S.N. & Lu, Q. (2012) 'Formation and release of arrestin domain-containing protein 1-mediated microvesicles (ARMMs) at plasma membrane by recruitment of TSG101 protein', *Proceedings of the National Academy of Sciences of the United States of America*, 109(11), pp. 4146–4151.

Najmeh, S., Cools-Lartigue, J., Rayes, R.F., Gowing, S., Vourtzoumis, P., Bourdeau, F., Giannias, B., Berube, J., Rousseau, S., Ferri, L.E. & Spicer, J.D. (2017) 'Neutrophil extracellular traps sequester circulating tumor cells via ß1-integrin mediated interactions', *International Journal of Cancer*, 140(10), pp. 2321–2330.

Nanou, A., Miller, M.C., Zeune, L.L., de Wit, S., Punt, C.J.A., Groen, H.J.M., Hayes, D.F., de Bono, J.S. & Terstappen, L.W.M.M. (2020) 'Tumour-derived extracellular vesicles in blood of metastatic cancer patients associate with overall survival', *British Journal of Cancer*, 122(6), pp. 801–811.

Nath, A. & Chan, C. (2016) 'Genetic alterations in fatty acid transport and metabolism genes are associated with metastatic progression and poor prognosis of human cancers', *Scientific Reports*, 6.

Nath, A., Li, I., Roberts, L.R. & Chan, C. (2015) 'Elevated free fatty acid uptake via CD36 promotes epithelial-mesenchymal transition in hepatocellular carcinoma', *Scientific Reports*, 5.

Ngo, B., Kim, E., Osorio-Vasquez, V., Doll, S., Bustraan, S., Liang, R.J., Luengo, A., Davidson, S.M., Ali, A., Ferraro, G.B., Fischer, G.M., Eskandari, R., Kang, D.S., Ni, J., Plasger, A., Rajasekhar, V.K., Kastenhuber, E.R., Bacha, S., Sriram, R.K., et al. (2020) 'Limited environmental serine and glycine confer brain metastasis sensitivity to PHGDH inhibition', *Cancer Discovery*, 10(9), pp. 1352–1373.

van Niel, G., Carter, D.R.F., Clayton, A., Lambert, D.W., Raposo, G. & Vader, P. (2022) 'Challenges and directions in studying cell–cell communication by extracellular vesicles', *Nature Reviews Molecular Cell Biology*, 23(5), pp. 369–382.

van Niel, G., Charrin, S., Simoes, S., Romao, M., Rochin, L., Saftig, P., Marks, M.S., Rubinstein, E. & Raposo, G. (2011) 'The tetraspanin CD63 regulates ESCRT-independent and dependent endosomal sorting during melanogenesis', *Developmental cell*, 21(4), p. 708.

Van Niel, G., D'Angelo, G. & Raposo, G. (2018) 'Shedding light on the cell biology of extracellular vesicles', *Nature Reviews Molecular Cell Biology 2018 19:4*, 19(4), pp. 213–228.

Nobre, A.R., Risson, E., Singh, D.K., Di Martino, J.S., Cheung, J.F., Wang, J., Johnson, J., Russnes, H.G., Bravo-Cordero, J.J., Birbrair, A., Naume, B., Azhar, M., Frenette, P.S. & Aguirre-Ghiso, J.A. (2021) 'Bone marrow

NG2+/Nestin+ mesenchymal stem cells drive DTC dormancy via TGF-ß2', *Nature Cancer 2021 2:3*, 2(3), pp. 327–339.

Nogueira, V., Park, Y., Chen, C.C., Xu, P.Z., Chen, M.L., Tonic, I., Unterman, T. & Hay, N. (2008) 'Akt Determines Replicative Senescence and Oxidative or Oncogenic Premature Senescence and Sensitizes Cells to Oxidative Apoptosis', *Cancer Cell*, 14(6), pp. 458–470.

Novo, D., Heath, N., Mitchell, L., Caligiuri, G., MacFarlane, A., Reijmer, D., Charlton, L., Knight, J., Calka, M., McGhee, E., Dornier, E., Sumpton, D., Mason, S., Echard, A., Klinkert, K., Secklehner, J., Kruiswijk, F., Vousden, K., Macpherson, I.R., et al. (2018) 'Mutant p53s generate pro-invasive niches by influencing exosome podocalyxin levels', *Nature Communications*, 9(1), pp. 1–17.

O'Prey, J., Sakamaki, J., Baudot, A.D., New, M., Van Acker, T., Tooze, S.A., Long, J.S. & Ryan, K.M. (2017) 'Application of CRISPR/Cas9 to Autophagy Research', *Methods in Enzymology*, 588pp. 79–108.

Ocaña, O.H., Córcoles, R., Fabra, Á., Moreno-Bueno, G., Acloque, H., Vega, S., Barrallo-Gimeno, A., Cano, A. & Nieto, M.A. (2012) 'Metastatic Colonization Requires the Repression of the Epithelial-Mesenchymal Transition Inducer Prrx1', *Cancer Cell*, 22(6), pp. 709–724.

Oskarsson, T., Batlle, E. & Massagué, J. (2014) 'Metastatic stem cells: Sources, niches, and vital pathways'. Cell Stem Cell 14 (3) p.pp. 306–321.

Ostrowski, M., Carmo, N.B., Krumeich, S., Fanget, I., Raposo, G., Savina, A., Moita, C.F., Schauer, K., Hume, A.N., Freitas, R.P., Goud, B., Benaroch, P., Hacohen, N., Fukuda, M., Desnos, C., Seabra, M.C., Darchen, F., Amigorena, S., Moita, L.F., et al. (2010) 'Rab27a and Rab27b control different steps of the exosome secretion pathway', *Nature Cell Biology*, 12(1), pp. 19–30.

Padmanaban, V., Krol, I., Suhail, Y., Szczerba, B.M., Aceto, N., Bader, J.S. & Ewald, A.J. (2019) 'E-cadherin is required for metastasis in multiple models of breast cancer', *Nature*, 573(7774), pp. 439–444.

Padua, D., Zhang, X.H.F., Wang, Q., Nadal, C., Gerald, W.L., Gomis, R.R. & Massagué, J. (2008) 'TGFß Primes Breast Tumors for Lung Metastasis Seeding through Angiopoietin-like 4', *Cell*, 133(1), pp. 66–77.

Paget, S. (1889) 'THE DISTRIBUTION OF SECONDARY GROWTHS IN CANCER OF THE BREAST.', *The Lancet*, 133(3421), pp. 571–573.

Palumbo, J.S., Talmage, K.E., Massari, J. V., La Jeunesse, C.M., Flick, M.J., Kombrinck, K.W., Jirousková, M. & Degen, J.L. (2005) 'Platelets and fibrin(ogen) increase metastatic potential by impeding natural killer cell-mediated elimination of tumor cells', *Blood*, 105(1), pp. 178–185.

Panchaud, N., Péli-Gulli, M.P. & De Virgilio, C. (2013) 'Amino acid deprivation inhibits TORC1 through a GTPase-activating protein complex for the Rag family GTPase Gtr1', *Science Signaling*, 6(277), .

Pantano, F., Croset, M., Driouch, K., Bednarz-Knoll, N., Iuliani, M., Ribelli, G., Bonnelye, E., Wikman, H., Geraci, S., Bonin, F., Simonetti, S., Vincenzi, B., Hong, S.S., Sousa, S., Pantel, K., Tonini, G., Santini, D. & Clézardin, P. (2021) 'Integrin alpha5 in human breast cancer is a mediator of bone metastasis and a therapeutic target for the treatment of osteolytic lesions', *Oncogene*, 40(7), pp. 1284–1299.

Parashuraman, S. & D'Angelo, G. (2019) 'Visualizing sphingolipid biosynthesis in cells', *Chemistry and Physics of Lipids*, 218pp. 103–111.

Parry, G., Bartholomew, J.C. & Bissell, M.J. (1980) 'Role of src gene in growth regulation of Rous sarcoma virus-infected chicken embryo fibroblasts', *Nature 1980 288:5792*, 288(5792), pp. 720–722.

Pascual, G., Avgustinova, A., Mejetta, S., Martín, M., Castellanos, A., Attolini, C.S.O., Berenguer, A., Prats, N., Toll, A., Hueto, J.A., Bescós, C., Di Croce, L. & Benitah, S.A. (2017) 'Targeting metastasis-initiating cells through the fatty acid receptor CD36', *Nature*, 541(7635), pp. 41–45.

Pastushenko, I., Brisebarre, A., Sifrim, A., Fioramonti, M., Revenco, T., Boumahdi, S., Van Keymeulen, A., Brown, D., Moers, V., Lemaire, S., De Clercq, S., Minguijón, E., Balsat, C., Sokolow, Y., Dubois, C., De Cock, F., Scozzaro, S., Sopena, F., Lanas, A., et al. (2018) 'Identification of the tumour transition states occurring during EMT', *Nature 2018 556:7702*, 556(7702), pp. 463–468.

Paul, N.R., Allen, J.L., Chapman, A., Morlan-Mairal, M., Zindy, E., Jacquemet, G., Fernandez del Ama, L., Ferizovic, N., Green, D.M., Howe, J.D., Ehler, E., Hurlstone, A. & Caswell, P.T. (2015) 'α5β1 integrin recycling promotes Arp2/3-independent cancer cell invasion via the formin FHOD3', *Journal of Cell Biology*, 210(6), pp. 1013–1031.

Paul, N.R., Jacquemet, G. & Caswell, P.T. (2015) 'Endocytic Trafficking of Integrins in Cell Migration'. Current Biology 25 (22) p.pp. R1092–R1105.

Pavlova, N.N. & Thompson, C.B. (2016) 'The Emerging Hallmarks of Cancer Metabolism'. Cell Metabolism 23 (1) p.pp. 27–47.

Peinado, H., Alečković, M., Lavotshkin, S., Matei, I., Costa-Silva, B., Moreno-Bueno, G., Hergueta-Redondo, M., Williams, C., García-Santos, G., Ghajar, C.M., Nitadori-Hoshino, A., Hoffman, C., Badal, K., Garcia, B.A., Callahan, M.K., Yuan, J., Martins, V.R., Skog, J., Kaplan, R.N., et al. (2012) 'Melanoma exosomes educate bone marrow progenitor cells toward a pro-metastatic phenotype through MET', *Nature medicine*, 18(6), pp. 883–891.

Peinado, H., Zhang, H., Matei, I.R., Costa-Silva, B., Hoshino, A., Rodrigues, G., Psaila, B., Kaplan, R.N., Bromberg, J.F., Kang, Y., Bissell, M.J., Cox, T.R., Giaccia, A.J., Erler, J.T., Hiratsuka, S., Ghajar, C.M. & Lyden, D. (2017) 'Pre-metastatic niches: Organ-specific homes for metastases'. Nature Reviews Cancer 17 (5) p.pp. 302–317.

Pfefferle, A.D., Herschkowitz, J.I., Usary, J., Harrell, J.C., Spike, B.T., Adams, J.R., Torres-Arzayus, M.I., Brown, M., Egan, S.E., Wahl, G.M., Rosen, J.M. & Perou, C.M. (2013) 'Transcriptomic classification of genetically engineered mouse models of breast cancer identifies human subtype counterparts', *Genome Biology*, 14(11), p. R125.

Piskounova, E., Agathocleous, M., Murphy, M.M., Hu, Z., Huddlestun, S.E., Zhao, Z., Leitch, A.M., Johnson, T.M., Deberardinis, R.J. & Morrison, S.J. (2015) *Oxidative stress inhibits distant metastasis by human melanoma cells*. 527 (7577).

Placke, T., Örgel, M., Schaller, M., Jung, G., Rammensee, H.G., Kopp, H.G. & Salih, H.R. (2012) 'Platelet-derived MHC class I confers a pseudonormal phenotype to cancer cells that subverts the antitumor reactivity of natural killer immune cells', *Cancer Research*, 72(2), pp. 440–448.

Podsypanina, K., Du, Y.C.N., Jechlinger, M., Beverly, L.J., Hambardzumyan, D. & Varmus, H. (2008) 'Seeding and propagation of untransformed mouse mammary cells in the lung', *Science*, 321(5897), pp. 1841–1844.

Pollard, J.W. (2016) 'Defining Metastatic Cell Latency', *New England Journal of Medicine*, 375(3), pp. 280–282.

Pollari, S., Käkönen, S.M., Edgren, H., Wolf, M., Kohonen, P., Sara, H., Guise, T., Nees, M. & Kallioniemi, O. (2011) 'Enhanced serine production by bone metastatic breast cancer cells stimulates osteoclastogenesis', *Breast Cancer Research and Treatment*, 125(2), pp. 421–430.

Porporato, P.E., Payen, V.L., Pérez-Escuredo, J., De Saedeleer, C.J., Danhier, P., Copetti, T., Dhup, S., Tardy, M., Vazeille, T., Bouzin, C., Feron, O., Michiels, C., Gallez, B. & Sonveaux, P. (2014) 'A mitochondrial switch promotes tumor metastasis', *Cell Reports*, 8(3), pp. 754–766.

del Pozo Martin, Y., Park, D., Ramachandran, A., Ombrato, L., Calvo, F., Chakravarty, P., Spencer-Dene, B., Derzsi, S., Hill, C.S., Sahai, E. & Malanchi, I. (2015) 'Mesenchymal Cancer Cell-Stroma Crosstalk Promotes Niche Activation, Epithelial Reversion, and Metastatic Colonization', *Cell Reports*, 13(11), pp. 2456–2469.

Psaila, B. & Lyden, D. (2009) 'The metastatic niche: Adapting the foreign soil'. Nature Reviews Cancer 9 (4) p.pp. 285–293.

Qian, B., Deng, Y., Im, J.H., Muschel, R.J., Zou, Y., Li, J., Lang, R.A. & Pollard, J.W. (2009) 'A distinct macrophage population mediates metastatic breast cancer cell extravasation, establishment and growth', *PLoS ONE*, 4(8), .

Qian, B.Z., Li, J., Zhang, H., Kitamura, T., Zhang, J., Campion, L.R., Kaiser, E.A., Snyder, L.A. & Pollard, J.W. (2011) 'CCL2 recruits inflammatory monocytes to facilitate breast-tumour metastasis', *Nature*, 475(7355), pp. 222–225.

Qian, B.Z., Zhang, H., Li, J., He, T., Yeo, E.J., Soong, D.Y.H., Carragher, N.O., Munro, A., Chang, A., Bresnick, A.R., Lang, R.A. & Pollard, J.W. (2015) 'FLT1 signaling in metastasis-associated macrophages activates an inflammatory signature that promotes breast cancer metastasis', *Journal of Experimental Medicine*, 212(9), pp. 1433–1448.

Rabas, N., Palmer, S., Mitchell, L., Ismail, S., Gohlke, A., Riley, J.S., Tait, S.W.G., Gammage, P., Soares, L.L., Macpherson, I.R. & Norman, J.C. (2021) 'Pink1 drives production of mtDNA-containing extracellular vesicles to promote invasiveness', *Journal of Cell Biology*, 220(12), .

Rainero, E., Caswell, P.T., Muller, P.A.J., Grindlay, J., Mccaffrey, M.W., Zhang, Q., Wakelam, M.J.O., Vousden, K.H., Graziani, A. & Norman, J.C. (2012) 'Diacylglycerol kinase α controls RCP-dependent integrin trafficking to promote invasive migration', *The Journal of cell biology*, 196(2), pp. 277–295.

Rainero, E., Howe, J.D., Caswell, P.T., Jamieson, N.B., Anderson, K., Critchley, D.R., Machesky, L. & Norman, J.C. (2015) 'Ligand-Occupied Integrin Internalization Links Nutrient Signaling to Invasive Migration', *Cell Reports*, 10(3), pp. 398–413.

Reczek, C.R. & Chandel, N.S. (2017) 'The two faces of reactive oxygen species in cancer', *Annual Review of Cancer Biology*, 1pp. 79–98.

Revill, K., Wang, T., Lachenmayer, A., Kojima, K., Harrington, A., Li, J., Hoshida, Y., Llovet, J.M. & Powers, S. (2013) 'Genome-wide methylation analysis and epigenetic unmasking identify tumor suppressor genes in hepatocellular carcinoma', *Gastroenterology*, 145(6), .

Rhim, A.D., Mirek, E.T., Aiello, N.M., Maitra, A., Bailey, J.M., McAllister, F., Reichert, M., Beatty, G.L., Rustgi, A.K., Vonderheide, R.H., Leach, S.D. & Stanger, B.Z. (2012) 'EMT and dissemination precede pancreatic tumor formation', *Cell*, 148(1–2), pp. 349–361.

Ridley, A.J. (2006) 'Rho GTPases and actin dynamics in membrane protrusions and vesicle trafficking'. Trends in Cell Biology 16 (10) p.pp. 522–529.

Riihimäki, M., Thomsen, H., Sundquist, K., Sundquist, J. & Hemminki, K. (2018) 'Clinical landscape of cancer metastases', *Cancer Medicine*, 7(11), p. 5534.

Rinaldi, G., Pranzini, E., Van Elsen, J., Broekaert, D., Funk, C.M., Planque, M., Doglioni, G., Altea-Manzano, P., Rossi, M., Geldhof, V., Teoh, S.T., Ross, C., Hunter, K.W., Lunt, S.Y., Grünewald, T.G.P. & Fendt, S.M. (2021) 'In Vivo Evidence for Serine Biosynthesis-Defined Sensitivity of Lung Metastasis, but

Not of Primary Breast Tumors, to mTORC1 Inhibition', *Molecular Cell*, 81(2), pp. 386-397.e7.

Rios Garcia, M., Steinbauer, B., Srivastava, K., Singhal, M., Mattijssen, F., Maida, A., Christian, S., Hess-Stumpp, H., Augustin, H.G., Müller-Decker, K., Nawroth, P.P., Herzig, S. & Berriel Diaz, M. (2017) 'Acetyl-CoA Carboxylase 1-Dependent Protein Acetylation Controls Breast Cancer Metastasis and Recurrence', *Cell Metabolism*, 26(6), pp. 842-855.e5.

Risson, E., Nobre, A.R., Maguer-Satta, V. & Aguirre-Ghiso, J.A. (2020) 'The current paradigm and challenges ahead for the dormancy of disseminated tumor cells'. Nature cancer 1 (7) p.pp. 672–680.

Rivera, I.G., Ordoñez, M., Presa, N., Gangoiti, P., Gomez-Larrauri, A., Trueba, M., Fox, T., Kester, M. & Gomez-Muñoz, A. (2016) 'Ceramide 1-phosphate regulates cell migration and invasion of human pancreatic cancer cells', *Biochemical Pharmacology*, 102pp. 107–119.

Robe, P.A., Martin, D.H., Nguyen-Khac, M.T., Artesi, M., Deprez, M., Albert, A., Vanbelle, S., Califice, S., Bredel, M. & Bours, V. (2009) 'Early termination of ISRCTN45828668, a phase 1/2 prospective, randomized study of sulfasalazine for the treatment of progressing malignant gliomas in adults', *BMC Cancer*, 9(1), p. 372.

Roberts, M., Barry, S., Woods, A., Van der Sluijs, P. & Norman, J. (2001) 'PDGF-regulated rab4-dependent recycling of αvβ3 integrin from early endosomes is necessary for cell adhesion and spreading', *Current Biology*, 11(18), pp. 1392–1402.

Roberts, M.S., Woods, A.J., Dale, T.C., van der Sluijs, P. & Norman, J.C. (2004) 'Protein Kinase B/Akt Acts via Glycogen Synthase Kinase 3 To Regulate Recycling of αvβ3 and α5β1 Integrins', *Molecular and Cellular Biology*, 24(4), pp. 1505–1515.

Robinson, B.D., Sica, G.L., Liu, Y.F., Rohan, T.E., Gertler, F.B., Condeelis, J.S. & Jones, J.G. (2009) 'Tumor microenvironment of metastasis in human breast carcinoma: A potential prognostic marker linked to hematogenous dissemination', *Clinical Cancer Research*, 15(7), pp. 2433–2441.

Rocha, N., Kuijl, C., Van Der Kant, R., Janssen, L., Houben, D., Janssen, H., Zwart, W. & Neefjes, J. (2009) 'Cholesterol sensor ORP1L contacts the ER protein VAP to control Rab7-RILP-p150Glued and late endosome positioning', *Journal of Cell Biology*, 185(7), pp. 1209–1225.

Rodrigues, G., Hoshino, A., Kenific, C.M., Matei, I.R., Steiner, L., Freitas, D., Kim, H.S., Oxley, P.R., Scandariato, I., Casanova-Salas, I., Dai, J., Badwe, C.R., Gril, B., Tešić Mark, M., Dill, B.D., Molina, H., Zhang, H., Benito-Martin, A., Bojmar, L., et al. (2019) 'Tumour exosomal CEMIP protein promotes cancer cell colonization in brain metastasis', *Nature Cell Biology*, 21(11), pp. 1403–1412.

Roh-Johnson, M., Bravo-Cordero, J.J., Patsialou, A., Sharma, V.P., Guo, P., Liu, H., Hodgson, L. & Condeelis, J. (2014) 'Macrophage contact induces RhoA GTPase signaling to trigger tumor cell intravasation', *Oncogene*, 33(33), pp. 4203–4212.

Rohan, T.E., Xue, X., Lin, H.M., D'Alfonso, T.M., Ginter, P.S., Oktay, M.H., Robinson, B.D., Ginsberg, M., Gertler, F.B., Glass, A.G., Sparano, J.A., Condeelis, J.S. & Jones, J.G. (2014) 'Tumor microenvironment of metastasis and risk of distant metastasis of breast cancer', *Journal of the National Cancer Institute*, 106(8), .

Roussos, E.T., Balsamo, M., Alford, S.K., Wyckoff, J.B., Gligorijevic, B., Wang, Y., Pozzuto, M., Stobezki, R., Goswami, S., Segall, J.E., Lauffenburger, D.A.,

Bresnick, A.R., Gertler, F.B. & Condeelis, J.S. (2011) 'Mena invasive (Mena INV) promotes multicellular streaming motility and transendothelial migration in a mouse model of breast cancer', *Journal of Cell Science*, 124(13), pp. 2120–2131.

Rowland, A.F., Fazakerley, D.J. & James, D.E. (2011) 'Mapping Insulin/GLUT4 Circuitry'. Traffic 12 (6) p.pp. 672–681.

Rutkute, K., Asmis, R.H. & Nikolova-Karakashian, M.N. (2007) 'Regulation of neutral sphingomyelinase-2 by GSH: A new insight to the role of oxidative stress in aging-associated inflammation', *Journal of Lipid Research*, 48(11), pp. 2443–2452.

Ryan, D.G., Yang, M., Prag, H.A., Blanco, G.R., Nikitopoulou, E., Segarra-Mondejar, M., Powell, C.A., Young, T., Burger, N., Miljkovic, J.L., Minczuk, M., Murphy, M.P., von Kriegsheim, A. & Frezza, C. (2021) 'Disruption of the TCA cycle reveals an ATF4-dependent integration of redox and amino acid metabolism', *eLife*, 10.

Sahai, E. (2005) 'Mechanisms of cancer cell invasion', *Current Opinion in Genetics & Development*, 15(1), pp. 87–96.

Sancak, Y., Peterson, T.R., Shaul, Y.D., Lindquist, R.A., Thoreen, C.C., Bar-Peled, L. & Sabatini, D.M. (2008) 'The rag GTPases bind raptor and mediate amino acid signaling to mTORC1', *Science*, 320(5882), pp. 1496–1501.

Sanjana, N.E., Shalem, O. & Zhang, F. (2014) 'Improved vectors and genome-wide libraries for CRISPR screening', *Nature methods*, 11(8), p. 783.

Savina, A., Fader, C.M., Damiani, M.T. & Colombo, M.I. (2005) 'Rab11 promotes docking and fusion of multivesicular bodies in a calcium-dependent manner', *Traffic*, 6(2), pp. 131–143.

Savina, A., Furlán, M., Vidal, M. & Colombo, M.I. (2003) 'Exosome release is regulated by a calcium-dependent mechanism in K562 cells', *Journal of Biological Chemistry*, 278(22), pp. 20083–20090.

Saxena, M., Kalathur, R.K.R., Neutzner, M. & Christofori, G. (2018) 'PyMT-1099, a versatile murine cell model for EMT in breast cancer', *Scientific Reports*, 8(1), pp. 1–12.

Sayin, V.I., Leboeuf, S.E., Singh, S.X., Davidson, S.M., Biancur, D., Guzelhan, B.S., Alvarez, S.W., Wu, W.L., Karakousi, T.R., Zavitsanou, A.M., Ubriaco, J., Muir, A., Karagiannis, D., Morris, P.J., Thomas, C.J., Possemato, R., Vander Heiden, M.G. & Papagiannakopoulos, T. (2017) 'Activation of the NRF2 antioxidant program generates an imbalance in central carbon metabolism in cancer', *eLife*, 6.

Schafer, Z.T., Grassian, A.R., Song, L., Jiang, Z., Gerhart-Hines, Z., Irie, H.Y., Gao, S., Puigserver, P. & Brugge, J.S. (2009) 'Antioxidant and oncogene rescue of metabolic defects caused by loss of matrix attachment', *Nature*, 461(7260), pp. 109–113.

Schlesinger, M. (2018) 'Role of platelets and platelet receptors in cancer metastasis 06 Biological Sciences 0601 Biochemistry and Cell Biology'. Journal of Hematology and Oncology 11 (1).

Schueller, G. & Herold, C.J. (2003) 'Lung metastases'. Cancer Imaging 3 (2) p.pp. 126–128.

Schumacher, D., Strilic, B., Sivaraj, K.K., Wettschureck, N. & Offermanns, S. (2013) 'Platelet-Derived Nucleotides Promote Tumor-Cell Transendothelial Migration and Metastasis via P2Y2 Receptor', *Cancer Cell*, 24(1), pp. 130–137.

Schwalm, S., Erhardt, M., Römer, I., Pfeilschifter, J., Zangemeister-Wittke, U. & Huwiler, A. (2020) 'Ceramide Kinase Is Upregulated in Metastatic Breast Cancer Cells and Contributes to Migration and Invasion by Activation of PI 3-

Kinase and Akt', *International Journal of Molecular Sciences*, 21(4), .
Schwörer, S., Berisa, M., Violante, S., Qin, W., Zhu, J., Hendrickson, R.C., Cross, J.R. & Thompson, C.B. (2020) 'Proline biosynthesis is a vent for TGFß-induced mitochondrial redox stress', *The EMBO Journal*, 39(8), .
Sellers, K., Fox, M.P., Ii, M.B., Slone, S.P., Higashi, R.M., Miller, D.M., Wang, Y., Yan, J., Yuneva, M.O., Deshpande, R., Lane, A.N. & Fan, T.W.M. (2015) 'Pyruvate carboxylase is critical for non-small-cell lung cancer proliferation', *Journal of Clinical Investigation*, 125(2), pp. 687–698.
Shalem, O., Sanjana, N.E., Hartenian, E., Shi, X., Scott, D.A., Mikkelsen, T.S., Heckl, D., Ebert, B.L., Root, D.E., Doench, J.G. & Zhang, F. (2014) 'Genome-scale CRISPR-Cas9 knockout screening in human cells', *Science*, 343(6166), pp. 84–87.
Shao, B., Wahrenbrock, M.G., Yao, L., David, T., Coughlin, S.R., Xia, L., Varki, A. & McEver, R.P. (2011) 'Carcinoma mucins trigger reciprocal activation of platelets and neutrophils in a murine model of Trousseau syndrome', *Blood*, 118(15), pp. 4015–4023.
Shinde, A., Wilmanski, T., Chen, H., Teegarden, D. & Wendt, M.K. (2018) 'Pyruvate carboxylase supports the pulmonary tropism of metastatic breast cancer', *Breast Cancer Research : BCR*, 20(1), .
Shinde, S.R. & Maddika, S. (2017) 'PTEN Regulates Glucose Transporter Recycling by Impairing SNX27 Retromer Assembly', *Cell Reports*, 21(6), pp. 1655–1666.
La Shu, S., Yang, Y., Allen, C.L., Maguire, O., Minderman, H., Sen, A., Ciesielski, M.J., Collins, K.A., Bush, P.J., Singh, P., Wang, X., Morgan, M., Qu, J., Bankert, R.B., Whiteside, T.L., Wu, Y. & Ernstoff, M.S. (2018) 'Metabolic reprogramming of stromal fibroblasts by melanoma exosome microRNA favours a pre-metastatic microenvironment', *Scientific Reports*, 8(1), pp. 1–14.
Sinha, S., Hoshino, D., Hong, N.H., Kirkbride, K.C., Grega-Larson, N.E., Seiki, M., Tyska, M.J. & Weaver, A.M. (2016) 'Cortactin promotes exosome secretion by controlling branched actin dynamics', *The Journal of cell biology*, 214(2), pp. 197–213.
Sosa, M.S., Bragado, P. & Aguirre-Ghiso, J.A. (2014) 'Mechanisms of disseminated cancer cell dormancy: an awakening field', *Nature Reviews Cancer 2014 14:9*, 14(9), pp. 611–622.
Spiegel, A., Brooks, M.W., Houshyar, S., Reinhardt, F., Ardolino, M., Fessler, E., Chen, M.B., Krall, J.A., Decock, J., Zervantonakis, I.K., Iannello, A., Iwamoto, Y., Cortez-Retamozo, V., Kamm, R.D., Pittet, M.J., Raulet, D.H. & Weinberg, R.A. (2016) 'Neutrophils suppress intraluminal NK cell-mediated tumor cell clearance and enhance extravasation of disseminated carcinoma cells', *Cancer Discovery*, 6(6), pp. 630–649.
Steinberg, F., Gallon, M., Winfield, M., Thomas, E.C., Bell, A.J., Heesom, K.J., Tavaré, J.M. & Cullen, P.J. (2013) 'A global analysis of SNX27-retromer assembly and cargo specificity reveals a function in glucose and metal ion transport', *Nature Cell Biology*, 15(5), pp. 461–471.
Stockwell, B.R., Friedmann Angeli, J.P., Bayir, H., Bush, A.I., Conrad, M., Dixon, S.J., Fulda, S., Gascón, S., Hatzios, S.K., Kagan, V.E., Noel, K., Jiang, X., Linkermann, A., Murphy, M.E., Overholtzer, M., Oyagi, A., Pagnussat, G.C., Park, J., Ran, Q., et al. (2017) 'Ferroptosis: A Regulated Cell Death Nexus Linking Metabolism, Redox Biology, and Disease', *Cell*, 171(2), pp. 273–285.
Stuffers, S., Sem Wegner, C., Stenmark, H. & Brech, A. (2009) 'Multivesicular Endosome Biogenesis in the Absence of ESCRTs', *Traffic*, 10(7), pp. 925–937.
Sun, X., Berger, R.S., Heinrich, P., Marchiq, I., Pouyssegur, J., Renner, K., Oefner,

P.J. & Dettmer, K. (2020) ‘Optimized Protocol for the In Situ Derivatization of Glutathione with N-Ethylmaleimide in Cultured Cells and the Simultaneous Determination of Glutathione/Glutathione Disulfide Ratio by HPLC-UV-QTOF-MS’, *Metabolites*, 10(7), pp. 1–15.

Szczerba, B.M., Castro-Giner, F., Vetter, M., Krol, I., Gkountela, S., Landin, J., Scheidmann, M.C., Donato, C., Scherrer, R., Singer, J., Beisel, C., Kurzeder, C., Heinzelmann-Schwarz, V., Rochlitz, C., Weber, W.P., Beerenwinkel, N. & Aceto, N. (2019) ‘Neutrophils escort circulating tumour cells to enable cell cycle progression’, *Nature*, 566(7745), pp. 553–557.

Sznurkowska, M.K. & Aceto, N. (2021) ‘The gate to metastasis: key players in cancer cell intravasation’. FEBS Journal 289 (15) p.pp. 4336–4354.

Takasugi, M., Yoshida, Y., Hara, E. & Ohtani, N. (2022) ‘The role of cellular senescence and SASP in tumour microenvironment’. FEBS Journal

Tasdogan, A., Faubert, B., Ramesh, V., Ubellacker, J.M., Shen, B., Solmonson, A., Murphy, M.M., Gu, Z., Gu, W., Martin, M., Kasitinon, S.Y., Vandergriff, T., Mathews, T.P., Zhao, Z., Schadendorf, D., DeBerardinis, R.J. & Morrison, S.J. (2020) ‘Metabolic heterogeneity confers differences in melanoma metastatic potential’, *Nature*, 577(7788), pp. 115–120.

Terunuma, A., Putluri, N., Mishra, P., Mathe, E.A., Dorsey, T.H., Yi, M., Wallace, T.A., Issaq, H.J., Zhou, M., Killian, J.K., Stevenson, H.S., Karoly, E.D., Chan, K., Samanta, S., Prieto, D., Hsu, T.Y.T., Kurley, S.J., Putluri, V., Sonavane, R., et al. (2014) ‘MYC-driven accumulation of 2-hydroxyglutarate is associated with breast cancer prognosis.’, *The Journal of clinical investigation*, 124(1), pp. 398–412.

Théry, C., Witwer, K.W., Aikawa, E., Alcaraz, M.J., Anderson, J.D., Andriantsitohaina, R., Antoniou, A., Arab, T., Archer, F., Atkin-Smith, G.K., Ayre, D.C., Bach, J.M., Bachurski, D., Baharvand, H., Balaj, L., Baldacchino, S., Bauer, N.N., Baxter, A.A., Bebawy, M., et al. (2018) ‘Minimal information for studies of extracellular vesicles 2018 (MISEV2018): a position statement of the International Society for Extracellular Vesicles and update of the MISEV2014 guidelines’, *https://doi.org/10.1080/20013078.2018.1535750*, 7(1), .

Timmerman, L.A., Holton, T., Yuneva, M., Louie, R.J., Padró, M., Daemen, A., Hu, M., Chan, D.A., Ethier, S.P., van ’t Veer, L.J., Polyak, K., McCormick, F. & Gray, J.W. (2013) ‘Glutamine sensitivity analysis identifies the xCT antiporter as a common triple-negative breast tumor therapeutic target.’, *Cancer cell*, 24(4), pp. 450–65.

Timpson, P., McGhee, E.J., Erami, Z., Nobis, M., Quinn, J.A., Edward, M. & Anderson, K.I. (2011) ‘Organotypic collagen I assay: A malleable platform to assess cell behaviour nin a 3-dimensional context’, *Journal of Visualized Experiments*, (56), pp. 1–4.

Tiu, Y.C., Gong, L., Zhang, Y., Luo, J., Yang, Y., Tang, Y., Lee, W. mui & Guan, X.Y. (2022) ‘GLIPR1 promotes proliferation, metastasis and 5-fluorouracil resistance in hepatocellular carcinoma by activating the PI3K/PDK1/ROCK1 pathway’, *Cancer Gene Therapy 2022*, pp. 1–11.

Tkach, M. & Théry, C. (2016) ‘Communication by Extracellular Vesicles: Where We Are and Where We Need to Go’. Cell 164 (6) p.pp. 1226–1232.

Tominaga, N., Kosaka, N., Ono, M., Katsuda, T., Yoshioka, Y., Tamura, K., Lötvall, J., Nakagama, H. & Ochiya, T. (2015) ‘Brain metastatic cancer cells release microRNA-181c-containing extracellular vesicles capable of destructing blood-brain barrier’, *Nature Communications*, 6(1), pp. 1–12.

Townsend, D.M., Tew, K.D. & Tapiero, H. (2003) ‘The importance of glutathione

in human disease'. Biomedicine and Pharmacotherapy 57 (3) p.pp. 145–155.
Trajkovic, K., Hsu, C., Chiantia, S., Rajendran, L., Wenzel, D., Wieland, F., Schwille, P., Brügger, B. & Simons, M. (2008) 'Ceramide triggers budding of exosome vesicles into multivesicular endosomes', *Science*, 319(5867), pp. 1244–1247.
Trimboli, A.J., Fukino, K., De Bruin, A., Wei, G., Shen, L., Tanner, S.M., Creasap, N., Rosol, T.J., Robinson, M.L., Eng, C., Ostrowski, M.C. & Leone, G. (2008) 'Direct Evidence for Epithelial-Mesenchymal Transitions in Breast Cancer', *Cancer Research*, 68(3), pp. 937–945.
Ubellacker, J.M., Tasdogan, A., Ramesh, V., Shen, B., Mitchell, E.C., Martin-Sandoval, M.S., Gu, Z., McCormick, M.L., Durham, A.B., Spitz, D.R., Zhao, Z., Mathews, T.P. & Morrison, S.J. (2020) 'Lymph protects metastasizing melanoma cells from ferroptosis', *Nature*, 585(7823), pp. 113–118.
Vanlandingham, P.A. & Ceresa, B.P. (2009) 'Rab7 Regulates Late Endocytic Trafficking Downstream of Multivesicular Body Biogenesis and Cargo Sequestration', *The Journal of Biological Chemistry*, 284(18), p. 12110.
Vettore, L.A., Westbrook, R.L. & Tennant, D.A. (2021) 'Proline metabolism and redox; maintaining a balance in health and disease', *Amino Acids*, 53(12), pp. 1779–1788.
Vielhaber, G., Brade, L., Lindner, B., Pfeiffer, S., Wepf, R., Hintze, U., Wittern, K.P. & Brade, H. (2001) 'Mouse anti-ceramide antiserum: a specific tool for the detection of endogenous ceramide', *Glycobiology*, 11(6), pp. 451–457.
Villarroya-Beltri, C., Baixauli, F., Mittelbrunn, M., Fernández-Delgado, I., Torralba, D., Moreno-Gonzalo, O., Baldanta, S., Enrich, C., Guerra, S. & Sánchez-Madrid, F. (2016) 'ISGylation controls exosome secretion by promoting lysosomal degradation of MVB proteins', *Nature Communications*, 7.
Vleminckx, K., Vakaet, L., Mareel, M., Fiers, W. & Roy, F. Van (1991) 'Genetic manipulation of E-cadherin expression by epithelial tumor cells reveals an invasion suppressor role', *Cell*, 66(1), pp. 107–119.
Voorde, J. Vande, Ackermann, T., Pfetzer, N., Sumpton, D., Mackay, G., Kalna, G., Nixon, C., Blyth, K., Gottlieb, E. & Tardito, S. (2019) 'Improving the metabolic fidelity of cancer models with a physiological cell culture medium', *Science Advances*, 5(1), p. eaau7314.
Waldmeier, L., Meyer-Schaller, N., Diepenbruck, M. & Christofori, G. (2012) 'Py2T Murine Breast Cancer Cells, a Versatile Model of TGFβ-Induced EMT In Vitro and In Vivo', *PLOS ONE*, 7(11), p. e48651.
Wallis, R., Mizen, H. & Bishop, C.L. (2020) 'The bright and dark side of extracellular vesicles in the senescence-associated secretory phenotype', *Mechanisms of Ageing and Development*, 189p. 111263.
Wang, J., Li, J., Gu, J., Yu, J., Guo, S., Zhu, Y. & Ye, D. (2015) 'Abnormal methylation status of FBXW10 and SMPD3, and associations with clinical characteristics in clear cell renal cell carcinoma', *Oncology Letters*, 10(5), pp. 3073–3080.
Wang, T., Wei, J.J., Sabatini, D.M. & Lander, E.S. (2014) 'Genetic screens in human cells using the CRISPR-Cas9 system', *Science (New York, N.Y.)*, 343(6166), pp. 80–84.
Wang, X., Liu, R., Zhu, W., Chu, H., Yu, H., Wei, P., Wu, X., Zhu, H., Gao, H., Liang, J., Li, G. & Yang, W. (2019) 'UDP-glucose accelerates SNAI1 mRNA decay and impairs lung cancer metastasis', *Nature*, 571(7763), pp. 127–131.
Wang, Y., Hodgkinson, V., Zhu, S., Weisman, G.A. & Petris, M.J. (2011) 'Advances in the understanding of mammalian copper transporters', *Advances in*

Nutrition, 2(2), pp. 129–137.
Wang, Y., Yen, F.S., Zhu, X.G., Timson, R.C., Weber, R., Xing, C., Liu, Y., Allwein, B., Luo, H., Yeh, H.W., Heissel, S., Unlu, G., Gamazon, E.R., Kharas, M.G., Hite, R. & Birsoy, K. (2021) 'SLC25A39 is necessary for mitochondrial glutathione import in mammalian cells', *Nature*, 599(7883), pp. 136–140.
Warburg, O. (1925) 'über den Stoffwechsel der Carcinomzelle', *Klinische Wochenschrift*, 4(12), pp. 534–536.
WARBURG, O. (1956) 'On the origin of cancer cells.', *Science (New York, N.Y.)*, 123(3191), pp. 309–314.
Wculek, S.K. & Malanchi, I. (2015) 'Neutrophils support lung colonization of metastasis-initiating breast cancer cells', *Nature*, 528(7582), pp. 413–417.
Wei, Y., Wang, D., Jin, F., Bian, Z., Li, L., Liang, H., Li, M., Shi, L., Pan, C., Zhu, D., Chen, X., Hu, G., Liu, Y., Zhang, C.Y. & Zen, K. (2017) 'Pyruvate kinase type M2 promotes tumour cell exosome release via phosphorylating synaptosome-associated protein 23', *Nature Communications*, 8.
Weigelt, B., Peterse, J.L. & Van't Veer, L.J. (2005) 'Breast cancer metastasis: Markers and models'. Nature Reviews Cancer 5 (8) p.pp. 591–602.
Weis, S., Cui, J., Barnes, L. & Cheresh, D. (2004) 'Endothelial barrier disruption by VEGF-mediated Src activity potentiates tumor cell extravasation and metastasis', *Journal of Cell Biology*, 167(2), pp. 223–229.
Wen, S.W., Sceneay, J., Lima, L.G., Wong, C.S.F., Becker, M., Krumeich, S., Lobb, R.J., Castillo, V., Wong, K.N., Ellis, S., Parker, B.S. & Möller, A. (2016) 'The biodistribution and immune suppressive effects of breast cancer-derived exosomes', *Cancer Research*, 76(23), pp. 6816–6827.
Westbrook, R.L., Bridges, E., Roberts, J., Escribano-Gonzalez, C., Eales, K.L., Vettore, L.A., Walker, P.D., Vera-Siguenza, E., Rana, H., Cuozzo, F., Eskla, K.L., Vellama, H., Shaaban, A., Nixon, C., Luuk, H., Lavery, G.G., Hodson, D.J., Harris, A.L. & Tennant, D.A. (2022) 'Proline synthesis through PYCR1 is required to support cancer cell proliferation and survival in oxygen-limiting conditions', *Cell Reports*, 38(5), p. 110320.
Wexler, H., Minton, J.P. & Ketcham, A.S. (1965) 'A comparison of survival time and extent of tumor metastases in mice with transplanted, induced and spontaneous tumors', *Cancer*, 18(8), pp. 985–994.
White, D.P., Caswell, P.T. & Norman, J.C. (2007) 'αvβ3 and α5β1 integrin recycling pathways dictate downstream Rho kinase signaling to regulate persistent cell migration', *Journal of Cell Biology*, 177(3), pp. 515–525.
Wiel, C., Le Gal, K., Ibrahim, M.X., Jahangir, C.A., Kashif, M., Yao, H., Ziegler, D. V., Xu, X., Ghosh, T., Mondal, T., Kanduri, C., Lindahl, P., Sayin, V.I. & Bergo, M.O. (2019) 'BACH1 Stabilization by Antioxidants Stimulates Lung Cancer Metastasis', *Cell*, 178(2), pp. 330-345.e22.
Wieman, H.L., Wofford, J.A. & Rathmell, J.C. (2007) 'Cytokine stimulation promotes glucose uptake via phosphatidylinositol-3 kinase/Akt regulation of Glut1 activity and trafficking', *Molecular Biology of the Cell*, 18(4), pp. 1437–1446.
Williams, E.D., Gao, D., Redfern, A. & Thompson, E.W. (2019) 'Controversies around epithelial–mesenchymal plasticity in cancer metastasis', *Nature reviews. Cancer*, 19(12), p. 716.
Wilson, B.J., Allen, J.L. & Caswell, P.T. (2018) 'Vesicle trafficking pathways that direct cell migration in 3D matrices and in vivo'. Traffic 19 (12) p.pp. 899–909.
Winnard, P.T., Vesuna, F., Muthukumar, S. & Raman, V. (2020) 'Divergent organ-specific isogenic metastatic cell lines identified using multi-omics exhibit

differential drug sensitivity', *PLoS ONE*, 15(11), .

Winnard, P.T., Zhang, C., Vesuna, F., Kang, J.W., Garry, J., Dasari, R.R., Barman, I. & Raman, V. (2017) 'Organ-specific isogenic metastatic breast cancer cell lines exhibit distinct Raman spectral signatures and metabolomes', *Oncotarget*, 8(12), p. 20266.

Woods, A.J., White, D.P., Caswell, P.T. & Norman, J.C. (2004) 'PKD1/PKCμ promotes αvß3 integrin recycling and delivery to nascent focal adhesions', *EMBO Journal*, 23(13), pp. 2531–2543.

Wu, Y., Zanotelli, M.R., Zhang, J. & Reinhart-King, C.A. (2021) 'Matrix-driven changes in metabolism support cytoskeletal activity to promote cell migration', *Biophysical Journal*, 120(9), pp. 1705–1717.

Wyckoff, J.B., Jones, J.G., Condeelis, J.S. & Segall, J.E. (2000) 'A critical step in metastasis: In vivo analysis of intravasation at the primary tumor', *Cancer Research*, 60(9), pp. 2504–2511.

Wyckoff, J.B., Wang, Y., Lin, E.Y., Li, J.F., Goswami, S., Stanley, E.R., Segall, J.E., Pollard, J.W. & Condeelis, J. (2007) 'Direct visualization of macrophage-assisted tumor cell intravasation in mammary tumors', *Cancer Research*, 67(6), pp. 2649–2656.

Yáñez-Mó, M., Siljander, P.R.M., Andreu, Z., Zavec, A.B., Borràs, F.E., Buzas, E.I., Buzas, K., Casal, E., Cappello, F., Carvalho, J., Colás, E., Cordeiro-Da Silva, A., Fais, S., Falcon-Perez, J.M., Ghobrial, I.M., Giebel, B., Gimona, M., Graner, M., Gursel, I., et al. (2015) 'Biological properties of extracellular vesicles and their physiological functions'. Journal of Extracellular Vesicles 4 (2015) p.pp. 1–60.

Yang, J. & Holman, G.D. (2005) 'Insulin and contraction stimulate exocytosis, but increased AMP-activated protein kinase activity resulting from oxidative metabolism stress slows endocytosis of GLUT4 in cardiomyocytes', *Journal of Biological Chemistry*, 280(6), pp. 4070–4078.

Yano, S., Takehara, K., Kishimoto, H., Tazawa, H., Urata, Y., Kagawa, S., Bouvet, M., Fujiwara, T. & Hoffman, R.M. (2016) 'In vivo selection of intermediately- and highly- malignant variants of triple-negative breast cancer in orthotopic nude mouse models', *Anticancer Research*, 36(12), pp. 6273–6277.

Ye, X., Brabletz, T., Kang, Y., Longmore, G.D., Nieto, M.A., Stanger, B.Z., Yang, J. & Weinberg, R.A. (2017) 'Upholding a role for EMT in breast cancer metastasis', *Nature*, 547(7661), pp. E1–E6.

Ye, X., Tam, W.L., Shibue, T., Kaygusuz, Y., Reinhardt, F., Ng Eaton, E. & Weinberg, R.A. (2015) 'Distinct EMT programs control normal mammary stem cells and tumour-initiating cells', *Nature*, 525(7568), pp. 256–260.

Young, K.A., Biggins, L. & Sharpe, H.J. (2021) 'Protein tyrosine phosphatases in cell adhesion', *Biochemical Journal*, 478(5), p. 1061.

Yu, L., McPhee, C.K., Zheng, L., Mardones, G.A., Rong, Y., Peng, J., Mi, N., Zhao, Y., Liu, Z., Wan, F., Hailey, D.W., Oorschot, V., Klumperman, J., Baehrecke, E.H. & Lenardo, M.J. (2010) 'Termination of autophagy and reformation of lysosomes regulated by mTOR', *Nature*, 465(7300), pp. 942–946.

Zanotelli, M.R., Goldblatt, Z.E., Miller, J.P., Bordeleau, F., Li, J., VanderBurgh, J.A., Lampi, M.C., King, M.R. & Reinhart-King, C.A. (2018) 'Regulation of ATP utilization during metastatic cell migration by collagen architecture', *Molecular Biology of the Cell*, 29(1), pp. 1–9.

Zaoui, M., Morel, M., Ferrand, N., Fellahi, S., Bastard, J.P., Lamazière, A., Larsen, A.K., Bérézіat, V., Atlan, M. & Sabbah, M. (2019) 'Breast-associated adipocytes secretome induce fatty acid uptake and invasiveness in breast cancer cells via CD36 independently of body mass index, menopausal status

and mammary density', *Cancers*, 11(12), .

Zech, T., Calaminus, S.D.J., Caswell, P., Spence, H.J., Carnell, M., Insall, R.H., Norman, J. & Machesky, L.M. (2011) 'The Arp2/3 activator WASH regulates α5β1-integrin-mediated invasive migration', *Journal of Cell Science*, 124(22), pp. 3753–3759.

Zhang, H., Deng, T., Liu, R., Bai, M., Zhou, L., Wang, Xia, Li, S., Wang, Xinyi, Yang, H., Li, J., Ning, T., Huang, Di., Li, H., Zhang, L., Ying, G. & Ba, Y. (2017) 'Exosome-delivered EGFR regulates liver microenvironment to promote gastric cancer liver metastasis', *Nature Communications 2017 8:1*, 8(1), pp. 1–11.

Zhang, H., Freitas, D., Kim, H.S., Fabijanic, K., Li, Z., Chen, H., Mark, M.T., Molina, H., Martin, A.B., Bojmar, L., Fang, J., Rampersaud, S., Hoshino, A., Matei, I., Kenific, C.M., Nakajima, M., Mutvei, A.P., Sansone, P., Buehring, W., et al. (2018) 'Identification of distinct nanoparticles and subsets of extracellular vesicles by asymmetric flow field-flow fractionation', *Nature Cell Biology 2018 20:3*, 20(3), pp. 332–343.

Zhang, H., Wong, C.C.L., Wei, H., Gilkes, D.M., Korangath, P., Chaturvedi, P., Schito, L., Chen, J., Krishnamachary, B., Winnard, P.T., Raman, V., Zhen, L., Mitzner, W.A., Sukumar, S. & Semenza, G.L. (2012) 'HIF-1-dependent expression of angiopoietin-like 4 and L1CAM mediates vascular metastasis of hypoxic breast cancer cells to the lungs', *Oncogene*, 31(14), pp. 1757–1770.

Zhang, Z.Z., Lee, E.E., Sudderth, J., Yue, Y., Zia, A., Glass, D., Deberardinis, R.J. & Wang, R.C. (2016) 'Glutathione depletion, pentose phosphate pathway activation, and hemolysis in erythrocytes protecting cancer cells from vitamin C-induced oxidative stress', *Journal of Biological Chemistry*, 291(44), pp. 22861–22867.

Zhao, Y., Zhao, M.F., Jiang, S., Wu, J., Liu, J., Yuan, X.W., Shen, D., Zhang, J.Z., Zhou, N., He, J., Fang, L., Sun, X.T., Xue, B. & Li, C.J. (2020) 'Liver governs adipose remodelling via extracellular vesicles in response to lipid overload', *Nature Communications*, 11(1), pp. 1–17.

Zheng, W. & Pollard, J.W. (2017) 'What DKKtates where to metastasize'. Nature Cell Biology 19 (10) p.pp. 1146–1148.

Zhou, B., Moodie, A., Blanchard, A.A.A., Leygue, E. & Myal, Y. (2015) 'Claudin 1 in breast cancer: New insights'. Journal of Clinical Medicine 4 (12) p.pp. 1960–1976.

Zhu, J., Schwörer, S., Berisa, M., Kyung, Y.J., Ryu, K.W., Yi, J., Jiang, X., Cross, J.R. & Thompson, C.B. (2021) 'Mitochondrial NADP(H) generation is essential for proline biosynthesis', *Science*, 372(6545), .

Zhu, J. & Thompson, C.B. (2019) 'Metabolic regulation of cell growth and proliferation'. Nature Reviews Molecular Cell Biology 20 (7) p.pp. 436–450.

Zhu, M., Meng, P., Ling, X. & Zhou, L. (2020) 'Advancements in therapeutic drugs targeting of senescence'. Therapeutic Advances in Chronic Disease 11.

Zhuang, X., Zhang, H., Li, Xiaoyan, Li, Xiaoxun, Cong, M., Peng, F., Yu, J., Zhang, X., Yang, Q. & Hu, G. (2017) 'Differential effects on lung and bone metastasis of breast cancer by Wnt signalling inhibitor DKK1', *Nature Cell Biology*, 19(10), pp. 1274–1285.

Zimmerman, B., Kelly, B., McMillan, B.J., Seegar, T.C.M., Dror, R.O., Kruse, A.C. & Blacklow, S.C. (2016) 'Crystal Structure of a Full-Length Human Tetraspanin Reveals a Cholesterol-Binding Pocket', *Cell*, 167(4), pp. 1041-1051.e11.